CHARACTERIZATION OF YBR074 (PFF1), A CONSERVED VACUOLAR MEMBRANE METALLOPROTEASE FAMILY MEMBER

by

Karen Alice Hecht

H.B.Sc. Biochemistry, University of Toronto, Toronto Canada, 2006

Submitted to the Graduate Faculty of

The Kenneth P. Dietrich School of

Arts and Sciences in partial fulfillment

of the requirements for the degree of

Doctor of Philosophy

University of Pittsburgh

2013

UNIVERSITY OF PITTSBURGH

FACULTY OF DIETRICH SCHOOL OF ARTS AND SCIENCES

This dissertation was presented

by

Karen Alice Hecht

It was defended on

July 27, 2012

and approved by

Meir Aridor, Associate Professor, Cell Biology and Physiology

Karen M. Arndt, Professor, Biological Sciences

Michael Grabe, Assistant Professor, Biological Sciences

Joseph A. Martens, Assistant Professor, Biological Sciences

Committee chair: Jeffrey L. Brodsky, Professor, Biological Sciences

CHARACTERIZATION OF YBR074 (PFF1), A CONSERVED VACUOLAR MEMBRANE METALLOPROTEASE FAMILY MEMBER

Karen Alice Hecht, PhD

University of Pittsburgh, 2013

In yeast, the vacuole is the principal intracellular compartment associated with protein degradation. The vacuole acts as a buffering organelle that accumulates nutrients in times of plenty, and releases them into the cytosol during periods of nutrient starvation. This important biological function is mediated by vacuolar proteases, which exhibit a variety of conserved catalytic mechanisms. Metalloproteases represent one of the most diverse classes of proteases, and they are defined by a characteristic dependence on coordinated metal ions for their catalytic activity.

In higher eukaryotes, metalloproteases are associated with both intracellular homeostasis and remodeling of the extracellular environment. In humans, remodeling of the extracellular matrix is mediated by secreted matrix metalloproteases regulating cell motility during development and wound healing, and also serving as markers of cancer metastasis. Within the cell, metalloproteases play a major role in the maturation and trafficking of proteins, as well as in the turnover of long-lived, superfluous, or damaged proteins and organelles.

This dissertation represents the first characterization of the putative yeast metalloprotease Ybr074, which is named herein, protein in FXNA-related family (Pff1). Pff1 is a member of the conserved family of M28 metalloproteases, which includes the mammalian ortholog, FXNA. FXNA has been reported to be localized in the endoplasmic reticulum (ER), and is expressed in

multiple tissues in rats, where it has been implicated in ovarian development. This dissertation shows that, unlike the ER-localized FXNA, Pff1 is a vacuolar protein. This finding is in agreement with extensive data, presented herein, demonstrating that Pff1 is not involved in protein quality control in the ER. However, genetic and chemical-genetic analyses suggest that Pff1 may have a role in yeast cell wall maintenance. Finally, this dissertation describes proteomic approaches employed in an attempt to identify endogenous substrates of Pff1, and outlines additional strategies aimed at defining the biological function of this novel vacuolar protease family member.

TABLE OF CONTENTS

PREFACE ..... **XIV**

1.0 INTRODUCTION **1**

1.1 STRUCTURE AND FUNCTION OF THE YEAST VACUOLE **2**

1.1.1 Proteolysis **8**

1.1.1.1 Autophagy **8**

1.1.1.2 Microautophagy **13**

1.1.1.3 Endocytosis **13**

1.1.2 Trehalose metabolism **17**

1.1.3 Other functions of the vacuole **18**

1.2 VACUOLAR PROTEASES **20**

1.2.1 Soluble vacuolar proteases. **21**

1.2.2 Membrane-bound vacuolar protease **30**

1.3 METALLOPROTEASE FAMILY MEMBERS IN YEAST **31**

1.4 QUESTIONS FOR FUTURE RESEARCH ON YEAST VACUOLAR FUNCTION **35**

1.5 DISSERTATION GOALS AND OVERVIEW **36**

2.0 CHARACTERIZATION AND LOCALIZATION OF YBR074 ..... **41**

2.1 INTRODUCTION **41**

2.2 MATERIALS AND METHODS 42
2.2.1 Computational Methods 42
2.2.2 Strains, plasmids, yeast growth conditions, and molecular techniques 43
2.2.3 Protein localization 49
2.2.4 Cycloheximide chase analysis of Ybr074 stability 52
2.3 RESULTS 53
2.4 CONCLUSIONS 70
3.0 ATTEMPTS TO DEFINE THE FUNCTION OF YBR074 71
3.1 INTRODUCTION 71
3.2 MATERIALS AND METHODS 72
3.2.1 Strains 72
3.2.1.1 Generating double mutant strains by yeast mating 73
3.2.2 Growth Assays 73
3.2.3 Molecular Techniques 75
3.2.4 Assays examining ER-Associated Degradation (ERAD) 75
3.2.4.1 Cycloheximide chase analyses 75
3.2.4.2 Cycloheximide pulse chase analyses 78
3.2.5 Analysis of phylogenetic profiling data 79
3.2.6 Proteomic analysis methods 79
3.3 RESULTS 81
3.3.1 Is Ybr074 a quality control protease? 81
3.3.1.1 Does Ybr074 function as a general protease during ERAD? 82

3.3.1.2 Does Ybr074 help resolve ERAD substrates with large lumenal domains? 87

3.3.1.3 Do Ybr074 and the 26S proteasome function in synergy during the degradation of CFTR? 90

3.3.1.4 Does ablation of *YBR074* and 26S proteasome function lead to synergistic effects on cell growth? 92

3.3.2 Do genetic and chemical-genetic interactions between *YBR074* and other genes link this protein to cellular processes? 95

3.3.2.1 Does *YBR074* play a role in yeast mating? 100

3.3.2.2 Does *YBR074* function in the transition to pseudohyphal growth in nutrient-limited conditions? 101

3.3.3 Does the phylogenetic profile of *YBR074* hint at its function? 103

3.3.4 Can a substrate for Ybr074 be identified using proteomic approaches? 106

3.4 CONCLUSIONS 120

4.0 CELL WALL INTEGRITY 122

4.1 MATERIALS AND METHODS 124

4.1.1 Strains and Molecular Techniques 124

4.1.2 Zymolyase sensitivity Assay 124

4.1.3 β-1,3-glucan quantification assay 124

4.1.4 Killer toxin halo assay 125

4.2 RESULTS 126

4.2.1 Does *YBR074* interact with the cell wall integrity function of *CDC48*? .. 129

4.2.2 Does the loss of *YBR074* affect the function of *CDC48* during ERAD? .. 134

4.2.3 Are β-glucan levels affected by disruption of Ybr074 and Cdc48 function? 137

4.3 CONCLUSIONS 143

5.0 DISCUSSION AND FUTURE DIRECTIONS 144

BIBLIOGRAPHY 171

LIST OF TABLES

Table 1: *Saccharomyces cerevisiae* vacuolar proteases 20

Table 2: Metalloproteases of the yeast *Saccharomyces cerevisiae* 34

Table 3: Yeast strains used in this study. 47

Table 4: Plasmids used in this study. 48

Table 5: Members of the FXNA-related gene family. 57

Table 6: ERAD substrate expression vectors 77

Table 7: Genes tested for chemical-genetic interactions in conjunction with *ybr074Δ* 97

Table 8: Compounds used to test chemical-genetic interactions 98

Table 9: Genes related to *YBR074* by evolutionary rate of covariation. 105

Table 10: Candidate substrates identified by 2D DiGE 111

Table 11: GFP-tagged proteins exhibiting increased levels in ybr074Δ strain compared to wild type 113

Table 12: GFP-tagged proteins exhibiting reduced levels in *ybr074Δ* strain compared to wild type 118

Table 13: Pff1 protease domain constructs designed for purification 154

Table 14: Vectors used in attempts to clone Pff1 protease domain for purification 158

Table 15: Refolding buffers tested on PD_2 in a 96-well plate format 166

LIST OF FIGURES

Figure 1: Protein trafficking pathway and vacuolar sorting pathways 7

Figure 2: Steps mediating autophagy. 9

Figure 3: Schematic of endocytosis 16

Figure 4: Global sequence alignment of Ape3 and Ybr074. 29

Figure 5: Global sequence alignment of FXNA and Ybr074. 40

Figure 6: The *YBR074W* locus. 53

Figure 7: Ybr074 is a transmembrane protein with a conserved M28 metalloprotease domain that is predicted to reside in the ER lumen. 55

Figure 8: Ybr074 is modified by N-linked glycans. 59

Figure 9: Assignment of Ybr074 topology by protease protection assay 62

Figure 10: Sub-cellular localization of Ybr074 as assessed using indirect immunofluorescence microscopy. 63

Figure 11: Live cell imaging of GFP-Ybr074 localization. 65

Figure 12: Ybr074-HA is retained in the ER 67

Figure 13: Stability of N- and C-terminally tagged Ybr074 constructs 69

Figure 14: The cytosolic 26S proteasome and lumenal Ybr074 putative protease 82

Figure 15: Optimization of cycloheximide chase analysis using the substrate CFTR 85

Figure 16: Ybr074 has no effect on the degradation of known ERAD substrates. 86

Figure 17: Degradation of CPY*-DHFR(Pro) and CPY*-DHFR is not dependent on Ybr074 ... 89

Figure 18: Comparison of CFTR-derived fragments in wild type, *ybr074Δ*, *rpn4Δ*, and *ybr074Δ rpn4Δ* strains. 92

Figure 19: Growth curve of strains impaired for Ybr074 and/or 26S proteasome function. 94

Figure 20: Genes interacting with *YBR074* by Synthetic Genetic Array (SGA) analysis 99

Figure 21: Qualitative mating assay showing no Ybr074-dependent defect in mating. 101

Figure 22: Pseudohyphal growth does not require Ybr074 103

Figure 23: 2D DiGE comparing wild type and *ybr074Δ* protein levels 107

Figure 24: Apparent shift of spots 14 and 35 from a higher molecular weight in the *ybr074Δ* sample to a lower molecular weight in the wild type sample. 108

Figure 25: Rhr2 expression in wild type and *ybr074Δ* strains. 110

Figure 26: *CDC48* mutant alleles. 127

Figure 27: Sensitivity of *ybr074Δ* and *cdc48-2* to cell wall stress inducing agents CFW and CR. 130

Figure 28: *cdc48-3*, *cdc48 R155H*, and *cdc48 A232E* do not exhibit a chemical-genetic interaction in the *ybr074Δ* genetic background. 132

Figure 29: Individual *ybr074Δcdc48-2* isolates do not exhibit a consistent chemical-genetic interaction of CFW. 133

Figure 30: ERAD efficiency of *cdc48-2* strains is not exacerbated by disruption of Ybr074 function. 136

Figure 31: Analysis of β-1,3-glucan levels 140

Figure 32: K1 killer toxin halo assay shows slight resistance of *ybr074Δ* and *ybr074Δ cdc48-2* strains compared to wild type. 142

Figure 33: Schematic of Ybr074 (Pff1) active site 149

Figure 34: Pff1 secondary structure predication using PSIPRED version 3.0 157

Figure 35: Expression of PD_2 from the pBAD vector 158

Figure 36: Pilot purification of PD2 161

Figure 37: PD_2 in batch purification gel 163

Figure 38: Refolding of PD_2 by dialysis 164

Figure 39: Fast dilution of PD_2 in refolding buffer containing L-arginine or L-histidine 168

PREFACE

What's in a name? One would hope to find a lot of meaning in a name. Pff1 is a name that is drawn from the comparison of related protein sequences. Although none of the members of the Brodsky lab are related (as far as I know), they have certainly come to feel like family over the course of my six years as a graduate student, and as lab mates go, they are beyond compare. So, I'll take this space to thank them in writing, so that they know I really mean it.

Many thanks go to Dr. Jeffrey Brodsky for holding me to a high standard by entrusting me with a challenging, and intellectually stimulating project. I've flitted about most of yeasts' cellular biology, chasing one hypothesis after another. Consequently, I've learned many things over the course of my graduate career, and not just about yeast biology. Thank you for teaching me by example how to manage a project, being guided both by the "big picture" and the gritty details. Thank you for fostering my creativity and encouraging me to try new experiments, even if it meant ordering bizarre reagents and making oddly colored agar plates. Thank you too, for your continued support in developing my career as a scientist. I hope to continue enjoying your mentorship for as long as I begin sentences with, "to test this hypothesis…"

Thank you, Jen Goeckeler, for being a powerhouse of a lab manager and keeping me supplied with those bizarre reagents I mentioned earlier. Your insightful comments at lab meeting, your encyclopedic knowledge, and your generosity in sharing advice, laughter, and baked goods have been a joy.

To my very first mentors in the lab, Dr. Kunio Nakatsukasa and Dr. Shruthi Vembar, thank you for being such strong science role models. You made my transition into the lab delightful, and I felt there was no end to what I could learn from you.

No North is quite as true as True North. Thank you, Alex Kolb, for being a brilliant bay mate. I could always count on you to receive my data with a stream of critically important questions. I don't know how you think so fast, but if it ever came down to a question quick-draw at high noon, I'd be glad to have you on my side. I can't wait to see you launch your next start-up. Reach for the stars, Alex; they don't stand a chance against you.

To my classmates, Sandlin and Joe, thank goodness for you two! Sandlin, I thank you for your constant support in science, and for your friendship. You taught me not just to watch my time in grad school unfold, but to create opportunities for myself and build a career out of them. Joe, your ambition and passion are inspiring, and as a fellow ORF researcher, I've often drawn strength from your tenaciousness and creativity. Science is lucky to have you.

Dr. Teresa Buck, thank you for your good advice and great company over the years, and for the maple bars. Your executive approach towards ENaC has been an inspiration. Dr. Cristy Gelling, thank you for giving me hope that it is possible to know nearly everything about yeast and still be a delightful and eloquent person. Dr. Annette Chiang, thank you for your constant support and kindness and for sharing your secret stash of 50mL pipettes (oops! Secret's out). Dr. Chris Guerriero, you are such a natural mentor. I was always very glad to have your spotless scientific rigor close at hand, and your calming influence (must have been the expert whistling). Dr. Patrick Needham, thank you for being my biochemistry guru in times of extreme insolubility, and for being strong enough to open any bottle, no matter how encrusted in dextrose. Dr. Allison O'Donnell, you've been instrumental during this time of dissertation writing. Thank you for the

lessons, the paper service, and for helping me to keep it real. Dr. Lucia Zacchi, thank you for always spurring me into action and letting me draw strength from your purposeful nature. Thank you all, too, for being my friends.

Sarah, even when it seems that your "to do" list might never end, you take on every challenge with grace and confidence. I admire you a lot, and I'm glad to know that a lot more people will have to chance to learn from you like I have.

To the newest members of the lab, Lynley and Mike, your enthusiasm and curiosity is so positively rejuvenating to this ancient 6th year. I'm so glad you've joined the lab, and I can't wait to see you succeeding wildly in your thesis projects.

A very special thank you goes out to my undergraduate mentees, Sarah Richards and Torie Wytiaz. You probably didn't know what you were getting into when you picked up a pipette against Pff1, but you didn't let the ORF get the better of you. Thank you for being brave, persistent, and always delightful. I'm so lucky to have had you on my team and I know you'll do fantastic things with your future. Thank you to all our undergraduate students for being such an integral part of the lab. Besides making things much easier for us test-tube sullying, buffer-guzzling grad students, you make the lab a much more fun and rewarding place.

Thank you to Dr. Heather Hendrickson for being one of the most influential people I've met in Pittsburgh, for sharing your passion for science and life at large, and introducing me to almost everyone I know and love in this city- that means you, Marek, Matt, Jenney and Thiago.

Thank you to my wonderful parents, Julia and Igor, for teaching me to love learning and for encouraging me to aim high. I hope that I can make you as proud of me as I am of you. Finally, thank you to Seth for his uncanny ability to make me feel good about life no matter what is happening in or out of the lab. Sticking with you is the most inspired thing I've ever done.

1.0 INTRODUCTION

The characterization of Ybr074 was initiated when *YBR074* was found to be induced in yeast cells exogenously expressing the mammalian cystic fibrosis transmembrane conductance regulator (CFTR). Since CFTR is a multi-domain protein that folds inefficiently, it was hypothesized that novel protein quality factors could be identified among genes upregulated in response to general stress conditions caused by CFTR expression in yeast. Preliminary evidence suggested that a yeast strain in which *YBR074* was partially disrupted, exhibited stabilization of CFTR (Ahner & University of Pittsburgh. School of Arts and Sciences, 2005). Since Ybr074 was computationally predicted to be an ER-localized protein with homology to a family of metalloproteases, it was hypothesized that it may play a role in the degradation of CFTR, and perhaps other quality control substrates.

The results presented in this dissertation show that the putative protease Ybr074 is not involved in CFTR quality control. Furthermore, this work demonstrates that Ybr074 is localized to the vacuole. In order to understand what role Ybr074 may be fulfilling in the vacuole, this chapter will focus on the various biological functions associated with the vacuole and the proteases found therein. The chapter concludes with an overview, in which I describe the significance and goals of my research, and outline the content of each chapter in this dissertation.

1.1 STRUCTURE AND FUNCTION OF THE YEAST VACUOLE

The yeast vacuole is a prominent organelle that can occupy ~20% of the cell volume. It is functionally similar to the plant vacuole and the lysosome of higher eukaryotes, with an important role in degradation, storage, homeostasis, and detoxification. (Broach et al, 1991; Li & Kane, 2009)

The vacuole was first described in the 1930's from light microscopy images of plant cells showing large "empty" (*vacuus*, in Latin) structures within the cytosol (Marty, 1999). However, the vacuole in yeast is host to numerous proteases, lipases, nucleases, and transporters (Broach et al, 1991; Klionsky et al, 1990; Veses et al, 2008).

The vacuole is a dynamic organelle that undergoes fusion and fission events in response to the cell cycle, and to environmental cues. Logarithmically growing cells have a multi-lobed vacuole, while in stationary phase cells, or cells starved of a carbon source, these lobes fuse to produce a single round vacuolar structure (Wiemken et al, 1970).

The vacuole maintains a slightly acidic environment (pH 6.2), compared to the cytosolic pH 7.2 in logarithmically growing yeast (Orij et al, 2009; Preston et al, 1989). This proton gradient is generated by the vacuolar ATPase, V-type ATPase, which pumps protons into the vacuolar lumen. In addition to decreasing the pH of the vacuole, the V-ATPase also generates a membrane potential of 75 mV, vacuole interior positive (Bowman & Bowman, 1986; Kakinuma et al, 1981). This potential difference is maintained by cation channels and chloride transport (Klionsky et al, 1990). These transporters include the Na^+/H^+ and K^+/H^+ cation exchanger Nxh1, and the chloride transporter Gef1 (Braun et al, 2010; Qiu, 2012).

The vacuole also has a characteristic lipid composition. Ergosterol and sphingolipid levels increase along the secretory pathway, with the plasma membrane having the highest

proportion of both these lipids and the ER having the lowest levels (Zinser et al, 1993). However, the vacuole has a relatively low ergosterol to phospholipid ratio and a reduced concentration of sphingolipids (Zinser et al, 1991). Regulating the lipid composition of the vacuolar membrane is essential to its function. In particular, phosphoinositides, ergosterol, and diacyglycerol regulate proteins that mediate vacuolar fusion events. For example, misregulation of vacuolar phosphoinositides disrupts vacuolar fusion and results in fragmented vacuoles (Fratti et al, 2004; Li & Kane, 2009).

A specific host of vacuolar proteins also define the function of this organelle. Approximately 200 of the 6000 yeast genes are annotated as encoding proteins having vacuolar localization, and 27% of those are described as having transporter function (Li & Kane, 2009). The remaining proteins comprising the vacuole possess functions in macromolecule hydrolysis, membrane fusion, protein sorting and targeting to the vacuole, acidification, and cell wall biogenesis (Wiederhold et al, 2009). A proteomic study found five cell wall biogenesis proteins enriched in the vacuole, which are thought to be targeted to the vacuole for degradation. These are Chs2, involved in chitin synthesis; Gas1 and Fks1, involved in β-glucan synthesis; Bgl2, a β-glucanase; and Yjl171, a glycosylphosphatidylinositol- (GPI) anchored cell wall protein of unknown function (Wiederhold et al, 2009).

Most proteins are targeted to the vacuole via the secretory pathway. The secretory pathway relays proteins and lipids to the subcellular compartment where their function is required. Secretory proteins are translated in the cytosol by ribosomes and are post-translationally or co-translationally inserted into the endoplasmic reticulum (ER) via the Sec61 protein channel known as the translocon (Marie et al, 2008; Mellman & Warren, 2000). Secretory proteins that are translocated co-translationally bear a signal sequence peptide with a

characteristic stretch of 8-20 hydrophobic residues that are recognized by the Signal Recognition Particle (SRP) associated with the ribosome (Janda et al, 2010). The SRP-ribosome nascent chain complex docks at the translocon, at which point soluble proteins are inserted into the ER lumen, while transmembrane proteins are inserted into the membrane through a lateral gating mechanism of the translocon (Alder & Johnson, 2004; Egea & Stroud, 2010). Once in the ER, nascent proteins fold with the assistance of chaperones, including those in the heat shock protein (Hsp) 70 family and Hsp40 family, and undergo post-translational modifications, including proteolytic cleavage of the signal peptide, disulphide bond formation, and addition of carbohydrate residues (Braakman & Bulleid, 2011; Hebert & Molinari, 2007).

Once secretory proteins have folded correctly in the ER, they are packaged into coat protein complex-II (COPII) vesicles for deliver to the Golgi. The COPII complex is made up of the Sar1 GTP-binding protein, the Sec23-Sec24 complex, and the Sec13-Sec31 complex (Hughes & Stephens, 2008). Transmembrane cargo can bind directly to COPII-coat proteins via a cytosolic ER exit signal located at the C-terminus of the cargo protein. The ER exit signal can be a di-hydrophobic sequence such as Phe-Phe, Tyr-Try, Ile-Ile, or Leu-Leu. The ER exit signal might also be comprised of the di-acidic motif Asp/Glu-Xaa-Asp/Glu (where Xaa is any amino acid). Other types of ER exit signals have also been characterized, including Phe-Tyr, Leu-Val, Ile-Leu, Phe-Xaa, Xaa-Val, and Tyr-Xaa-Xaa-Phi (where Phi is a bulky hydrophobic amino acid) (Nufer et al, 2002; Watanabe & Riezman, 2004). It is important to note these C-terminal ER exit signal are not always sufficient for vesicle budding, and that other signals within the cargo protein may be required in combination with a C-terminal signal to direct ER exit (Otte & Barlowe, 2002). Furthermore, soluble protein cargos require membrane-spanning adaptor

proteins to interact with the cytosolic COPII coat. These adaptor proteins, or cargo receptors, include Erv29 and Erv14 (Sato & Nakano, 2007).

Vesicle fusion to the Golgi is mediated by soluble n-ethylmaleimide sensitive factor adaptor protein receptor (SNARE) proteins that form a complex in trans between the vesicle-specific SNAREs (v-SNAREs) and the target membrane-specific SNAREs (t-SNAREs) of the Golgi (Brittle & Waters, 2000). Once cargo has been successfully delivered to the Golgi, the SNARE complex is disassembled by the dissociation chaperones Sec17 and Sec18, which in mammalian cells are SNAP (Soluble NSF-Attachment Protein) and NSF (N-ethylmaleimide-Sensitive Factor), respectively (Brittle & Waters, 2000). COPI vesicles direct retrograde transport of v- SNAREs back to the ER. The COPI coat also retrieves other factors from the Golgi, such as the ER chaperones Kar2 and Pdi1, by recognition of an ER-retention signal: KDEL for soluble ER-resident proteins, and KKXX for transmembrane ER-resident proteins (Duden, 2003).

In the Golgi, carbohydrate residues of secretory proteins are modified and extended, particularly on secretory proteins destined for the cell wall (Goto, 2007; Yan & Lennarz, 2005). It is at this point, in the Golgi, that cargo proteins reach a cross-road in the secretory pathway, and can be retained in the Golgi, targeted to the plasma membrane, or targeted to the vacuole. The adaptor protein (AP) 1 complex is involved in targeting cargo to endosomes (Valdivia et al, 2002). The AP-3 complex is more specific for delivery of cargo from the Golgi to the vacuole (Cowles et al, 1997).

The principle routes described for vacuolar sorting of secretory proteins are known as the carboxypeptidase Y (CPY) pathway and the alkaline phosphatase (ALP) pathway (Bowers & Stevens, 2005). The CPY pathway targets proteins to the pre-vacuolar compartment, also known

as the multivesicular body (MVB), which subsequently fuses with the vacuole. The CPY pathway involves sorting into vesicles associated with clathrin and adaptor proteins Gga1 and Gga2 (Bonifacino, 2004; Bowers & Stevens, 2005). The ubiquitin ligase, Rsp5, appends a K63-linked polyubiquitin signal on cargo, which ensures targeting to the MVB instead of the plasma membrane (Lauwers et al, 2010). This is achieved by association with the ubiquitin-binding endosomal sorting complex required for transport (ESCRT) complexes (Van Den Hazel et al, 1996). These vesicles are subsequently tethered to the MVB by a multi-subunit tethering complex (MTC) known as the homotypic fusion and vacuole protein sorting (HOPS) complex (Brocker et al, 2012). The HOPS complex, together with the Rab family GTPase, Ypt7, and SNARE proteins direct vesicle fusion to the MVB, and fusion of the MVB to the vacuole (Lachmann et al, 2011). In contrast, the ALP pathway bypasses the MVB completely, such that vesicles budding from the Golgi are targeted directly to the vacuole by AP-3 complex in a clathrin-independent manner (Bowers & Stevens, 2005). These pathways are summarized in Figure 1.

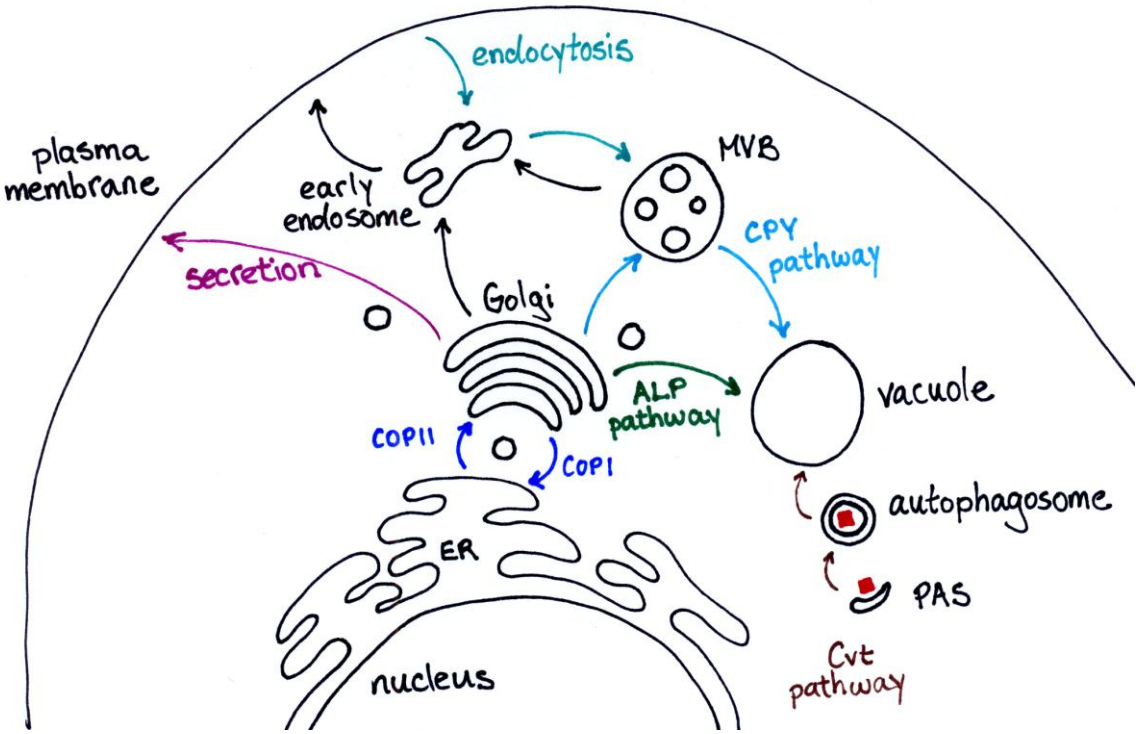

Figure 1: Protein trafficking pathway and vacuolar sorting pathways

Cellular compartments are labeled in black and secretory pathways discussed in this chapter are highlighted and color coded. Of particular note are the vacuolar sorting pathways: the CPY pathway, shown in light blue; the ALP pathway, shown in green; and the Cvt pathway, shown in brown. This image was adapted from Bowers *et al.* 2005.

1.1.1 Proteolysis

The vacuole is host to numerous exopeptidases and endopeptidases that contribute to what is often considered the vacuole's principal function, protein degradation (Van Den Hazel et al, 1996). The vacuole maintains protein homeostasis under physiological conditions by degrading senescent, superfluous, and damaged proteins and organelles. It is also important under conditions of nutrient stress, when cell growth and proliferation are down-regulated, and macromolecules are broken down in the vacuole so that their constituent amino acids can be recycled (Thumm, 2000). Degradation of up to ~85% of the cell's intracellular protein content has been observed during nutrient starvation (Teichert et al, 1989). Such nutrient stress is encountered when cells reach stationary phase, or when they are undergoing sporulation. Some of the cues known to trigger nutrient stress include carbon and nitrogen starvation, and to a lesser extent a lack of essential amino acids, nucleotides, and sulphates (Mizushima, 2007; Takeshige et al, 1992). This section discusses the various degradation functions attributed to the vacuole.

1.1.1.1 Autophagy

Autophagy, also known as macroautophagy, is a process whereby bulk cytoplasmic material and organelles are isolated in a double-membrane vesicle known as an autophagosome (Mari et al, 2011). The autophagosome fuses with the vacuole, where its contents are degraded and their constituent parts recycled. This mechanism is conserved throughout eukaryotes, and is used to maintain cellular homeostasis under physiological conditions by eliminating long-lived proteins and damaged organelles. Autophagy can also be induced under conditions of nutrient stress, and

during specific stages in the cell cycle such as in stationary phase or during sporulation (Hopper et al, 1974; Reggiori & Klionsky, 2002). Autophagy is mediated by over 30 autophagy-related proteins, known as Atg proteins encoded by *ATG* genes (Xie & Klionsky, 2007).

Autophagy is described in a series of sequential steps: induction, cargo recognition, vesicle nucleation, expansion and completion of the autophagosome, Atg protein recycling, fusion of the autophagosome with the vacuole, vesicle breakdown, and macromolecule recycling (Figure 2).

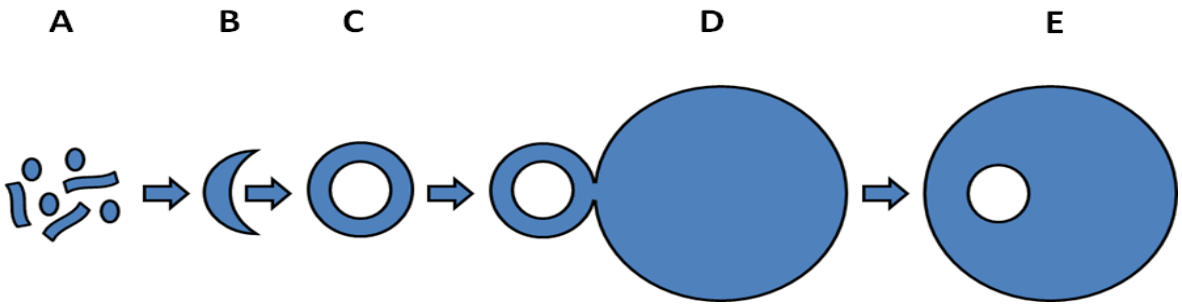

Figure 2: Steps mediating autophagy.

A) The phagophore assembly site (PAS) recruits cargo and Atg proteins required to extend the vesicle membrane to form a B) phagophore, which closes to form a double membrane vesicle called the C) autophagosome, which D) fuses to the vacuole, resulting in an internalized single membrane vesicle called the E) autophagic body. Ultimately, the autophagic membrane is broken down, releasing its contents into the vacuolar lumen for degradation.

In yeast, autophagy is regulated by the protein kinase known as Target of rapamycin (Tor). Under nutrient-rich conditions, a Tor-containing complex (TORC1) is active and inhibits autophagy. During nutrient limitation, TORC1 is inactive, resulting in induction of autophagy (Mizushima, 2007). Inactivation of TORC1 allows the Atg1 kinase to associate with

hypophosphorylated Atg13 and Atg17. Formation of the Atg1-Atg13-Atg17 kinase complex increases the activity of Atg1. Although the substrate of Atg1 has not been identified, formation of this complex is associated with increased levels of autophagy (He & Klionsky, 2009).

Once autophagy has been induced, Atg proteins begin to accumulate at the Phagophore Assembly Site (PAS). In yeast, the PAS is found adjacent to the vacuole, and acts as a nucleation site for recruitment of Atg proteins, cargo, and lipids needed to form the phagophore. This event is marked by accumulation of the transmembrane protein, Atg9, which is a core member of the autophagy machinery and is conserved amongst eukaryotes (Suzuki et al, 2001). The scaffold proteins Atg11 and Atg17 also localize to the PAS and facilitate its expansion by recruiting other Atg proteins (Kabeya et al, 2009; Xie & Klionsky, 2007).

Another protein with a putative role in PAS nucleation is the lipid kinase Vps34. This phosphatyidylinositol 3-kinase forms at least two distinct complexes in yeast, denoted Complex I and II. It is thought that Vps34 produces phosphatidylinositol-3-phosphate at the PAS, which serves as a binding site for Atg proteins containing phox homology (PX) domains, such as Atg20 and Atg24 (Nice et al, 2002). However, the role of these PX domain-containing proteins is not understood.

Expansion of the phagosome is dependent on two ubiquitin-like protein conjugating systems involving the ubiquitin-like proteins Atg12 and Atg8. Based on structural data derived from studies on plant Atg12 and mammalian Atg8, these proteins display a ubiquitin fold at the C-terminus, even though they are not considered homologs based on sequence similarity (Paz et al, 2000; Suzuki et al, 2005). During autophagy, Atg12 is activated by the E1-like protein Atg7, which mediates the transfer of Atg12 to the E2-like protein Atg10. Atg12 is then covalently linked to a lysine residue on Atg5. The Atg12-Atg5 conjugate then associates with Atg16 to form

an Atg12-Atg5-Atg16 ternary complex that coats the outer membrane of the expanding phagophore and is thought to drive membrane curvature and to prevent premature fusion with the vacuole (Yang & Klionsky, 2009).

The second uniquitin-like conjugating system required for phagosome formation involves the cleavage of the ubiquitin-like protein Atg8 by the cysteine protease Atg4, followed by conjugation of the cleaved Atg8 to phosphatidylenthanolamine (PE) by the E2-like enzymes Atg7 and Atg3. Atg8-PE is associated with both the inner and outer membranes of the phagophore and serves to link cargo to the phagophore membrane (Pyo et al, 2012). Intriguingly, Atg8-PE has been shown to interact with Shp1, a co-factor of the AAA^+ ATPase Cdc48, which will be discussed in detail in Chapter 2. It is thought that Cdc48 together with Shp1 play an important, though uncharacterized role in phagosome maturation (Dargemont & Ossareh-Nazari, 2012; Krick et al, 2010).

Once expansion of the phagophore is complete the resulting double membrane vesicle enclosing its cargo is referred to as the autophagosome. Atg8-PE on the outer membrane is cleaved by Atg4 and recycled. Other Atg proteins are also recycled at this stage by an uncharacterized mechanism. Fusion of the outer membrane of the autophagosome with the vacuole is mediated by SNAREs, Vam3 and Vam7; the ATPase Sec18; and the Rab-family GTP-binding protein, Ypt7 (Yang & Klionsky, 2009). Once internalized by the vacuole, the cytoplasmic cargo encapsulated by the inner membrane of the autophagosome is referred to as an autophagic body. The membrane of the autophagic body is degraded by the lipase Atg15, and its contents are hydrolyzed by vacuolar proteases (Epple et al, 2001). It is interesting to note that Atg15 is currently the only known vacuolar lipase.

Although autophagy is generally considered to be non-selective, a few forms of selective autophagy have been described. These involve degradation of superfluous or damaged organelles. Unlike non-selective autophagy, phagophores associated with selective autophagy engulf very little cytoplasmic material besides the target organelle. These selective forms of autophagy are known to target the ER, lipid droplets, mitochondria, the nucleus, peroxisomes, and ribosomes, and are referred to as ERphagy, lipophagy, mitophagy, Piecemeal Microautophagy of the Nucleus (PMN), pexophagy, and ribophagy, respectively (Beau et al, 2008; Bernales et al, 2007; Dong & Czaja, 2011; Dunn et al, 2005; Kissova et al, 2007; Kraft et al, 2009; Krick et al, 2008).

Another notable type of selective autophagy is known as the cytoplasm-to-vacuole targeting (Cvt) pathway. Unlike the forms of autophagy discussed previously, the Cvt pathway occurs during nutrient-rich conditions and is a constitutive process (Khalfan & Klionsky, 2002). The Cvt pathway mediates the selective transport of homooligomeric vacuolar proteins. Only three substrates are known to be targeted to the vacuole by this method: aminopeptidase I (Ape1), α-mannosidase 1 (Ams1), and aminopeptidase 4 (Ape4). Notably, Ape1 and Ams1 are resident vacuolar proteins, while Ape4 is cytosolic under physiological conditions, with Cvt-mediated vacuolar targeting occurring during nutrient starvation conditions (Yuga et al, 2011).

Cvt substrates are synthesized in the cytoplasm as precursors, where they homooligomerize and bind to Atg19. Atg19 acts as a receptor for Cvt substrates and recruits them to the PAS in an Atg11-dependent manner (Baba et al, 1997; Hutchins & Klionsky, 2001; Scott et al, 1997; Yuga et al, 2011). The autophagosomes associated with the Cvt pathway are smaller, and take approximately 10 times longer to form than those associated with autophagy (Kraft et al, 2009).

The Cvt pathway may be an important alternative trafficking mechanism to target vacuolar resident proteins that may otherwise be damaging to secretory pathway residents. Alternatively, the Cvt pathway may facilitate transport of stable oligomeric proteins which are too large to traverse the vacuolar membrane via transporters. The Cvt pathway may also facilitate vacuolar localization of membrane-associated proteins, such as Ams1, which lack a signal sequence to direct their translocation into the secretory pathway (Figure 1) (Hutchins & Klionsky, 2001).

1.1.1.2 Microautophagy

Microautophagy differs from macroautophagy because cargo is engulfed directly by vacuolar membrane extensions and not by *de* novo synthesis of a phagophore membrane. Microautophagy is constitutively active but can also be induced to higher levels under starvation conditions. Microautophagy targets both cytosolic proteins and organelles. Internalization of cargo is achieved by invagination of the vacuolar membrane, or by protruding vacuolar membrane extensions known as autophagic tubes. The cytosolic material is engulfed and the resulting vacuolar vesicle pinches off and becomes completely internalized by the vacuole. The vesicle and its contents are then degraded, and constituent parts may be recycled. It is thought that the uptake of vacuolar boundary membrane by microautophagy is required to balance the influx of autophagosomal membranes resulting from macroautophagy (Li et al, 2012; Uttenweiler & Mayer, 2008).

1.1.1.3 Endocytosis

Endocytosis represents another pathway targeting proteins to the vacuole for degradation. Endocytosis is a conserved mechanism that mediates protein turnover at the cell surface, nutrient

uptake, and adaptation to the extracellular environment (Boettner et al, 2012). Yeast must both internalize plasma membrane proteins that have become superfluous and deliver new ones to replace them. The most well characterized endocytic pathway is clathrin-mediated endocytosis (CME), which is mediated by ~60 proteins (Weinberg & Drubin, 2012). Until recently, the CME was the only demonstrated mechanism for endocytosis in yeast. However clathrin-independent pathways are beginning to be described as well (Prosser et al, 2011).

The process of endocytosis can be divided into a stationary phase, in which early proteins, early coat proteins, and cargo are recruited, and a mobile phase, in which intermediate and late coat proteins mediate membrane deformation and actin polymerization that drives invagination of the endocytic vesicle. The process is completed by vesicle scission and uncoating. This allows recycling of coat proteins and vesicle fusion with the early endosome (Figure 3).

The mechanism that leads to endocytic site selection is not understood, but is marked by recruitment of early proteins Ede1 and Syp1 to sites of the plasma membrane inner leaflet referred to as eisosomes (Moreira et al, 2009). Syp1 contains an F-BAR domain, which binds lipid and deforms membranes. Ede1 is a ubiquitin-binding protein that plays an important role in the recruitment of proteins involved in later stages of endocytosis. Recruitment of these early proteins is followed by enrichment of endocytic cargo proteins to these sites, and association of early coat proteins including clathrin, and cargo-specific adaptors such as the AP-2 complex and Yap1801/Yap1802. Syp1 also functions as a cargo-specific adaptor for the cell wall stress sensor Mid2 (Boettner et al, 2012).

The subsequent recruitment of intermediate coat proteins brings together machinery that mediates coupling of actin assembly and vesicle formation. For example, the intermediate coat

protein, Sla2, serves as an adaptor linking the plasma membrane, clathrin coat, and actin at the site of endocytosis. The Sla2 N-terminal domain binds phosphoinositol-4-5-bisphosphate (PIP2) at the endocytic membrane, its central coiled-coil region interacts with clathrin light chain, and its C-terminal domain interacts with actin filaments (Sun et al, 2005). Furthermore, a number of late coat protein are recruited, which act as nucleation promoting factors (NPFs) that activate the Arp2/3 complex mediating actin assembly. These NPFs include Pan1, Las17 (mammalian Wiskott-Aldrich syndrome protein; WASP), Myo3, Myo5, and Abp1. Actin polymerization provides a directional pulling force and the tensile strength required to extend the membrane deformation inward, forming an elongated tubule with a clathrin-coated tip (Girao et al, 2008; Weinberg & Drubin, 2012). Although dynamin is essential for scission in mammalian cells, its yeast counterpart, Vps1, it thought to plays a lesser role in this process (Weinberg & Drubin, 2012). It is thought that the combination of actin assembly, membrane deformation by BAR and F-BAR proteins, such as Syp1 and the heterodimeric Rvs161/167 complex, and lipid phase separation between the plasma membrane and endocytic vesicle are the key factors facilitating vesicle scission (Liu et al, 2006; Weinberg & Drubin, 2012). Finally, vesicle uncoating is facilitated by the PIP2 phosphatase Sjl2 and other late coat proteins, such as Lsb5 and Gts1 (Weinberg & Drubin, 2012). The uncoated endocytic vesicle undergoes a series of fusion events with the early endosome, the late endosome, and finally the vacuole. Vesicle fusion is facilitated by Rab GTPases, multisubunit tethering complexes (MTC) and SNAREs (Boettner et al, 2012; Munn et al, 1999).

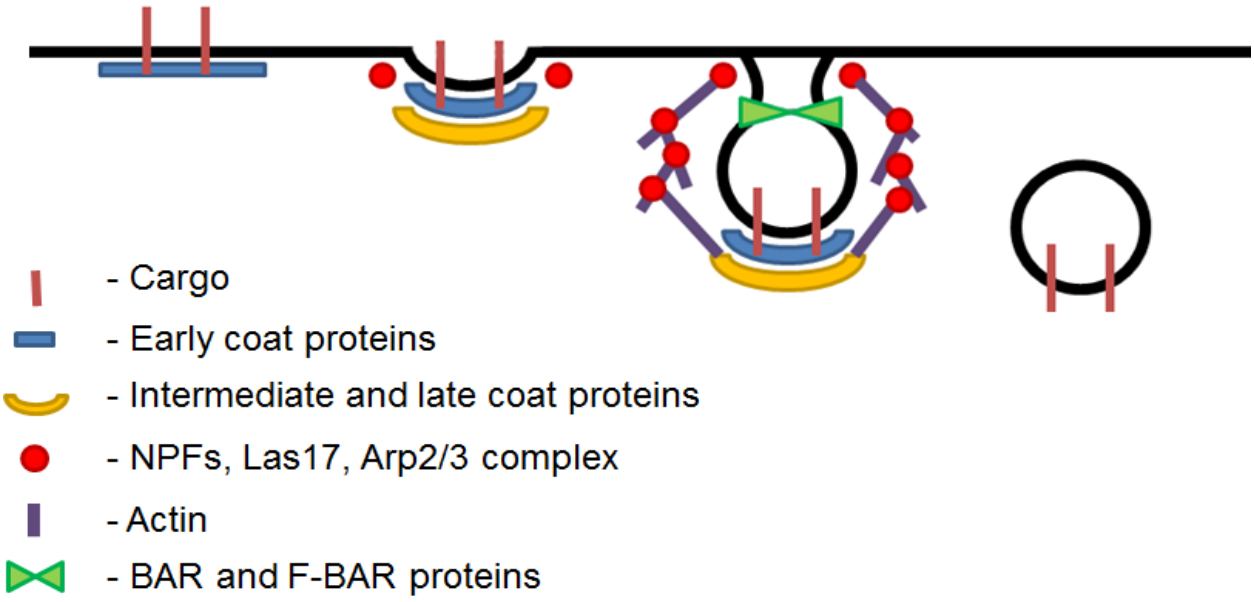

Figure 3: Schematic of endocytosis

Early, early coat protein and cargo are recruited to endocytic sites. Intermediate and late coat proteins, as well as actin remodeling proteins assemble. Invagination of the endocytic vesicle is mediated by actin assembly, as well as BAR and F-BAR proteins. The endocytic vesicle undergoes scission and uncoating. This diagram was adapted from Weinberg J. *et al.* 2012.

1.1.2 Trehalose metabolism

Trehalose is a disaccharide that accumulates in yeast during stationary phase, and in response to various stress conditions, including salt stress, heat or cold stress, oxidative stress, and dehydration (Garre & Matallana, 2009; Nwaka & Holzer, 1998). Trehalose is thought to act as a protectant of membranes under conditions of stress by forming hydrogen bonds with lipid polar head groups, and maintaining appropriate spacing between lipid acyl chains. This mechanism of trehalose-mediated membrane protection is known as the water replacement hypothesis (Golovina et al, 2009). Under conditions of heat stress, trehalose associates with and stabilizes proteins, and prevents misfolded proteins from aggregating. Furthermore, recovery of cells after heat stress is associated with rapid degradation of trehalose, which is thought to be required in order to allow Hsps access to misfolded proteins in order to facilitate their re-folding (Singer & Lindquist, 1998).

Degradation of trehalose into two glucose molecules is mediated by the cytosolic trehalases, Nth1 and Nth2, as well as the vacuolar trehalase, Ath1 (Garre & Matallana, 2009). Although Ath1 is considered a vacuolar enzyme, whose activity is optimal at acidic pH, some evidence suggests Ath1 is also found in the periplasmic space (Jules et al, 2004). Although a role for Ath1 in trehalose degradation after stress has not been ruled out, it is thought that the principal role of Ath1 in trehalose hydrolysis is its utilization as a carbon source. In fact, an *ath1Δ* strain was unable to grow on media in which trehalose was the sole carbon source (Nwaka et al, 1996). However, *ATH1* was also induced by the high osmolarity glycerol (HOG) pathway

under conditions of salt stress, suggesting that a role for Ath1 in stress tolerance may yet be discovered (Garre & Matallana, 2009).

1.1.3 Other functions of the vacuole

In addition to proteolytic functions, the vacuole has other important roles in the maintenance of cellular homeostasis. The vacuole acts as a storage compartment for amino acids, phosphates, Ca^{2+}, and metal ions (Li et al, 2012). It stores basic and neutral amino acids at particularly high levels in order to buffer a decrease in cytosolic levels of amino acids arising during nutrient starvation (Broach et al, 1991; Li et al, 2012). The vacuole stores inorganic phosphate and polyphosphate, which are used in the synthesis of nucleotides, and phospholipids (Shirahama et al, 1996). Polyphosphates may also help regulate vacuolar pH by releasing protons when hydrolyzed. They also play an important role as counterions, facilitating the retention of basic amino acids and positively charged ions, such as Ca^{2+}. Calcium ATPase and Ca^{2+}/H^{+} transporters facilitate calcium storage in the vacuole, and regulate cytosolic levels of this important signaling molecule. Ca^{2+} mediates the cell wall stress response, release from pheromone-induced cell cycle arrest, and the salt stress response (Pittman, 2011; Rusnak & Mertz, 2000). The vacuole also stores other physiologically relevant ions such as Mg^{2+} and Zn^{2+}, which may have deleterious effects on the cell if allowed to accumulate in the cytosol (Klionsky et al, 1990). The vacuole sequesters toxic compounds, such as Cd^{2+}, Co^{2+}, and Pb^{2+}, in the form of glutathione S-conjugates (Broach et al, 1991). Interestingly, a screen for genes required for transition metal tolerance revealed 18 genes required for tolerance on all six metals tested in this screen: Zn^{2+}, Ni^{2+}, Mn^{2+}, Fe^{2+}, Cu^{2+}, and Co^{2+}. These included subunits of the V-ATPase, an ER-resident ATPase assembly factor, Vma21, and members of the Regulator of the H^{+}-ATPase of the

Vacuolar and Endosomal membranes (RAVE) complex, which is involved in assembly of the V-ATPase. Factors involved in vacuolar protein sorting, such as the Rho family GTPase Ypt7, and the phosphatidylinositol kinases Vps34 and Fab1, were also isolated (Bleackley et al, 2011). These findings highlight the importance of vacuolar sequestration in mediating tolerance to metals. Finally, cross-talk between the yeast vacuole and mitochondria has been shown to regulate apoptosis in response to external pro-apoptotic signals such as acetic acid (Sousa et al, 2011). This process is thought to be mediated by translocation of Pep4 from the vacuole into the cytosol as a result of vacuolar membrane permeabilization (Mason et al, 2005; Schauer et al, 2009). Pep4 release from the vacuole appears to protect cells from apoptosis by facilitating the removal of damaged mitochondria by an uncharacterized, and autophagy-independent mechanism (Pereira et al, 2010).

1.2 VACUOLAR PROTEASES

The yeast vacuole contains seven known vacuolar proteases, only one of which is a transmembrane protease. Of these, three are metalloproteases, three are serine proteases, and one is an aspartyl protease. The vacuolar proteases include three aminopeptidases, two carboxypeptidases, and two endopeptidases. This section describes the known characteristics and function of these proteases, which are summarized in Table 1.

Table 1: *Saccharomyces cerevisiae* vacuolar proteases

Protease	Gene	Activity	Proteolytically activated by	Trafficking pathway	Function	Known P1 site amino acids
Proteinase A	*PEP4*	aspartyl endoprotease	Pep4 and Prb1	secretory	Initiator of protease activation cascade; protein degredation	Phe, Leu, Tyr, Trp, Thr, Asn, Gln, Glu, Lys, Ala, Ile
Proteinase B	*PRB1*	serine endoprotease	Pep4 and Prb1	secretory	protease activation; protein degradation	Leu, Arg, Phe, Tyr, Gln, Lys
Carboxypeptidase Y	*PRC1*	serine carboxypeptidase	Pep4 and Prb1	CPY pathway	peptide degradation	Ala, Gly, Val, Leu, Ile, Met, Phe
Carboxypeptidase S	*CPS1*	zinc metalloprotease	Prb1	CPY pathway	peptide degradation	Gly, Leu
Aminopeptidase I	*APE1*	zinc metalloprotease	Prb1	Cvt pathway	glutathione degradation	Leu, Cys/Gly
Aminopeptidase Y	*APE3*	metalloprotease	Prb1	secretory	unknown	Pro, Ala, Leu, Met, Phe, Tyr, Ser, Lys, Arg
Dipeptidylaminopeptidase B	*DAP2*	serine dipeptidase	none	CPY pathway	unknown	Xaa-Ala, Xaa-Pro

The MEROPS peptidase database (http://merops.sanger.ac.uk) has classified known proteases into evolutionarily related groups, which will be referenced in the following discussion of vacuolar proteases. A protease clan refers to proteases derived from a single common

ancestor. Clans are subdivided into families. A protease family refers to a sub-group of proteases that share sequence similarity, either throughout the entire protein sequence or only within the catalytic domain (Rawlings & Barrett, 1993). Protease families are assigned a letter referring to the catalytic mechanism of the protease: M for metalloprotease, S for serine protease, and A for aspartyl protease. The catalytic designation is followed by a numeric identifier for the family (Rawlings et al, 2012). Another important nomenclature refers to the site of cleavage of the substrate. The amino acid on the N-terminal side of the hydrolyzed peptide bond is referred to as P1, while the amino acid on the C-terminal side is referred to a P1'. Similarly, the site on the proteolytic enzyme known to bind to the P1 residues is referred to as S1, while the site recognizing the P1' residue is referred to as S1'.

Briefly, serine proteases comprise a large family whose enzymatic activity is mediated by a characteristic "catalytic triad" consisting of Asp, His, and Ser. The members, substrates and catalytic mechanism of the serine type proteases is reviewed in Hedstrom *et al*. (Hedstrom, 2002). Metalloproteases depend on metal ions, especially Zn^{2+}, for their catalytic function, and are discussed in detail in Section 1.3 (Rawlings & Barrett, 1995). The aspartyl proteases are characterized by two catalytic Asp residues mediating an acid-base hydrolysis reaction (Tang & Wong, 1987). The structure and function of aspartyl proteases was reviewed by Dunn (Dunn, 2002).

1.2.1 Soluble vacuolar proteases.

Proteinase A (PrA), encoded by the *PEP4* gene, is a monomeric 42 kDa aspartyl endoprotease of the A1 family of proteases. PrA is targeted to the vacuole via the secretory pathway (Broach et al, 1991; Van Den Hazel et al, 1996; Westphal et al, 1996). It is a key vacuolar enzyme in the

vacuolar protease activation cascade. Many vacuolar hydrolases, including PrA, are initially produced as inactive precursor forms, known as zymogens (van den Hazel et al, 1992). Zymogens are not activated until they have been delivered to the vacuole where an inhibitory propeptide is removed by proteolysis. This allows hydrolase activity to be sequestered within the vacuole, and protects substrates outside the vacuole from proteolytic damage. The vacuolar proteases, proteinase B (PrB), carboxypeptidase Y (CPY), and aminopeptidase I (API), which are discussed in detail below, all depend on PrA for proteolytic activation, and PrA mutant strains are deficient in the activity of these proteases (Van Den Hazel et al, 1996).

PrA is initially synthesized as an inactive precursor referred to as preproPrA. PreproPrA is 405 amino acids in length and has a molecular mass of 52 kDa. PreproPrA has a hydrophobic 22 amino acid signal sequence that directs its translocation into the ER, where it is modified by N-linked glycans at Asn67 and Asn266 (Mechler et al, 1982; Parr et al, 2007). The signal peptide is cleaved by the signal peptidase to produce ProPrA, which is then transported to the Golgi. The carbohydrate residues of ProPrA are mannosylated in the Golgi. ProPrA is then recognized by the vacuolar protein sorting receptor,Vps10, which targets it to the vacuole (Jorgensen et al, 1999). Either within the transport vesicle or the vacuole, proPrA undergoes autocatalytic activation, whereby a 54 amino acid propeptide is removed to produce active PrA. Active PrA preferentially cleaves substrates between two hydrophobic amino acids, such as Phe, Ile, Leu, Glu, and Ala (Kondo et al, 1998).

Proteinase B (PrB) is a serine endoprotease of the S8 family, encoded by the *PRB1* in yeast. The zymogen preproPrB is initially synthesized in a 76 kDa form that is translocated into the ER where it is modified by a single N-linked glycan, and its 20 amino acid signal peptide is removed (Moehle et al, 1989). PreproPrB undergoes autocatalytic cleavage in the ER, removing

an N-terminal 260 amino acid propeptide (Nebes & Jones, 1991). The ER-resident protein, Pbn1, acts as a chaperone in this process to facilitate proper folding of proPrB, which is a pre-requisite for autocatalytic cleavage of the proPrB propeptide (Naik & Jones, 1998; Subramanian et al, 2006). ProPrB is further modified by O-linked glycans in the Golgi resulting in a 42 kDa species (Moehle et al, 1989). The N-terminal propeptide is thought to remain non-covalently associated with proPrB, partially inhibiting its enzymatic activity, until proPrB is targeted to the vacuole where the N-terminal propeptide is degraded by PrA (Naik & Jones, 1998). In the vacuole a C-terminal propeptide (~30 amino acids) of proPrB is cleaved by PrA to produce a 37 kDa PrB species. The final cleavage event is mediated autocatalytically by PrB, removing a C-terminal peptide modified by a single N-linked glycan, and yielding the mature 31 kDa PrB (Moehle et al, 1989). Intriguingly, while disrupting PrA activity leads to accumulation of proPrB and the N-terminal propeptide, proPrB retains residual catalytic activity (Van Den Hazel et al, 1996).

Information on the substrate specificity of PrB comes from studies of PrB isolated from both *Saccharomyces cerevisiae* and *Candida albicans*. Both artificial peptides and non-yeast proteins, such as insulin, were used to test PrB substrate specificity in these studies (Farley et al, 1986; Kominami et al, 1981). Based on these studies, PrB has a broad substrate specificity that may depend on amino acid context. The protease cleaves substrates at Arg, Leu, Tyr, Phe, Lys, or Asp in the P site, and Phe, Tyr, Val, Gly, Leu, Glu, or His in the P' site (Farley et al, 1986; Kominami et al, 1981).

Carboxypeptidase Y (CPY) is a serine carboxypeptidase of the S10 family, which is encoded by *PRC1* in yeast. CPY is initially synthesized as ~60 kDa precursor 532 amino acids in length. It is translocated into the ER where a 20 amino acid signal peptide is removed by signal peptidase and four N-linked glycan residues are appended to produce a 67 kDa from called p1-

CPY (Jung et al, 1999). CPY protein folding in the ER involves the formation of five disulphide bonds and is facilitated by a 91 amino acid propeptide, which acts as an intramolecular chaperone (Tang et al, 2002). The p1-CPY protein is delivered to the Golgi where glycan residues are extended to produce a 69 kDa form referred to as p2-CPY. In the Golgi, p2-CPY is recognized by Vps10 via a QRPL recognition sequence in the propeptide region for delivery to the MVB, which subsequently fuses with the vacuole (Jung et al, 1999; Marcusson et al, 1994; Van Den Hazel et al, 1996). This vacuolar targeting pathway, named the CPY pathway, was described in Section 1.1 and is used by other substrates targeted to the vacuole, two of which are discussed below. In the vacuole, the propeptide of CPY is removed by the sequential action of PrA and PrB to produce active CPY (Broach et al, 1991; Jung et al, 1999).

CPY contains a catalytic triad characteristic of serine proteases, which is comprised of Ser146, His397, and Asp338 (Jung et al, 1999). The enzyme is active at low pH and high salt concentrations, which are characteristic of the vacuolar environment. Substrates of CPY are recognized via their C-terminal carboxyl group, which associates with CPY by hydrogen bonding near the S1' binding pocket. The S1' subsite in the substrate binding pocket is large and can recognize both hydrophobic and hydrophilic residues. However, the hydrophobic S1 subsite exhibits greater specificity towards hydrophobic amino acids by virtue of being lined with bulky Tyr residues and having a Leu at the bottom of the binding pocket (Jung et al, 1999).

Carboxypeptidase S (CpS) is a zinc-dependent metallo-carboxypeptidase of the M20 family, which is encoded by *CPS1* in yeast. CpS is synthesized as a ~64 kDa precursor containing a signal anchor sequence spanning amino acids 20 through 40 that is inserted into the ER membrane such that CpS is oriented with its C-terminus facing the lumen (Spormann et al, 1991). The CpS membrane-bound precursor is glycosylated at 2 or 3 N-glycan acceptor sites and

passes through the Golgi before being targeted to the vacuole via the CPY pathway (Lauwers et al, 2009).

Once in the vacuole, CpS is processed by PrB, and is released in its soluble form into the vacuolar lumen. Both 74 kDa and 77 kDa mature forms of CpS are observed, representing CpS modified by 2 or 3 N-linked glycans, respectively. It is interesting to note that the membrane-bound form of CpS also shows proteolytic activity (Spormann et al 1992).

CpS has partially overlapping substrate specificity with CPY, contributing ~60% of the enzymatic activity required to hydrolyze the synthetic dipeptide Cbz-Gly-Leu, where Cbz is the amine protecting group benzyloxycarbonyl (Wolf & Ehmann, 1981). In a *prc1Δ* strain, CpS is required for growth on media where Cbz-Gly-Leu is the sole nitrogen and leucine source (Spormann et al, 1991). Finally, CpS has also been found to play a role in sporulation efficiency. Disrupting PrB activity produces a partial defect in sporulation. However, when PrB activity is disrupted together with CPY and CpS activity, cells lose nearly all capacity for sporulation (Wolf & Ehmann, 1981).

Aminopeptidase I (Ape1) is a zinc-dependent metallo-aminopeptidase of the M18 family, encoded by the *APE1* gene in yeast. Ape1 is synthesized as 61 kDa precursor known as preApe1, which contains a 45 amino acid N-terminal helix-loop-helix domain that is required for vacuolar localization. PreApe1 homooligomerizes in the cytoplasm, forming a dodecamer complex with a molecular mass of 372 kDa (Kim et al, 1997). Unlike other protease precursors, the preApe1 complex is catalytically active. It is thought that preApe1 dodecamers aggregate into large complexes in order to inhibit protease activity (Adachi et al, 2007). This Ape1 complex is recognized by its receptor Atg19, which interacts with Atg11 to tether the preApe1 complex to the PAS (Morales Quinones et al, 2012). The preApe1 complex is encapsulated in a Cvt vesicle

that fuses with the vacuole. Exposure to the acidic pH of the vacuolar lumen results in disassembly of the preApe1 complex to preApe1 dodecamers (Adachi et al, 2007). Finally, PrB cleaves the N-terminal propeptide of the preApe1 subunits in the vacuole to produce 50 kDa mApe1 subunits (Morales Quinones et al, 2012; Schu, 2008).

ApeI, is also known as Lap4 because it was initially characterized as a leucine aminopeptidase in a screen for yeast mutants defective in their ability to hydrolyze the synthetic substrate leucine beta-naphthylamide (Trumbly & Bradley, 1983). Ape1 was also shown to mediate resistance to Cd^{2+}, which is a toxic metal ion that induces oxidative stress in yeast (Adamis et al, 2009). Yeast sequesters Cd^{2+} in the vacuole as a glutathione (GSH) S-conjugate. GSH is a tripeptide made up of Glu, Cys, and Gly residues. The Glu residue is linked to the Cys residue by a gamma peptide bond, where the carboxyl group of the Glu side-chain is bound to the amine group of the Cys peptide backbone. The GSH is recycled from the vacuole by the action of gamma-glutamyltranspeptidase (Ecm38), which hydrolyzes Glu, leaving a Cys-Gly dipeptide which is thought to be further degraded by Ape1 (Adamis et al, 2009). However, more recent work has identified an alternative GSH degradation pathway involving the cytosolic dipeptidase, Dug1, of the M20 family of metalloproteases. This study demonstrated that Ape1 was not required for growth of a *met15Δ* strain on media in which GSH was the only source of sulphur (Ganguli et al, 2007).

There are three other leucine aminopeptidases in yeast: Lap1 is found in the cytosol and periplasm, Lap2 is found in the cytosol and nucleus, and Lap3 is found in the cytosol. Cells in which all four leucine aminopeptidase-encoding genes have been deleted are viable, suggesting these enzymes do not play an essential role or that enzymes such as Dug1 have overlapping activity with the leucine aminopeptidases (Schu, 2008).

Aminopeptidase Y (Ape3), encoded by the gene *APE3*, is a metallo- aminopeptidase of the same M28 family of proteases as Ybr074 (see Chapter 2). Like *YBR074*, the *APE3* locus is found on chromosome II. Global pairwise sequence alignment of Ape3 and Ybr074, shown in Figure 4, reveals 5.7% amino acid sequence identity, while comparison of the M28 protease domains share 21.9% sequence identity (Myers & Miller, 1988).

```
                10        20        30        40        50        60
Ape3   MHFSLKQLAVAAFYATNLGSAYVIPQFFQEAFQQEEPIENYLPQLNDDDSSAVAANIPKP

Ybr074 ------------------------------------------------------------

                70        80        90       100       110       120
Ape3   HIPYFMKPHVESEKLQDKIKVDDLNATAWDLYRLANYSTPDYGHPTRVIGSKGHNKTMEY

Ybr074 ------------------------------------------------------------

               130       140       150       160       170       180
Ape3   ILNVFDDMQDYYDVSLQEFEALSGKIISFNLSDAETGKSFANTTAFALSPPVDGFVGKLV
                                          .  . : ..  .  .     ..
Ybr074 ---------------------------------MKLKSVFRSVLKYRKTNLSLLLLITYS
                                                   10        20
               190       200       210       220       230       240
Ape3   EIPNLGCEEKDYASVVPPRHNEKQIALIERGKCPFGDKSNLAGKFGFTAVVIYDNEPKSK
        :  :   ...  ..  :...:.   . .  .  .:: . ....:     .  .:.
Ybr074 IITLLYIFDHERYKLNLPKEDEHP-EFNDLLETAWGDLQIITASF--HPYTSKENDKVHD
        30        40        50         60        70          80
               250       260       270       280       290       300
Ape3   EGLHGTLGEPTKHTVATVGVPYKVGKKLIANIALNIDYSLYFAMDSYVEFIKTQNIIADT
         :. .:    . . :.:.   .  .... .    .. :  :   : : .....::..
Ybr074 YLLKRVLEITGNSSFASVSDDKESERSILFQQQDPFNESSRF---SRVTYFESSNILVKL
           90       100       110       120          130       140
               310       320       330       340       350
Ape3   KHGDPDNI-VALGAHSDSVEEGPGINDDGSGTISLLNVAKQLTHFKINNKVRFAWWAAEE
       .  .:..  . :.:: :::  : : .::: :..:::   :   . . :  . : .   ::
Ybr074 EGKNPEEEGLLLSAHFDSVPTGYGATDDGMGVVSLLANLKYHIKHRPNRTLIFNFNNNEE
             150       160       170       180       190       200
     360       370       380       390       400       410
Ape3   EGLLGSNFYAYNLTKEENSKIRVFMDYDMMASPNYEYEIYDANNKENPKGSEELKNLYVD
        ::::.. : .. .  . .:  . ..    ..    ..  :... .  . : . . .  .
Ybr074 FGLLGASTY-FDHSWSNLTKYVINLEGTGAGGKAVLFRTSDTSTARIYQQSVKENPFGNS
             210       220       230       240       250       260
     420       430       440       450       460       470
Ape3   YYKAHHLNYTLVPFDGRSDYVGFINNGIPAGGIATGAEKNNVNNGKVLDRCYHQLCDDVS
        :.    .  .    ...::  . .::. .  .:    .:  .. :       ..    .
Ybr074 IYQQGFYSRYV---RSETDYKIYEENGMRGWDVAFYKPRNLYHTIK------DSIQYTSK
               270          280       290       300             310
     480       490       500       510       520       530
Ape3   NLSWDAFITNTKLIAHSVATYADSFEGFPKRETQKHKEVDILNAQQPQFKYRADFLII--
         :  . :. .: :. ...  :. .  :    .      .. . .  : .   ::..
Ybr074 ASLWHMLHTSLQLSAYVASNSLDTADQTPACYFDFIGLKFFVISAKTLFYWNCIFLLVSP
             320       330       340       350       360       370

Ape3   ------------------------------------------------------------

Ybr074 VVAIGLYLISRDRMTWKSYSWLSWTRFPLSLAAGIIVQKLFSNDIIRSNPLTFSRNYFWP
             380       390       400       410       420       430

Ape3   ------------------------------------------------------------

Ybr074 ISAFFTQVIFTSYVLINCSNFFFPCADMKSLSIIELFIILWTILLFTSKLLYSSDYRYTG
             440       450       460       470       480       490
```

```
Ape3   ------------------------------------------------------------

Ybr074 LYPLSIFFLLSTIAAILRLLALALGMRTRKRLGRECRDHHSNYSSHSQIDMERDGQENLE
             500       510       520       530       540       550

Ape3   ------------------------------------------------------------

Ybr074 QPQDQLTSSQDDQASIQDDNVSTTSAGPSHNVDEDHGMDSSSQQHDERVPLLKGSNSMEE
             560       570       580       590       600       610

Ape3   ------------------------------------------------------------

Ybr074 GLSTRENSLKLEYTDYAWIIQFLLIVPIPSFILFNSVDVIMDALNHTVQEGSKATFDVLR
             620       630       640       650       660       670

Ape3   ------------------------------------------------------------

Ybr074 FGMVGSILIALPILPFFYKVNYITISLTALLFLISASKTLLVHPFTNSNPLKVRFSQNID
             680       690       700       710       720       730

Ape3   ------------------------------------------------------------

Ybr074 LSQGNAASVHVLGREGNFLKPMLQDLPSIKYSSTHINCTSVTNGMELCMYDGMQPNLLST
             740       750       760       770       780       790

Ape3   ------------------------------------------------------------

Ybr074 NGNTNISSMVKVHVLHNNRNSTERSPYEPIVAELLLEVKENRACTLTFESRHQAKSPVRE
             800       810       820       830       840       850

Ape3   ------------------------------------------------------------

Ybr074 ITVYQKKNSAPQKANITKTIKSASGINELQLHKLDFDQETYHIGVQWFPKLLTDGNVEDD
             860       870       880       890       900       910

Ape3   ------------------------------------------------------------

Ybr074 KLGTKDELSVSISCYWGEYDSESVVNGTAVRKIPAFDELINYAPLSFSFTNEQKGLVIVK
             920       930       940       950       960       970

Ape3   -----

Ybr074 DAIIL
```

Figure 4: Global sequence alignment of Ape3 and Ybr074.

Global sequence alignment without end-gap penalty was performed using Lalign version 2.2 and default parameters (Huang & Miller, 1991). The M28 domains of Ape3 and Ybr074 are highlighted in yellow according to the Pfam domain boundaries.

Ape3 is synthesized as 60 kDa precursor bearing a 21 amino acid signal sequence directing its translocation into the ER (Nishizawa et al, 1994). The signal sequence is cleaved in the ER, and the Ape3 precursor is targeted to the Golgi, where it is recognized by Vps10 and targets Ape3 to the vacuole (Jorgensen et al, 1999). In the vacuole a 35 amino acid N-terminal propeptide is cleaved by PrB, producing mature Ape3 (Yasuhara et al, 1994). The mature Ape3 protein exists in both a 70 kDa and 75 kDa form that differ in the extent of glycan modification, as Ape3 has eight acceptor sites for N-linked glycans but only 5-7 sites are used (Yasuhara et al, 1994).

Ape3 enzymatic activity was tested by Yasuhara *et al.* using synthetic peptides with a C-terminal 4-methylcoumaryl-7-amide (MCA) protecting group (Yasuhara et al, 1994). Ape3 exhibits a preference for cleaving the basic residue Lys. However, it also cleaves N-terminal Pro, Ala, Leu, Met, Ser, Phe, and Tyr residues (Yasuhara et al, 1994). The catalytic activity of Ape3 is affected by treatment with Co^{2+}. Specifically, the hydrolysis of amino acid-MCAs and dipeptides was enhanced in the presence of Co^{2+}, while that of dipeptidyl-MCAs and larger unmodified peptides was inhibited. Surprisingly, although M28 family metalloproteases commonly bind two catalytic zinc ions, the authors suggested zinc is inhibitory to Ape3 proteolytic activity (Yasuhara et al, 1994).

1.2.2 Membrane-bound vacuolar protease

Dipeptidylaminopeptidase B (Dap2) is serine protease of the S9 family and is encoded by *DAP2* in yeast. Dap2 has a hydrophobic transmembrane segment, positioned 30 amino acids from the N-terminus, that serves both as an ER-targeting sequence and membrane anchor. Dap2 is a type II membrane protein, having a cytosolic N-terminus and lumenal C-terminus, and is initially

synthesiszed as a 93 kDa protein 818 amino acids in length. Dap2 has eight N-glycans and is modified in the ER with anywhere between 5 and 8 N-linked glycan residues, which undergo minimal extension in the Golgi. This results in a final ~120 kDa product. Dap2 is targeted to the vacuole via the secretory pathway and, unlike other vacuolar proteases, is not modified by proteolytic processing in the vacuole (Roberts et al, 1989; Van Den Hazel et al, 1996).

Although the substrate specificity of Dap2 is unknown, its Golgi-resident homolog, dipeptidylaminopeptidase A (Ste13) is known to process repeating -X-Ala- dipeptides from the yeast α factor mating pheromone (Julius et al, 1983). Disrupting Ste13 function prevents maturation of α factor and results in sterile *MATα* cells. This defect in mating was partially restored when Dap2 was overexpressed 10 fold in a *MATα ste13* mutant strain (Julius et al, 1983).

1.3 METALLOPROTEASE FAMILY MEMBERS IN YEAST

Metalloproteases comprise 24% of all proteases with assigned MEROPS identifiers, and 27% of proteases with solved structures listed in the Protein Data Bank (PDB) (Rawlings et al, 2012). The metalloproteases are divided in the MEROPS database into 16 clans, each representing a group of metalloproteases derived from a common ancestor. Each clan is sub-divided into families of protease sharing sequence similarity. The largest clan, MA, is comprised of 37 families. The MH clan, to which Ybr074 belongs, is comparatively small, consisting of only 4 families: M18, M20, M28, and M42 (Rawlings et al, 2012).

The mechanism of catalysis of metalloproteases involves a water molecule that is polarized by interaction with a divalent metal ion. This “activation” of the water molecule

enables it to hydrolyze the substrate peptide bond via nucleophilic attack. Most metalloproteases function using Zn^{2+} as the catalytic ion, but a few proteases make use of Mn^{2+}, Co^{2+}, Ni^{2+}, or Cu^{2+} instead. While 11 of the 16 clans bind a single metal ion, clans MF, MG, MH, MN, and MQ bind two co-catalytic metal ions (Mansfeld, 2007).

The known metalloproteases in *Saccharomyces cerevisiae* are listed in Table 2. A gene ontology (GO) term analysis of these metalloproteases reveals that 36% of them are mitochondrial proteases involved in protein targeting, maturation, and quality control, as well as mitochondrial organization (Gakh et al, 2002). For information on these mitochondrial proteases, the reader is referred to an excellent review by Koppen and Langer (Koppen & Langer, 2007).

Notably, all four proteases involved in maturation of the **a**-factor mating pheromone are classified as metalloproteases (Boyartchuk & Rine, 1998). These are Ste24, an ER-localized transmembrane protein; Ste23, a peripherally associated membrane protein; Rce1, an ER-localized transmembrane protein; and Axl1, a peripherally associated membrane protein that is found at the bud neck, the tip of mating projections, and the cell periphery (Alper et al, 2009; Huh et al, 2003). Some additional substrates have been identified for these proteases. For example, Ste24 is also involved in chitin biosynthesis, although the substrate linking it to this process is not known (Meissner et al, 2010). In addition, mammalian Ste24 plays an important role in the maturation of lamin A, and disruption of this activity results in progeroid disorders in humans (Barrowman & Michaelis, 2009). Ste23 shares sequence similarity with the mammalian insulin-degrading enzyme, and was found to hydrolyze this substrate *in vitro*, as well as the amyloid-beta peptide associated with Alzheimer's disease (Alper et al, 2009). Rce1 is also known to process the precursor form of the signaling molecule Ras GTPase in yeast (Manandhar

et al, 2010). Therefore, the physiological functions of this group of metalloproteases may be more diverse than is currently known.

A group of four metalloproteases in yeast were associated with the vacuolar compartment by GO term analysis. Of these, Ape1, Ape3, and Cps1 have been discussed in Section 1.2, while Ape4 was discussed in Section 1.1.1. It is interesting to note that Ecm14 and Tre1, which are non-catalytic metalloprotease homologs, are also associated with the vacuolar compartment by GO term analysis. Ecm14 has been found to associate with the vacuolar membrane in a proteomic analysis and in a high-throughput screen of GFP-tagged proteins (Huh et al, 2003; Wiederhold et al, 2009). The function of Ecm14 is poorly understood, but it has been found to affect adhesion in *Saccharomyces cerevisiae* by contributing to the shedding of flocculin, Flo11, from the cell surface (Karunanithi et al, 2010). Tre1 and Tre2 together with Bsd2 function as an adaptor complex linking the ubiquitin ligase, Rsp5, to its substrate, Smf1. Rsp5-mediated ubiquitination of the metal transporter, Smf1, which facilitates Smf1 endocytosis and targeting to the vacuole for degradation via the vacuolar protein sorting pathway (Leon & Haguenauer-Tsapis, 2009).

Other metalloproteases include Rpn11 and Rpn8, which are notable members of the 26S proteasome. The proteasome is a 2.5 MDa cytosolic protein complex mediating the degradation of ubiquitinated proteins via the ubiquitin-proteasome system (Finley, 2009). Rpn11 is a subunit of the 19S regulatory subunit of the proteasome that functions as a proteasome substrate deubiquitinating enzyme (Lee et al, 2011). Rpn8 is also a subunit of the 19S regulatory particle and shares sequence similarity with Rpn11 (Glickman et al, 1999).

Table 2: Metalloproteases of the yeast *Saccharomyces cerevisiae*

Clan	Family	MEROPS ID	Gene	SGD Description
MA	M1	M01.006	*APE2*	Role in obtaining leucine from dipeptide substrates; cytosolic and mitochondrial
MA	M1	M01.007	*AAP1*	Arg/Ala aminopeptidase, overproduction stimulates glycogen accumulation; cytoplasm and nucleus
MA	M1	M01.017	*TMA108*	Cytoplasmic protein involved in ribosome biogenesis
MA	M1	M01.034	*LAP2*	Leucyl aminopeptidase yscIV with epoxide hydrolase activity; cytoplasmic and nuclear
MA	M1	non-peptidase homologue	*TAF2*	TFIID subunit (150 kDa), involved in RNA polymerase II transcription initiation; nuclear
MA	M3	M03.003	*PRD1*	Degradation of mitochondrial proteins and of presequence peptides
MA	M3	M03.006	*MIP1*	Mitochondrial DNA polymerase
MA	M41	M41.002	*AFG3*	Mediates degradation of misfolded or unassembled mitochondrial proteins
MA	M41	M41.003	*YTA12*	Mediates degradation of misfolded or unassembled mitochondrial proteins
MA	M41	M41.004	*YTA11*	Degradation of unfolded or misfolded mitochondrial gene products
MA	M48	M48.001	*STE24*	Functions in two steps of a-factor maturation; ER
MA	M48	M48.018	*OMA1*	Involved in turnover of mitochondrial inner membrane-embedded proteins
MA	M49	M49.001	*YOL057W*	Dipeptidyl-peptidase III
MA	M80	M80.001	*WSS1*	Sumoylated protein that localizes to a single spot on the nuclear periphery
MC	M14	non-peptidase homologue	*ECM14*	Required for normal cell wall assembly
ME	M16	M16.003	*MAS1*	Smaller subunit of the mitochondrial processing protease (MPP)
ME	M16	M16.007	*AXL1*	Performs one of two N-terminal cleavages during maturation of a-factor; cell periphery and bud neck
ME	M16	M16.008	*STE23*	N-terminal processing of pro-a-factor to the mature form
ME	M16	M16.013	*CYM1*	Mitochondrial intermembrane space; degrades proteins and presequence peptides
ME	M16	M16.971	*MAS2*	Larger subunit of the mitochondrial processing protease (MPP)
ME	M16	M16.973	*COR1*	Core subunit of the ubiquinol-cytochrome c reductase complex in mitochondria
ME	M16	M16.974	*COR2*	Subunit 2 of the ubiquinol cytochrome-c reductase complex in mitochondria
ME	M16	M16.A04	*YOL098C*	Putative metalloprotease
MG	M24	M24.001	*MAP1*	Removal of N-terminal methionine of nascent polypeptides; cytosolic and nuclear
MG	M24	M24.002	*MAP2*	Removal of N-terminal methionine from nascent polypeptides; cytosolic
MG	M24	M24.026	*ICP55*	Cleaves the N termini of imported mitochondrial proteins after MPP
MG	M24	unassigned	*FRA1*	Cytosolic negative regulator of transcription of the iron regulon
MG	M24	unassigned	*YFR006W*	Putative X-Pro aminopeptidase
MH	M18	M18.001	*APE1*	Vacuolar aminopeptidase I; marker for autophagy and Cvt pathway
MH	M18	M18.002	*APE4*	Cytoplasmic aspartyl aminopeptidase that may also function in the vacuole
MH	M20	M20.002	*CPS1*	Vacuolar carboxypeptidase; induced under low-nitrogen conditions
MH	M20	M20.017	*DUG1*	Cys-Gly di-peptidase; degrades glutathione (GSH) with Dug2 and Dug3
MH	M20	non-peptidase homologue	*DUG2*	Component of glutamine amidotransferase (GATase II); degrades GSH; cytosolic
MH	M28	M28.001	*APE3*	Vacuolar aminopeptidase Y, processed to mature form by Prb1p
MH	M28	M28.006	*YDR415c*	Putative protein of unknown function
MH	M28	M28.974	*YFR018C*	Putative protein of unknown function
MH	M28	M28.A05	*YBR074W*	Putative metalloprotease
MH	M28	non-peptidase homologue	*TRE2*	Regulates ubiquitylation and vacuolar degradation of the metal transporter Smf1
MH	M28	non-peptidase homologue	*VPS70*	Protein of unknown function involved in vacuolar protein sorting
MH	M28	non-peptidase homologue	*TRE1*	Plasma membrane protein, regulates ubiquitylation and vacuolar degradation of the metal transporter Smf1
MJ	M38	non-peptidase homologue	*DAL1*	Converts allantoin to allantoate in the first step of allantoin degradation
MK	M22	M22.005	*QRI7*	Essential for modification of mitochondrial tRNAs that decode ANN codons
MK	M22	unassigned	*KAE1*	ATPase of HSP70/DnaK family; involved in modification of mitochondrial tRNAs
MP	M67	M67.001	*RPN11*	Metalloprotease subunit of the 19S regulatory particle of the 26S proteasome lid
MP	M67	M67.973	*RPN8*	Essential, non-ATPase regulatory subunit of the 26S proteasome
MP	M67	unassigned	*RRI1*	Catalytic subunit of the COP9 signalosome (CSN) complex; cytosolic
M-	M79	M79.001	*RCE1*	CAAX prenyl protease; maturation of Ras and the a-factor mating pheromone

1.4 QUESTIONS FOR FUTURE RESEARCH ON YEAST VACUOLAR FUNCTION

Given the diverse functions associated with the vacuole, issues that need to be addressed in future research into the mechanisms regulating this specialized organelle are very broad. This section highlights only a few of the many important questions requiring attention in this field.

While the substrate specificity of many of the vacuolar proteases has been defined using synthetic substrates, not much information is available in the context of endogenous substrates of vacuolar proteases. The current view is that vacuolar proteases are generally indiscriminant enzymes because the need for substrate specificity is obviated by the presence of the vacuolar membrane, which acts as a physical barrier separating these general proteases from the rest of the cell. However, this does not explain why so many different protease (eight, including Ybr074) are associated with the vacuole. Do certain proteases have dominant roles in response to certain physiological conditions requiring vacuole-dependent degradation? For example, are different vacuolar proteases more active or more abundant during sporulation than under conditions triggering apoptosis? Furthermore, are there functional characteristics that differentiate soluble vacuolar proteases from membrane-bound vacuolar proteases? Perhaps membrane-bound proteases associate more readily with membrane-bound substrates.

In the study of autophagy, the source of autophagosome membranes still represents an outstanding question. Although many sources have been cited, including the ER, mitochondria and plasma membrane, it is not clear whether different lipid donors contribute structural or

functional differences to the autophagosomes they generate (Weidberg et al, 2011). Could the composition of autophagosomes affect cargo selectivity?

1.5 DISSERTATION GOALS AND OVERVIEW

Ybr074 is an uncharacterized, putative metalloprotease of the M28 family in yeast. Ybr074 has a conserved protease domain related to a putative mammalian metalloprotease known as FXNA, or ER Metalloprotease 1 (ERMP1). Both Ybr074 and FXNA are predicted to be multi-pass transmembrane proteins, with Ybr074 having nine predicted transmembrane segments and FXNA having eight predicted transmembrane segements (TopPredII, upper cut-off) (Claros & von Heijne, 1994). Knock-down of FXNA in rat ovaries, achieved using shRNA delivered using a lentiviral vector, resulted in a defect in ovarian development. More specifically, the organization of somatic granulosa cells around the oocyte was impaired upon FXNA knockdown, presumably disrupting intercellular contacts required for the development of the ovarian follicle (Garcia-Rudaz et al, 2007).

FXNA is expressed in other rat tissues, including the kidneys, the adrenal gland, and various areas of the brain (Garcia-Rudaz et al, 2007). Therefore, FXNA may have more extensive, and as yet, undiscovered functions in these tissues. Since the protease domain of Ybr074 shares 32.5% sequence identity with that of FXNA, I hoped that using yeast as a model organism would illuminate the functions of both Ybr074 and FXNA. Nevertheless, the sequence similarity between FXNA and Ybr074 does not extend beyond the protease domain (Figure 5). Therefore, the biological functions and endogenous substrates of Ybr074 and FXNA may well differ.

Even if Ybr074 does not inform directly on the function of FXNA, understanding its biological function has intrinsic value to the field of yeast biology. The role of Ybr074 in the context of the yeast proteome has the potential to inform on pathways connecting vacuolar function and cellular protein homeostasis. These more general biological pathways may be analogous in higher eukaryotes. Furthermore, an understanding of the influence of Ybr074 on the maintenance of the cell wall, described in Chapter 4, may contribute novel targets against pathological yeast associated with human disease (Santamaria et al, 2011). For example, the pathogenic fungus *Candida albicans* is the fourth most common cause of bloodstream infection in cancer patients. A class of antifungal drugs, known as the echinocandins, is used to combat this type of fungal infection. Echinocandins, such as caspofungin, function by inhibiting glucan synthesis in the cell wall of *C. albicans* (Kofla & Ruhnke, 2011). The importance of cell wall glucans in maintaining cell wall integrity will be discussed further in Chapter 4. Furthermore, metalloproteases, such as Ybr074, have important industrial applications. For example, metalloproteases are used to improve beer filtration and reduce calorie content in the brewing industry. Metalloproteases have been used to remove protein coatings to restore old documents and artworks. Metalloproteases are also widely used in the food industry to add flavor-enhancing peptides (Mansfeld, 2007).

Finally, metalloproteases are important pharmaceutical targets. For example, matrix metalloproteases (MMPs) are secreted proteins that normally remodel the extracellular matrix (ECM) to facilitate important physiological functions such as cellular proliferation, cellular migration, wound healing, growth, and development (Klein & Bischoff, 2011). However, MMPs are also linked to a number of pathologies in humans, including cancer, lung disease, vascular disease, inflammation, and neurodegenerative disease (Sbardella et al, 2012). Therefore,

understanding the function of the putative metalloprotease Ybr074, identifying its substrates and its interaction partners is an inherently valuable endeavor.

In the following chapters, I describe the first characterization of Ybr074, such as its topology and sub-cellular localization (Chapter 2). In Chapter 3, I elaborate on genetic techniques used in an attempt to identify the biological function of Ybr074. This chapter also describes proteomic techniques used in an attempt to isolate endogenous substrates of Ybr074. I explore a potential link between Ybr074 and maintenance of the cell wall in Chapter 4. Chapter 5 will conclude with a discussion of the findings presented in this dissertation, and future directions for further characterization of Ybr074.

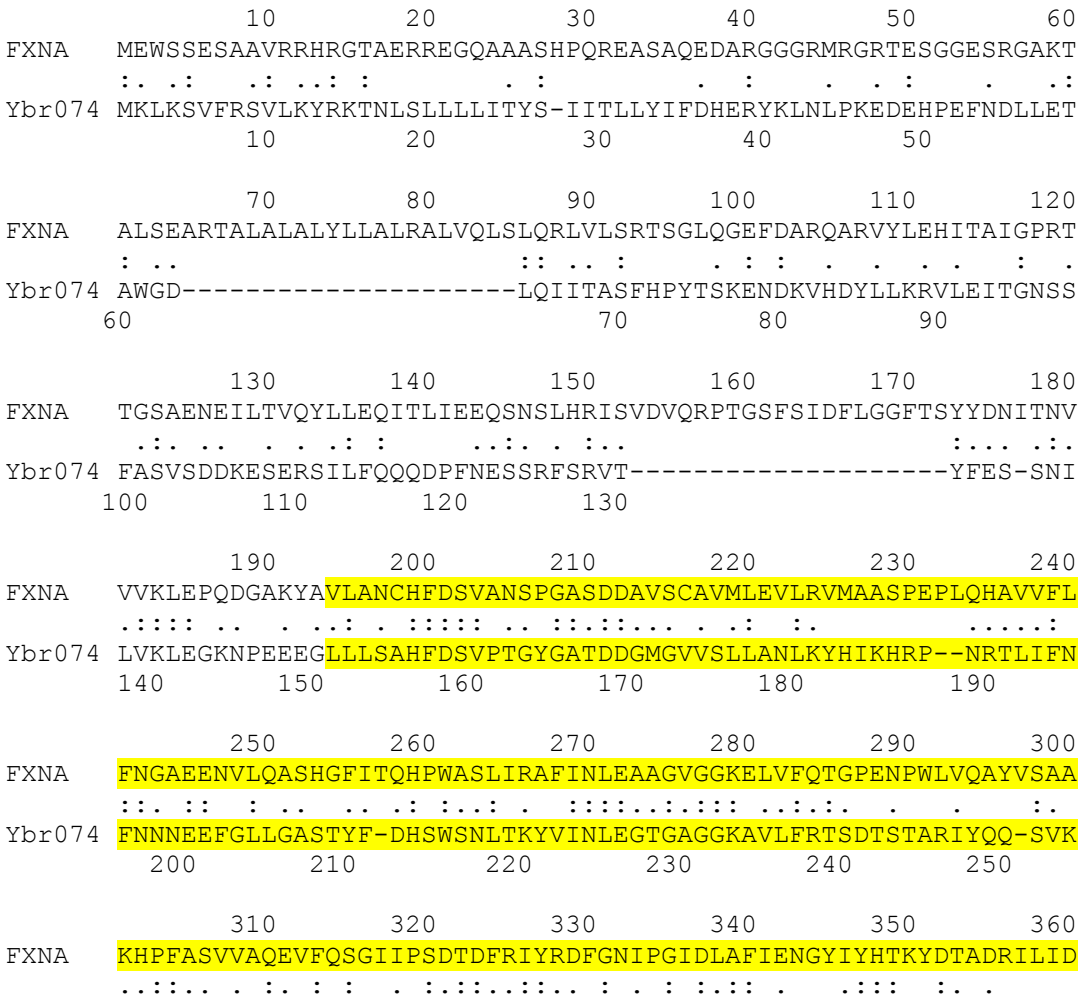

```
Ybr074 ENPFGNSIYQQGFYSRYVRSETDYKIYEENG-MRGWDVAFYKPRNLYHTIKDSIQYTSKA
           260       270       280       290       300       310

               370       380       390       400       410
FXNA   SIQRAGDNILAVLKYLATSDMLASSSE---YRHGSMVFFDVLGLLVIAYPSRVGSIINYM
       :. .   . : .  :.:.... ....    :     . : :..  .. : . .  ... .
Ybr074 SLWHMLHTSLQLSAYVASNSLDTADQTPACYFDFIGLKFFVISAKTLFYWNCIFLLVSPV
           320       330       340       350       360       370

       420       430       440       450       460
FXNA   VVMAVVLYLGRKLLRPNHSNSNYVRDFLC-GLGITFISWFTSLVTVL------------I
       :.... :    ..   ..:  ...:  :  . ::   . :.. .               :
Ybr074 VAIGLYLISRDRMTWKSYSWLSWTRFPLSLAAGIIVQKLFSNDIIRSNPLTFSRNYFWPI
           380       390       400       410       420       430

          470          480       490       500          510
FXNA   IAVFVSLIGQS---LSWYNYFYIAVCLYGTATVAKIILIHTL----AKRFYYVNA--SDL
        : :...:  :   ..  :.:.  . . . . .  .:.. :.    .: .:  .   . :
Ybr074 SAFFTQVIFTSYVLINCSNFFFPCADMKSLSIIELFIILWTILLFTSKLLYSSDYRYTGL
           440       450       460       470       480       490

         520       530                   540       550
FXNA   YLGELFFDTSLFVHCGFLVALT------------AQGFCSAFMSAVWVAFPL--------
       :   .::  : ..    :.::.              .   : . :   . .
Ybr074 YPLSIFFLLSTIAAILRLLALALGMRTRKRLGRECRDHHSNYSSHSQIDMERDGQENLEQ
           500       510       520       530       540       550

          560                 570       580                 590
FXNA   -LTKLCVYKD---------FKKHGAKGRFIALYLLGM---------FIPYLYGLYLIWAV
          .:   .:           .  .:     .    ::          .: : :   .
Ybr074 PQDQLTSSQDDQASIQDDNVSTTSAGPSHNVDEDHGMDSSSQQHDERVPLLKGSNSMEEG
           560       570       580       590       600       610

        600       610       620       630       640            650
FXNA   FEMFTPILGRSGSEIPPDVVLASILAVCVMILSSYFITFIYLVNST-----KKTILTLIL
       .      :    ..    . .  :. .  .:: .   ...  .: :     : :. .: .
Ybr074 LSTRENSLKLEYTDYAWIIQFLLIVPIPSFILFNSVDVIMDALNHTVQEGSKATFDVLRF
           620       630       640       650       660       670

             660       670        680            690       700
FXNA   VCAVTFLLVCSGAFFPYSSNPDSPK-PKRVFLQHVSRT-----FHNLEGSVVKRDSGIWI
         . ..:..     : :. :  . .    .::  .:.:     : : .   :. ...: .
Ybr074 GMVGSILIALPILPFFYKVNYITISLTALLFLISASKTLLVHPFTNSNPLKVRFSQNIDL
           680       690       700       710       720       730

                710       720        730          740       750
FXNA   N----------GFDYTGMSHVTPHIPEIN-DTIRAHCE---ENAPLCGFPWYLPVHFLIR
       .          : . . .. .   .: :. .. . .:    ..  :: .  . :   :.
Ybr074 SQGNAASVHVLGREGNFLKPMLQDLPSIKYSSTHINCTSVTNGMELCMYDGMQPN--LLS
           740       750       760       770       780          790

             760       770       780                       790
FXNA   KNWYLPAPEISPRNPAHFRLVSKEKMPWDSI-------------KLTFEAT--GPSHMS
        :      .   .  :    : :. :.. :               ::::.   . : .
Ybr074 TNGNTNISSMVKVHVLHNNRNSTERSPYEPIVAELLLEVKENRACTLTFESRHQAKSPVR
              800       810       820       830       840       850
```

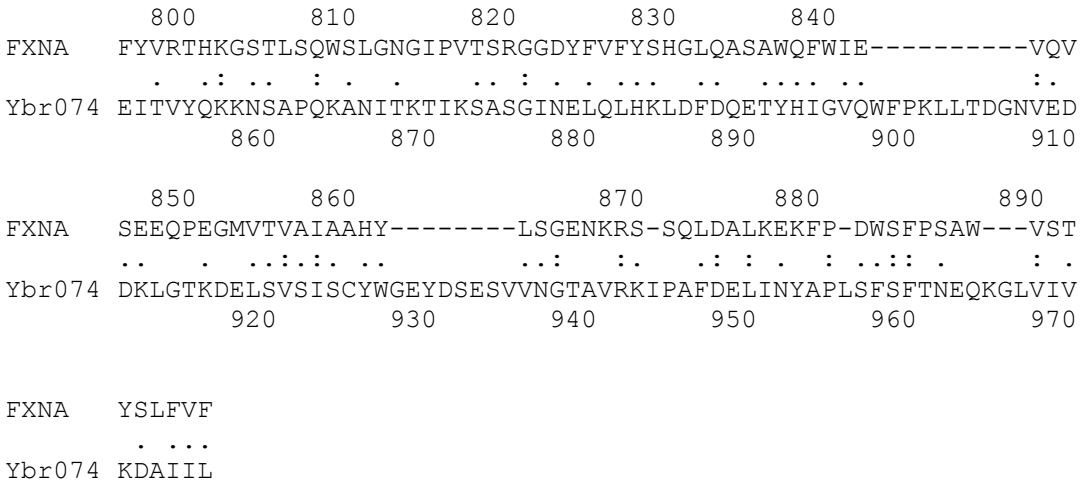

Figure 5: Global sequence alignment of FXNA and Ybr074.

Global sequence alignment was performed using Lalign version 2.2 and default parameters (Huang & Miller, 1991). The M28 domains of FXNA and Ybr074 are highlighted in yellow according to the Pfam domain boundaries.

2.0 CHARACTERIZATION AND LOCALIZATION OF YBR074

2.1 INTRODUCTION

Saccharomyces cerevisiae was the first eukaryote to have its entire genome sequenced (Goffeau et al, 1996). Since then it has served as a model organism for higher eukaryotes and as a tool in the on-going efforts to surmount the challenge facing the "post-genomic era": to characterize and annotate the information gleaned from genome sequencing. In 2007, soon after this thesis project began, the biological function of approximately 21% of the *Saccharomyces cerevisiae* genome (>1000 genes) remained uncharacterized, including that of 11 putative proteases (Pena-Castillo & Hughes, 2007). It is likely that many of these uncharacterized genes do not have strong phenotypes when disrupted, resulting in their under-representation in the research literature. This may be due to functional redundancy, or because of the limited number of conditions testable in a laboratory environment (Pena-Castillo & Hughes, 2007). In order to develop hypotheses about the function of these genes, numerous computational analyses, based on nucleotide or amino acid sequence, are available (Friedberg, 2006). Among these computational methods, sequence pattern searching and structure-based similarity searches were used in this study to predict biological functions of Ybr074. This chapter will focus on the computational predictions that led to testable hypotheses.

Based on the presence of several distinct hydrophobic amino acid motifs, Ybr074 was predicted and demonstrated to be a transmembrane protein. Local sequence similarity comparisons to proteins of known function identified a conserved domain belonging to the M28 family of metalloproteases. Computational predictions of Ybr074's sub-cellular localization suggested that this protein might be ER-localized. Finally, topological predictions placed the protease domain of Ybr074 on the lumenal side of the ER. Although the results detailed below do show that Ybr074 is a transmembrane protein and is modified by N-linked glycans in the ER, it resides in the vacuolar membrane, contrary to what was predicted, with its protease domain facing the vacuolar lumen.

2.2 MATERIALS AND METHODS

2.2.1 Computational Methods

The amino acid sequence of Ybr074 was analyzed using the default parameters of the Position-Specific Iterative Basic Local Alignment Search Tool (PSI-BLAST) to identify proteins in the non-redundant protein sequences database, which shared local sequence similarity with Ybr074 (Altschul et al, 1997; Altschul et al, 2005). The European Molecular Biology Library-European Bioinformatics Institute (EMBL-EBI), InterPro Scan sequence search tool, and the PANTHER Classification System version 7.2 were also used to examine proteins related to Ybr074 using default parameters (Mi et al, 2010).

The M28 protease domain of Ybr074, and its putative catalytic and zinc-binding residues, were identified using the National Center for Biotechnology Information (NCBI) Conserved

Domain Database (CDD) (Marchler-Bauer et al, 2011). The M28 protease domain boundaries of Ybr074 were analyzed using Pfam version 26.0 (Punta et al, 2012).

The presence and position of transmembrane segments, as well as the topology of Ybr074 were predicted using ConPredII (Arai et al, 2004), TopPred 2 (von Heijne, 1992), Membrane Protein Explorer, MPEx (Snider et al, 2009), and PSORT II under default settings (Nakai & Horton, 1999). N-linked glycosylation sites were predicted using the NetNGlyc 1.0 server, under default settings, from the Eukaryotic Linear Motif (ELM) resource for functional sites in proteins (Blom et al, 2004). Sub-cellular localization of Ybr074 was predicted using PSORT, PSORT II, and WoLF PSORT under default settings (Horton et al, 2007). Structural homology predictions for the M28 protease domain and C-terminal domain of Ybr074 were analyzed using Protein Homology/analogY Recognition Engine 2 (PHYRE2) under default settings (Kelley & Sternberg, 2009).

2.2.2 Strains, plasmids, yeast growth conditions, and molecular techniques

Strains used in this study are listed in Table 3. Standard growth conditions and molecular techniques were used, unless otherwise indicated (Adams et al, 1998). A chromosomally-integrated P_{GAL1}-*GFP-YBR074* strain was generated using the integration vector pFA6a-His3MX6-P_{GAL1}-GFP, as described (Longtine et al, 1998). Briefly, the His3MX6-P_{GAL1}-GFP cassette was amplified using the following primers, forward primer: AAA TTA TCT ACA AGG AAA TAA ATT GAT AGG TAA AGT TAA AGA ATC ACG GCG AAT TCG AGC TCG TTT AAA C; reverse primer: TTT GTT TTC CGG TAC TTT AGA ACT GAT CTG AAT ACA CTT TTT AAT TTC ATT TTG TAT AGT TCA TCC ATG C, and were transformed into the BY4742 strain. Transformed cells were selected on synthetic medium lacking histidine. Integration of the

His3MX6-P_{GAL1}-GFP cassette was confirmed by amplification of a region upstream of *YBR074* and internal to the His3MX6-P_{GAL1}-GFP cassette (forward primer: CAA TGA CGC CAA ATA TGG ACA CT; reverse primer: TTT GTA TAG TTC ATC CAT GC) from purified genomic DNA (Adams et al, 1998).

Plasmids used in this study are listed in Table 4. To generate an N-terminally HA-tagged *YBR074* construct, *YBR074* was PCR amplified using vector pGP564_1_b11 from the yeast overexpression plasmid library (Jones et al, 2008) (forward primer: AAT CAC GGA TCC AAA TTA AAA AGT GTA TTC AGA TCA GTT CTA AAG; reverse primer: AGA ACT CGA GTT ATA AAA TTA TAG CAT CCT TGA CAA TAA CTA ATC CTT TCT G), and ligated into the BamHI/XhoI sites of yeast expression vector pKN16 (Table 4). The $P_{GAL1/10}$ promoter of the resulting plasmid was removed using SacI/SpeI and replaced with the endogenous promoter of *YBR074* (forward primer: ATG GAG AGC TCG ACA AGT GCG CTG GAT TTA CAA AAG AAA ATG AAT GA; reverse primer: TCA TAC TAG TGC CGT GAT TCT TTA ACT TTA CCT ATC AAT TTA TTT CCT). This construct was verified by DNA sequence analysis (IDT, Coralville, IA).

To generate the *YBR074*-M28HA expression constructs a single HA tag was inserted at Pro45, within the M28 metalloprotease domain, using a two-stage PCR method (Wang & Malcolm, 1999). Secondary structure prediction programs, SSPro version 4.5 (Cheng et al, 2005) and PSIPRED version 3.0 (Buchan et al, 2010), were used to identify a region for insertion of the HA tag without disrupting secondary structures. Specifically, the tag was inserted following residue Leu55, in a predicted coil region between transmembrane segment 1 and the first alpha helix predicted to compose the M28 protease domain (Pollastri et al, 2002). Briefly, the endogenous promoter and coding sequence of *YBR074* were PCR amplified as two separate

fragments, PCR1 (forward primer A: ATG GAG AGC TCG ACA AGT GCG CTG GAT TTA CAA AAG AAA ATG AAT GA; reverse primer B: TGC ATA GTC CGG GAC GTC ATA CGG ATA TGG TAG ATT GAG TTT ATA ACG TTC ATG ATC AAA GAT ATA G) and PCR2 (forward primer C: TAT CCG TAT GAC GTC CCG GAC TAT GCA AAA GAG GAT GAG CAC CCT GAA TTC AAT GAC; reverse primer D: AGA ACT CGA GTT ATA AAA TTA TAG CAT CCT TGA CAA TAA CTA ATC CTT TCT G). A third reaction, PCR3 (forward primer A, reverse primer D) was carried out in which a mixture of 5% PCR1 and 5% PCR2 (vol/vol) was used as a template for amplification. The resulting P_{ENDG}-*YBR074*-M28HA cassette was inserted into pRS316 or pRS426 at the SacI/XhoI sites, and the constructs were verified by DNA sequence analysis, as above.

Sensitivity to killer toxin was tested based on previously described protocols (Boone et al, 1990; Santos et al, 2000). In brief, the killer toxin secreting strain 1368, described in Table 3, was grown to saturation overnight in Yeast Peptone Dextrose (YPD), pH 4.5, at room temperature. The growth medium was separated from cells by centrifugation at ~1000 *g* for 3 min, and filtered using a 0.22 μm diameter filter (Millipore, Franklin Lakes, NJ). The filtered medium was concentrated 200-fold using an ultrafiltration Amicon Ultra-15 unit with a 10 KDa molecular mass cut-off (Millipore, Billerica, MA). Test strains were grown in YPD to log phase, and 1 OD_{600} cell equivalents were harvested and re-suspended in 100 μL Sterile Double Distilled Water (SDDW). The 2-fold concentrated YPD, pH 4.5, medium was incubated in a 37°C water bath before being added to an equal volume of autoclaved 4% Bacto agar, supplemented with 30 μg/mL methylene blue. Once equilibrated to approximately 37°C, the molten medium was seeded with the test strain, and the medium was poured and allowed to solidify. A sterile filter

disc spotted with 10 μL of the concentrated killer toxin medium was added to seeded plates and the plates were incubated for 4 days at room temperature.

Sensitivity to killer toxin was measured as the diameter of the halo using ImageJ software (Schneider et al, 2012). The diameter of each halo was taken as the average of four measurements. Each strain was tested in three individual replicates and the average halo diameter and standard error were calculated using Microsoft Excel 2010.

Table 3: Yeast strains used in this study.

Strain	Genotype	Source or reference
BY4742	MAT α *his3Δ1 leu2Δ0 lys2Δ0 ura3Δ0*	Brachmann C.B. *et al.* 1998
OY209	MAT α *cdc48-2::NATMX can1Δ::STE2pr-Sp_his5 lyp1Δ::STE3pr-LEU2* his3Δ1 leu2Δ0 ura3Δ0	C. Boone, University of Toronto, Toronto, Canada
kre1Δ	MAT α *kre1::KANMX his3Δ1 leu2Δ0 lys2Δ0 ura3Δ0*	Open Biosystems Yeast Knockout Collection
slt2Δ	MAT α *slt2::KANMX his3Δ1 leu2Δ0 lys2Δ0 ura3Δ0*	Open Biosystems Yeast Knockout Collection
cdc48-3	MAT α *his3Δ1 leu2Δ0 lys2Δ0 ura3Δ0 cdc48-3*	J.R. Tran, University of Pittsburgh, Pittsburgh, PA
CDC48 R155H	MAT α *his3Δ1 leu2Δ0 lys2Δ0 ura3Δ0 cdc48::KANMX* pRS315-*CDC48-myc*-R155H	J.R. Tran, University of Pittsburgh, Pittsburgh, PA
CDC48 A232E	MAT α *his3Δ1 leu2Δ0 lys2Δ0 ura3Δ0 cdc48::KANMX* pRS315-*CDC48-myc*-A232E	J.R. Tran, University of Pittsburgh, Pittsburgh, PA
KH01 (also referred to as wild type)	MAT α *his3Δ1 leu2Δ0 LYS2 MET15 ura3Δ0*	this study
KH02 (also referred to as *ybr074Δ*)	MAT α *ybr074::KANMX his3Δ1 leu2Δ0 LYS2 ura3Δ0*	this study
KH03 (also referred to as *cdc48-2*)	MAT α *cdc48-2::NATMX his3Δ1 leu2Δ0 LYS2 ura3Δ0*	this study
KH04 (also referred to as *cdc48-2 ybr074*Δ)	MAT α *cdc48-2::NATMX ybr074::KANMX his3Δ1 leu2Δ0 LYS2 ura3Δ0*	this study
KH05 (also referred to as GFP-Ybr074)	MAT α *his3Δ1 leu2Δ0 lys2Δ0 ura3Δ0 ybr074::PGAL1-GFP-YBR074*	this study
1368	MAT α his[KIL-b] L-A-HNBM1	R. Wickner, NIH, Bethesda, MD
Y825	MAT a *ura3-52 leu2Δ0*	Jin, R. *et al.* 2008
Y825 *ybr074*Δ	MAT a *ybr074::KANMX ura3-52 leu2Δ0*	this study
*pep4*Δ	MAT α *pep4::KANMX his3Δ1 leu2Δ0 lys2Δ0 ura3Δ0*	Open Biosystems Yeast Knockout Collection
*pdr5*Δ	MAT α *pdr5::KANMX his3Δ1 leu2Δ0 lys2Δ0 ura3Δ0*	Open Biosystems Yeast Knockout Collection

Table 4: Plasmids used in this study.

Plasmid Name	Description	Selectable Marker	Source or reference
pGP564_1_b11	2µ overexpression chromosome II: 378129-393468, including *YBR074*	*LEU2*	Jones G.M. *et al.* 2008
pFA6a-*His3MX6-PGAL1-GFP*	P_{GAL1}-GFP integration plasmid	*HIS3MX6*	Longtine, M.S. *et al.* 1998
pRS400	*KANMX* integration vector	N/A	Brachmann, C.B. *et al.* 1998
pFA6a-*NAT-MX6*	*NATMX* integration vector	N/A	Vembar, S.S. *et al.* 2010
pKN16	pRS316-$P_{GAL1/10}$ expression vector	*URA3*	K. Nakatsukasa, Nagoya University, Nagoya, Japan
pRS316-*3HA-YBR074*	Ybr074 expression	*URA3*	This study
pRS426-*3HA-YBR074*	Ybr074 expression	*URA3*	This study
pRS316-*YBR074-M28HA*	Ybr074 expression	*URA3*	This study
pRS426-*YBR074-M28HA*	Ybr074 expression	*URA3*	This study
pRS316-*YBR074-HA*	Ybr074 expression	*URA3*	This study
pRS426-*YBR074-HA*	Ybr074 expression	*URA3*	This study
pMF616	Gas1p* integration plasmid	*URA3*	Fujita M. *et al.* 2006
pRS316-*3HA-Gas1p**	Gas1p* expression plasmid	*URA3*	This study
pRS316-*CPY*-3HA*	CPY* expression plasmid	*URA3*	Bhamidipati A. *et al.* 2005
CPY*-DHFR	CPY*-DHFR-3HA expression vector	*URA3*	Bhamidipati, A. et al. 2005
CPY*-DHFR(Pro)	CPY*-DHFR(Pro)-3HA expression vector with DHFR mutations A29P, W30P, F31P	*URA3*	Bhamidipati, A. et al. 2005
pSM1152	CFTR-3HA overexpression vector	*URA3*	Zhang, Y. et al. 2002
pSM1911	Ste6p*-HA overexpression vector	*URA3*	Huyer, G. et al. 2004
PGAL-3HA-RHR2	Rhr2 overexpression vector	*URA3*	This study

2.2.3 Protein localization

Immunofluorescence assays were performed, as described previously, with minor modifications (Adams et al, 1998). Spheroplasted cells were incubated in poly-lysine coated wells for 10 min at room temperature. Cells were then washed three times with 30 μL of sterile filtered blocking solution (PBS, pH 7.4, 0.5% BSA, 0.5% ovalbumin, 0.01% fish skin gelatin; Sigma, St. Louis, MO) supplemented with 0.1% Triton X-100 (Sigma, St. Louis, MO). Cells were then incubated in blocking solution, including Triton X-100, for 30 min in a humidified chamber, followed by an overnight incubation with 1:500 mouse anti-HA (Roche, Indianapolis, IN) and 1:500 rabbit anti-Kar2 (Brodsky et al, 1993), or 1:100 rabbit anti-HA (Cell Signaling Technology, Beverly, MA) and 1:750 mouse anti-Vph1 (Invitrogen/Molecular Probes, Carlsbad, CA) overnight at 4°C in a humidified chamber. The next day, cells were washed four times with 30 μL blocking solution, and incubated with 1/250 Alexa Fluor 488 goat anti-mouse IgG and 1:250 Alexa Fluor 568 goat anti-rabbit IgG (Invitrogen, Moecular Probes, Eugene OR). Images were visualized using a Leica TCS SP5 (Leica microsystems, Buffalo Grove, IL).

Live cell imaging of GFP-Ybr074 was examined in the BY4742 strain with chromosomally-integrated GFP-Ybr074 under the control of a galactose promoter, and selected using the HIS3MX gene as described above. Cells were grown in medium lacking histidine and supplemented with 2% galactose to induce expression, or 2% raffinose as a negative control. Cells were induced overnight at 30°C and harvested at an OD_{600} of ~0.8. Approximately 0.4 OD_{600} cell equivalents were harvested by centrifugation at 13,000 *g* for 30 sec and washed in 1mL PBS, pH 7.4. Cells were re-suspended in PBS, pH 7.4, to a concentration of 4 OD_{600}/mL

and 5 μL were mounted on a glass slide for visualization. Cells were visualized using the Olympus BX60 fluorescence microscope and QED InVivo software. No expression of GFP-Ybr074 was observed when cells were grown in media supplemented with raffinose instead of galactose (data not shown).

Cell fractionation by sucrose density centrifugation was performed as described (Hong et al 1996). The wild type strain, BY4742, expressing HA-tagged YBR074 from its endogenous promoter on a 2μ plasmid was grown in 100 mL selective media to OD_{600} of 0.6-0.8. Harvested cells were re-suspended in 400 μL 10% EDTA buffer (10 mM Tris-HCl, pH 7.6, 10 mM EDTA) or 10% Mg^{2+} buffer (10 mM Tris-HCl, pH 7.6, 2 mM MgCl2) including protease inhibitors (PMSF, Leupeptin, Pepstatin A). Cells were lysed by agitation on a Vortex mixer with glass beads for four 30 sec pulses followed by 30 sec on ice. The homogenate was cleared of unbroken cells at 2000 rpm for 2 min at 4°C using a Microfuge 22R centrifuge (Beckman Coulter, Palo Alto, CA). A step gradient was made using 2 mL steps of 70%, 60%, 50%, and 40% sucrose followed by 1.5 mL steps of 30% and 20% sucrose in EDTA or Mg^{2+} buffer. The gradient was loaded with 400 μL of cleared cell homogenate and centrifuged at 139,000 *g* (28,500 rpm) for 18.5 h at 4°C in an SW41 Ti rotor using an L8-70M Ultracentrifuge (Beckman Coulter, Brea, CA). Fractions were collected by pipetting from the top of the gradient in 500 μL increments, and total protein was precipitated in 10% trichloroacetic acid (TCA) for 15 min on ice (Fischer Scientific, Fair Lawn, NJ). Precipitated proteins were pelleted, and were washed in acetone, spun down again, and re-suspended in 30 μL TCA buffer (80mM Tris-HCl, pH 8, 8mM EDTA, 120 mM DTT, 3.5% SDS, 10% glycerol, 0.08% Tris base, 0.01% Bromophenol Blue). Samples were immediately loaded onto a 10% SDS-polyacrylamide gel, and after electrophoresis proteins were transferred to nitrocellulose. Blots were incubated using the following primary antibodies:

1:5000 mouse anti-HA (Roche, Indianapolis, IN), 1:3000 rabbit anti-Pma1 (Dr. C. Slayman, Yale School of Medicine, New Haven, CT), 1:3000 rabbit anti-Anp1 (Dr. S. Munro, Medical Research Council Laboratory of Molecular Biology, Cambridge, UK), 1:5000 rabbit anti-Sec61 (Stirling et al, 1992). The bound antibodies were visualized using Super Signal West Femto kit (Thermo Scientific, Rockford, IL) on a Kodak 440CF Image Station (Eastman Kodak, Rochester, NY).

Protease protection assays were performed using microsomes derived from wild type yeast expressing HA-tagged *YBR074* from its endogenous promoter on a *CEN* plasmid. Microsomes were isolated using the "medium" preparation method (Nakatsukasa & Brodsky, 2010). Reactions were prepared in B88 (20mM HEPES, pH 6.8, 150 mM potassium acetate, 5 mM magnesium acetate, 250 mM sorbitol) using 100-500 μg of total microsomal protein, and were incubated in the presence or absence of 100 μg/mL proteinase K (Sigma, St. Louis, MO) and 1% Triton X-100. Reactions were incubated on ice and 25 μL fractions were taken at 0, 10, 30, and 60 min and precipitated in 10% TCA and processed as described above.

The presence of N-linked glycans on Ybr074 was tested by digestion with Endoglycosidase H (Roche, Indianapolis, IN). Microsomes were prepared as described above from a BY4742 strain expressing HA-tagged *YBR074* from its endogenous promoter on a *CEN* plasmid. Approximately 100 μg of protein were incubated in 50mM citrate buffer, pH 5.5, 1 mM PMSF, 1 μg/mL leupeptin, and 0.5 μg/mL pepstatin A (Sigma, St. Louis, MO) in the presence or absence of 0.005 units of endoglycosidase H overnight at 4°C. Digested protein was resolved by 10% SDS-PAGE and proteins were visualized by western blot analysis using 1:5000 HRP-conjugated mouse anti-HA antibody (Roche, Indianapolis, IN) as described above. The molecular mass of the resulting protein bands was determined by Rf analysis.

Carbonate extraction was performed using microscomes prepared as described above from a BY4742 strain expressing HA-tagged *YBR074* from its endogenous promoter on a *CEN* plasmid (Parlati et al, 1995). Approximately 200 μg of microsomal protein was re-suspended in 1 mL B88 or 0.1 M Na_2CO_3, pH 11.5, in the presence of protease inhibitors (PMSF, leupeptin, pepstatin A; Sigma, St. Louis, MO) at 4°C and incubated for 30 min. Soluble protein was separated from membrane bound protein by ultracentrifugation at 13,500 *g* (50,000 rpm) for 1 h at 4°C in a Sorvall LC M120-EX Micro Ultracentrifuge using a Sorvall S100AT5 fixed angle rotor. The supernatant was isolated and processed by TCA precipitation as described above. The pellet was washed with B88 containing protease inhibitors, and spun again at 198,000 *g* (60,000 rpm) for 10 min at 4°C. The supernatant from the second spin was removed and discarded, and the pellet was re-suspended in sample buffer. Samples were resolved by 10% SDS-PAGE and proteins were visualized by western blot analysis as described above.

2.2.4 Cycloheximide chase analysis of Ybr074 stability

To examine dependence on the 26S proteasome for degradation of tagged Ybr074 constructs, cells expressing tagged Ybr074 were grown to logarithmic phase (OD_{600} = 0.4-0.8) and treated with 100 μM MG132 (Peptide institute, Inc., Osaka, Japan) for 30 min at 30°C before addition of 250 μg/mL cycloheximide (Sigma, St. Louis, MO). At the indicated times, 1 mL from each culture was transferred to a tube containing sodium azide at a final concentration of 20 mM. Cells were harvested by centrifugation at 18,000 *g* for 30 sec at 4°C and then washed with 1mL of ice cold 10 mM sodium azide to block respiration. Cells were centrifuged as above, the supernatant was aspirated, and the cell pellets were flash frozen in liquid nitrogen before being

processed the next day by TCA precipitation, according to an established protocol (Nakatsukasa et al, 2008).

2.3 RESULTS

When the genome of *Saccharomyces cerevisiae* was first sequenced, *YBR074W* and *YBR075W* were annotated as two separate open reading frames (ORFs) (Goffeau et al, 1996). When the genome of the closely related filamentous fungus *Ashbya gossypii* was sequenced years later, a comparison of these two genomes resulted in the fusion of *YBR074W* and *YBR075W*, and this fused ORF was re-named *YBR074W* (Figure 6) (Brachat et al, 2003; Dietrich et al, 2004; Goffeau et al, 1996).

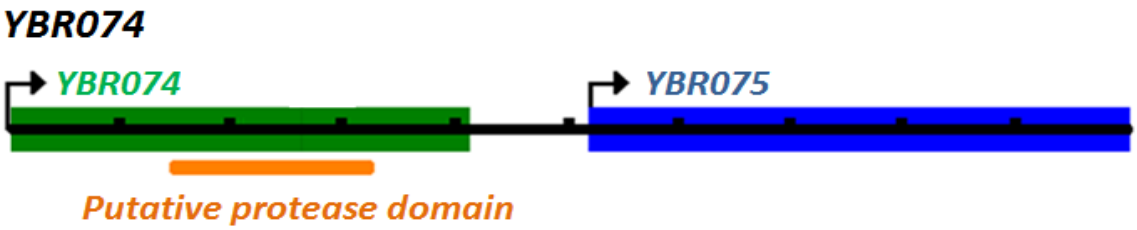

Figure 6: The *YBR074W* locus.

The coding sequence of *YBR074W* (2931 bp) is drawn to scale, and each tick on the black line corresponds to 300 bp. The green and blue shaded regions represent the ORFs *YBR074W* and *YBR075W* prior to the gene being fused and re-annotated. The region underlined in orange represents the M28 metalloprotease domain boundaries as predicted by Pfam.

YBR074W is predicted to encode nine transmembrane segments based on a computational analysis of amino acid segments above a threshold level of hydrophobicity (Ikeda et al, 2002). In order to examine whether Ybr074 is a transmembrane protein, a sodium carbonate extraction experiment was conducted whereby a crude microsomal fraction from cells expressing N-terminally HA-tagged Ybr074 were treated with sodium carbonate at pH 11.5. Under these conditions sodium carbonate disrupts electrostatic interactions mediating the peripheral association of proteins with the lipid bilayer (Fujiki et al, 1982). Microsomes were then separated into membrane and soluble fractions by ultra-centrifugation. I found that 3HA-Ybr074 partitioned in the membrane fraction, as anticipated (Figure 7B). The peripherally membrane associated protein, Pdi1, was used as a negative control, and shown to transition from the membrane fraction to the soluble fraction upon treatment with sodium carbonate. The transmembrane protein, Sec61, was used as a positive control and remained in the membrane fraction even after treatment with sodium carbonate, as anticipated.

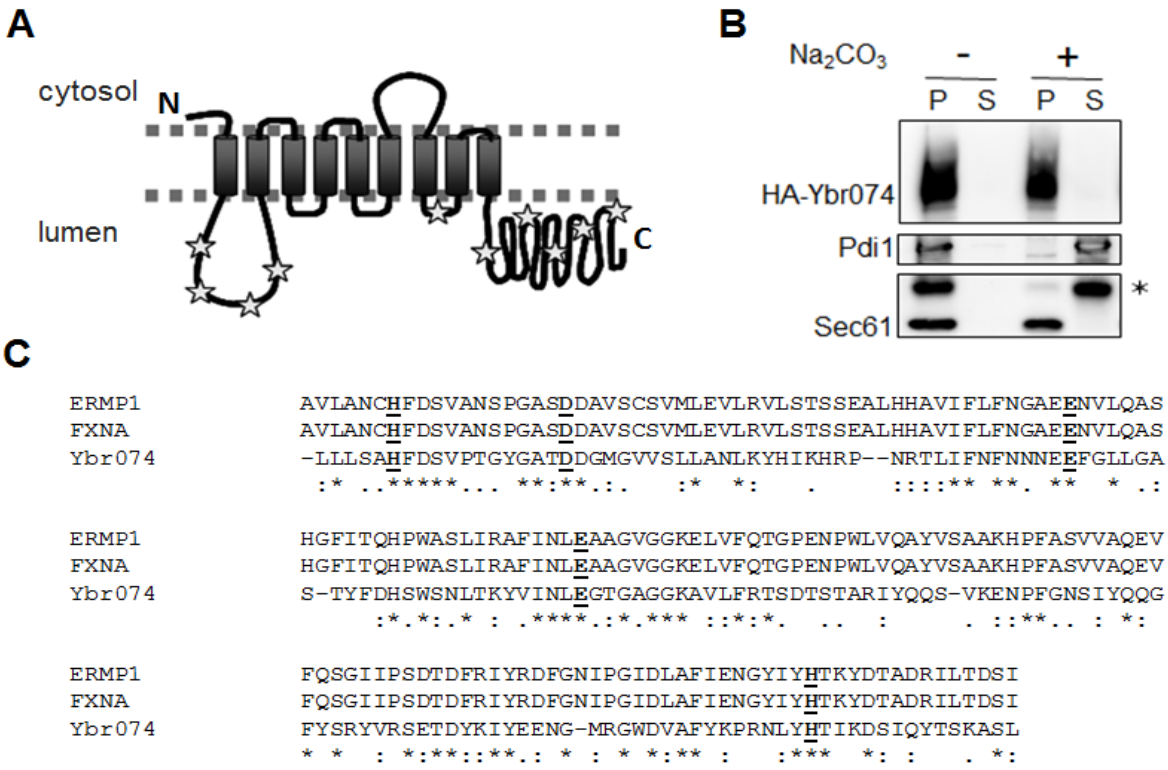

Figure 7: Ybr074 is a transmembrane protein with a conserved M28 metalloprotease domain that is predicted to reside in the ER lumen.

A) Computationally predicted topology of Ybr074 with putative lumenal glycosylation sites indicated by stars (Asn96, Asn121, Asn189, Asn217, Asn656, Asn768, Asn796, Asn811, Asn866, and Asn937). The N-terminus (N) and C-terminus (C) are labeled. The conserved M28 metalloprotease domain (Leu151-Leu314) is located in the first lumenal loop between transmembrane segments 1 and 2. B) Ybr074 is an integral membrane protein. ER-derived microsomes were treated with 0.1M sodium carbonate, pH 11.5, and the pellet (P) and soluble (S) fractions were isolated. Ybr074 and Sec61 are transmembrane proteins, and Pdi1 is a peripheral ER membrane protein. * denotes a soluble non-specific protein recognized by rabbit anti-Sec61 antibody. C) Multiple sequence alignment between M28 metalloprotease domains of Ybr074, GI: 341941012; the human ortholog, ERMP1, GI: 55749804; and the rat ortholog,

FXNA, GI: 42476352. Boundaries for the protease domain sequence were determined using Pfam. Catalytic residues are underlined. Note that the conserved M28 catalytic motifs, His-Phe-Asp and Glu-Glu, are present in Ybr074, ERMP1, and FXNA.

Analysis of Ybr074 by multiple sequence alignment and domain searching using the Protein family database (Pfam) uncovered a conserved M28 family metalloprotease domain (Punta et al, 2012). The M28 family of metalloproteases contains both amino- and carboxy-peptidases whose enzymatic activities depend on a pair of co-catalytic zinc ions and the catalytic residues His-Xaa-Asp and Glu-Glu, which are required for catalysis (Fundoiano-Hershcovitz et al, 2004; Rawlings & Barrett, 1995; Rawlings et al, 2012).

Based on the Protein ANalysis THrough Evolutionary Relationships (PANTHER) Classification System version 7.2, *YBR074W* is a member of a gene family known as FXNA-related (PTHR12147), which includes 46 orthologous genes from 22 different species (Table 5) (Mi et al, 2010; Thomas et al, 2003). The human ortholog of *YBR074W* is known as Endoplasmic Reticulum MetalloPeptidase 1 (ERMP1). Its putative residence at the ER is inferred based on sequence similarity with the rat ortholog known as Felix-ina (FXNA). A C-terminally Flag tagged FXNA construct expressed in COS7 cells was shown by Garcia-Rudaz *et al.* to co-localize with the ER marker Protein Disulphide Isomerase (PDI). Furthermore, knock-down of FXNA using shRNA delivered using a lentivirus vector to rat ovaries was shown to lead to defects in ovarian follicle development by an unknown mechanism (Garcia-Rudaz et al, 2007). It was therefore hypothesized that Ybr074 would also be an ER-resident protein. In fact, PSORT, a program for the prediction of protein localization, suggested the Ybr074 most likely resided in the ER (Nakai & Horton, 1999). However, it is important to note that a proteomic

analysis of yeast vacuolar membranes found Ybr074 enriched there, suggesting Ybr074 may be a vacuolar protease (Wiederhold et al, 2009). In order to resolve this discrepancy, the localization of Ybr074 will be analyzed later in this chapter.

Table 5: Members of the FXNA-related gene family.

Gene Symbol	Gene ID	Relevant References
AgaP_AGAP003423	1272796	
AgaP_AGAP003078	1273752	
AgaP_AGAP003432	1272805	
AgaP_AGAPP007676	1269552	
AgaP_AGAP007677	1269551	
aq_1891	1193539	
AT5G20660	832189	(Lu et al, 2009)
AT1G67420	843062	
AGOS_AGL209W	4622751	
AGOS_ADR123W	4620380	
AN3918.2	2873338	
ywaD	937350	
ERMP1	541094	
C44B7.11	183431	
B0495.7	174245	
ERMP1	484188	
CHLREDRAFT_186822	5725281	
CG33013	318830	
CG33012	36342	
CG10051	37222	
CG10073	37225	
CG30047	246414	
CG11961	37221	
CG10081	37226	
CG9416	37223	
CG30043	246412	
CG13160	36343	
CG30049	246416	
CG10062	37224	
ERMP1	426644	

Gene Symbol	Gene ID	Relevant References
ERMP1	79956	
ERMP1	717415	
ERMP1	100015108	
ERMP1	226090	
NCU04133	3877453	
NCU04479	3873191	
NCU04994	3871961	
Os07g0295800	4342962	
ERMP1	373544	(Garcia-Rudaz et al, 2007)
APE3	852589	(Nishizawa et al, 1994; Yasuhara et al, 1994)
YBR074W	852366	(Wiederhold et al, 2009)
SPCC1919.12c	2539157	
SPCC1259.02c	2539040	
SCO1226	1096649	
SCO4589	1100029	
SCO5043	1100484	

As a first step toward testing the hypothesis that Ybr074 is an ER-resident protein, the presence of N-linked glycans on Ybr074 was examined, as it is known that these post-translational modifications occur within the ER (Lederkremer, 2009; Schwarz & Aebi, 2011). To test this hypothesis, microsomes containing 3HA-Ybr074 were treated with Endo H, which cleaves N-linked glycans that lack extended chains from proteins and causes a downward shift as observed by SDS-PAGE. Indeed, treatment of Ybr074 with Endo H produced a protein band shift of from ~147 kDa to ~123 kDa (Figure 8). Given that each N-linked glycan is estimated to contribute ~3 kDa to the molecular mass of a protein, this shift corresponds to removal of roughly 8 N-linked glycans (Helenius & Aebi, 2004). This is less than the 10 N-linked glycosylation sites on Ybr074, which are predicted to be lumenal based on ConPredII analysis. However, it is possible that some N-linked glycosylation sites are inaccessible to glycosylation because the required enzymes are sterically hindered from modifying Asn residues near the

membrane, or because the tertiary structure precludes modification. It was also noted that the molecular mass of Endo H-treated Ybr074 was higher than predicted (114 kDa). It is possible that Ybr074 may bear additional post-translational modifications, such as O-linked glycosylation or phosphorylation, which were not examined. More trivially, membrane proteins often resolve by SDS-PAGE with migrations that do not correspond precisely to their masses. Furthermore, calculations of shifts in molecular mass may be limited by the resolution of the gel, and therefore should be considered as estimates rather than exact measurements.

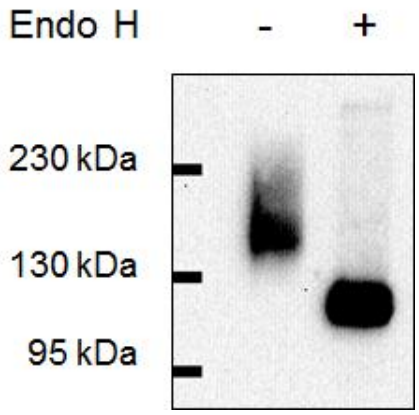

Figure 8: Ybr074 is modified by N-linked glycans.

ER-derived microsomes were prepared from strains expressing an N-terminally HA-tagged Ybr074 from its endogenous promoter on a *CEN/ARS* plasmid. The microsomes were either Endo H treated or left in buffer, as indicated. The apparent molecular mass of glycosylated Ybr074 is 147 kDa. The apparent molecular mass of unglycosylated Ybr074 is 123 kDa. The difference in molecular mass between the glycosylated and unglycosylated forms of Ybr074 suggests that eight of the ten predicted glycosylation sites are modified by N-linked glycans.

In order to understand the biological function of Ybr074, it was important to determine on which side of the membrane its protease domain resides. The computationally predicted topology calculated using ConPredII suggested that the M28 protease domain of Ybr074 faces the ER lumen. In order test this hypothesis, microsomes were isolated from yeast expressing tagged Ybr074 constructs. These microsomes represent crude membrane fractions containing both ER and vacuolar membranes. Microsomes isolated from strains expressing Ybr074 HA-tagged at the N-terminus, at the M28 protease domain, or at the C-terminus were subjected to a protease protection assay. Constructs in which the HA-tag is positioned outside the microsome should be susceptible to degradation by a protease. Conversely, constructs in which the HA-tag is positioned inside the microsome should be protected from degradation by proteinase K, unless Triton X-100 is included in the reaction to disrupt the integrity of the microsome membrane.

Western blot analysis of N-terminally HA-tagged Ybr074-containing microsomes indicated that the N-terminus of Ybr074 is mostly protected from degradation by Proteinase K (Figure 9). Proteinase K-treated 3HA-Ybr074 is observed to shift to a lower molecular mass as compared to microsomes that were not treated with proteinase K. This is indicative of partial degradation of Ybr074 in the presence of proteinase K, although the HA tag itself was not degraded. However, addition of Triton X-100 resulted in near complete degradation of the N-terminal HA tag after 30 min of Proteinase K treatment. Since the N-terminus is computationally predicted to face the cytosol, and therefore to be outside the microsome and susceptible to Proteinase K treatment, this result was surprising. However, the N-terminus, which is predicted to be only 14 amino acids in length, may be too closely associated with the membrane, resulting in its protection from Proteinase K. Although unlikely, an alternative explanation is that the first transmembrane segment (TM1) may not span the membrane as predicted, or it may be cleaved

by signal peptidase in the ER via a non-canonical cleavage site. To further test these possibilities, a strain expressing GFP-Ybr074 was also tested. This construct expresses a longer GFP moiety that is appended to the protein's N-terminus, (238 amino acids, GI: 262348071). A protease protection assay using this construct showed the N-terminus of Ybr074 was not protected from Proteinase K digestion, consistent with the N-terminus facing the cytosol.

The Ybr074 construct tagged using HA within the M28 domain was also protected from degradation by proteinase K except when treated together with Triton X-100 to disrupt microsome integrity (Figure 9). This suggests that the M28 protease domain is lumenal, as predicted. However, it should be noted that the position of the HA tag is also predicted to be close to the membrane (approximately 10 amino acids), similar to the N-terminally HA-tagged Ybr074 construct. Therefore, protection from proteinase K treatment may also be the result of close association with the microsome membrane or association with Ybr074's tertiary structure. Nevertheless, this region also harbors many of the predicted N-linked glycosylation sites, adding further evidence that this domain is lumenal.

The C-terminally HA-tagged Ybr074 construct appeared to be resistant to the protease even after treatment for 60 min in the presence of Triton X-100. This suggests that the C-terminal domain may assume a stable fold resistant to degradation. However, some degradation was observed in protease treated microsomes as compared to untreated microsomes, suggesting that the C-terminus of Ybr074 is also lumenal, as predicted.

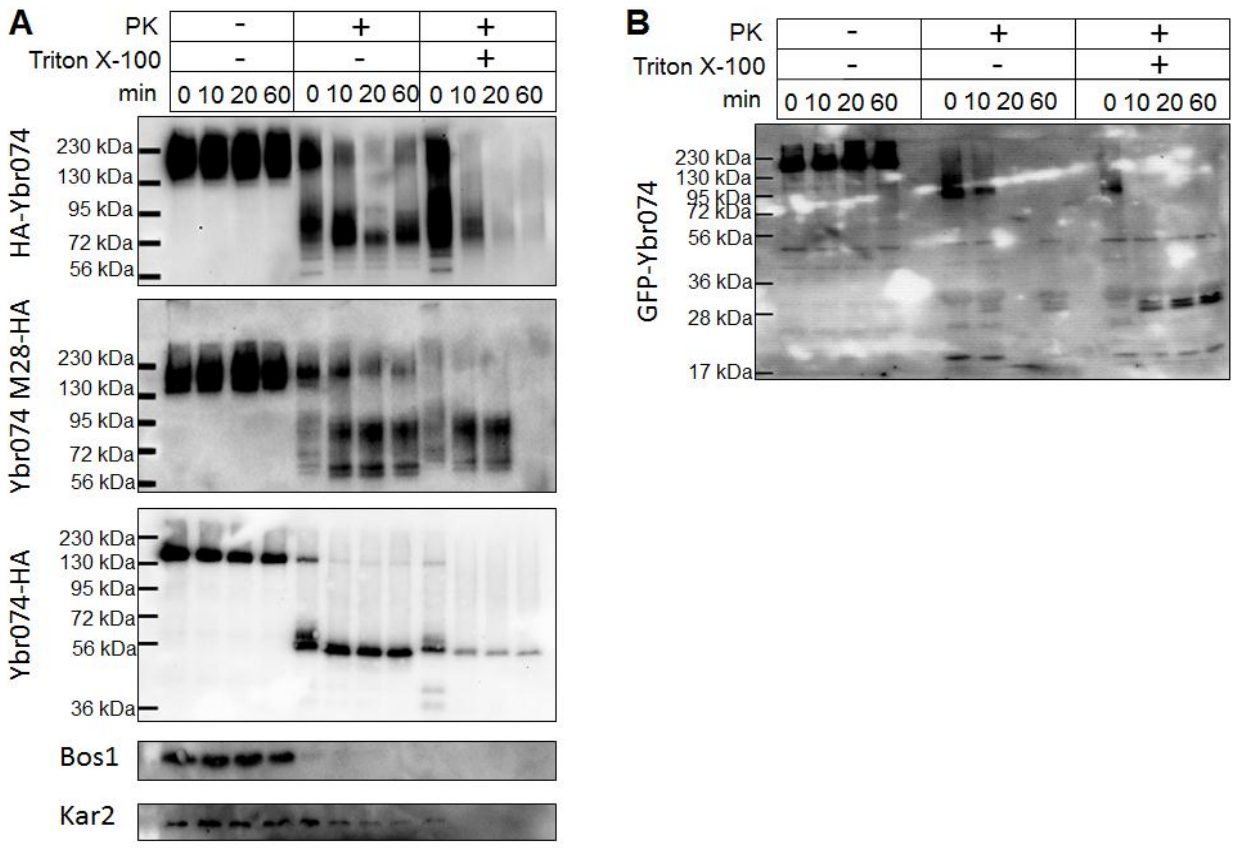

Figure 9: Assignment of Ybr074 topology by protease protection assay

Samples were treated in the presence or absence of 100µg/mL proteinase K and Triton X-100, as indicated. The cytosolic membrane anchored protein, Bos1, and the lumenal protein, Kar2 were used as controls for protease sensitivity and protection, respectively. A) A protease protection assay was performed using ER-derived microsomes from yeast expressing N-terminally HA-tagged Ybr074 (*CEN* vector), Ybr074 HA-tagged within the M28 domain (2µ vector), and C-terminally HA-tagged Ybr074 (2µ vector). Each protein was expressed from its endogenous promoter. B) Protease protection of chromosomally integrated GFP-Ybr074 expressed from a galactose-inducible promoter.

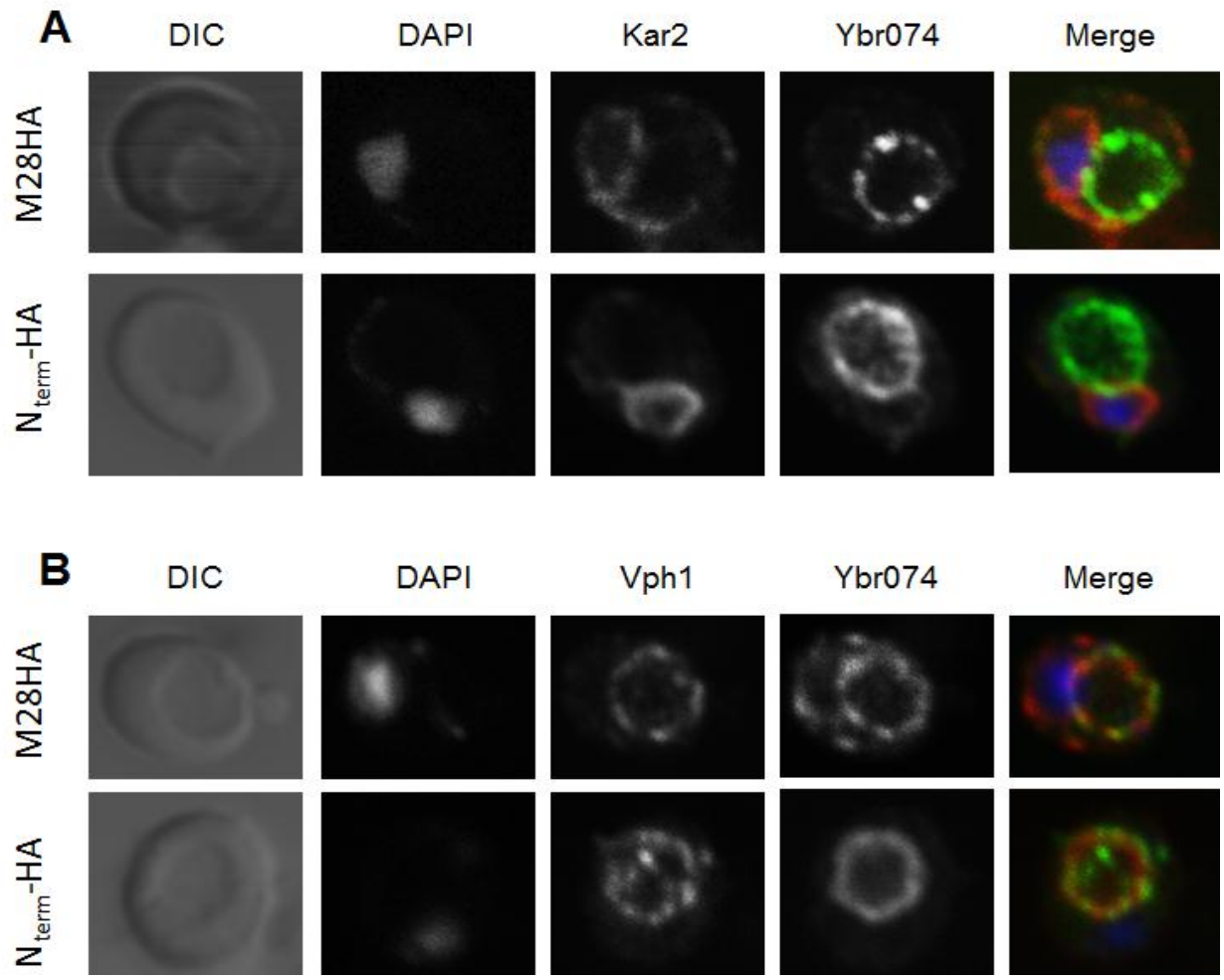

Figure 10: Sub-cellular localization of Ybr074 as assessed using indirect immunofluorescence microscopy.

Yeast expressing HA-tagged Ybr074 in the putative M28 protease domain or at the N-terminus were processed as described in the Methods section. A) A mouse anti-HA antibody was used to detect Ybr074, and is shown in green in the merged images. A rabbit anti-Kar2 antibody was used to detect the ER-resident protein Kar2, and is shown in red in the merged images. Nuclear staining using DAPI is shown in blue. B) A rabbit anti-HA antibody was used to detect Ybr074, which is shown in red in the merged images. A mouse anti-Vph1 antibody was used to detect the vacuolar protein, Vph1, which is shown in green in the merged images.

As previously mentioned, although Ybr074 was computationally predicted to be ER-localized and its rat ortholog, FXNA, was found in the ER of COS7 cells, a proteomic analysis of yeast vacuolar membranes suggested Ybr074 was a vacuolar protein (Garcia-Rudaz et al, 2007; Wiederhold et al, 2009). In order to examine the sub-cellular localization of Ybr074, HA-tagged constructs were subjected to indirect immunofluorescence microscopy. I also examined the localization of the ER marker, Kar2, and the vacuolar membrane marker, Vph1. Both Ybr074 constructs tagged at the N-terminus or the putative M28 protease domain showed strong co-localization with the vacuolar membrane marker, Vph1, suggesting that Ybr074 is a vacuolar resident protein (Figure 10). Interestingly, a small proportion of Ybr074 was also observed to co-localize with Kar2, as exemplified in Figure 10. Specifically, a faint peri-nuclear ring, corresponding to the ER, is visible in the Ybr074 staining shown in the panels labeled "M28HA" and "N_{term}-HA" of Figure 10A, and in the panel labeled "M28HA" of Figure 10B. This is consistent with the Endo H sensitivity data indicating that Ybr074 traffics through the ER (Figure 8).

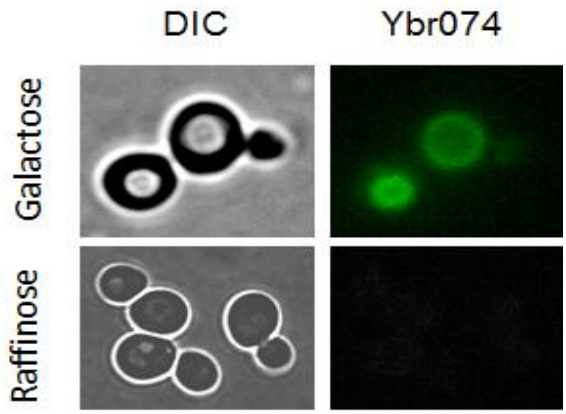

Figure 11: Live cell imaging of GFP-Ybr074 localization.

Live cell images are shown using a wild type strain, KH1, expressing a chromosomally-integrated form of GFP-tagged Ybr074 from a galactose-inducible promoter (see Table 3). GFP-Ybr074 expression was induced with galactose, and raffinose was used as a negative control. Differential Interference Contrast (DIC) images are shown on the left, with vacuoles appearing as a lighter shade due to their lower refractive index compared to the cytosol. The images on the right show GFP fluorescence only in galactose-treated cells.

As further support of Ybr074 vacuolar localization, a chromosomally-integrated GFP-tagged form of Ybr074 (GFP-Ybr074) was over-expressed from a galactose-inducible promoter. As shown in Figure 11, GFP-Ybr074 also showed vacuolar membrane localization. Furthermore, the proteomic study that identified Ybr074 in isolated vacuolar membranes did not rely on epitope tagging (Wiederhold et al, 2009).

In contrast to localization data shown in Figure 10, Ybr074 HA-tagged at the C-terminus appears to co-localize with the ER marker, Kar2 by indirect immunofluorescence microscopy (Figure 12). These data suggest that appending an HA epitope to the C-terminus of Ybr074 interferes with the vacuolar localization of Ybr074 (also see Discussion Chapter 5).

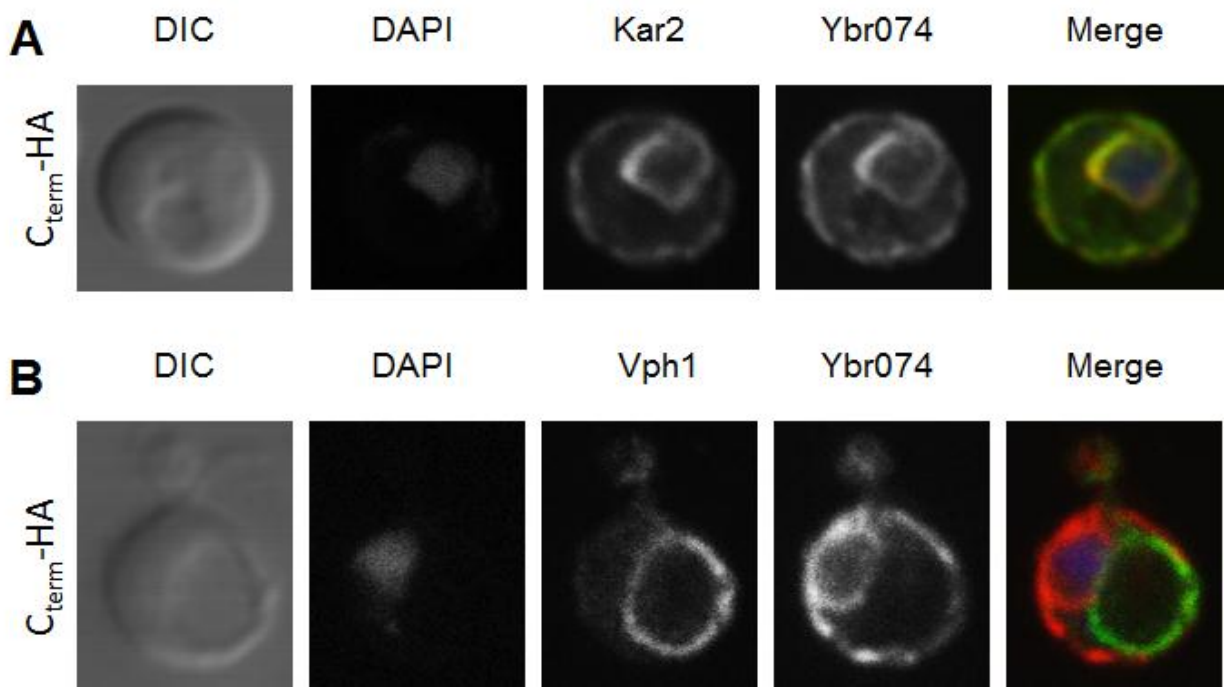

Figure 12: Ybr074-HA is retained in the ER

A) Ybr074-HA co-localizes with the ER marker, Kar2, forming at a peri-nuclear position. The vacuole appears as a circular depression by DIC imaging. In the merged image, DAPI signal, marking the nucleus, is shown in blue; Kar2 signal, corresponding to the ER, is shown in red; and Ybr074-HA signal is shown in green. The signal is yellow where Kar2 and Ybr074-HA signals overlap. B) Ybr074-HA signal was observed as a peri-nuclear ring, typical of ER protein staining. The vacuolar marker, Vph1, was localized to a ring coinciding with the vacuole observed by DIC imaging. The merged image shows the DAPI signal in blue, the Ybr074-HA signal in red, and the Vph1 signal in green.

If a C-terminally tagged Ybr074 construct is inappropriately retained in the ER, it might be expected to be less stable than a Ybr074 construct that is correctly targeted to the vacuole. To test this hypothesis, cycloheximide chase analyses were conducted to compare the stabilities of N-terminally and C-terminally HA-tagged Ybr074 constructs.

The C-terminally HA-tagged Ybr074 construct, found in the ER, was significantly less stable than the vacuolar N-terminally HA-tagged Ybr074 in wild type cells (Figure 13A). To determine if the vacuole plays a role in the degradation of Ybr074, the stability of Ybr074 was examined in a *pep4Δ* strain. Since Pep4 (proteinase A) is required for the proteolytic activation of many vacuolar proteases, disruption of Pep4 activity impairs vacuolar proteolytic function (van den Hazel et al, 1992). Results indicate that C-terminally tagged Ybr074 is dependent on vacuole activity for degradation, while N-terminally tagged Ybr074 stability is not affected by in the absence of Pep4 activity (Figure 13A).

To determine whether degradation of Ybr074 was dependent on the 26S proteasome, Ybr074 stability was examined in a *pdr5Δ* strain in which deletion of the multidrug transporter, Pdr5, allows cells to retain the 26S proteasome inhibitor MG132 (Collins et al, 2010). While C-terminally tagged Ybr074 was significantly stabilized when 26S proteasome activity was inhibited by MG132, stability of the N-terminally tagged Ybr074 was not dependent on 26S proteasome activity (Figure 13B).

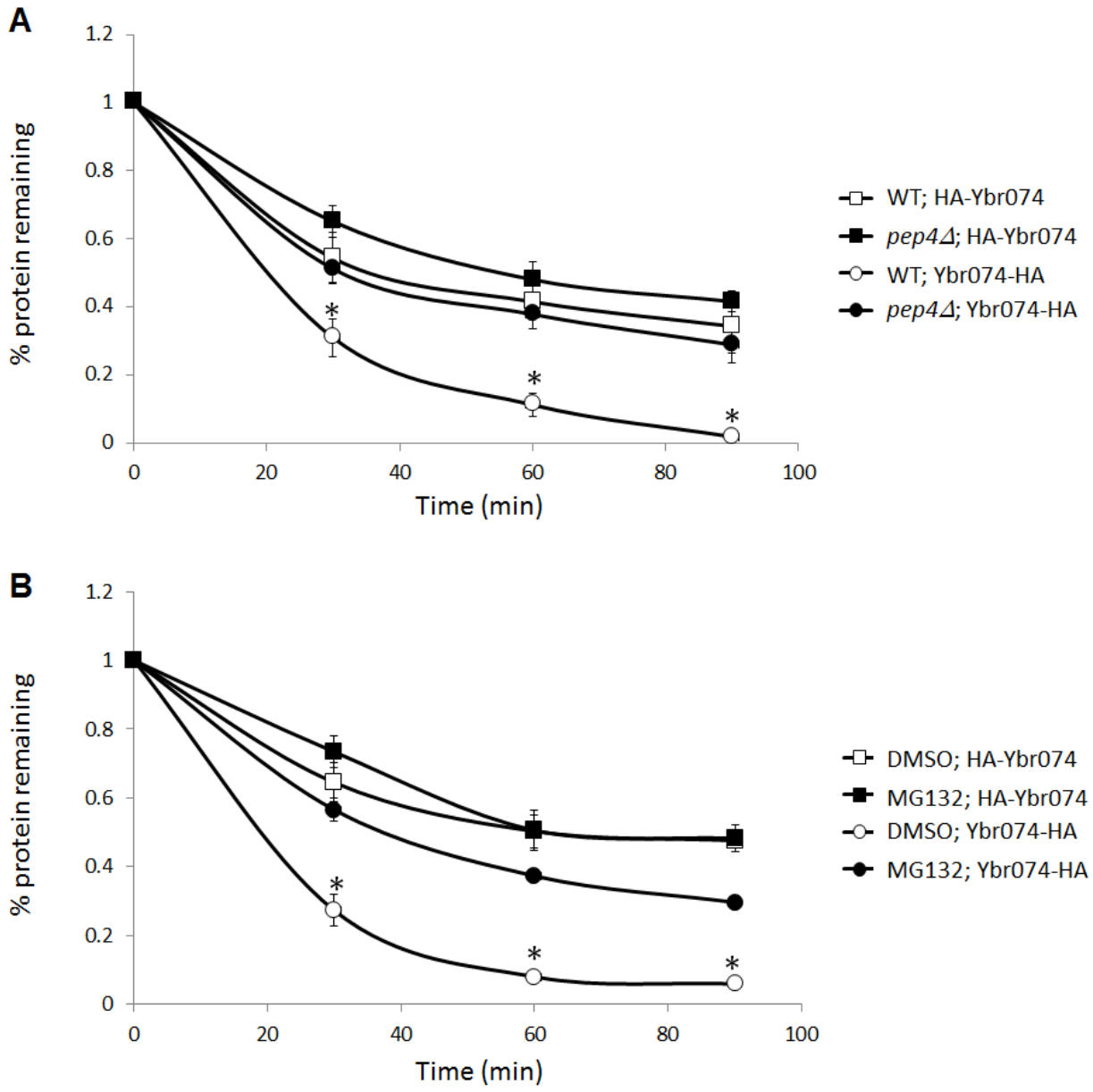

Figure 13: Stability of N- and C-terminally tagged Ybr074 constructs

A) Wild type (WT) and *pep4Δ* strains expressing N-terminally HA-tagged (HA-Ybr074) or C-terminally HA-tagged (Ybr074-HA) Ybr074 constructs were analyzed by cycloheximide chase analysis. B) A *pdr5Δ* strain expressing HA-Ybr074 or Ybr074-HA were treated for 30 min at 30°C with DMSO or 100 µM MG132 before addition of cycloheximide. * = $p<0.05$

2.4 CONCLUSIONS

Computational analyses indicated that Ybr074 is a member of the FXNA-related family of proteins, harbors a protease domain, and belongs to the M28 family of metalloproteases. Ybr074 was demonstrated to be a transmembrane protein and is glycosylated, indicating that Ybr074 trafficks through the ER. Protease protection assays suggest that the M28 and C-terminal domains of Ybr074 are lumenal, as expected. Surprisingly, the HA-tagged N-terminus appeared lumenal as well, either suggesting that the topological prediction was incorrect, or that the N-terminal epitope was not accessible to protease due to proximity to the membrane. A protease protection assay conducted using Ybr074 tagged with GFP at the N-terminus showed the N-terminus is cytosolic. Since the larger GFP tag is likely more accessible to digestion by proteinase K, this result may be more reliable and is consistent with the predicted topology of Ybr074. Furthermore, Ybr074 was shown both by indirect immunofluorescence microscopy and live cell imaging to be a vacuolar membrane protein. This is contrary to its computationally predicted ER localization. The localization of Ybr074 contrasts to that reported for FXNA, which was shown to be ER-localized in COS7 cells using a C-terminally FLAG-tagged FXNA construct (Garcia-Rudaz et al, 2007). However, it is worth noting that FXNA and Ybr074 may display cross-specifies differences. Furthermore, appending a tag at the C-terminus of Ybr074 causes this protein to be targeted for degradation in a 26S proteasome and vacuole dependent manner. Therefore, it is likely that Ybr074 is normally targeted to the vacuole. It is important to emphasize that an untagged Ybr074 was found enriched in the vacuolar membrane by proteomic analysis (Wiederhold et al, 2009). Therefore, appending a C-terminal tag to Ybr074 may destabilize the protein and cause the quality control machinery to prevent its trafficking to the vacuole by targeting Ybr074 for degradation. This scenario is discussed in Chapter 5.

3.0 ATTEMPTS TO DEFINE THE FUNCTION OF YBR074

3.1 INTRODUCTION

In parallel to discovering that Ybr074 is most likely a vacuolar protein, several approaches were taken to test the role of Ybr074 in ER quality control. In this chapter, I used molecular, genetic, phylogenomic, and proteomic methods to ask if Ybr074 participates in the degradation of ERAD substrates, to identify Ybr074's genetic interactions, and to search for Ybr074 substrates. As my extensive data suggest, Ybr074 does not affect the degradation of any ERAD substrates tested. Genetic analysis indicated a potential role for Ybr074 is maintenance of cell wall integrity. Although proteins exhibiting evolutionary co-variance with Ybr074 using phylogenomic analysis did not produce statistically significant enrichment of any Gene Ontology (GO) terms, the data did support a potential role for Ybr074 is affecting trafficking of proteins involved in cell wall maintenance. Finally, a proteomic analysis revealed a potential Ybr074 substrate, Rhr2, but further analysis showed that Rhr2 is not a Ybr074 substrate.

3.2 MATERIALS AND METHODS

3.2.1 Strains

Deletion of *YBR074* in the BY4742 and BY4741 backgrounds were carried out using Polymerase Chain Reaction (PCR)-mediated gene disruption (Brachmann et al, 1998). Briefly, the BY4742 strain was transformed with a *ybr074::KANMX* cassette which was amplified from the pRS400 vector (forward primer: AAA TTA TCT ACA AGG AAA TAA ATT GAT AGG TAA AGT TAA AGA ATC ACG GCA GAT TGT ACT GAG AGT GCA C; reverse primer: CAG TAG GCG AAT TTG AGT TTA TAA AAA TTT ACA TTT AAA ACT AAT TAG AAC TGT GCG GTA TTT CAC ACC G). Transformants were selected on yeast-peptone containing 2% dextrose (YPD) and 250 μg/mL Geneticin (G-418; Invitrogen, Carlsbad, CA). Colonies incorporating the *ybr074::KANMX* cassette were verified by PCR using primers flanking the *YBR074* open reading frame (ORF) (upstream primer: CAA TGA CGC CAA ATA TGG ACA CT; downstream primer: AAG AGA GCA CCG TAG AAT GGT T). To generate the *ybr074::NATMX* strain, the *NATMX* cassette was PCR amplified from the *pFA6a-NAT-MX6* vector using Forward primer: CAA GGA AAT AAA TTG ATA GGT AAA GTT AAA GAA TCA CGG CCG GAT CCC CGG GTT AAT TAA and Reverse primer: ATT TGA GTT TAT AAA AAT TTA CAT TTA AAA CTA ATT AGA AGA GCT CGT TTA AAC TGG ATG (Vembar et al, 2010). The *NATMX* cassette was transformed into BY4742 and BY4741 strains as described (Adams et al, 1998). Cells were selected on YPD medium supplemented with nourseothricin (NAT), and integration of the *NATMX* cassette was verified by PCR using the same primers used to check for integration of the *KANMX* cassette.

3.2.1.1 Generating double mutant strains by yeast mating

To generate double mutant strains, such as the *cdc48-2 ybr074Δ* strain, yeast mating was conducted as in the example that follows. The *cdc48-2* MAT α strain (OY209) was mixed with *ybr074::KANMX* strain in a patch on solid YPD medium containing 2% Bacto agar. Parental strains were allowed to mate overnight at room temperature before selecting for diploids on YPD containing 250 μg/mL G-418 and 100 μg/mL NAT (clonNAT; Werner BioAgents, Jena, Germany) for 3 d at room temperature. Diploid colonies were patched onto GNA presporulation media (3% Difco nutrient broth, 1% Difco yeast extract, 5% dextrose, 2% Bacto agar; BD, Sparks, MD) overnight at room temperature before being transferred to liquid sporulation media (2% potassium acetate, 0.005% zinc acetate) and incubated in a roller drum for 3-7 d at room temperature. Spores were then dissected and genotyped as described (Adams et al, 1998). Strains KH01, KH02, and KH03 were isolated by this same method (Table 3).

3.2.2 Growth Assays

The growth curve assay was conducted using wild type BY4742, *ybr074Δ*, *pdr5Δ*, and *ybr074Δpdr5Δ* strains, which were either grown in YPD or transformed with a plasmid engineered for the expression of the Cystic Fibrosis Transmembrane conductance Regulator (CFTR), and grown in selective media lacking uracil (Zhang et al, 2001). Cells were grown at 30°C to log phase before being diluted back to OD_{600} = 0.15. The cells were then incubated in the presence or absence of 25 μM MG132 (Peptides International, Louisville, KY) and OD_{600} readings collected every 40 min for 6 h.

Serial dilution growth assays were conducted by harvesting 0.5 OD_{600} equivalents from logarithmic phase cultures grown in YPD. Cells were washed in sterile double distilled water (SDDW), re-suspended in SDDW at 1 OD_{600}/mL, and used to make 10x serial dilutions in SDDW. Samples were spotted onto media containing 50 μg/mL calcofluor white (CFW; Sigma, St. Louis, MO) or 50 μg/mL Congo Red (CR; Sigma, St. Louis, MO), with or without 1M sorbitol, and grown at the indicated temperatures for 4 d.

The assay for adhesion and invasion of agar was conducted using the wild type strain Y285 and the *ybr074Δ* strain in the Y285 strain background, as described (Guldal & Broach, 2006). Briefly, cells were grown to saturation overnight in YPD medium at 30°C and diluted back to OD_{600}= 1.5 the next day. A total of 200 μL of cells were spotted onto synthetic complete solid medium supplemented with 2% dextrose, or 0.2% dextrose. Cells were grown at 30°C for 5 d and then rinsed with distilled water to observe adhesion onto agar medium. To observe invasion of the agar, cells on the surface of the agar medium were removed in distilled water by rubbing the surface of the plate with a gloved finger. Growth, adhesion, and invasion of agar were captured using the Epson Perfection 3490 photo scanner.

Qualitative mating assays were performed as described (Shei & Broach, 1995). Briefly, *MAT α* and *MAT a* strains were grown to logarithmic phase (OD_{600}= 0.4-0.8) and 0.5 OD_{600} cell equivalents of each were collected, washed in SDDW, and re-suspended to 1 OD_{600}/mL in SDDW. Serial dilutions of *MAT α* cells were mixed with 200 μL of *MAT a* cells, and *vice versa*. The serial dilutions containing both *MAT α* and *MAT a* cell were plated on synthetic media lacking lysine and methionine to select for diploids, synthetic media lacking lysine to select for *MAT α* cells, and synthetic media lacking methionine to select for *MAT a* cells.

3.2.3 Molecular Techniques

The 3HA-Gas1* expression construct was generated by sub-cloning P_{GAS1}-*3HA-GAS1*-T_{GAS1} from the pMF616 integration plasmid, described in Table 3, using the BamHI/SpeI sites and ligated into the pRS315 expression vector. The construct was verified by DNA sequence analysis (IDT, Coralville, IA).

RHR2 was PCR amplified from genomic DNA isolated from the BY4742 strain as described, using Forward primer: GAT CGG ATC CCC TTT GAC CAC AAA ACC TTT ATC TTT G, and Reverse primer: GAT CGA ATT CTT ACC ATT TCA ACA AGT CAT CCT TAG CGT (Adams et al, 1998). Amplified *RHR2* was inserted into the pKN16 expression vector by ligation using BamHI/XhoI sites. The construct was verified by DNA sequence analysis (IDT, Coralville, IA).

3.2.4 Assays examining ER-Associated Degradation (ERAD)

The assays described in this section aim at testing the role of Ybr074 in ERAD, and assessing whether it acts in synergy with the 26S proteasome, as shown in Figure 12.

3.2.4.1 Cycloheximide chase analyses

Vectors expressing the indicated ERAD substrates were transformed into the specified yeast strains and grown in selective media lacking uracil or leucine, as required (see Table 6). Alternative transformation methods were used to transform the *ybr074Δcdc48-2* strain, which could not be transformed using the standard LiAc method (Adams et al, 1998). The CPY*

expression vector was introduced by mating *ybr074Δ* and *cdc48-2* strains containing the CPY*-3HA expression vector, detailed in Table 6. Strain construction by yeast mating, sporulation, tetrad dissection, and genotyping were conducted as described (Adams et al, 1998).To express Gas1* in the *ybr074Δcdc48-2* strain, cells were transformed with both the *LEU2*-marked Gas1* expression vector (Table 6), and the *URA3*-marked 3HA-Ybr074 expression vector (Table 3). Cells were grown on selective media lacking both uracil and leucine, followed by growth on media lacking leucine and supplemented with 5-fluoroorotic acid (5-FOA) to counter-select for the *URA3*-marked 3HA-Ybr074 expression plasmid (Boeke et al, 1987). Finally, cells containing only the Gas1* expression vector were grown on media lacking leucine. Cells expressing the desired ERAD substrate were grown to logarithmic phase (OD_{600} = 0.4-0.8) and treated by one of three methods illustrated in Figure 14A. Briefly, cells were either concentrated by centrifugation at 1,000 *g* for 5 min, and re-suspended to 1 OD_{600}/mL, or transferred directly to a water bath at the indicated temperature without concentrating the cells. At the various temperatures tested, cells were either immediately treated with 250 μg/mL cycloheximide, or pre-incubated for 90 min before the addition of cycloheximide (Sigma, St. Louis, MO). At the indicated times, 1 mL from each culture was transferred to a tube containing sodium azide at a final concentration of 20 mM. Cells were harvested by centrifugation at 18,000 *g* for 30 sec at 4°C and then washed with 1mL of ice cold 10 mM sodium azide to block respiration. Cells were centrifuged as above, the supernatant was aspirated, and the cell pellets were flash frozen in liquid nitrogen before being processed the next day by TCA precipitation, according to an established protocol (Nakatsukasa et al, 2008).

Table 6: ERAD substrate expression vectors

Plasmid name	Description	Selectable marker	Source or Reference
pSM1152	CFTR-3HA overexpression vector	*URA3*	Zhang, Y. et al. 2002
3HA-Gas1p*	3HA-Gas1p* expression vector	*LEU2*	this study
pMF616	3HA-Gas1p* integration vector	*URA3*	Fujita, M. *et al.* 2006
pSM1911	Ste6p*-HA overexpression vector	*URA3*	Huyer, G. et al. 2004
CPY*-3HA	CPY*-3HA expression vector	*URA3*	Bhamidipati, A. et al. 2005
CPY*-DHFR	CPY*-DHFR-3HA expression vector	*URA3*	Bhamidipati, A. et al. 2005
CPY*-DHFR(Pro)	CPY*-DHFR(Pro)-3HA expression vector with DHFR mutations A29P, W30P, F31P	*URA3*	Bhamidipati, A. et al. 2005

3.2.4.2 Cycloheximide pulse chase analyses

To examine whether Ybr074 contributes to the degradation of CPY*-DHFR, CPY*-DHFR(Pro), or CFTR, a cycloheximide pulse chase analysis was conducted using the indicated strains as described (Brodsky et al, 1998; Zhang et al, 2001). Briefly, cells transformed with CPY*-DHFR or CPY*-DHFR(Pro) were grown in selective medium lacking uracil and supplemented with glucose to an OD_{600} ~ 0.5. Cells were concentrated to 10 OD_{600} cell equivalents per mL and equilibrated to 30°C for 30 min. Cells were then labeled using Express ^{35}S (Perkin-Elmer, Boston, MA) at a final concentration of 100 μCi/mL for 10 min at 30°C. Protein synthesis was quenched using cycloheximide at a final concentration of 200 μg/mL, and 4 OD_{600} cell equivalents were collected at the indicated time points. The cells were washed in B88 and pellets were processed by glass bead lysis in extraction buffer (50 mM Tris-HCl, pH 7.4, 1% SDS, 1 mM EDTA, 1 mM PMSF, 1 ug/mL pepstatin and leupeptin). The resulting cell homogenate, containing ~10^7 cpm in total, was incubated with mouse anti-HA (Roche, Indianapolis, IN) antibody overnight at 4°C and then washed before adding Protein A Sepharose (GE Healthcare, Uppsala, Sweden) and incubating for 1-2 h. Immunoprecipitates were washed and the proteins were resolved by 10% SDS-PAGE followed by phosphorimage analysis.

3.2.5 Analysis of phylogenetic profiling data

Saccharomyces cerevisiae genes whose Evolutionary Rate Covariation (ERC) clustered with that of Ybr074 were kindly calculated by Dr. Nathan L. Clark (Dept. of Computational and Systems Biology, University of Pittsburgh, Pittsburgh, PA) as described (Clark et al, 2012).

3.2.6 Proteomic analysis methods

Cell lysates were prepared on-site and subjected to 2D DiGE by Applied Biomics, Inc., Hayward, CA. The BY4741 and *ybr074::NATMX MAT a* strains were grown in YPD at 30°C to OD_{600}= 0.6. Cells were harvested by centrifugation at 4,900 *g* (5,500 rpm) for 5 min at 4°C, using a Sorvall RC 5B Plus centrifuge and a GSA rotor. Cell pellets were re-suspended in 10 mL PBS, pH 8, and harvested by centrifugation at 5,000 *g* (6,500 rpm) for 5 min at 4°C, using a Sorvall RC 5B Plus centrifuge and an SS-34 rotor. The final cell pellets were re-suspended in 1 mL standard lysis buffer containing 8M urea, 1% CHAPS, 10 mM Tris-HCl, pH 8, 5mM magnesium acetate at 4°C. Cells were sonicated using the VirTis VirSonic 475 sonicator at 10% output power with three 10 sec pulses with 1 min intervals at 4°C between each pulse. Cell lysate were flash frozen in liquid nitrogen and delivered to Applied Biomics, Inc., for further processing, as described (May et al, 2012). Briefly, cell lysates were labeled with size and charge matched CyDye DiGE fluorophores to enable separation of both samples on the same 2D gel. Cell lysate from the BY4741 strain was labeled with Cy2 dye, and cell lysate from the *ybr074Δ* strain was labeled with Cy3 dye. Cell lysates were separated by isoelectric focusing (IEF) in the first dimension, followed by SDS-PAGE in the second dimension. The gel was scanned with a Typhoon image scanner to visualize Cy2 dye and Cy3 dye signals. ImageQuant software was

used to generate images of each sample and the overlayed samples. Quantitative comparitive analysis of all the protein spots on the gel were analyzed using DeCyder "in gel" software to calculate protein expression ratios across the two samples using a threshold value of 1.3. Protein spots chosen for identification by mass spectrometry were picked using the Ettan Spot Picker.

To test whether Rhr2 was a Ybr074 substrate, BY4742 and *ybr074Δ* strains containing the empty vector pKN16 or the 3HA-Rhr2 overexpression vector (see Table 4) were grown to logarithmic phase (OD_{600}= 0.4-0.8) at 30°C in synthetic complete media lacking uracil and supplemented with 2% glucose. Cells were harvested by centrifugation at 1000 *g* at room temperature and re-suspended in synthetic media lacking uracil and supplemented with 2% galactose to induce Rhr2 expression at 30°C for 6.5 h. Cells were harvested by centrifugation at 1000 *g* and processed by TCA precipitation, as above. Cell lysates were resolved by 12.5% SDS-PAGE and transferred to nitrocellulose. Protein was visualized by Western blot analysis using HRP-conjugated anti-HA antibody at 1:5000 for 1 h at room temperature (Roche Diagnostics, Indianapolis, IN). Glycerol-3-phosphate dehydrogenase (G6PDH) was used as a loading control, and was detected using anti- G6PDH antibody at 1:5000 for 1 h at room temperature (Sigma, St. Louis, MO). The bound antibodies were visualized using Super Signal West Pico kit (Thermo Scientific, Rockford, IL) on a Kodak 440CF Image Station (Eastman Kodak, Rochester, NY).

To identify putative Ybr074 substrates, an analysis of a GFP-tagged protein library in the *ybr074Δ* strain background was conducted by members of the Schuldiner lab, Department of Molecular Genetics, The Weizmann Institute of Science Rehovot, Israel as described (Cohen & Schuldiner, 2011). Briefly, the *ybr074::NATMX* strain was mated with the GFP-tagged *MAT a* collection using Synthetic Genetic Array (SGA) techniques as described (Cohen & Schuldiner, 2011; Tong & Boone, 2006). Haploid cells expressing a GFP-tagged protein in the *ybr074Δ*

background were selected and grown to logarithmic growth phase in synthetic complete medium at 30°C in 384-well growth plates. Cells were then transferred to 384-well microscope plates (Matrical Bioscience) and visualized using an automated inverted fluorescence microscope ScanR system (Olympus) using a swap robot (Hamilton). Images were then manually reviewed using ScanR analysis program and processed by Adobe Photoshop CS3 software.

3.3 RESULTS

3.3.1 Is Ybr074 a quality control protease?

Based on computational predictions, I initially hypothesized that Ybr074 is an ER-resident protease that may help degrade terminally misfolded proteins in the ER. To test this hypothesis, a number of assays to measure the degradation of ERAD substrates were employed. First, cycloheximide chase analyses were conducted, monitoring the degradation of CFTR, Ste6p*, CPY*, and Gas1p* in wild type and *ybr074Δ* strains. Second, pulse chase analysis of the ERAD substrate CPY* fused to a stably folded dihydrofolate reductase (DHFR) domain (CPY*-DHFR), or an unstable mutant form of DHFR (CPY*-DHFR(Pro)), were examined for Ybr074-dependent differences in their degradation fragment profiles. Third, a pulse chase analysis was used to examine the fragments resulting from the ERAD of CFTR in strains in which the function of Ybr074, the 26S proteasome, or both were disrupted. Fourth, to determine whether Ybr074 and the 26S proteasome function in parallel degradation pathways under conditions of ER stress, the growth of cells expressing CFTR was investigated in the presence or absence of the 26S proteasome inhibitor, MG132, in wild type or *ybr074Δ* strains.

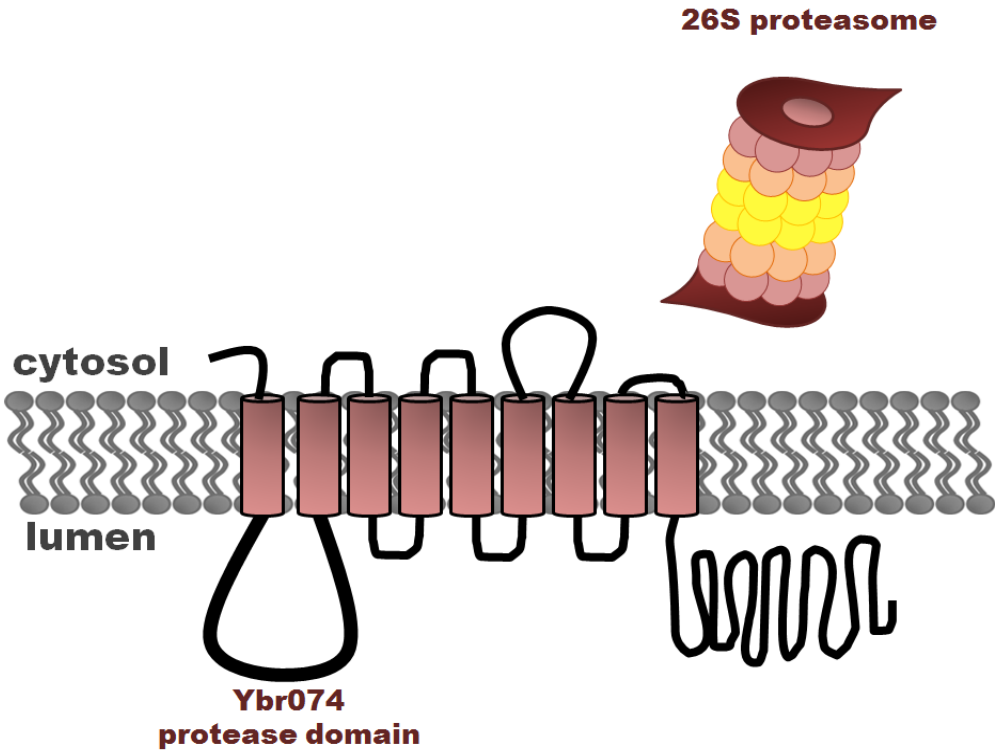

Figure 14: The cytosolic 26S proteasome and lumenal Ybr074 putative protease

The 26S proteasome functions in the cytosol, while the putative proteasome domain of Ybr074 faces the lumen. Do these proteases cooperate in the degradation of integrated membrane ERAD substrate on either side of the ER membrane?

3.3.1.1 Does Ybr074 function as a general protease during ERAD?

One third of all proteins enter the secretory pathway through the ER, where nascent proteins undergo folding and maturation (Ghaemmaghami et al, 2003). These proteins are either retained in the ER, where their function is required, or they are targeted for vesicle-mediated transport to an alternative sub-cellular compartment (Marie et al, 2008; Mellman & Warren, 2000). Proteins that fail to fold correctly, due to mutations, environmental stress, or spontaneous misfolding, accumulate in the ER and are targeted for degradation via ERAD (Smith et al, 2011;

Vembar & Brodsky, 2008). When this quality control mechanism was first described, it was thought that a degradation system consisting of one or more proteases residing in the ER was responsible for this phenomenon (Klausner et al, 1990; Lippincott-Schwartz et al, 1988). However, ER-lumenal proteases responsible for ER degradation were never identified, and in 1996, McCracken and Brodsky demonstrated that terminally misfolded proteins were selectively retrotranslocated from the ER and degraded in the cytosol (McCracken & Brodsky, 1996). Later, it was demonstrated that the cytosolic 26S proteasome was responsible for the degradation of ERAD substrates (Vembar & Brodsky, 2008; Werner et al, 1996). In this section, the hypothesis that Ybr074 represents an ER quality control protease was tested by comparing the ability of wild type and *ybr074Δ* strains to degrade a number of known ERAD substrates.

In order to optimize conditions for the cycloheximide chase protocol, several variables were tested using the ERAD substrate CFTR: strain background, temperature, and dilution. A study of genetic diversity in commonly used laboratory strains and wild strains of yeast has identified over 10, 000 "single-feature polymorphisms" (SFPs) contributing to allelic variation across yeast strains. Among numerous genes associated with these SFPs, 160 ORFs were related to proteolytic degradation, and 59 ORFs were related to protein folding and stability (van Dijken et al, 2000; Winzeler et al, 2003). Therefore, Ybr074-dependent effects on the ERAD of CFTR were tested in BY4742, W303, and YPH499 strain backgrounds. Because no Ybr074-dependent effect on CFTR degradation was observed in these strain backgrounds, all subsequent experiments were conducted in the BY4742 background (Figure 15B).

Previous studies of CFTR degradation have been conducted at 30°C, 37°C, or 40°C because temperature affects the efficiency of CFTR folding, the expression of ERAD components, and temperature-sensitive mutant alleles that may be relevant to the experiment

(Denning et al, 1992; Youker et al, 2004; Zhang et al, 2001). Cells are typically concentrated prior to addition of cycloheximide in order to enhance protein detection. However, centrifugation of cells causes a brief period of glucose starvation which is associated with a transcriptional response and activation of autophagy (Yorimitsu & Klionsky, 2007). Therefore, degradation of CFTR was tested at varying temperatures, with or without concentrating the cells prior to addition of cycloheximide. My results showed no Ybr074-dependent effect on CFTR degradation under the conditions tested. Therefore, subsequent experiments were conducted at 37°C without concentrating cells prior to addition of cycloheximide (Figure 15B).

The factors required for degradation of ERAD substrates can vary depending on the location of the lesion in the ERAD substrate. Lesions located in the cytosol, membrane, or lumen may be recognized by different factors, and may, in principle, exhibit differential dependence on Ybr074. Therefore, a variety of well characterized ERAD substrates were chosen to test this hypothesis: CPY* is a soluble protein found in the lumen, Gas1* is glycerophosphoinositol-(GPI) anchored protein closely associated with the ER membrane on the lumenal side, Ste6p* is multi-spanning transmembrane protein with a cytosolic lesion, and CFTR is an exogenous mammalian transmembrane protein predominantly exposed to the cytosol.

The degradation of each of these ERAD substrates was examined by cycloheximide chase analysis in both wild type and *ybr074Δ* strains. No statistically significant difference in the degradation of any of the ERAD substrates tested was found across these strains. These data suggest the Ybr074 is not involved in ER quality control.

A

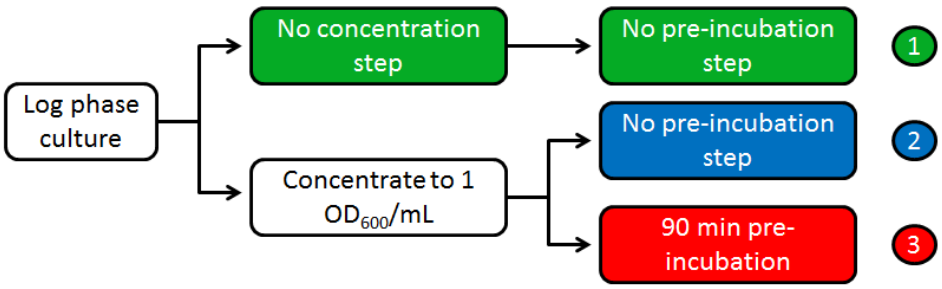

B

Experimental method	Wild Type	Mutant	Temperature	n =	Results
1	BY4742	*ybr075::KANMX*	30°C	5	CFTR stabilized in mutant strain
1	BY4742	*ybr075::KANMX*	30°C	9	Variable results
1	BY4742	*ybr074::NATMX*	30°C	2	No difference
2	BY4742	*ybr074::NATMX*	40°C	2	No difference
3	YPH499	*ybr074::KANMX*	30°C	4	No difference
3	YPH499	*ybr074::KANMX*	37°C	4	No difference
2	YPH499	*ybr074::KANMX*	40°C	3	No difference
2	W303-like	*ybr074::KANMX*	40°C	3	No difference

Figure 15: Optimization of cycloheximide chase analysis using the substrate CFTR

A) Cycloheximide chase experiments were conducted using logarithmic phase cultures that were either concentrated by centrifugation or not. Cultures were shifted from room temperature to 30°C, 37°C, or 40°C and cycloheximide was added either immediately, or after a 90 min pre-incubation period. B) Using experimental methods 1, 2, or 3 described above, wild type or mutant strains derived from the indicated genetic backgrounds were tested. The temperatures and number of replicates for each experiment are indicated. The *ybr074Δ* strain refers to the disruption of the entire *YBR074* ORF, while *ybr075Δ* refers to disruption of the *YBR074* coding sequence shown in blue in Figure 6. Results indicated in the first row of (B) were reported by Dr. A. Ahner (Ahner & University of Pittsburgh. School of Arts and Sciences, 2005), while I obtained all other results.

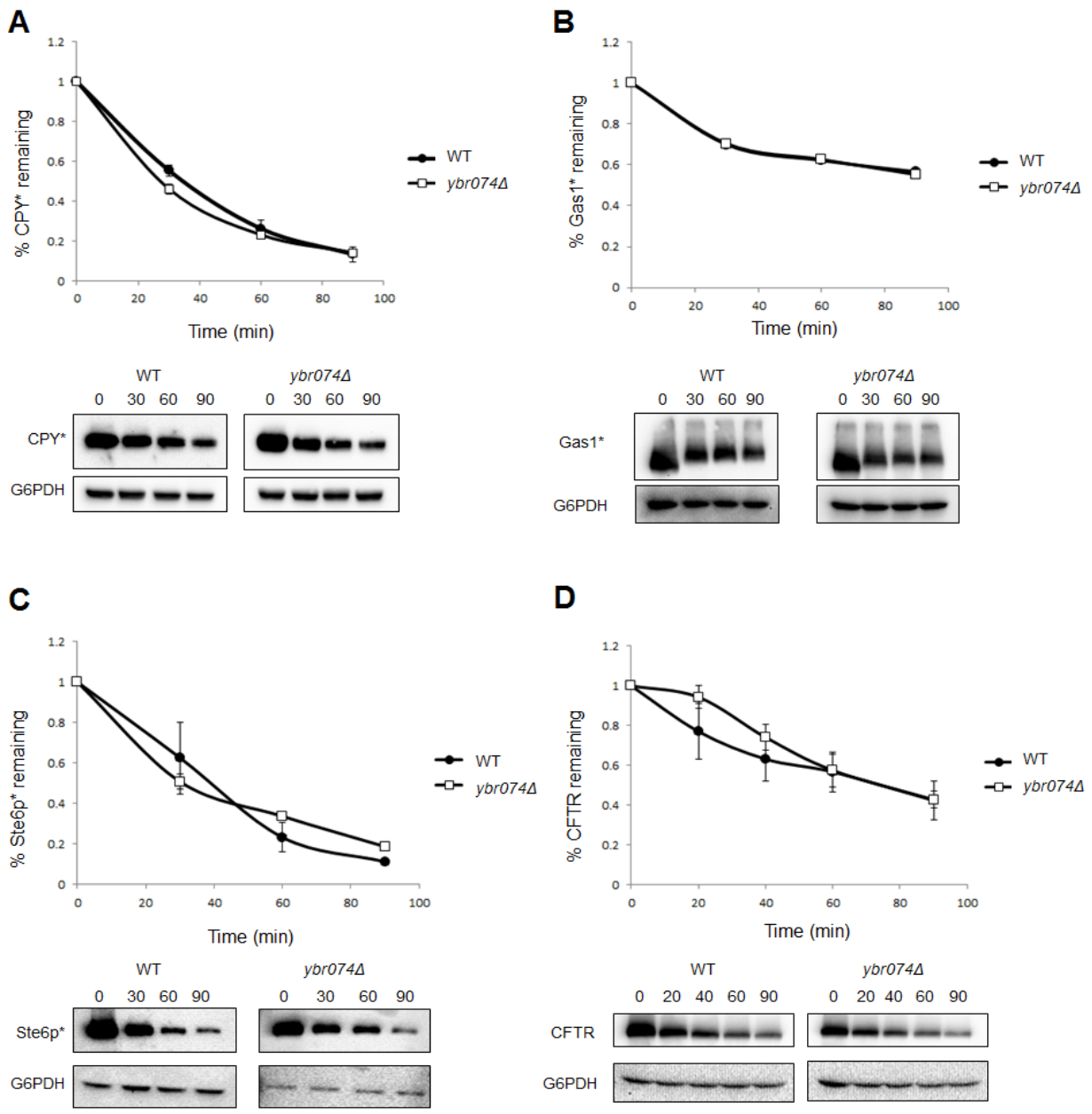

Figure 16: Ybr074 has no effect on the degradation of known ERAD substrates.

Results are shown as percentage protein remaining over time, ± SE. No statistically significant *YBR074*-dependent effect was found using the ERAD substrates above. A representative western blot of each ERAD substrate and the loading control, glucose-6-phosphate dehydrogenase (G6PDH) is shown for both wild type and *ybr074Δ* strains. A) Strains expressing CPY* were shifted from room temperature to 37°C for 1 h prior to addition of cycloheximide

(n=4). B) Gas1* degradation was analyzed as above (n=7). C) Strains expressing Ste6p* were shifted from room temperature to 37°C for 2 h prior to addition of cycloheximide (WT, n=3; *ybr074Δ*, n=4). D) Strains expressing CFTR were shifted from 30°C to 40°C for 1.5 h prior to addition of cycloheximide (n=2).

3.3.1.2 Does Ybr074 help resolve ERAD substrates with large lumenal domains?

In order to translocate from the ER for proteasome-mediated degradation, it is thought that ERAD substrates must remain soluble, which is assisted by chaperone activity, and that any residual quaternary and tertiary structures must be disassembled (Nishikawa et al, 2001; Romisch, 2005). Soluble ERAD substrates, such as CPY*, depend on retrotranslocation channels, such as Sec61, Hrd1 or Der1 for dislocation (Carvalho et al, 2010; Knop et al, 1996; Ng et al, 2000). However, multi-domain proteins containing stably folded lumenal domains may be physically impeded from passing through these retrotranslocation channels. As an example of this scenario, Weissman and colleagues designed an ERAD substrate comprised of CPY* fused at the C-terminus with *E.coli* DHFR (Bhamidipati et al, 2005). DHFR is ~20 kDa protein with a well characterized structure that has been shown in numerous studies to assume a stable conformation in the ER of both yeast and mammalian cells (Bhamidipati et al, 2005; Lee et al, 2001; Tirosh et al, 2003). It was observed that the CPY*-DHFR fusion protein was significantly stabilized in yeast as compared to CPY*. Furthermore, the DHFR domain was clipped by an uncharacterized protease and accumulated in the ER lumen (Bhamidipati et al, 2005). Therefore, I hypothesized that Ybr074 may play a role in resolving multi-domain ERAD substrates in order to facilitate their retrotranslocation. To test this hypothesis, wild type and *ybr074Δ* strains

expressing CPY*-DHFR, or CPY* fused to a destabilized mutant form of DHFR (CPY*-DHFR(Pro)) were examined for differences in the clipping of the resident DHFR motif.

Accumulation of two degradation fragments of ~40 kDa is evident by cycloheximide chase analysis of CPY*-DHFR (Figure 17A, C). These fragments are absent from the degradation profile of the destabilized CPY*-DHFR(Pro) substrate. I noted that the DHFR-CPY* fragments observed were a higher molecular mass than the previously published ~20 kDa fragments. This suggests there may be strain-dependent variation in the degradation profile of this ERAD substrate. In any event, degradation of CPY*-DHFR(Pro) was not dependent on Ybr074. No statistically significant difference in the degradation of CPY*-DHFR was observed when comparing wild type and *ybr074Δ* strains, except at 40 min (Figure 17B,D; $p=0.048$). It is possible that disruption of Ybr074 function causes an initial delay in CPY*-DHFR degradation, which is resolved at later time points by other proteases, or there is delivery of the accumulated substrate to the vacuole. However, my data suggest that Ybr074 is not required for the degradation of CPY*-DHFR. Furthermore, no statistically significant difference between wild type and *ybr074Δ* was observed when accumulation of CPY*-DHFR degradation fragments was quantified (Figure 17E; $p>0.4$).

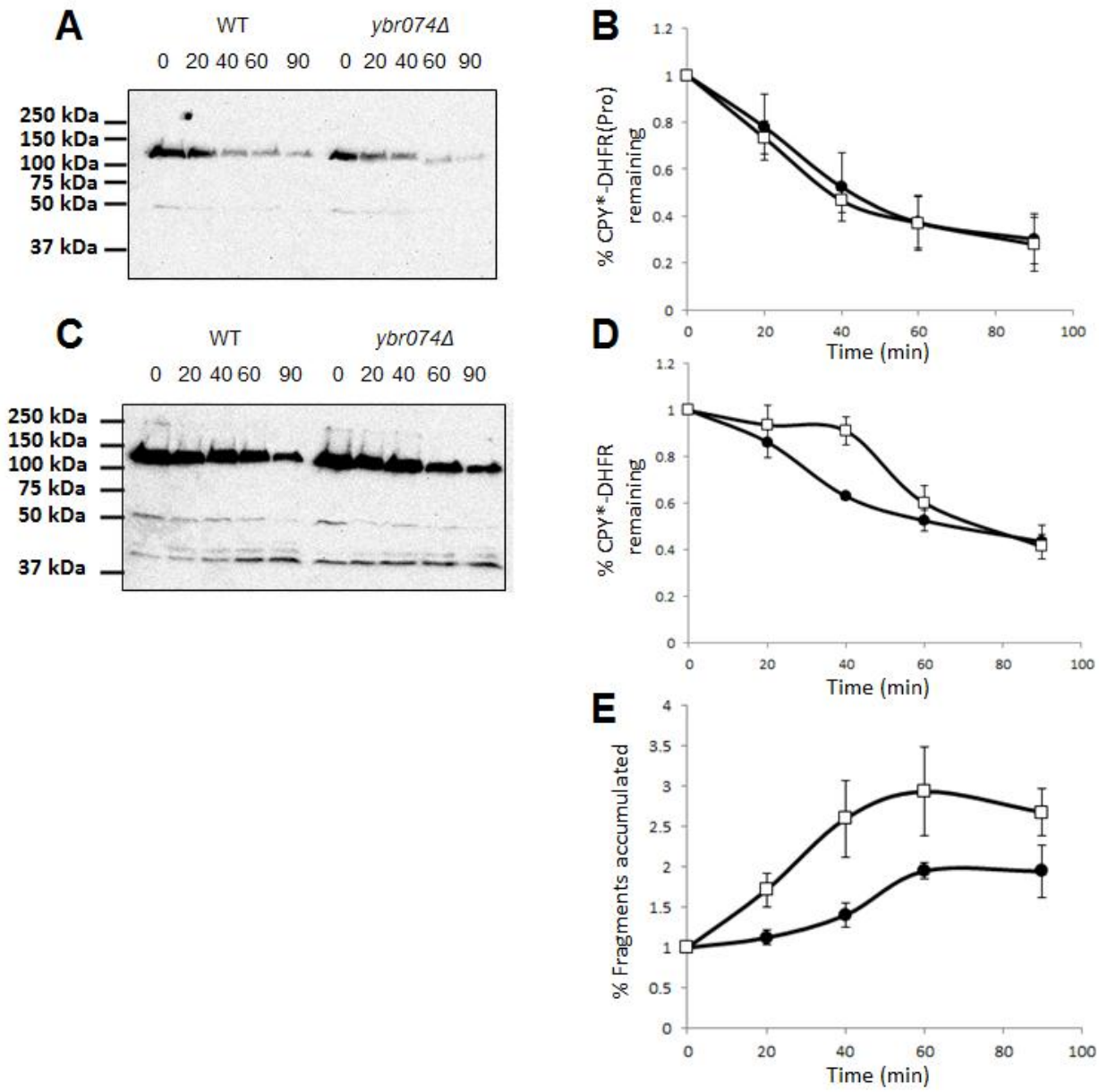

Figure 17: Degradation of CPY*-DHFR(Pro) and CPY*-DHFR is not dependent on Ybr074

A) CPY*-DHFR(Pro)-HA and C) CPY*-DHFR-HA degradation was examined by cycloheximide chase. Degradation of full length B) CPY*-DHFR(Pro) and D) CPY*-DHFR was quantified at the indicated time points as a percentage of initial protein. Data from wild type strains is shown as black circles, and data from the *ybr074Δ* mutant are shown as white squares. E) Accumulation of the two ~40 kDa CPY*-DHFR fragments over time is shown. Error bars represent SE n=3.

3.3.1.3 Do Ybr074 and the 26S proteasome function in synergy during the degradation of CFTR?

The Cystic Fibrosis Transmembrane conductance Regulator (CFTR) is a mammalian cAMP-regulated chloride channel that normally trafficks through the secretory pathway to the plasma membrane of epithelial tissues. In mammalian systems CFTR is co-translationally translocated into the ER, where it folds and assumes a core-glycosylated precursor form of ~140kDa. CFTR assumes a complex structure, consisting of two six-pass transmembrane domains, two cytosolic nucleotide binding domains, and a cytosolic regulatory domain. It is an intrinsically unstable protein, and ~75% of the wild type CFTR synthesized in mammalian cells is targeted for degradation by ERAD (Jensen et al, 1995; Ward & Kopito, 1994; Ward et al, 1995).

A CFTR expression system in yeast was developed in the Brodsky lab and used to show that Hsp70, Hsp40, Hsp90, small heat shock proteins, and the peptidyl-prolyl-isomerase, FKBP8, are important factors modulating quality control of CFTR (Ahner et al, 2007; Hutt et al, 2012; Youker et al, 2004; Zhang et al, 2001). Yeast expressing exogenous wild type CFTR showed no growth defect when compared to yeast in which this mammalian protein is not expressed (unpublished observation). As occurs in mammals, CFTR is targeted for degradation by ERAD in yeast, demonstrating that yeast cells are able to respond to the introduction of this foreign and poorly folded protein (Zhang et al, 2001). Interestingly, the transcriptional response known as the Unfolded Protein Response (UPR), which is normally induced in response to ER stress is not triggered upon expression of CFTR in yeast (Zhang et al, 2001). This was somewhat surprising, as a prominent target of the UPR is ERAD. This result suggests there may be other factors that impact CFTR quality control in yeast. This section addresses the hypothesis that Ybr074,

functioning as a secretory pathway protease, may cooperate with the 26S proteasome to degrade complex transmembrane ERAD substrates, such as CFTR, from both sides of the ER membrane.

To test this hypothesis, a pulse chase analysis was conducted to examine CFTR peptide fragments resulting from its ERAD in strains in which Ybr074 function, 26S proteasome function, or both were disrupted.

First, in order to impair 26S proteasome function, its transcriptional activator, Rpn4, was disrupted, resulting in reduced proteasome levels (Xie & Varshavsky, 2001). Wild type, *ybr074Δ*, *rpn4Δ*, and *ybr074Δ rpn4Δ* strains expressing C-terminally HA-tagged CFTR were radiolabeled using ^{35}S-Met for 5 min at 30°C, followed by treatment with cycloheximide. Samples were collected immediately after addition of cycloheximide. CFTR was then immunoprecipitated using an anti-HA antibody or the 3g11 antibody, which recognizes an epitope within NBD1. CFTR-derived fragments that appeared in CFTR-expressing strains and not in the empty vector control were compared in each strain. However, the presence of CFTR-derived fragments was not observed to depend exclusively on either Ybr074 activity or 26S proteasome activity (Figure 18).

Fewer CFTR-derived fragments were observed than were expected, suggesting that a longer incubation period after addition of cycloheximide may be required in order to detect CFTR-derived fragments. Nevertheless, these results indicate that CFTR-derived fragments are evident when there is reduced proteasome activity at this early time point, and that no Ybr074-dependent clipping of CFTR is taking place when comparing wild type and *ybr074Δ* strains along (Figure 18).

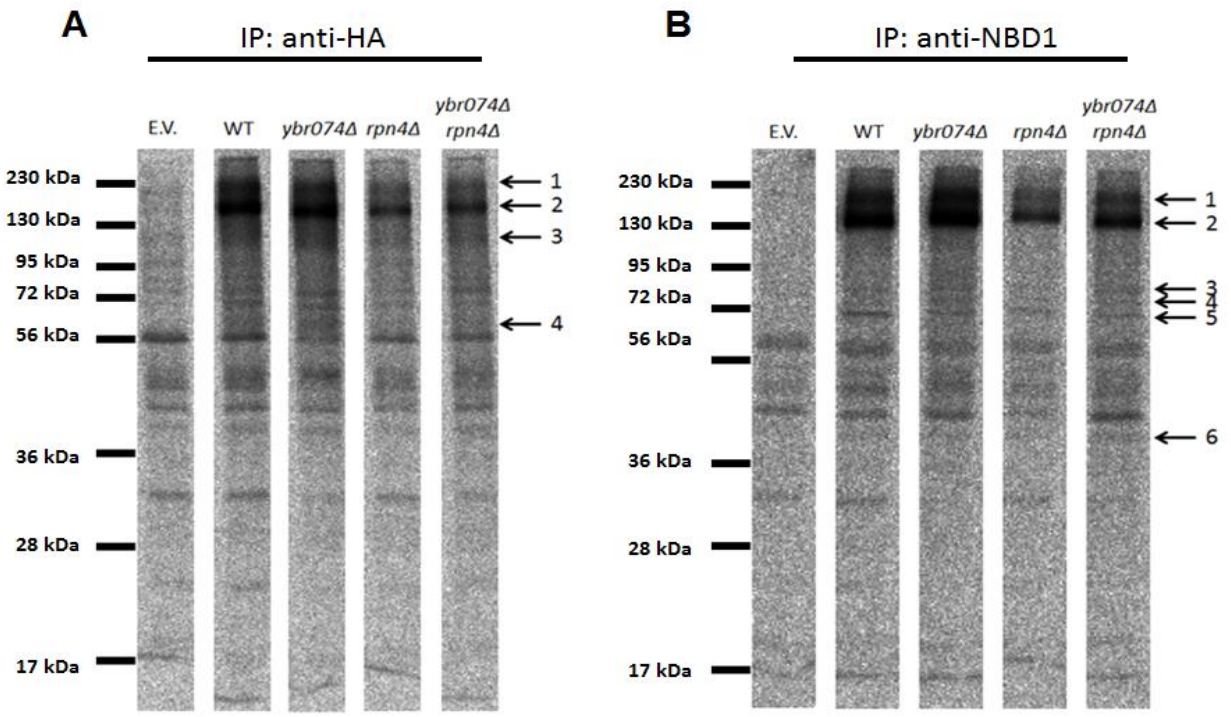

Figure 18: Comparison of CFTR-derived fragments in wild type, *ybr074Δ*, *rpn4Δ*, and *ybr074Δ rpn4Δ* strains.

Bands indicated by arrows appear in strains expressing CFTR and not in a wild type strain transformed with an empty vector (E.V.). Band 2 represents full-length CFTR, ~140 kDa. Strains expressing CFTR-HA were immunoprecipitated using an A) anti-HA antibody or B) the anti-NBD1 antibody, 3g11. All CFTR-derived fragments appear in all of the strains tested (n=2).

3.3.1.4 Does ablation of *YBR074* and 26S proteasome function lead to synergistic effects on cell growth?

Accumulation of misfolded proteins in the ER can lead to cytotoxicity, as has been documented in cases of human endocrine ER storage diseases and liver disease (Guerriero & Brodsky, 2012; Kim & Arvan, 1998). As mentioned above, in yeast and in mammals, when the nascent protein

folding capacity of the ER is overwhelmed by the accumulation of misfolded proteins, a transcriptional stress response known as the UPR is induced. This transcriptional program results in the upregulation of genes involved in both ERAD and protein folding in response to ER stress (Travers et al, 2000). Overexpression of the ERAD substrate CPY* in yeast induces both the UPR and an "overflow" pathway that targets excess CPY* to the vacuole for degradation. However, when the gene encoding a vacuolar protease, Pep4, is disrupted in this strain, the accumulation of CPY* in the ER becomes toxic (Spear & Ng, 2003).

It was also noted above that the expression of CFTR in yeast is neither toxic nor does it induce the UPR (Zhang et al, 2001). Furthermore, immunofluorescence analysis has demonstrated that CFTR is localized in the ER and not the vacuole in yeast (Sullivan et al, 2003; Zhang et al, 2001). In the absence of UPR induction or a vacuolar "overflow" pathway, an alternative mechanism may be protecting cells from CFTR-induced toxicity. To address the hypothesis that Ybr074 is involved in mediating CFTR tolerance in yeast, strains expressing CFTR were examined for growth defects under conditions when Ybr074 function, the 26S proteasome function, or both were disrupted.

To impair 26S proteasome activity, the multidrug transporter, Pdr5, was disrupted in order to allow retention of the 26S proteasome peptide aldehyde inhibitor, MG132 (Lee & Goldberg, 1998). In the absence of MG132, wild type, *ybr074Δ*, *pdr5Δ*, and *pdr5Δ ybr074Δ* strains expressing CFTR exhibited similar growth rates. However, inhibition of 26S proteasome activity using MG132 slowed down the growth of both *pdr5Δ*, and *pdr5Δ ybr074Δ* strains. Since these strains were affected to a similar extent by the addition of MG132, it appears that Ybr074 and the 26S proteasome do not function in synergy to mediate the quality control of CFTR.

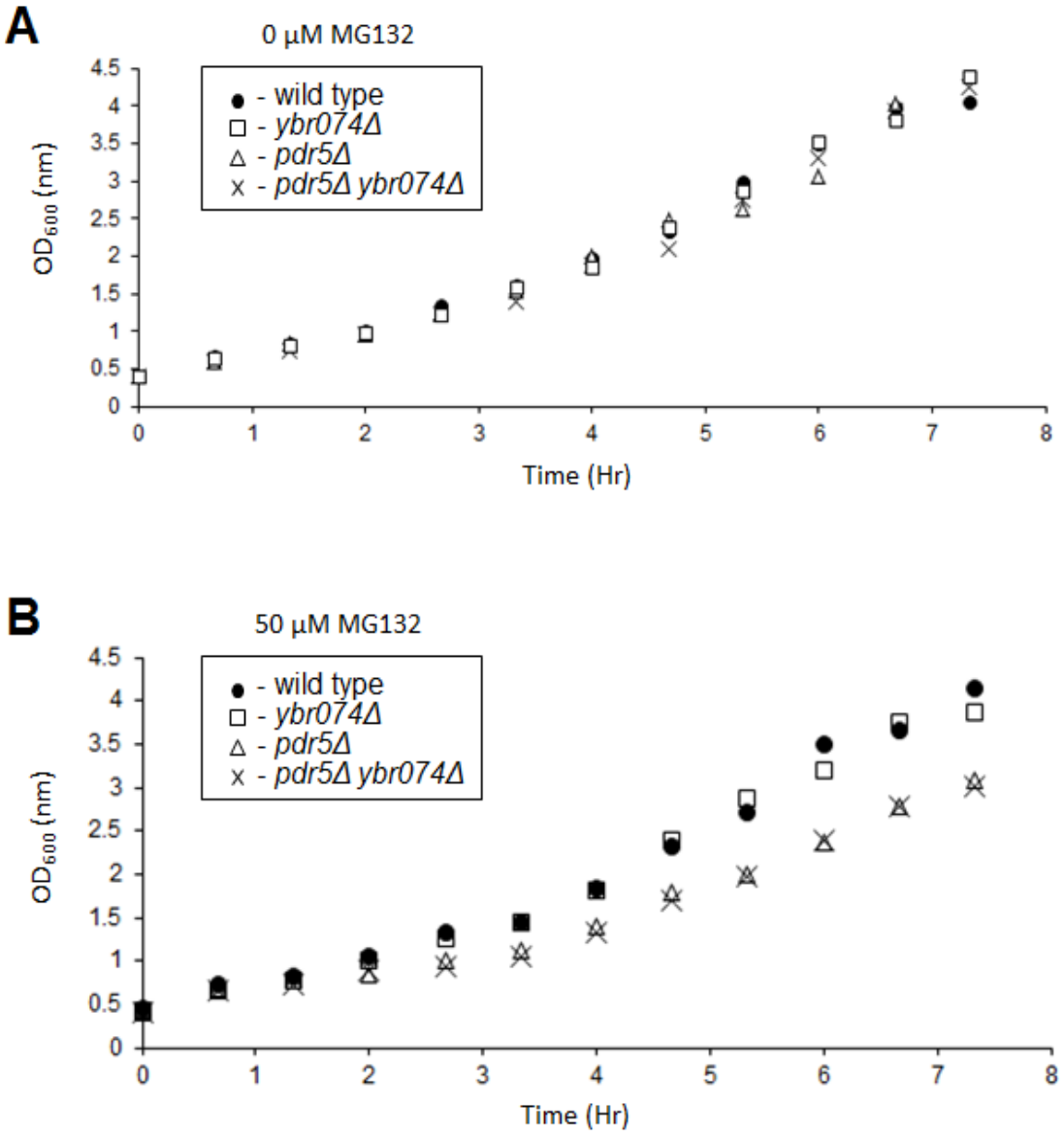

Figure 19: Growth curve of strains impaired for Ybr074 and/or 26S proteasome function.

All strains shown above were expressing CFTR and were grown in selective media lacking uracil. A) In the absence of the 26S proteasome inhibitor, MG132, the indicated strains exhibit similar growth curves at 30°C. B) In the presence of 50 µM MG132, *pdr5Δ*, and *pdr5Δybr074Δ* exhibit a growth curve lagging to a similar extent as compared to wild type and *ybr074Δ* strains (n=1).

3.3.2 Do genetic and chemical-genetic interactions between *YBR074* and other genes link this protein to cellular processes?

A genetic approach toward understanding the function of Ybr074 was employed primarily using genetic interaction data from a synthetic genetic array (SGA) screen conducted by the Boone lab (University of Toronto, Toronto, Canada) (Tong & Boone, 2006). SGA is an automated, high-throughput method of double mutant yeast strain construction intended for analysis of genetic interactions. Robotic manipulations are used to systematically cross a query single deletion strain to an array of single gene deletion mutants (Tong & Boone, 2006). Genetic interactions are identified using colony size as an indicator of fitness. A genetic interaction is identified when double mutant progeny exhibit an unexpected phenotype compared to the fitness of each individual parental strain: a "negative" interaction refers to progeny exhibiting fitness lower than expected, and a "positive" interaction refers to progeny exhibiting fitness greater than expected. Genetic interactions are quantified using an SGA score (ε), which is calculated by: $\varepsilon = f_{ab} - (f_a \times f_b)$, where f_{ab} represents progeny fitness, while f_a and f_b represent the fitness of individual parental strains (Koh et al, 2010).

When non-essential genes of the yeast genome were organized based on common genetic interaction profiles, genes with shared biological function clustered together. This resulted in the "guilt by association" hypothesis, which posits that the function of an uncharacterized gene can be inferred based on the function of known genes found in the same cluster (Tong et al, 2001).

Another method used to infer the function of uncharacterized genes involves characterizing drug sensitivity profiles. This method uses bioactive compounds with known targets to disrupt a specific biochemical pathway and identify genes linked to this pathway by

chemical-genetic interaction (Parsons et al, 2004). These chemical-genetic interactions were also used to examine biological functions of Ybr074.

To date, 1673 potential ORFs have been queried by SGA analysis against an array of strains representing 3885 ORFs. Although the *ybr074Δ* strain was not itself used as a query strain, it was represented on the array. Therefore, although this is not an exhaustive list of *YBR074* genetic interactions, Figure 20A,B show that 34 out of 1673 query genes exhibited a genetic interaction with *YBR074*.

Using the Gene Ontology Term Finder, no significantly enriched GO function and GO process terms were identified among the 34 genes exhibiting genetic interaction with *YBR074*. However, ~85% of genes were categorized under the GO component term "membrane-bound organelle" (GO ID: 43227). In the absence of any clear links to any biological function, I manually curated the gene list and classified them into nine broad functional categories: lipid-related function, metabolic function, chromatin remodeling and transcription, ER quality control, translation, cell cycle, cell adhesion, secretion, and unknown function (Figure 20C). Of these candidates, *FUS1*, *TMN3*, and genes involved in lipid-related functions were selected for further analysis for the reasons detailed below.

A selection of genes shown in Table 7 was examined for chemical-genetic interactions using the compounds listed in Table 8. Double mutant strains grown on YPD or YPD supplemented with a stress-inducing chemical compound were compared against wild type and the parental single mutant strains. However, due to variability among tested colonies, no consistent phenotypes were observed. The only exception was an alleviating interaction observed upon treatment of *cdc48-2 ybe074Δ* strain with calcofluor white. However, this phenotype may

be caused by an unidentified third site mutation, as discussed in Section 4.2.1. Therefore, no chemical-genetic interactions can be said to have been identified by this method.

Table 7: Genes tested for chemical-genetic interactions in conjunction with *ybr074Δ*

Gene	Allele	Localization	Function
SEC63	*sec63-1*	ER	Essential subunit of the Sec63 post-translational translocation complex
CDC48	*cdc48-2*	cytosol, ER, nucleus, mitochondria, mating projection tip	AAA+ ATPase involved in retrotranslocation of ERAD substrates, autophagy, and cell wall maintenance
DEP1	*dep1Δ*	N/A	Transcriptional modulator involved in regulation of structural phospholipid biosynthesis genes
FUS1	*fus1Δ*	mating projection tip	Membrane protein localized to shmoo tip, required for cell fusion
GFA1	*gfa1-97*	N/A	Glutamine-fructose-6-phosphate amidotransferase catalyzes first step of chitin synthesis
NCR1	*ncr1Δ*	vacuole	Vacuolar membrane protein involved in sphingolipid metabolism; functional orthologue of human Niemann Pick C1 (NPC1) protein
OPI1	*opi1Δ*	ER, nucleus	Transcriptional regulator of phospholipid biosynthetic genes
STE24	*ste24Δ*	ER, nucleus, mitochondria	Highly conserved zinc metalloprotease that functions in two steps of a-factor maturation
VPS21	*vps21Δ*	late endosome, mitochondira, cytoplasm, nucleus	GTPase required for transport during endocytosis and correct sorting of vacuolar hydrolases

Table 8: Compounds used to test chemical-genetic interactions

Compound	Concentration	Effect
Cadmium chloride	50 μM	Induces oxidative stress, leads to DNA damage, triggers heavy metal stress response
Caffeine	15 mM	Inhibits Tor1 kinase, activates Pkc1-dependent Cell Wall Integrity (CWI) pathway, inhibits Ras/cAMP pathway
Calcofluor white	50 μg/mL	Binds chitin, disrupts cell wall structure and morphogenesis, activates CWI pathway
Diamide	1 mM	Induces oxidative stress by depleting glutathion, triggers CWI pathway and High Osmolarity Glycerol (HOG) pathway
Tunicamycin	1 μg/mL	Inhibits N-glycosylation of nascent proteins in the ER, induces Unfolded Protein Response (UPR) and HOG pathways

A Negative Interactions

Query ORF	Query gene name	Localization	Function
YCL027W	FUS1	shmoo tip	Membrane protein required for cell fusion; expression regulated by mating pheromone
YNL194C	YNL194C	cell periphery	Integral membrane protein required for sporulation and plasma membrane sphingolipid content
YER098W	UBP9	cytoplasm	Ubiquitin carboxyl-terminal hydrolase
YKL104C_tsq991	gfa1-97	unknown	Glutamine-fructose-6-phosphate amidotransferase; catalyzes first step of chitin biosynthesis
YDL232W	OST4	endoplasmic reticulum	Subunit of the oligosaccharyltransferase complex of the endoplasmic reticulum; type I membrane protein
YLR393W	ATP10	mitochondria	Mitochondrial inner membrane protein required for assembly of the mitrochondrial F1F0 ATP synthase
YOR294W_tsq687	rrs1-124	nucleus, nucleolus	Essential protein required for nuclear export of the 60S pre-ribosomal complex during ribosome biogenesis
YDL180W	YDL180W	vacuole	Putative protein of unknown function
YHR162W	YHR162W	mitochondria	Putative protein of unknown function
YHL020C	OPI1	nucleus	Transcriptional regulator of phospholipid biosynthetic genes
YDR540C	IRC4	cytoplasm, nucleus	Putative protein of unknown function
YGL071W	AFT1	cytoplasm, nucleus	Transcription factor involved in iron utilization and homeostasis
YAL013W	DEP1	Rpd3L complex	Transcriptional modulator involved in regulation of structural phospholipid biosytnthesis genes
YOR089C	VPS21	late endosome	GTPase required for transport during endocytosis and correct sorting of vacuolar hydrolases
YKR072C	SIS2	cytoplasm, nucleus	Involved in regulating co-enzyme A biosynthesis
YPR120C	CLB5	nucleus	B-type cyclin involved in DNA replication during S phase
YKR028W	SAP190	cytoplasm	Protein involved in cell wall cytoskeleton organization
YAL026C	DRS2	Golgi	Aminophospholipid translocase (flippase) maintains membrane lipid asymmetry in post-Golgi secretory vesicles
YGL064C	MRH4	mitochondria	ATP-dependent RNA helicase of the DEAD-box family with essential role in mitochondrial function
YDL126C_tsq209	cdc48-2	cytosol, endoplasmic reticulum membrane, mitochondria, nucleus	AAA+ ATPase involved in retrotranslocation of ERAD substrates, autophagy, and cell wall maintenance

B Positive Interactions

Query ORF	Query gene name	Localization	Function
YFR037C_tsq1000	rsc8-ts16	nucleus	Component of the RSC chromatin remodeling complex
YJL176C	SWI3	nucleus	Subunit of the SWI/SNF chromatin remodeling complex
YDL064W_tsq370	ubc9-2	nucleus	SUMO-conjugating enzyme required for mitotic control
YDL215C	GDH2	mitochondria	NAD+-dependent glutamate dehydrogenase involved in nitrogen metabolism
YOR254C_tsq231	sec63-1	endoplasmic reticulum	Essential subunit of the Sec63 post-translational tranlocation complex
YER113C	TMN3	Golgi	Nuclear pore protein involved in export of pre-tRNA and mature tRNA after retrograde import from the cytoplasm
YKL205W	LOS1	cytoplasm, nucleus	Protein with role in cell adhesion and filamentous growth
YMR194C-B	CMC4	mitochondria	Protein localized to mitochondrial intermembrane space
YNR010W	CSE2	nucleus	Subunit of the RNAP II mediator complex required for regulation of RNA polymerase II activity
YMR044W	IOC4	nucleus	Acts within coding regions to coordinate transcription elongation with termination and processing
YGR156W_tsq477	pti1-ts7	nucleus	Essential component of cleavage and polyA factor involved in 3' end formation of snoRNA and mRNA
YOR311C	DGK1	endoplasmic reticulum	Diacylglycerol kinase
YGL235W	YGL235W	unknown	Putative protein of unknown function
YGL084C	GUP1	plasma membrane, endoplasmic reticulum	Plasma membrane protein involved in remodeling GPI anchors, and in glycerol transport

C

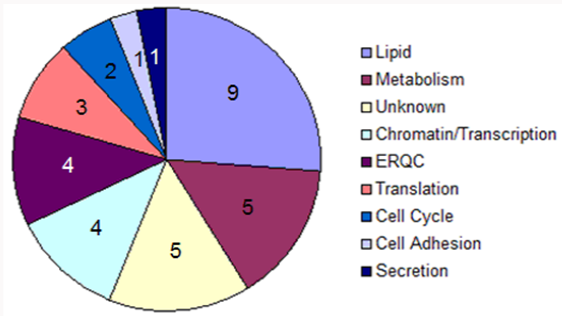

Figure 20: Genes interacting with *YBR074* by Synthetic Genetic Array (SGA) analysis

A) Genes that exhibit a negative genetic interaction with *YBR074* by SGA analysis are shown. B) Genes that exhibit a positive genetic interaction with *YBR074* by SGA analysis are shown. C) Manually curated functional categories representing all 34 genes found to interact with *YBR074* by SGA analysis. Categories are based on descriptions of gene function obtained from the *Saccharomyces cerevisiae* Genome Database (SGD), www.yeastgenome.org.

3.3.2.1 Does *YBR074* play a role in yeast mating?

FUS1 encodes a membrane protein that localizes to the mating projection known as the shmoo tip, and facilitates membrane fusion between mating partners (Nolan et al, 2006). Because *FUS1* displayed the strongest genetic interaction with *YBR074*, a qualitative mating assay was conducted to determine whether Ybr074 plays a role in yeast mating.

Strains of one mating type were mixed with a serial dilution of the opposite mating type and spotted onto medium selective for diploids. As expected, *fus1Δ* strains of the opposite mating type did not fuse efficiently, and few diploids were recovered compared to wild type. However, *ybr074Δ* strains of the opposite mating type grew similarly to wild type on diploid selective medium (Figure 21). This suggests that *YBR074* is not required for efficient mating.

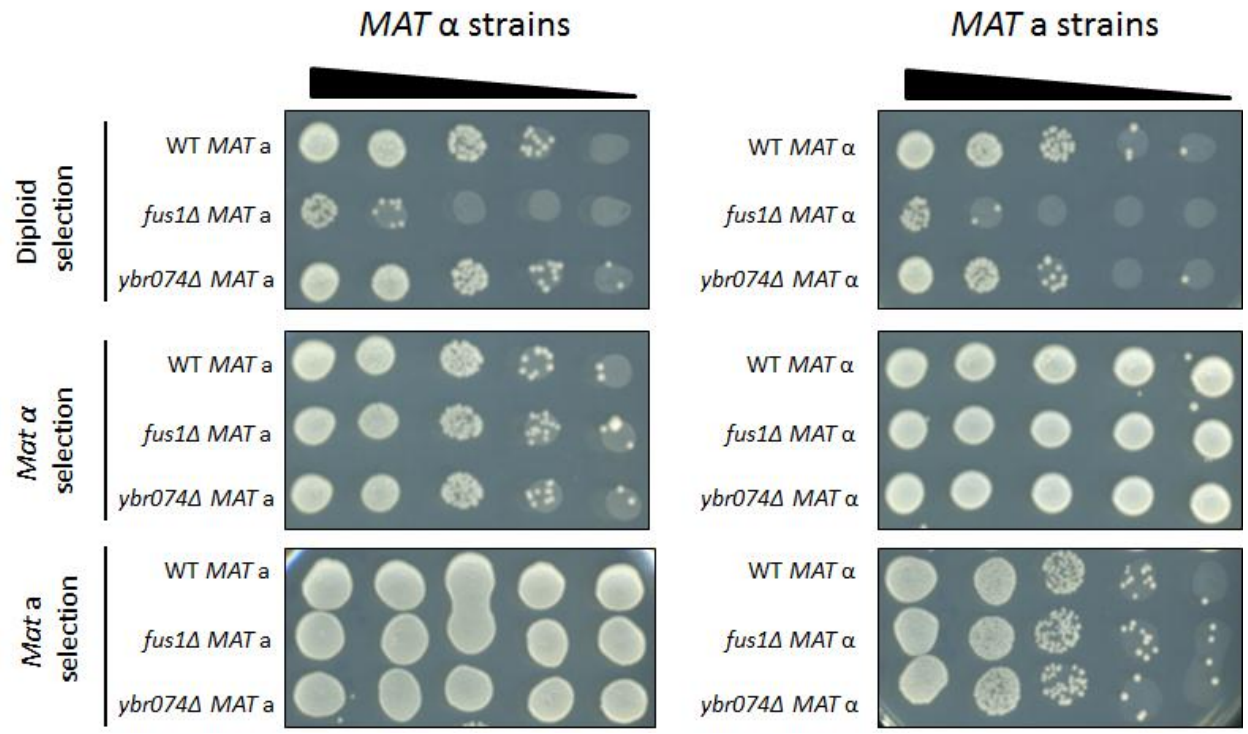

Figure 21: Qualitative mating assay showing no Ybr074-dependent defect in mating.

The left panel shows the *MAT* a strains, which were mixed with a serial dilution of *MAT* α strains. The right panel shows *MAT* α strains, which were mixed with a serial dilution of *MAT* a strains. Media lacking lysine and methionine is selective for diploids. Media lacking lysine is selective for *MAT* α strains and diploids. Media lacking methionine is selective for *MAT* a strains and diploids (n=2).

3.3.2.2 Does *YBR074* function in the transition to pseudohyphal growth in nutrient-limited conditions?

When exposed to certain environmental cues, such as nitrogen starvation, *S. cerevisiae* mounts a transcription response that alters the cell's morphology and budding pattern. This promotes a transition from a unicellular morphology to a filamentous morphology that mediates

substrate adhesion and invasion, and is thought to facilitate nutrient foraging. This adaptation is referred to as pseudohyphal growth, and depends largely on the activating transcription factor Flo8 (Froquet et al, 2008). However, the S288C-derived strain used predominantly in both this study and in the literature (BY4741 *MAT* a, and BY4742 *MAT* α), bears a mutation in the *FLO8* gene that inhibits formation of pseudohyphae. Intriguingly, *TMN3*, a gene involved in mediating pseudohyphal growth, displayed a genetic interaction with *YBR074*, suggesting that there may be a role for *YBR074* is pseudohyphal growth (Froquet et al, 2008).

To address this hypothesis, *YBR074* was disrupted in the strain Σ1278b, known to exhibit extensive filamentous growth under well-defined growth conditions (Gimeno et al, 1992; Grenson, 1966). Because fusel alcohols are a byproduct of amino acid metabolism under nitrogen starvation conditions, filamentous growth was induced in liquid culture using 1% butanol to examine cellular morphology as described (Jin et al, 2008; Lorenz et al, 2000). Cell adhesion and invasion were examined under starvation conditions on solid medium as described (Guldal & Broach, 2006). As expected, the S288C-derived strain, BY4741, did not form pseudohyphae under pseudohyphal-inducing conditions. However, both wild type and *ybr074Δ* strains in the Σ1278b genetic background displayed filamentous growth, adhesion, and invasion of solid media under pseudohyphal-inducing conditions (Figure 22). This suggests that *YBR074* is not required for transition to pseudohyphal growth.

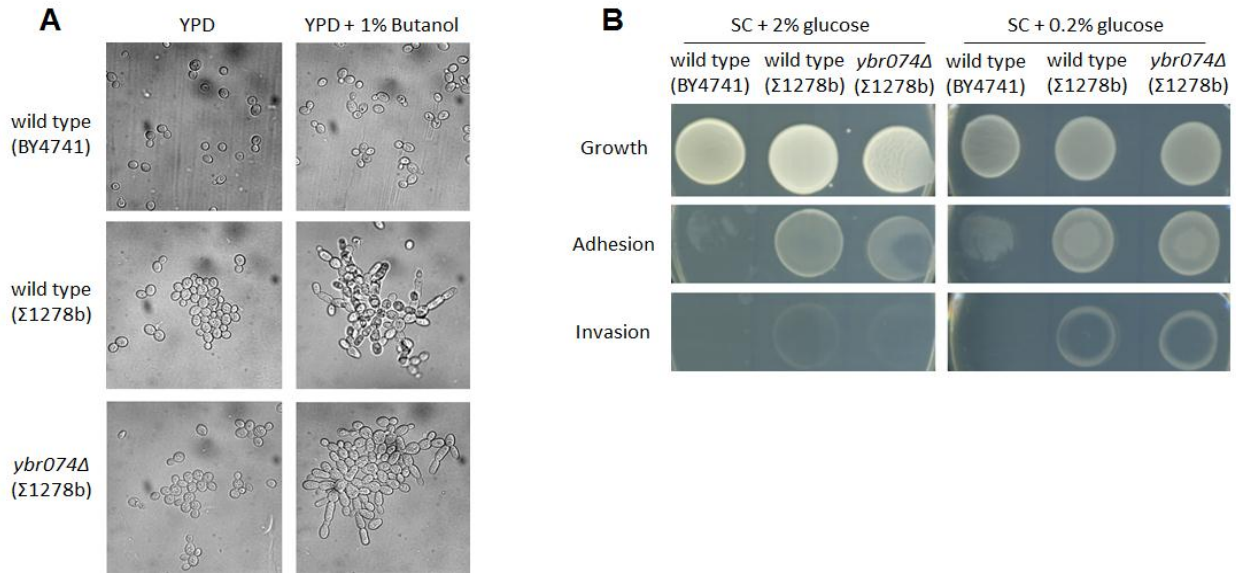

Figure 22: Pseudohyphal growth does not require Ybr074

A) Morphological changes induced by supplementing YPD with 1% butanol (vol/vol) were observed in both wild type and *ybr074Δ* strains in the Σ1278b genetic background. B) Growth, adhesion, and invasion of solid media are shown under nutrient rich (SC + 2% glucose) and nutrient starvation (SC + 0.2% glucose) conditions. Wild type and *ybr074Δ* strains in the Σ1278b genetic background exhibit the adhesion and invasion phenotypes, while the S288C-derived strain, BY4741, does not.

3.3.3 Does the phylogenetic profile of *YBR074* hint at its function?

Over the course of evolution, organisms experience environmental pressures that can accelerate or decelerate the mutability of their protein-coding genes. This produces a phylogenetic signature for each protein, which can be measured as its evolutionary rate of variation. Proteins that interact physically or functionally have been shown to exhibit similar phylogenetic signatures. Therefore, by measuring the evolutionary rate of covariation (ERC) of protein pairs across the

proteome of *Saccharomyces cerevisiae*, it may be possible to infer the function of Ybr074 by identifying its covarying proteins partners (Clark et al, 2012).

No statistically significant GO terms were enriched among the genes exhibiting evolutionary rate covariance with Ybr074 (Table 9) (Clark et al, 2012). However, it is interesting to note that six out of 30 genes were linked to vacuolar function (Vps41, Yhc3, Rcr2, Prb1, Vps13, Atg15), and seven out of 30 genes were linked to lipid or cell wall related function (Ymr086p, Rlm1, Yke4, Ydl109p, Sfl1, Lcl2, Gpi8).

Table 9: Genes related to *YBR074* by evolutionary rate of covariation.

Gene	Localization	Description
YMR086W	cell periphery	Protein of unknown function; possible component of the eisosome; expression is repressed by cAMP
YFL042C	N/A	Putative protein of unknown function; YFL042C is not an essential gene
VPS41	vacuolar membrane	Subunit of the homotypic vacuole fusion and vacuole protein sorting (HOPS) complex
HSF1	nucleus	Trimeric heat shock transcription factor
LRP1	N/A	Nuclear exosome-associated nucleic acid binding protein; involved in RNA processing, surveillance, degradation,
RLM1	cytoplasm, nucleus	MADS-box transcription factor, component of the protein kinase C-mediated MAP kinase pathway involved in the
YKE4	ER	Zinc transporter; localizes to the ER; null mutant is sensitive to calcofluor white, leads to zinc accumulation in cytosol
YHC3	vacuolar membrane	Protein involved in the ATP-dependent transport of arginine into the vacuole and possibly in balancing ion
PEX6	peroxisomes	AAA-peroxin, participates in the recycling of peroxisomal signal receptor Pex5p from the peroxisomal membrane to
BOI1	bud, bud neck, cell periphery, cytoplasm	Protein implicated in polar growth, functionally redundant with Boi2p; interacts with bud-emergence protein Bem1p
MRPL17	mitochondria	Mitochondrial ribosomal protein of the large subunit
YDL109C	N/A	Putative lipase; involved in lipid metabolism; YDL109C is not an essential gene
ICL2	mitochondria	2-methylisocitrate lyase of the mitochondrial matrix, functions in the methylcitrate cycle to catalyze the conversion of 2-methylisocitrate to succinate and pyruvate
FUN19	N/A	Non-essential protein of unknown function; expression induced in response to heat stress
RCR2	cytoplasm, vacuole	Vacuolar protein that presumably functions within the endosomal-vacuolar trafficking pathway
PRB1	vacuole	Vacuolar proteinase B (yscB), a serine protease of the subtilisin family; involved in protein degradation in the vacuole and required for full protein degradation during sporulation
SFL1	nucleus	Transcriptional repressor and activator; involved in repression of flocculation-related genes, and activation of stress
MLH3	N/A	Protein involved in DNA mismatch repair and crossing-over during meiotic recombination
MDV1	mitochondria	Peripheral protein of the cytosolic face of the mitochondrial outer membrane, required for mitochondrial fission
SRC1	nuclear periphery	Inner nuclear membrane protein that functions in regulation of subtelomeric genes and is linked to TREX
YOR296W	cytoplasm	Putative protein of unknown function; green fluorescent protein (GFP)-fusion protein localizes to the cytoplasm; expressed during copper starvation
VPS13	cytoplasm, endosomes	Involved in sporulation, vacuolar protein sorting and protein-Golgi retention;peripherally associated with membranes
YBP1	cytoplasm	Protein required for oxidation of specific cysteine residues of the transcription factor Yap1p, resulting in the nuclear localization of Yap1p in response to stress
LCL2	N/A	Putative protein of unknown function; mutant is deficient in amounts of cell wall mannosylphosphate; genetic interactions suggest a role in ERAD
ATG15	vacuole	Lipase required for intravacuolar lysis of autophagic bodies and Cvt bodies; targeted to intravacuolar vesicles during autophagy via the multivesicular body (MVB) pathway
SAM37	mitochondria	Component of the Sorting and Assembly Machinery (SAM or TOB complex) of the mitochondrial outer membrane
AIM11	N/A	Protein of unknown function; null mutant is viable but shows increased loss of mitochondrial genome and synthetic interaction with prohibitin (phb1)
GPI8	ER	ER membrane glycoprotein subunit of the glycosylphosphatidylinositol transamidase complex that adds glycosylphosphatidylinositol (GPI) anchors to newly synthesized proteins
SLD3	cytoplasm, nucleus	Protein involved in the initiation of DNA replication, required for proper assembly of replication proteins at the origins of replication; interacts with Cdc45p
DYN1	cytoplasm	Cytoplasmic heavy chain dynein, microtubule motor protein, required for anaphase spindle elongation

3.3.4 Can a substrate for Ybr074 be identified using proteomic approaches?

The following proteomic approaches were based on the notion that disrupting a protease would result in accumulation of its substrate(s). Two methods were used to attempt to identify the substrate(s) of Ybr074: 2D in-Gel Electrophoresis (DiGE), and a fluorescence-based proteomic screen using a library of yeast strains each expressing a different GFP-tagged protein (Cohen & Schuldiner, 2011; Huh et al, 2003; May et al, 2012; Rimon & Schuldiner, 2011).

DiGE is an approach whereby the total protein content of a wild type and a *ybr074Δ* strain is extracted and differentially labeled using unique fluorescent probes, most commonly cyanine-3 (Cy3) and cyanine-5 (Cy5). Labeled proteins from each strain are resolved on a single gel by 2D-gel electrophoresis and compared for differences in fluorescence intensity associated with each protein spot (Unlu et al, 1997). Protein spots can then be cut out of the gel and identified by mass spectrometry. This method informs on the average protein content of a population of cells, and has been used to detect changes in protein levels associated cancer-specific markers, for example (Zhou et al, 2002). This method can also be used to identify substrates of enzymes mediating post-translational modifications, as was achieved for the serine protease, granzyme B (Bredemeyer et al, 2004).

The relative abundance of each protein spot in wild type and *ybr074Δ* strains was compared by calculating the ratio of each *ybr074Δ* protein spot to its corresponding wild type protein spot. The majority of protein content (88.6%) visualized by this method was similar across both strains. The results did show 112 spots (5%) decreased in the *ybr074Δ* strain as compared to wild type, and 145 spots (6.4%) that had accumulated in the *ybr074Δ* strain as compared to wild type. As mentioned above, proteins that accumulated in the *ybr074Δ* strain

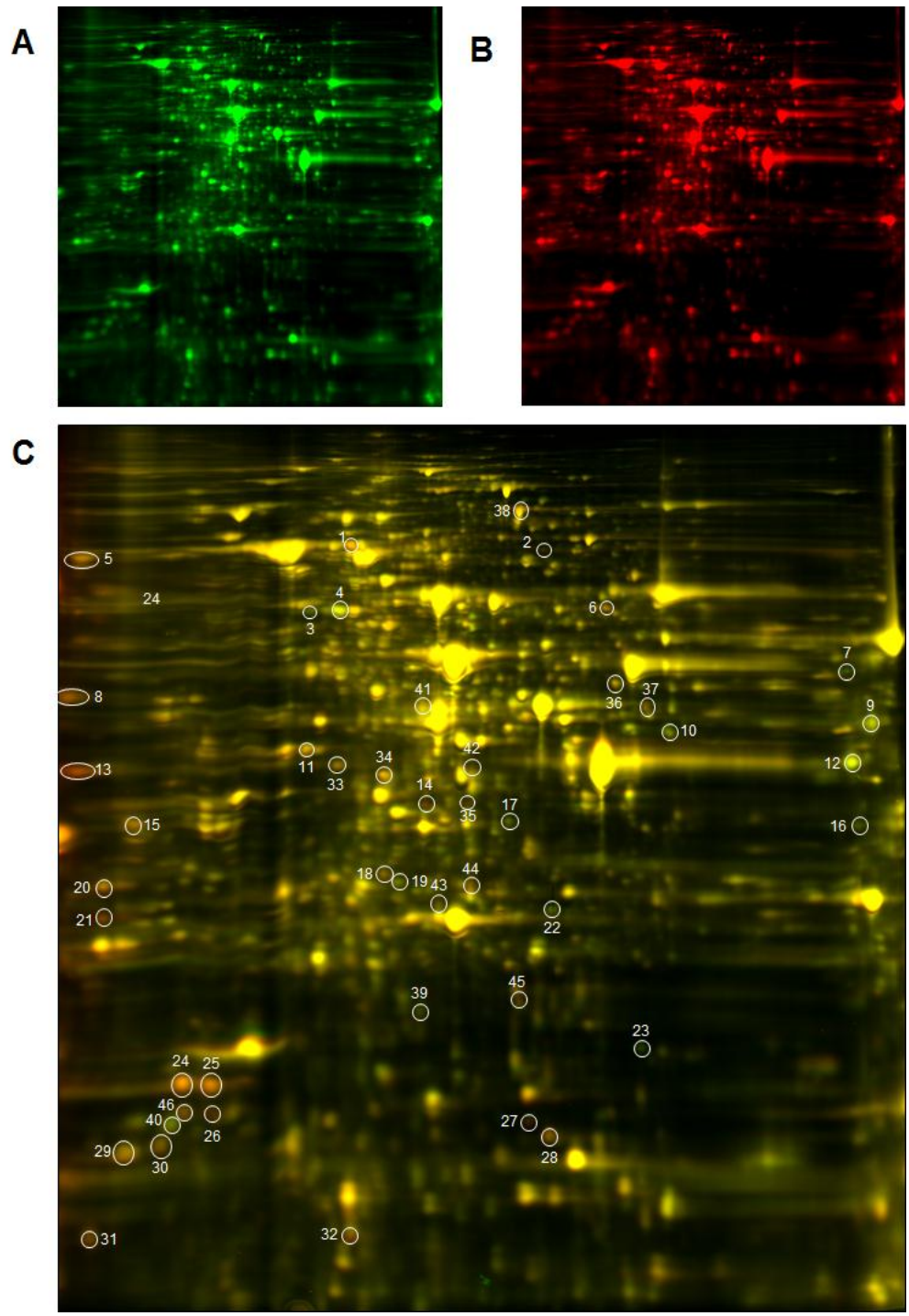

Figure 23: 2D DiGE comparing wild type and *ybr074Δ* protein levels

The relative abundance of protein from the A) wild type strain and B) *ybr074Δ* strain are quantitatively compared in the C) merge image, with protein spots showing noticeable changes in level of expression circled and numbered for identification.

may represent substrates of Ybr074. Alternatively, these proteins may have accumulated as an indirect effect of disrupting Ybr074 function. In order to differentiate between these possibilities, candidate protein spots were selected for identification and further investigation by western blot analysis in wild type and *ybr074Δ* strains.

Ten protein spots were selected for identification by mass spectrometry based on a high ratio of *ybr074Δ* to wild type levels, high molecular mass, or being in a close proximity to a protein spot of lower molecular mass that displayed a decrease in *ybr074Δ* to wild type levels, suggesting a Ybr074-dependent shift from a high molecular mass product, to a lower molecular mass product as exemplified by spots 14 and 35, shown in Figure 24.

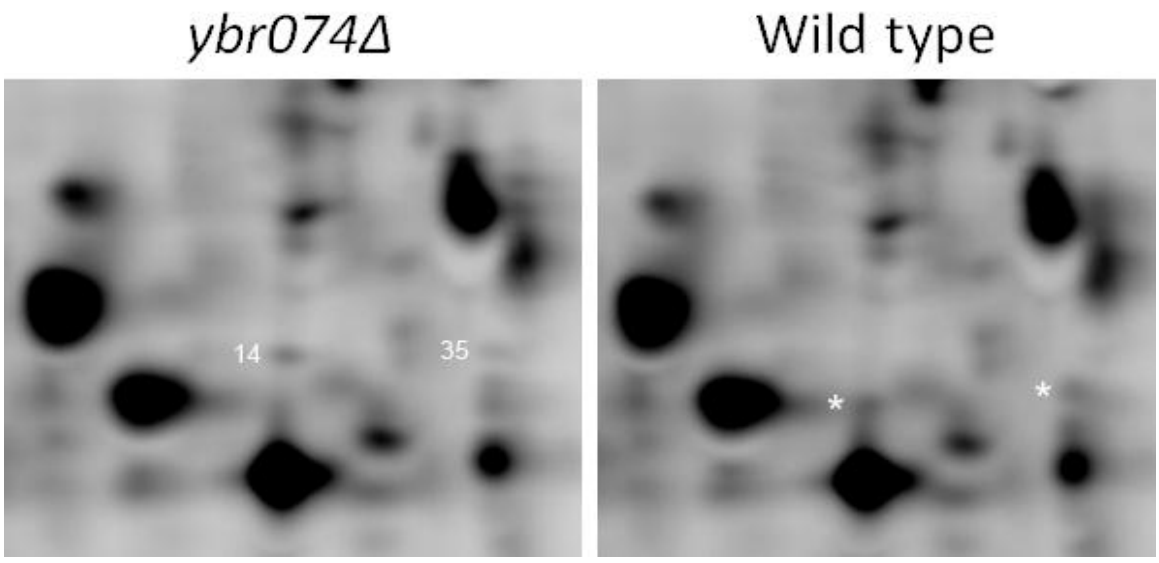

Figure 24: Apparent shift of spots 14 and 35 from a higher molecular weight in the *ybr074Δ* sample to a lower molecular weight in the wild type sample.

Protein spots 14 and 35 are labeled in the left panel. Spots neighboring 14 and 35, denoted by asterisks, appear more abundant in the wild type sample and have a lower molecular mass than spots 14 and 35.

The genes encoding the protein spots selected for identification are shown in Table 10. It is interesting to note that the vacuolar protease, Pep4, accumulated in a *ybr074Δ* strain. It is possible that loss of Ybr074 function at the vacuole is partially compensated for by increased abundance of Pep4.

Among the proteins identified in this assay, Rhr2 was intriguing because of its role in glycerol synthesis as a response to osmotic stress. Osmotic stress can be caused by damage to the cell wall upon treatment with the cell wall digesting enzyme, zymolyase. Cell wall damage caused in this manner results in the induction of two parallel signaling pathways known as the Cell Wall Integrity (CWI) and High-Osmolarity Glycerol (HOG) signaling pathways (Rodriguez-Pena et al, 2010). Since genetic interactions of *YBR074* with genes related to maintenance of cell wall integrity have been reported by the Boone lab, as previously mentioned, I was interested in verifying whether the accumulation of Rhr2 in the *ybr074Δ* strain resulted from loss of Ybr074-dependent degradation of Rhr2, or whether the accumulation might be attributed to an indirect effect of disrupting Ybr074 function.

To do this, N-terminally 3HA-tagged Rhr2 was constructed and expressed from a galactose promoter in wild type cells. 3HA-Rhr2 isolated from these cells was examined by Western blot analysis for Ybr074-dependent fragments that might result from degradation. However, no Ybr074-dependent Rhr2 fragments were observed (Figure 25). This suggests that accumulation of Rhr2 in *ybr074Δ* cells may have been an indirect effect of loss of Ybr074 function. (It is important to note that accumulation of Rhr2 was not expected in this experiment because the protein was highly overexpressed in order to better visualize any generated fragments).

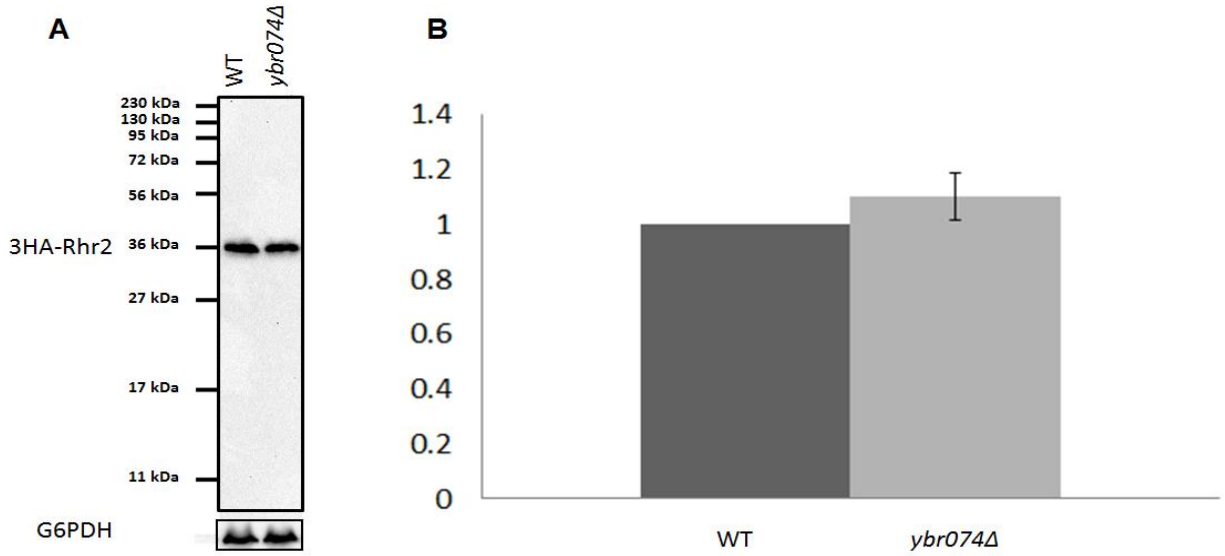

Figure 25: Rhr2 expression in wild type and *ybr074Δ* strains.

A) Total protein from cells expressing 3HA-Rhr2, which was induced by galactose for 6.5 h at 30°C, was separated by 12.5% SDS-PAGE. 3HA-Rhr2 and the loading control glyceraldehyde-6-phosphate dehydrogenase (G6PDH) were detected by Western blot. B) Relative abundance of full length Rhr2 was quantified and the SE is shown (n=4; $p>0.05$).

Table 10: Candidate substrates identified by 2D DiGE

Spot #	Systematic name	Standard name	GI #	Molecular Weight (kDa)	Protein PI	Description	Localization
1	*YJR045C*	*SSC1*	151945113	70.9	5.48	Hsp70 family ATPase, constituent of the import motor component of the Translocase of the Inner Mitochondrial membrane (TIM23 complex)	mitochondria
6	*YFL018C*	*LPD1*	15826394	51.5	6.54	Dihydrolipoamide dehydrogenase, the lipoamide dehydrogenase component (E3) of the pyruvate dehydrogenase and 2-oxoglutarate dehydrogenase multi-enzyme complexes	mitochondria
8	*YPL154C*	*PEP4*	7766834	35.7	4.35	Vacuolar aspartyl protease (proteinase A), required for the posttranslational precursor maturation of vacuolar proteinases; important for protein turnover after oxidative damage	vacuole
13	YGR167W	*CLC1*	1945336	25.5	4.31	Clathrin light chain, subunit of the major coat protein involved in intracellular protein transport and endocytosis	cytosol
14	YIL053W	*RHR2*	86558907	27.9	5.35	Constitutively expressed isoform of DL-glycerol-3-phosphatase; involved in glycerol biosynthesis	cytosol, nucleus
18	YDR399W	*HPT1*	6320607	25.2	5.46	Hypoxanthine-guanine phosphoribosyltransferase, catalyzes formation of purine nucleotides guanosine monophosphate and inosine monophosphate	cytosol nucleus
21	YKL056C	*TMA19*	151941490	18.7	4.41	Protein that associates with ribosomes; GFP-fusion protein localizes to the cytoplasm and relocates to the mitochondrial outer surface upon oxidative stress	cytosol, nucleus
25	YPR102C	*RPL11A*	6325359	19.7	9.92	Protein of the large 60S ribosomal subunit involved in ribosomal assembly	nucleus
29	YOL121C	*RPS19A*	6324451	15.9	9.61	Protein component of the small (40S) ribosomal subunit, required for assembly and maturation of pre-40 S particles	cytosol
35	YOL086C	*ADH1*	6324486	36.8	6.21	Alcohol dehydrogenase, required for the reduction of acetaldehyde to ethanol, the last step in the glycolytic pathway	cytosol

In a second approach, the fluorescence intensity was measured *in vivo* by high-content fluorescent microscopy in screening a collection of yeast strains each expressing a different GFP-tagged protein, both in the wild type or *ybr074Δ* genetic background. Using this approach, data are collected from individual cells rather than a population. This work was performed by Dr. Maya Schuldiner's group (Department of Molecular Genetics, Weizmann Insititute of Science, Rehovot, Israel). The Schuldiner lab has validated this approach in a related study aimed at identifying substrates dependent on the cargo receptor, Erv14, for ER exit. This was achieved by crossing an *erv14Δ* mutant strain to the GFP-tagged yeast library, and identifying GFP-tagged substrates that accumulated in the ER of mutant strains as compared to wild type strains (Herzig et al, 2012). Similarly, it was hypothesized that substrates of Ybr074 might accumulate in a *ybr074Δ* strain as compared to a wild type strain.

Results of the GFP-tagged yeast library screen identified 72 proteins that accumulated in the absence of Ybr074 activity, and 28 proteins with decreased levels in the absence of Ybr074 (Tables 11-12). No statistically significant GO terms were enriched among these candidates. It is interesting to note that the majority of proteins, ~70%, which accumulated in the *ybr074Δ* strain were annotated using the GO-Slim Component term "cytoplasm". However, it is important to keep in mind that ~60% of the yeast genome is annotated to this term. No vacuolar proteases were found among the proteins identified in this screen. However, the vacuolar protein sorting factor, Vps70 was among the proteins that accumulated in the absence of Ybr074 activity.

Table 11: GFP-tagged proteins exhibiting increased levels in ybr074Δ strain compared to wild type

Gene	Ratio	Localization	Description
SDA1	1.23	nucleus	Highly conserved nuclear protein required for actin cytoskeleton organization
SNZ1	1.25	N/A	Protein involved in vitamin B6 biosynthesis
ERR3	1.30	cytosol	Protein of unknown function, has similarity to enolases
YAL069W	1.32	N/A	Dubious open reading frame unlikely to encode a protein
YHR022C	1.39	N/A	Putative protein of unknown function
YIL169C	1.40	N/A	Putative protein; similar to YOL155C, a putative glucan alpha-1,4-glucosidase
EMI1	1.52	N/A	Required for induction of the early meiotic-specific transcription factor IME1
PUS5	1.53	mitochondria	Pseudouridine synthase, catalyzes formation of pseudouridine in mitochondrial 21S rRNA
SAG1	1.57	cell wall	Alpha-agglutinin of alpha-cells, binds to Aga1p, C-terminal half is GPI anchored
AVO1	1.89	cytosol, plasma membrane	Component of a membrane-bound complex containing the Tor2p kinase and other proteins
STE3	1.94	plasma membrane	Receptor for a factor pheromone, mediates pheromone response
VPS70	2.05	N/A	Protein of unknown function involved in vacuolar protein sorting
YDL218W	2.12	N/A	Putative protein; transcription is induced by starvation and aerobic conditions
DIN7	29.41	mitochondria	Mitochondrial nuclease functioning in DNA repair and replication
THI20	1.39	cytosol	Multifunctional protein with kinase involved in thiamine biosynthesis and degradation
FLC1	1.49	ER, bud neck, cell periphery, vacuole	Putative FAD transporter; required for uptake of FAD into ER; involved in cell wall maintenance
TNA1	1.39	plasma membrane, ER, mitochondria	High affinity nicotinic acid plasma membrane permease
HXT2	1.37	plasma membrane, vacuole	High-affinity glucose transporter of the major facilitator superfamily

Gene	Ratio	Localization	Description
CPA1	1.21	cytosol	Small subunit of carbamoyl phosphate synthetase; synthesis of citrulline, an arginine precursor
TEF1	1.24	cytosol, mitochondria	Translational elongation factor EF-1 alpha
RPL40B	1.25	cytosol, mitochondria	Fusion protein, cleaved to yield ubiquitin and a ribosomal protein of the 60S ribosomal subunit
YAT2	1.26	cytosol	Carnitine acetyltransferase; similar to Yat1p, a carnitine acetyltransferase associated with mitochondria
RPS19B	1.27	cytosol	Protein component of the 40S ribosomal subunit, required for assembly and maturation of pre-40S
YLR364W	1.27	cytosol	Glutaredoxin that employs a dithiol mechanism of catalysis
ADE17	1.29	cytosol, plasma membrane	Enzyme of 'de novo' purine biosynthesis
STM1	1.30	cytosol	Protein required for optimal translation under nutrient stress; involved in TOR signaling
SER1	1.33	cytosol	3-phosphoserine aminotransferase, required for serine and glycine biosynthesis
YML131W	1.34	cytosol	Putative protein of unknown function with similarity to medium chain dehydrogenase/reductases
SIP18	1.36	cytosol	Phospholipid-binding protein; expression is induced by osmotic stress
GCD11	1.45	cytosol	Gamma subunit of the translation initiation factor eIF2, involved in the identification of the start codon
ATX1	1.47	cytosol	Cytosolic copper metallochaperone; transports copper to the secretory vesicle copper transporter Ccc2p
RPS30B	1.50	cytosol	Protein component of 40S ribosomal subunit; nearly identical to Rps30Ap and similar to rat S30 ribosomal protein
GRE1	2.04	cytosol	Hydrophilin of unknown function; stress induced; regulated by the HOG pathway
PUB1	2.81	cytosol, nucleus	Poly (A)+ RNA-binding protein; required for stability of many mRNAs
SOL1	1.22	cytosol, nucleus	Protein with a possible role in tRNA export

Gene	Ratio	Localization	Description
ADH5	1.22	cytosol, nucleus	Alcohol dehydrogenase isoenzyme V; involved in ethanol production
ADE1	1.24	cytosol, nucleus	N-succinyl-5-aminoimidazole-4-carboxamide ribotide (SAICAR) synthetase; purine biosynthesis
GSP2	1.26	cytosol, nucleus	GTP binding protein; maintenance of nuclear organization, RNA processing and transport
SER2	1.26	cytosol, nucleus	Phosphoserine phosphatase of the phosphoglycerate pathway; serine and glycine biosynthesis
TDH2	1.27	cytosol, nucleus, plasma membrane, cell wall, lipid droplet, mitochondria	Glyceraldehyde-3-phosphate dehydrogenase; glycolysis and gluconeogenesis
SHP1	1.29	cytosol, nucleus	UBX domain-containing protein; degradation of ubiquitylated substrate with Cdc48
TKL2	1.34	cytosol, nucleus	Transketolase, functions in the pentose phosphate pathway; synthesis of aromatic amino acids
YNL313C	1.44	cytosol, nucleus	Essential protein of unknown function; GFP-tagged protein localizes to cytoplasm and nucleus
PIR1	1.50	cell wall, cytosol, nucleus	O-glycosylated protein required for cell wall stability
NTO1	1.58	cytosol, nucleus	Subunit of the NuA3 histone acetyltransferase complex that acetylates histone H3
HSH155	1.70	cytosol, nucleus	U2-snRNP associated splicing factor
SNF7	1.22	endosomes, cytosol	Subunit of the endosomal sorting complex required for transport III (ESCRT-III)
SEC65	1.34	ER, cytosol	Subunit of the signal recognition particle (SRP), involved in protein targeting to the ER
RTN2	1.29	ER	Protein of unknown function; similarity to mammalian RTNLA (reticulon-like A) subfamily
SED1	1.34	cell wall, ER, mitochondria	Major stress-induced structural GPI-cell wall glycoprotein in stationary-phase cells

Gene	Ratio	Localization	Description
SEC24	3.41	ER, Golgi	Component of the COPII vesicle coat; cargo selection in ER to Golgi transport
LSC1	1.23	mitochondria	Alpha subunit of succinyl-CoA ligase; mitochondrial enzyme of the TCA cycle
MRPS5	1.26	mitochondria	Mitochondrial ribosomal protein of the small subunit
YPR011C	1.33	mitochondria	Putative transporter, member of the mitochondrial carrier family
SEN54	1.39	mitochondria, cytosol	Subunit of the tRNA splicing endonuclease
ILV6	1.60	mitochondria	Regulatory subunit of acetolactate synthase; branched-chain amino acid biosynthesis
PDB1	8.26	mitochondria	E1 beta subunit of the pyruvate dehydrogenase (PDH) complex found in mitochondria
YGR283C	1.26	nucleolus, nucleus	Protein of unknown function; predicted to be involved in ribosome biogenesis
MAK5	1.22	nucleolus, nucleus	Essential nucleolar protein, putative DEAD-box RNA helicase; biogenesis of 60S ribosomal subunits
TAF6	1.20	nucleus	Subunit of TFIID and SAGA complexes; transcription initiation of RNA pol II and chromatin modification
LYS20	1.22	nucleus, mitochondria	Homocitrate synthase isozyme; lysine biosynthesis
TAL1	1.26	nucleus, cytosol	Transaldolase, enzyme in the non-oxidative pentose phosphate pathway
UTP21	1.26	nucleolus, nucleus	Subunit of U3-containing 90S preribosome and Small Subunit (SSU) processome complexes
SSL2	1.26	nucleus	Component of the holoenzyme form of RNA polymerase transcription factor TFIIH
RSC3	1.38	nucleus	Component of RSC chromatin remodeling complex; regulation of ribosomal genes and cell wall/stress response
MED4	1.42	nucleus	Subunit of the RNA polymerase II mediator complex
YGR043C	1.51	nucleus	Transaldolase of unknown function
TAF5	3.06	nucleus, cytosol	Subunit (90 kDa) of TFIID and SAGA complexes; RNA Pol II transcription initiation and chromatin modification

Gene	Ratio	Localization	Description
NCE102	1.22	plasma membrane, cytosol, vacuole, ER, mitochondria, mating projection, bud membrane	Protein of unknown function; involved in secretion of proteins that lack classical secretory signal sequences
RET3	1.47	N/A	Zeta subunit of the coatomer complex (COPI); involved in retrograde transport between Golgi and ER
GTR1	1.23	vacuole, cytosol, late endosome, nucleus	Cytoplasmic GTP binding protein; component of GSE complex, which is required for sorting of Gap1p
GNT1	1.24	Golgi, vacuole	N-acetylglucosaminyltransferase capable of modification of N-linked glycans in the Golgi apparatus

Table 12: GFP-tagged proteins exhibiting reduced levels in *ybr074Δ* strain compared to wild type

Gene	Ratio	Localization	Description
NTF2	0.47	nuclear envelope	Nuclear envelope protein, essential player in nucleocytoplasmic transport
YLR122C	0.47	N/A	Dubious open reading frame unlikely to encode a protein; partially overlaps the dubious ORF YLR123C
ARP9	0.15	nucleus	Component of SWI/SNF and RSC chromatin remodeling complexes
ILV5	0.50	mitochondria	Acetohydroxyacid reductoisomerase, mitochondrial protein; branched-chain amino acid biosynthesis
OPI9	0.41	N/A	Dubious open reading frame unlikely to encode a protein; partially overlaps the verified ORF VRP1/YLR337C
HSP30	0.47	plasma membrane	Hydrophobic plasma membrane localized, stress-responsive protein that negatively regulates the H(+)-ATPase Pma1p
RPL21B	0.31	cytosol	Protein component of the 60S ribosomal subunit, nearly identical to Rpl21Ap; similarity to rat L21 ribosomal protein
RPS6B	0.07	cytosol	Protein component of the 40S ribosomal subunit; identical to Rps6Ap; similarity to rat S6 ribosomal protein
PYC1	0.11	cytosol	Pyruvate carboxylase isoform, cytoplasmic enzyme that converts pyruvate to oxaloacetate
RPL19A	0.32	cytosol	Protein component of the large (60S) ribosomal subunit
RSE1	0.50	cytosol	Protein involved in pre-mRNA splicing; component of the pre-spliceosome; involved in ER to Golgi transport
SHM2	0.35	cytosol, nucleus, plasma membrane, mating projection tip	Cytosolic serine hydroxymethyltransferase; generating precursors for purine, pyrimidine, amino acid, and lipid biosynthesis
CDC48	0.46	cytosol, nucleus, ER, mating projection tip, mitochondria	ATPase in ER, nuclear membrane and cytosol; in a complex with Npl4p and Ufd1p participates in ERAD
DBP2	0.08	cytosol, nucleus, mitochondria	ATP-dependent RNA helicase of the DEAD-box protein family; nonsense-mediated mRNA decay and rRNA processing

Gene	Ratio	Localization	Description
MFA1	0.10	extracellular space	Mating pheromone a-factor; interacts with alpha cells to induce cell cycle arrest and other responses leading to mating
CAR2	0.35	cytosol, nucleus	L-ornithine transaminase (OTAse), catalyzes the second step of arginine degradation
RAD51	0.19	cytosol, nucleus	Strand exchange protein; involved in repair of double-strand breaks in DNA
KAP104	0.43	cytosol, nucleus, bud neck, bud tip	Transportin or cytosolic karyopherin beta 2; regulates asymmetric protein synthesis in daughter cells during mitosis
DIP2	0.49	cytosol, nucleus	Nucleolar protein of the small subunit (SSU) processome, required for 18S rRNA biogenesis
GYP1	0.47	cytosol, mitochondria, Golgi	Cis-golgi GTPase-activating protein (GAP) for the Rab family members; involved in vesicle docking and fusion
FAT1	0.19	lipid droplet, ER, peroxisome, plasma membrane	Very long chain fatty acyl-CoA synthetase and long chain fatty acid transporter; activates imported fatty acids
YJR041C	0.37	nucleolus, nucleus	Nucleolar protein required for metabolism of the rRNA primary transcript; ribosome biogenesis
SIK1	0.16	nucleolus, nucleus	Essential nucleolar protein component of the box C/D snoRNP complexes
HHF2	0.46	nucleus	Histone H4, core histone protein required for chromatin assembly and chromosome function
YRA1	0.22	nucleus	RNA binding protein required for export of poly(A)+ mRNA from the nucleus
RET1	0.47	nucleus	Second-largest subunit of RNA polymerase III, responsible for the transcription of tRNA and 5S RNA genes
STE2	0.18	plasma membrane, vacuole	Receptor for alpha-factor pheromone; GPCR that initiates the signaling response during mating
STE6	0.35	plasma membrane, mating projection tip, Golgi, vacuole	Plasma membrane ATP-binding cassette (ABC) transporter required for the export of a-factor

3.4 CONCLUSIONS

Ybr074 was not implicated in the ER quality control of any of the ERAD substrates tested, including CFTR, Ste6p*, Gas1*, CPY* and CPY*-DHFR. Similarly, Ybr074 does not act in synergy with the 26S proteasome in the degradation of ERAD substrates. This was evidenced by the absence of distinct Ybr074-dependent CFTR degradation fragments in the absence of 26S proteasome activity. Furthermore, no synergistic growth defect was observed when both Ybr074 and the 26S protease activity were disrupted in cells expressing CFTR. In hindsight, this is not surprising in light of the evidence discussed in Chapter 2, which indicated that Ybr074 is a vacuolar protein as opposed to an ER-localized protein. In fact, this may support the hypothesis presented in Chapter 2, suggesting that the ER accumulation of Ybr074 observed in cells expressing Ybr074-HA may represent an aberrantly localized, and perhaps misfolded, gene product.

Multiple methods designed to associate Ybr074 with a group of genes sharing a common biological function, including Synthetic Genetic Array (SGA) analysis, phylogenetics, and proteomics, did not place Ybr074 in any clear functional category. However, the presence of nine genes related to lipid metabolism and cell wall function, which were identified by SGA analysis, merited further investigation (see Chapter 4). Only five of 72 GFP-tagged proteins (Flc1, Hxt2, Nce102, Gtr1, Gnt1) that accumulated in a *ybr074Δ* strain are described as having vacuolar localization. It is interesting to note that none of these candidates are resident vacuolar proteins, but may be targeted to the vacuole for degradation under certain conditions. For example, high glucose levels trigger internalization and vacuolar targeting of the plasma

membrane glucose transporter, Hxt2 (Kruckeberg et al, 1999). An alternative strategy to identify endogenous substrates of Ybr074 will be discussed in Chapter 5.

4.0 CELL WALL INTEGRITY

The cell wall in yeast and other fungi forms a physical barrier between the cell and its environment. It is comprised of an inner network of linear and branched sugars, and an outer layer of highly glycosylated cell wall proteins (CWPs). The primary functions of the cell wall are to stabilize osmotic conditions within the cell, to provide mechanical strength and elasticity required for protection from physical stress, and to maintain cell shape and regulate morphogenesis (Lesage & Bussey, 2006).

The sugar polymers at the base of the cell wall are primarily responsible for providing the cell with tensile strength, and consist of the β-1,4-linked N-acetylglucosamine (GlcNAc) linear polymer known as chitin, a continuous network of helical β-1,3-glucan polymers that interact by hydrogen bonding, and highly branched, water-soluble β-1,6-glucan chains (Klis et al, 2006).

Mannoproteins forming the outer layer of the cell wall reduce its porosity and protect the polysaccharide layer from degrading enzymes. CWP functions include adhesion, iron uptake, cell wall remodeling, and signaling. The majority of CWPs are attached via a GPI anchor to β-1,6-glucan, which is attached in turn to β-1,3-glucan or chitin. Proteins with Internal Repeats-(PIR) CWPs are attached directly to β-1,3-glucan via an unidentified alkali-sensitive linkage. Other CWPs are non-covalently attached to neighboring CWPs via disulphide linkages.

Sugars and CWPs must be delivered to the cell wall to support growth and respond to changes in environmental conditions. CWPs are delivered via the secretory pathway, β-glucans

are delivered via poorly characterized, non-canonical pathways, and chitin is delivered via specialized vesicles known as chitosomes (Ziman et al, 1996).

The composition of the cell wall is known to vary with the cell cycle, and is subject to changes in oxygen levels, nutrient availability, and osmotic conditions (Jendretzki et al, 2011; Ziman et al, 1996). Two major mitogen-activated protein kinase (MAPK) signaling pathways are required for responding to these environmental cues and mounting transcriptional responses that allow cells to adapt to changing conditions. The Cell Wall Integrity (CWI) pathway is activated under condition of cell wall instability, while the High-Osmolarity Glycerol (HOG) pathway responds to osmotic stress (Rodriguez-Pena et al, 2010).

As was discussed in Chapter 3, *YBR074* exhibits genetic interactions with genes related to cell wall function: *FUS1*, involved in cell fusion during mating; *GFA1*, involved in the first step of chitin biosynthesis; *CDC48*, involved in numerous cellular functions including ERAD and cell wall maintenance; *TMN3*, involved in cellular adhesion and filamentous growth; and *GUP1*, involved in remodeling GPI anchors. *YBR074* also exhibits a chemical-genetic interaction under conditions of cell wall stress when deleted in the *cdc48-2* background (Figure 27, discussed below). In this chapter, the role of Ybr074 in cell wall integrity and its interaction with *CDC48* is examined.

4.1 MATERIALS AND METHODS

4.1.1 Strains and Molecular Techniques

Strains used in this chapter are described in Table 3. Serial dilutions were conducted as described in Chapter 3, using 50 μg/mL CR or 50 μg/mL CFW.

4.1.2 Zymolyase sensitivity Assay

Cells were grown in YPD at 30°C to logarithmic phase (OD_{600} = 0.4-0.8) and 0.5 OD_{600} equivalents of cells were harvested by centrifugation at ~13,000 *g*. Cells were washed in 10 mM Tris-HCl, pH 7.4, 1 mM EDTA buffer and re-suspended in the same buffer to a final concentration of 1 OD_{600}/mL. Cells were treated with 1 mg/mL zymolyase 20-T (MP Biomedicals, Solon, OH) for 1 h at 37°C. The OD_{600} of each strain was measured using a 10 fold dilution of cells into water at 0 min and 60 min. Sensitivity to zymolyase treatment was measured as a percentage of the initial OD_{600}.

4.1.3 β-1,3-glucan quantification assay

Quantification of 1,3-β-glucan was carried out as described (Watanabe et al, 2001). In brief, logarithmic phase cultures were washed twice and re-suspended in 10 mM TE buffer (10 mM Tris-HCl, pH 7.4, 1 mM EDTA) at 1.0 OD_{600} cell equivalents in 0.5 mL. Sodium hydroxide was added to a final concentration of 1 M, and the reactions were incubated at 80°C for 30 min to solubilize the 1,3-β-glucan. To the solubilized sample, 2.1 mL of aniline blue mix (40 volumes

of 0.1% aniline blue; Electron Microscopy Science, Hatfield, PA, in water, 21 volumes of 1 M HCl, and 59 volumes of 1 M glycine/NaOH, pH 9.5) was added, and incubated at 50°C for 30 min followed by a further incubation at room temperature for 30 min. Fluorescence was measured using an Aminco-Bowman Series 2 spectrometer and AB2 series 2 software at an excitation wavelength of 400 nm/16 nm bandpass, and an emission wavelength of 460 nm/16 nm bandpass (Thermo Spectronic, Rochester, NY). Curdlan was used to determine the linear range for fluorescence intensity (0-20 ug/mL) (InvivoGen, San Diego, CA).

4.1.4 Killer toxin halo assay

Sensitivity to killer toxin was tested based on previously described protocols (Boone et al, 1990; Santos et al, 2000). K1 killer toxin secreting strain, 1368, described in Table 3, was grown to saturation in YPD, pH 4.5, overnight at 25°C. Cells were separated from K1 killer toxin secreted into the medium by centrifugation at ~2000 *g* for 4 min at room temperature. The supernatant containing K1 killer toxin was filtered using a 0.22 μm filter (Millipore, Franklin Lakes, NJ). The filtered medium was concentrated 200-fold using an ultrafiltration Amicon Ultra-15 unit with a 10 kDa molecular mass cut-off (Millipore, Billerica, MA). Test strains were grown in YPD to log phase, and 1 OD_{600} cell equivalents were harvested and re-suspended in 100 μL sterile double distilled water. Two fold concentrated YPD, pH 4.5, medium was incubated in a 37°C water bath before being added to an equal volume of autoclaved 4% Bacto agar, supplemented with 30 μg/mL methylene blue. Once equilibrated to approximately 37°C, the molten medium was seeded with the test strain, and the medium was poured and allowed to solidify. A sterile filter disc spotted with 10 μL of the concentrated killer toxin medium was added to seeded plates and the plates were incubated for 4 d at room temperature. Sensitivity to

killer toxin was measured as the diameter of the halo using ImageJ software. The diameter of each halo was taken as the average of four measurements. Each strain was tested in three individual replicates and the average halo diameter and standard error were calculated using Microsoft Excel 2010.

4.2 RESULTS

Cdc48 is a homohexameric yeast ATPase Associated with diverse cellular Activities (AAA) protein, whose mammalian homolog is p97, also known as Valosin-Containing Protein (VCP). Broadly, Cdc48 and its cofactors, are required to segregate ubiquitinated substrates from protein complexes, membranes, and chromatin in order to facilitate their degradation (Meyer et al, 2012). Cdc48 facilitates ERAD, Golgi and ER membrane fusion, nuclear membrane re-assembly, cell cycle regulation, DNA repair, and autophagosome maturation. A distinct set of co-factors binds to the Cdc48 N-terminal domain in order to mediate each of these cellular functions. Cdc48 also contains a D1 ATPase domain required for hexamerization and heat-induced ATPase activity, as well as a D2 ATPase domain, which contributes most of the ATPase activity under physiological conditions (Yamanaka et al, 2012).

Recently, a role for Cdc48 in the maintenance of cell wall integrity during the cell cycle was described (Hsieh & Chen, 2011). Although the mechanism for Cdc48-dependent maintenance of cell wall integrity is undefined, these data are intriguing in light of the cell wall stress-dependent interaction between *CDC48* and *YBR074* observed in this study (see Figure 27).

A

Allele	Yeast	Human
IBMPFD	R165	R155H
IBMPFD	A242	A232E
cdc48-2	A547T	A537
cdc48-2	T803A	G780
cdc48-3	P257L	P247
cdc48-3	R387K	R377

B

MGEEHKPLLDASGVDPREEDKTATAILRRKKKDNMLLVDDAINDDNSVIAINSNTMDKLELFRG
DTVLVKGKKRKDTVLIVLIDDELEDGACRINRVVRNNLRIRLGDLVTIHPCPDIKYATRISVLP
IADTIEGITGNLFDVFLKPYFVEAYRPVRKGDHFVVRGGMRQVEFKVVDVEPEEYAVVAQDTII
HWEGEPINREDEENNMNEVGYDDIGGCRKQMAQIREMVELPLRHPQLFKAIGIKPPRGVLMYGP
PGTGKTLMARAVANETGAFFFLINGPEVMSKMAGESESNLRKAFEEAEKNAPAIIFIDEIDSIA
PKRDKTNGEVERRVVSQLLTLMDGMKARSNVVVIAATNRPNSIDPALRRFGRFDREVDIGIPDA
TGRLEVLRIHTKNMKLADDVDLEALAAETHGYVGADIASLCSEAAMQQIREKMDLIDLDEDEID
AEVLDSLGVTMDNFRFALGNSNPSALRETVVESVNVTWDDVGGLDEIKEELKETVEYPVLHPDQ
YTKFGLSPSKGVLFYGPPGTGKTLLAKAVATEVSTNFISVKGPELLSMWYGESESNIRDIFDKA
RAAAPTVVFLDELDSIAKARGGSLGDAGGASDRVVNQLLTEMDGMNAKKNVFVIGATNRPDQID
PAILRPGRLDQLIYVPLPDENARLSILNAQLRKTPLEPGLELTAIAKATQGFSGADLLYIVQRA
AKYAIKDSIEAHRQHEAEKEVKVEGEDVEMTDEGAKAEQEPEVDPVPYITKEHFAEAMKTAKRS
VSDAELRRYEAYSQQMKASRGQFSNFNFNDAPLGATATDNANSNNSAPSGAGAAFGSNAEEDDD
LYS

Figure 26: *CDC48* mutant alleles.

A) *CDC48* mutant alleles are shown along with the corresponding yeast and human nucleotide changes associated with each allele. When a converted amino acid is not indicated, it was not naturally occurring in this organism B) Amino acids associated with each mutant allele are highlighted using the corresponding colors shown in A). The N-terminal domain, D1 ATPase domain, and D2 ATPase domain, respectively, are highlighted in yellow according to the domain

In order to elucidate which of the Cdc48 functions is affected by disruption of Ybr074 function, ERAD and cell wall integrity phenotypes were examined in various *CDC48* mutant alleles (Figure 26) in the presence or absence of Ybr074 activity. *CDC48* has been linked to a human degenerative disorder known as Inclusion Body Myopathy associated with Paget disease of bone and Frontotemporal Dementia (IBMPFD) (Watts et al, 2004). Two mutant alleles associated with IBMPFD were used in this study: *cdc48* A232E and *cdc48* R155H. The A232E mutation affects the D1 ATPase domain. The R155H mutation occurs within the linker region between the N-terminal domain and D1 ATPase domain, and disrupts an important interaction with N387 in the D1 ATPase domain. The R155-N387 interaction normally allows conformational changes induced by ATP hydrolysis to be transmitted to the N-terminal domain (DeLaBarre & Brunger, 2003; Hubbers et al, 2007).

The thermosensitive mutant allele, *cdc48-3*, was isolated in yeast and bears two mutations in the D1 ATPase domain. The *cdc48-3* allele is associated with defects in ERAD at the non-permissive temperature of 37°C (Nakatsukasa et al, 2008). The *cdc48-2* allele bears two mutations, one in the D2 ATPase domain, and the second near the C-terminus. Although this allele is less well represented in the literature, it has been shown to cause an ERAD defect at 30°C (Garza et al, 2009).

These alleles were used to further examine the genetic interaction between *YBR074* and *CDC48*. Specifically, I assessed how *cdc48* mutants in a *ybr074Δ* background affect sensitivity to the cell wall stress inducing agents calcofluor white (CFW) and Congo red (CR), as well as ERAD efficiency. My results suggest that Ybr074 is not involved in modulating the ERAD function of Cdc48. Secondly, while Ybr074 does not appear to affect the composition of

polysaccharides in the cell wall, it may contribute to a *cdc48-2* allele-specific cell wall phenotype in the presence of CFW and Congo red.

4.2.1 Does *YBR074* interact with the cell wall integrity function of *CDC48*?

As previously mentioned above, CFW and CR induce cell wall stress by preferentially binding to chitin in the cell wall (Karreman & Lindsey, 2007; Ram & Klis, 2006). A serial dilution of wild type, *ybr074Δ*, *cdc48-2*, and *ybr074Δcdc48-2* cells was plated on YPD supplemented with 50 μg/mL CFW or CR. To differentiate between cell wall-related defects and other defects associated with the *CDC48* mutant strain, a serial dilution of cells was also plated on YPD supplemented with CFW or CR and with 1 M sorbitol, which acts as an osmotic stabilizer (Klis F.M. 2002). The *kre1Δ* strain was used as a positive control for CFW and CR sensitivity because it is involved in β-1,6-glucan assembly. Disruption of *KRE1* results in activation of the CWI pathway, which leads to a 2% to 20% compensatory increase in cellular chitin levels (Boone et al, 1990; Klis et al, 2002; Lesage et al, 2005). Strains with higher chitin content are more sensitive to CFW and CR, while strains with reduced chitin levels are more resistant to CFW and CR as compared to wild type yeast.

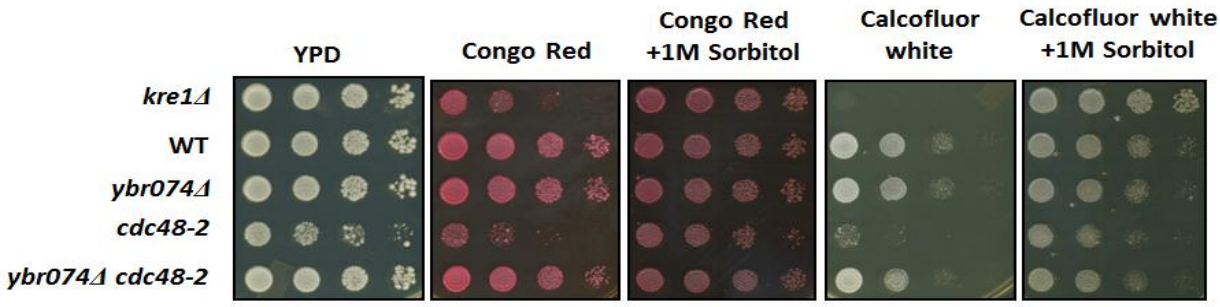

Figure 27: Sensitivity of *ybr074Δ* and *cdc48-2* to cell wall stress inducing agents CFW and CR.

A serial dilution of cells was spotted on YPD, YPD supplemented with CFW or CR, and YPD supplemented with CFW or CR and 1 M sorbitol, and incubated at 30°C. Although only one set is shown, this experiment was confirmed in five different colonies obtained from a single cross.

The positive control strain, *kre1Δ*, exhibits sensitivity to both CR and CFW as compared to wild type. This phenotype is rescued upon addition of sorbitol as an osmotic stabilizer, demonstrating that this is a cell wall specific defect (Figure 27). While *ybr074Δ* shows no sensitivity to CR or CFW as compared to the wild type, the *cdc48-2* strain is sensitive to these cell wall stress-inducing agents at 30°C. Interestingly, the sensitivity of the *cdc48-2* strain was partially rescued by addition of sorbitol, suggesting that much of the observed growth defect is induced by treatment with CR and CFW. The slight growth defect observed in the presence of sorbitol can be attributed to the temperature sensitivity observed in this strain at 30°C, and may be associated with defects in other functions of Cdc48 discussed above (Garza et al, 2009). Intriguingly, the *ybr074Δ cdc48-2* strain exhibits no growth defect compared to wild type upon treatment with either CR or CFW. This suggests the presence of an alleviating genetic interaction between *YBR074* and *CDC48*. The *ybr074Δ* and *cdc48-2* alleles in this double mutant strain are

marked with the drug resistance genes *KANMX* and *NATMX*, and their presence has been confirmed multiple times by plating the cells on YPD medium supplemented with G418 or NAT. The *cdc48-2* allele in this double mutant strain was also confirmed by DNA sequence analysis.

To confirm that the alleviating interaction observed in the *ybr074Δcdc48-2* strain on CFW and CR was attributed to mutations in only *YBR074* and *CDC48*, and not to a third mutation elsewhere in the genome, two more *ybr074Δcdc48-2* isolates were obtained from independent yeast matings, sporulation, tetrad dissection, and genotyping. Parental strains were mated on three separate occasions to produce three individual *ybr074Δcdc48-2* progeny. However, while the double mutant isolate shown in Figure 27, displayed an alleviating phenotype, the remaining two isolates exhibited sensitivity to CR and CFW similar to the *cdc48-2* strain alone (Figure 29). This result suggests that a third, suppressor mutation is responsible for conferring resistance to CR and CFW in the initial *ybr074Δcdc48-2* strain tested in Figure 27, or that a spontaneous gene duplication event occurred that restored Cdc48 function.

In order to confirm and remove this third suppressor mutation, the *ybr074Δcdc48-2* strain will be backcrossed to a wild type strain several times in order to restore the genetic background of this strain to wild type. If the third suppressor mutation is responsible for CR and CFW resistance, its elimination should result in a *ybr074Δcdc48-2* strain with similar susceptibility to CR and CFW.

Serial dilutions of double mutant strains, in which the *ybr074Δ* allele was combined with the remaining *CDC48* mutant alleles shown Figure 26, were not consistent with the alleviating phenotype observed for the *ybr074Δcdc48-2* strain (Figure 28). This supports the hypothesis that a third suppressor mutation is responsible for conferring resistance to CR and CFW. However, it is formally possible that the genetic interaction between *YBR074* and *CDC48* is allele specific.

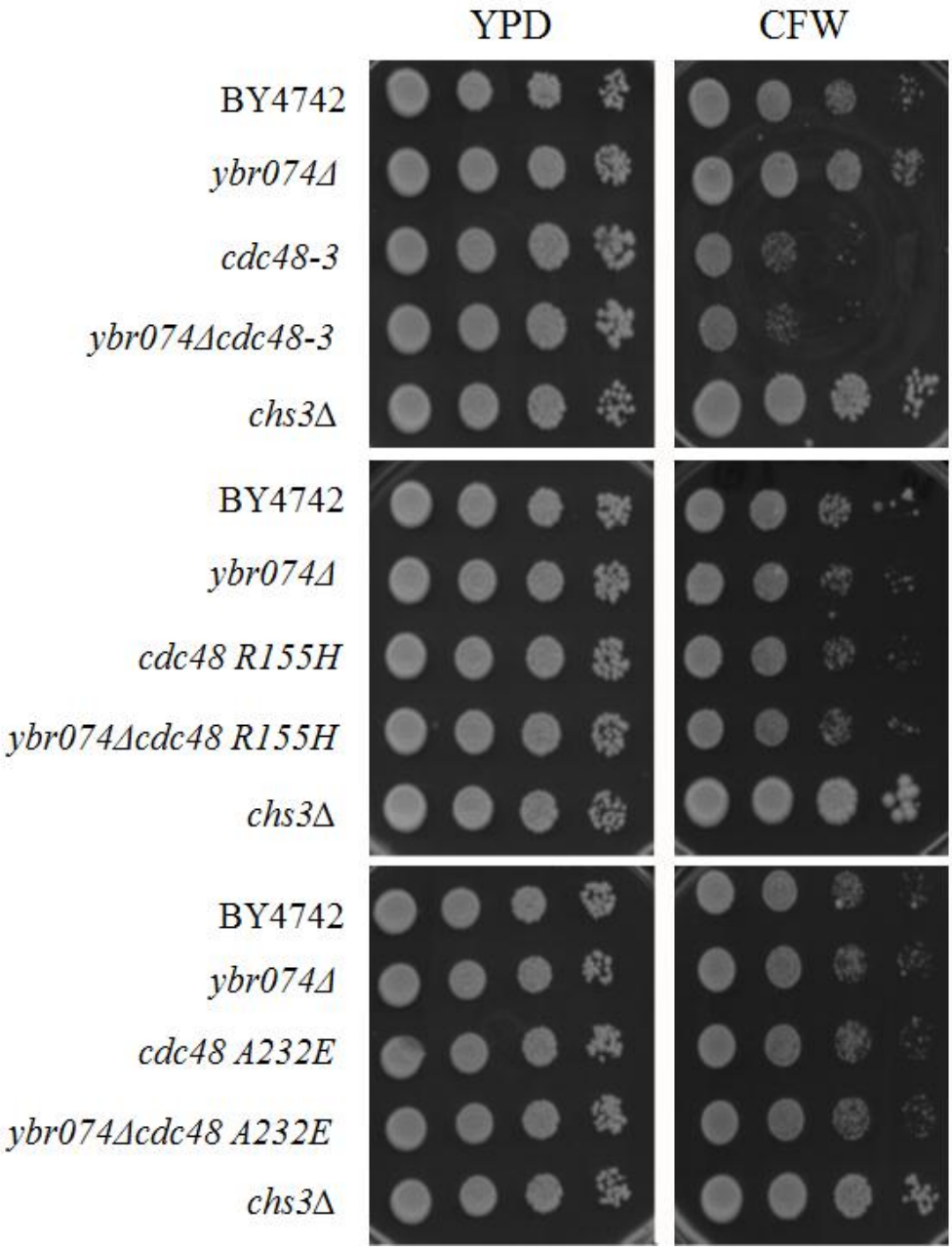

Figure 28: *cdc48-3*, *cdc48 R155H*, and *cdc48 A232E* do not exhibit a chemical-genetic interaction in the *ybr074Δ* genetic background.

Serial dilutions of the indicated strains were plated on YPD in the presence or absence of 50 μg/mL CFW. The *chs3Δ* strain, defective in biosynthesis of chitin, was used as a positive control for CFW resistance.

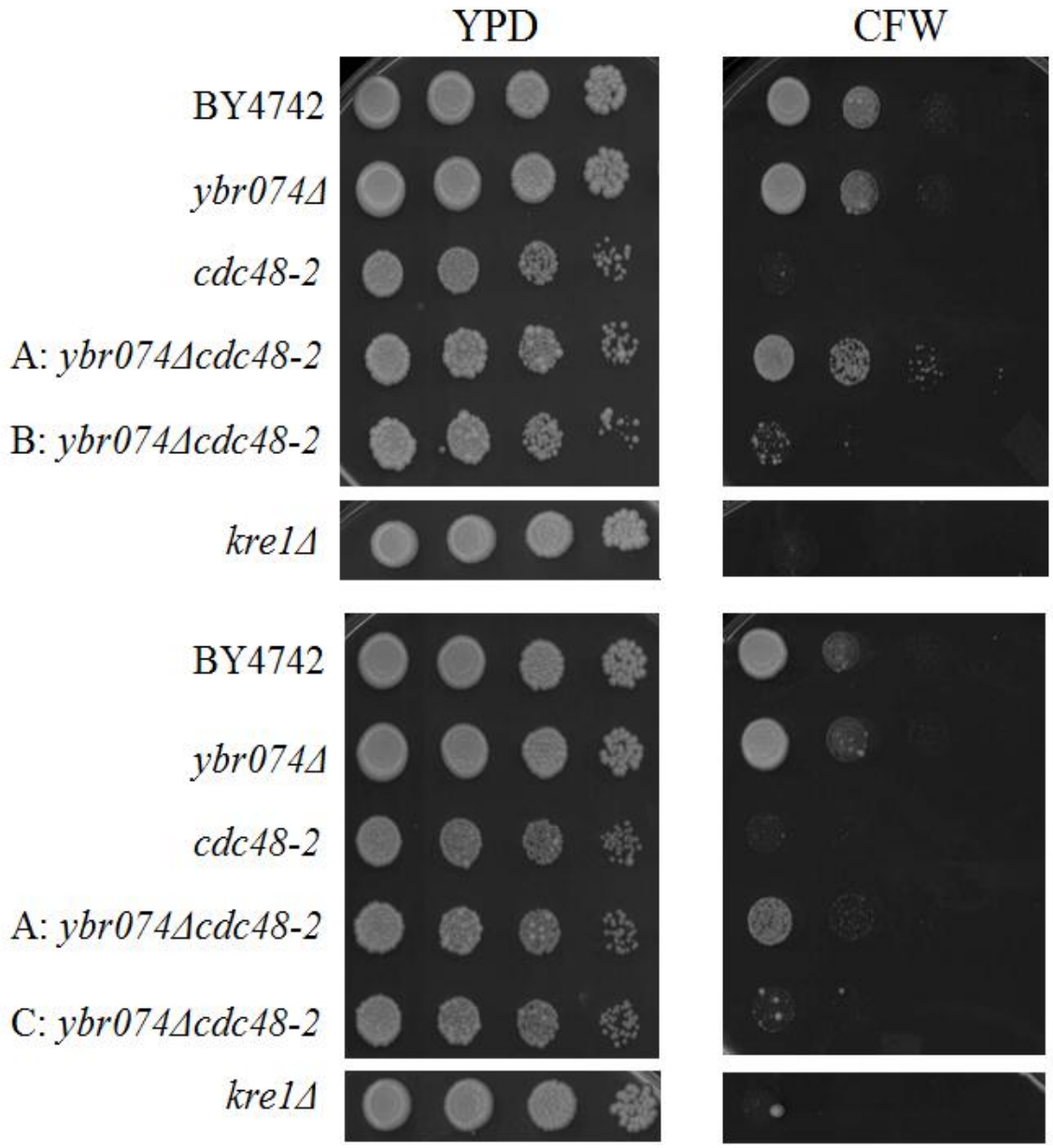

Figure 29: Individual *ybr074Δcdc48-2* isolates do not exhibit a consistent chemical-genetic interaction of CFW.

ybr074Δcdc48-2 isolate A, derived from cross 56, spore 7B, shows a phenotype similar to the wild type strain on YPD containing 50 μg/mL CFW. Isolate B, derived from cross 71, spore 11C, and isolate C, derived from cross 73, spore 9A are both more sensitive to CFW than the wild type strain.

4.2.2 Does the loss of *YBR074* affect the function of *CDC48* during ERAD?

The best characterized function of Cdc48 is its role in ERAD, where it couples the chemical energy derived from ATP hydrolysis to produce the mechanical force necessary to extract ubiquitinated ERAD substrates from the ER membrane into the cytosol for degradation by the 26S proteasome (Wolf & Stolz, 2012). In order to ascertain whether the ERAD-related function of Cdc48 might be affected by disruption of *YBR074*, cycloheximide assays were conducted using the ERAD substrates CPY* and Gas1*, which were discussed in the previous chapter.

The soluble substrate CPY* has been previously shown to depend on Cdc48 function for ERAD, and this dependence is re-capitulated in Figure 30A (Jarosch et al, 2002). It was hypothesized that Ybr074 may be compensating for the loss of Cdc48 function, since accumulation of CPY* upon its overexpression has been demonstrated to target CPY* to the vacuole (Spear & Ng, 2003). However, instead of the expected increase in CPY* stabilization in a *ybr074Δ cdc48-2* strain, my results demonstrate increased degradation of CPY* in this strain. This suggests that deletion of both *CDC48* and *YBR074* may be inducing a stress response that either facilitates delivery of CPY* to the vacuole, or induces expression of vacuolar proteases or an alternative degradation pathway.

The ERAD substrate Gas1* represents the misfolded form of the wild type Gas1 protein, which is responsible for the formation and maintenance of the β-1,3-glucan network of the yeast cell wall (Carotti et al, 2004). Gas1* bears the amino acid substitution, G291R, within a hydrophobic region of the protein. This mutation leads to Gas1* misfolding, ER retention, and 26S proteasome-dependent degradation (Fujita et al, 2006).

Gas1* is a unique ERAD substrate, in that it is subject to three different forms of quality control involving recognition of its protein, glycan and lipid elements. The misfolded protein is recognized by the ER chaperone Kar2, N-linked glycans are modified by the ER mannosidases Htm1 and Mns1 to promote ERAD, and O-linked glycans are appended by the O-mannosyltransferases Pmt1 and Pmt2 to mediate ER retention and association with Der1 (Goder & Melero, 2011; Hirayama et al, 2008). Finally, quality control of the GPI lipid anchor is mediated by the inositol GPI deacylase, Bst1, and members of the p24 complex, which function as an adaptor linking GPI-anchored substrates to the COPII coat (Castillon et al, 2011; Hirayama et al, 2008).

Intriguingly, Cdc48 has been found to be associated with Pmt1, Pmt2, and Der1 in a complex promoting the ERAD of Gas1* (Goder & Melero, 2011). However, Cdc48 has never been directly shown to contribute to Gas1* ERAD. Furthermore, although the function of the vacuolar protease, Pep4, is dispensable for Gas1*p degradation, it was shown to be required when in the absence of O-mannosylation was absent. This suggests that Gas1* is targeted for vacuolar degradation in Pep4-dependent manner when ERAD is impaired (Hirayama et al, 2008). It was therefore hypothesized that simultaneously crippling both ERAD and vacuolar degradation pathways in a *ybr074Δcdc48-2* mutant strain would result in exacerbated stabilization of Gas1*.

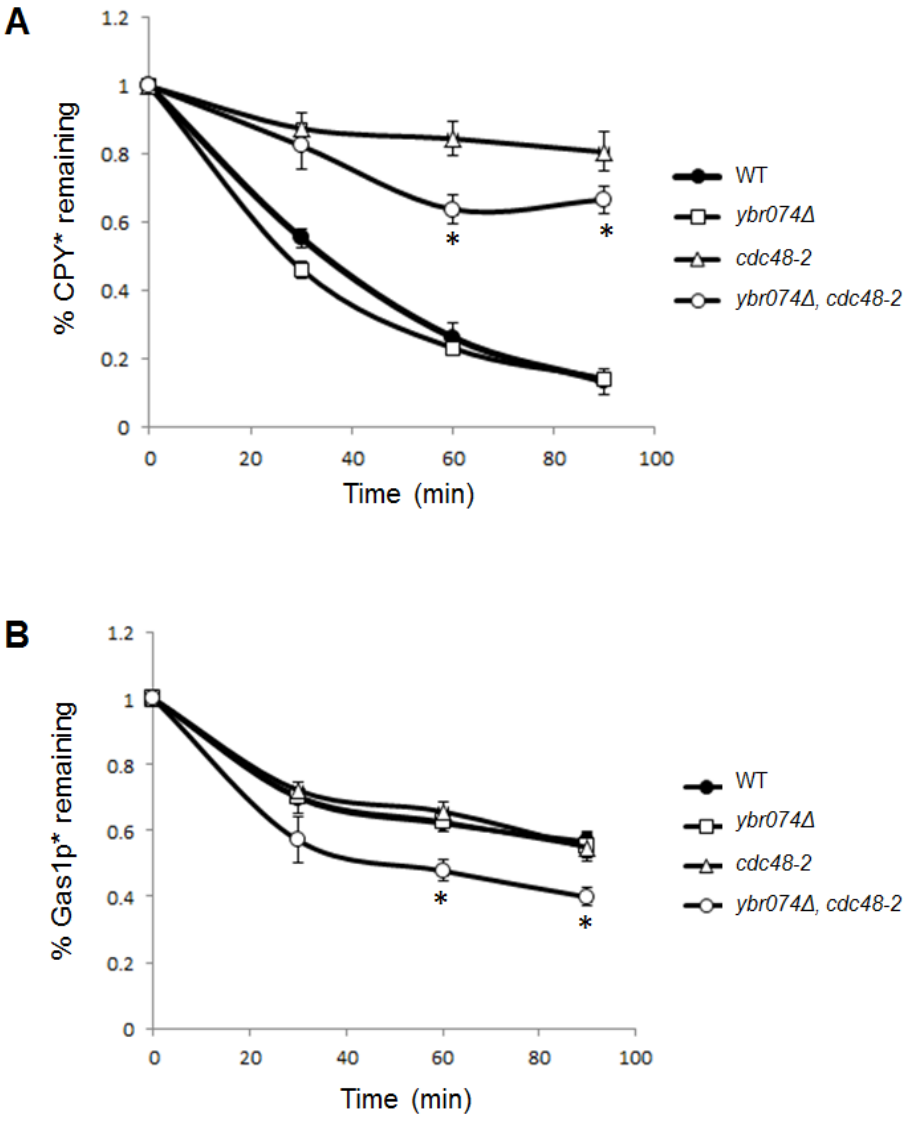

Figure 30: ERAD efficiency of *cdc48-2* strains is not exacerbated by disruption of Ybr074 function.

A) CPY* degradation in wild type (n=4), *ybr074Δ* (n=5), *cdc48-2* (n=6), and *ybr074Δ cdc48-2* (n=6) at 37°C. B) Gas1* degradation in wild type, *ybr074Δ* (n=5), *cdc48-2* (n=6), and *ybr074Δ cdc48-2* (n=6) at 37°C. *ybr074Δ*, *cdc48-2*, and *ybr074Δ cdc48-2* at 37°C (n=7). * = $p < 0.05$

To test this hypothesis, Gas1* degradation was monitored using cycloheximide chase analysis in wild type, *ybr074Δ*, *cdc48-2,* and *ybr074Δcdc48-2* strains. Degradation of Gas1* was not significantly different from wild type in either *ybr074Δ* or *cdc48-2* strains, indicating that Cdc48 is not required for degradation of Gas1* (Figure 30B). Formally, this may be the result of a compensatory vacuolar degradation pathway. Intriguingly, Gas1* was degraded to a greater extent in the *ybr074Δ cdc48-2* strain than in the wild type strain, suggesting that a compensatory degradation mechanism may be induced in this strain, and that Ybr074 is not specifically involved in quality control of GPI-anchored substrates. As a control for this experiment, I also examined CPY* dependence in each individual mutant strain and found that CPY* was stabilized in the *cdc48-2* strain, as expected (Rabinovich et al, 2002). However, CPY* was degraded slightly better in the *ybr074Δcdc48-2* strain as compared to the *cdc48-2* strain (Figure 30A). This indicates that Ybr074 is not involved in ERAD.

4.2.3 Are β-glucan levels affected by disruption of Ybr074 and Cdc48 function?

Given the results in Figure 27 suggesting Ybr074 may be affecting levels of chitin in the cell wall, I hypothesized that the more abundant β-glucan components of the cell wall may also be affected in a *ybr074Δ* strain. There are several ways to examine β-glucan levels in the yeast cell wall. In this section, enzymatic treatment using zymolyase and a quantitative fluorescence-based assay were used to assess β-1,3-glucan levels, while a killer toxin halo assay was used to detect β-1,6-glucan levels.

Zymolyase is an enzyme isolated from *Arthrobacter luteus* that specifically hydrolyses β-1,3-glucosidic bonds (Kitamura & Yamamoto, 1972). Yeast strains in which assembly of the β-glucan network is impaired are sensitive treatment with zymolyase, which eventually results in cell lysis (de Nobel et al, 2000; Garcia et al, 2009). As an example, the *kre1Δ* strain exhibits a cell wall weakened by a lack of β-1,6-glucan-mediated cross-linking of the β-1,3-glucan network. Consequently, the *kre1Δ* strain was observed to be approximately twice as sensitive to zymolyase treatment compared to wild type (Figure 31A). However, the *cdc48-2* and *ybr074Δ cdc48-2* strains did not display significantly different sensitivities to zymolyase compared to wild type. This result may be explained if the β-glucan levels in these strains remained unaltered compared to wild type, or if a reduction in β-glucan levels has been compensated for by an increase in mannoprotein levels. Increased mannoprotein levels may mask a zymolyase sensitivity phenotype by decreasing cell wall porosity and therefore, limiting access of zymolyase to the β-1,3-glucan layer of the cell wall (Shimoi et al, 1998). Surprisingly, the *ybr074Δ* strain was found to have a subtle, yet statistically significant increase in resistance to zymolyase treatment. This suggests *ybr074Δ* may have either increased levels of β-1,3-glucan or other cell wall components, which may mediate resistance to zymolyase compared to wild type yeast.

In order to examine β-1,3-glucan levels directly using a more quantitative approach, I employed the fluorescent dye, aniline blue, which binds specifically to β-1,3-glucans (Dubois et al, 1956). Purified β-1,3-glucan from yeast, known as Curdlan, was used to generate a standard curve for quantification of β-1,3-glucan levels in test strains. The results of this assay differed from the zymolyase sensitivity assay. In this case, the *ybr074Δ* strain did not exhibit any difference in β-1,3-glucan levels compared to wild type yeast, while both the *cdc48-2* and the

ybr074Δcdc48-2 strains had a statistically significant reduction in β-1,3-glucan levels to ~20% of wild type levels. This result suggests that there may be a zymolyase-specific stress response altering the cell wall structure in these strains via the HOG and/or CWI signaling pathways (Rodriguez-Pena et al, 2010). It is also possible that treatment with zymolyase for 1 h is sufficient to increase chitin levels in the *cdc48-2* strain, protecting it from zymolyase-induced cell lysis and increasing its sensitivity to CFW and CR. However, this explanation is inconsistent with the observation that the *ybr074Δ cdc48-2* strain is more resistant to CR and CFW. In this case, it is possible that an increase in mannoprotein levels at the cell wall may be contributing to CR and CFW resistance in this strain by reducing cell wall porosity (de Nobel et al, 1990). The cell wall protein Sed1 is a strong candidate for mediating resistance of the *ybr074Δ cdc48-2* strain to CFW. Sed1 was shown by Bermejo *et al.* to be strongly up-regulated in response to cell wall stress-inducing agents such as CR and zymolyase (Bermejo et al, 2010). Furthermore, Sed1 is known to mediate resistance to zymolyase and rescue the sensitivity of cell wall mutant strains to CFW (de Nobel et al, 2000; Shimoi et al, 1998). Intriguingly, Sed1 was observed to accumulate in a *ybr074Δ* strain, as shown in Table 11. Therefore, I hypothesize that Sed1 is upregulated in the *ybr074Δ cdc48-2*, and is responsible for mediating resistance to CFW in this strain. Examining *SED1* mRNA or protein levels in these strains may confirm this hypothesis if the *ybr074Δ cdc48-2* strain exhibits increased levels of Sed1 as compared to *ybr074Δ* or *cdc48-2* single mutant strains.

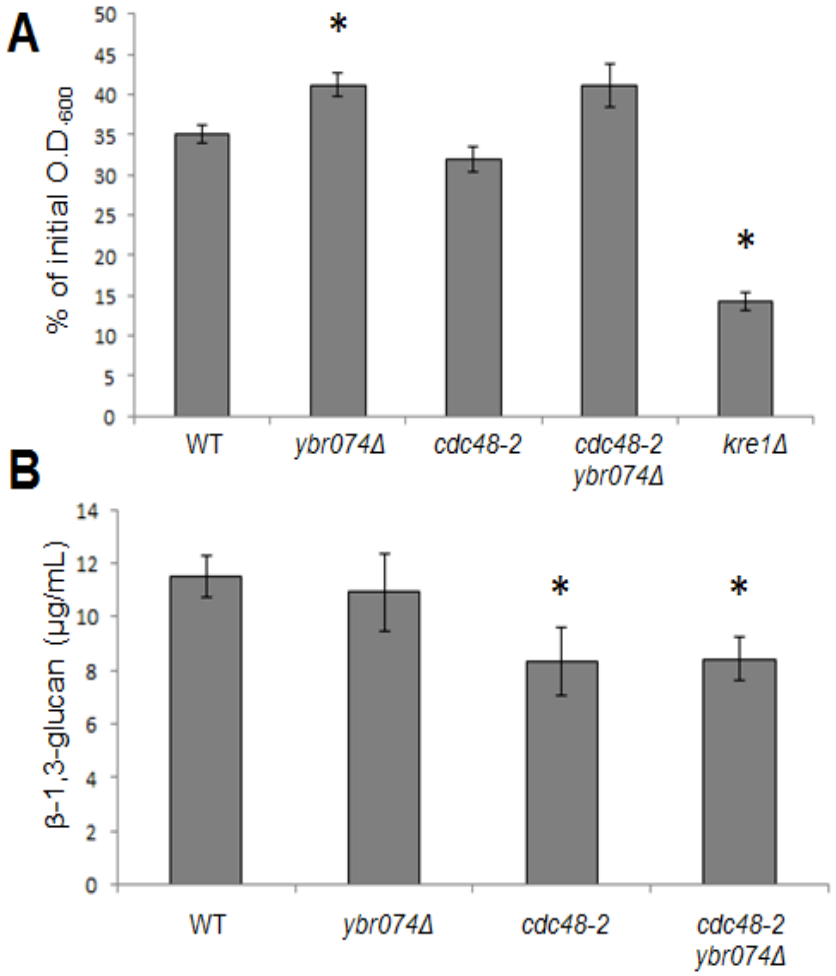

Figure 31: Analysis of β-1,3-glucan levels

A) Zymolyase sensitivity was measured as the percent OD_{600} of a culture after 1 h of treatment with zymolase compared to the initial OD_{600} (n=9; *, $p < 0.05$). B) Aniline blue fluorescence-based quantification of β-1,3-glucan levels are shown (n=2; *, $p < 0.05$).

In order to specifically examine β-1,6-glucan levels in these strains, a killer toxin halo assay was employed. In this experiment sensitivity to the K1 killer toxin protein was used as a measure of β-1,6-glucan levels in the cell wall of the test strain. K1 killer toxin binds specifically to β-1,6-glucans, forms pores in the plasma membrane, and results in lethality by impairing cellular ion homeostasis (Bussey, 1991).

Molten medium was seeded with test strains, and a filter disc containing K1 killer toxin was placed on the surface of the solidified medium. As the K1 killer toxin diffuses through the medium, it creates a circular region around the filter disc in which the test strain is killed. The diameter of this "halo" is used as a measure of K1 killer toxin sensitivity, and correlates with β-1,6-glucan levels. The *kre1Δ* strain, impaired in β-1,6-glucan synthesis, was used as a negative control, and exhibited no halo in this assay (Figure 32). The *slt2Δ* strain showed a slightly increased sensitivity to K1 killer toxin because the function of the MAPK, Slt2, normally mediating the CWI response, was disrupted. In hindsight, a *hog1Δ* strain would have been a stronger positive control, since this mutant strain displayed a stronger phenotype in a genome-wide mutant screen than *slt2Δ*, although the reason for this is not understood (Page et al, 2003). The *ybr074Δ* and *ybr074Δ cdc48-2* strains both exhibited a subtle, but statistically significant decrease in sensitivity to K1 killer toxin. This may be explained by reduced levels of β-1,6-glucan in the cell wall. Alternatively, it has been shown that increased cell wall thickness can result in resistance to killer toxin by blocking K1 killer toxin access to the plasma membrane. Increased resistance to K1 killer toxin is difficult to interpret because increased cell wall thickness can be attributed to a number of reasons, including impaired cortical actin assembly or impaired endocytosis (Li et al, 2002; Page et al, 2003). Paradoxically, over-production of β-1,6-glucan has also been linked to K1 killer toxin resistance. It is thought that increased K1 killer

toxin binding may reduce its effective concentration and inhibit pore formation (Page et al, 2003). Therefore, it may be informative to examine cell wall thickness in *ybr074Δ* and *ybr074Δcdc48-2* strains compared to wild type cells using electron microscopy, as previously published by our lab (Wright et al, 2007).

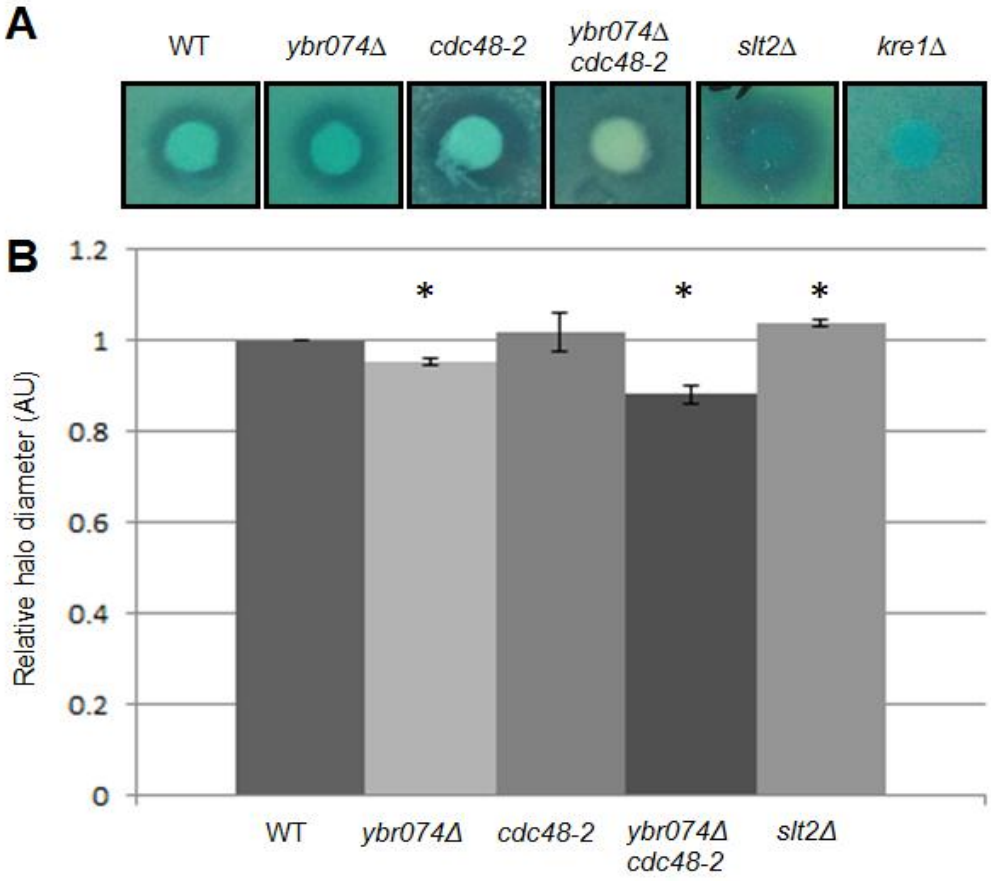

Figure 32: K1 killer toxin halo assay shows slight resistance of *ybr074Δ* and *ybr074Δ cdc48-2* strains compared to wild type.

A) K1 killer toxin halos and B) halo diameters in arbitrary units (AU), normalized to wild type, are shown for the indicated strain along with the standard error associated with each (n=3, * = $p < 0.05$).

4.3 CONCLUSIONS

An isolated *ybr074Δcdc48-2* strain displayed resistance to CR and CFW, as well as increased ERAD efficiency of CPY* and Gas1*p. Although these data suggest that the loss of both Ybr074 and Cdc48 function may be triggering a compensatory stress response that contributes to cell wall maintenance and ERAD, this conclusion is approached with caution because the possible presence of a third site mutation in this strain remains to be investigated.

The slight increase in zymolyase resistance of the *ybr074Δ* strain, as well as the data showing no difference in β-1,3-glucan levels in *ybr074Δ* compared to wild type yeast, suggest that a cell wall stress response independent of polysaccharide levels at the cell wall is protecting this strain from zymolyase treatment. This may be explained by an increase in mannoprotein levels at the cell wall, which would reduce its porosity and restrict access of zymolyase to the β-glucan substratum of the cell wall. In support of this hypothesis, the *ybr074Δ* strain was observed to be slightly resistance to K1 killer toxin, a phenomenon which has been linked to increased cell wall thickness and that is attributed to the accumulation of a mannoprotein layer. Therefore, future work should address this possibility using electron microscopy to examine cell wall thickness. Furthermore, results showing GFP-Sed1 accumulation in the *ybr074Δ* strain merit further investigation since Sed1 may be contributing to the accumulation of mannoproteins in the *ybr074Δ* strain as part of a response to cell wall stress. The *ybr074Δcdc48-2* phenotype will be confirmed by back-crossing to the BY4742 wild type strain, and these recently established cell wall assays will be repeated.

5.0 DISCUSSION AND FUTURE DIRECTIONS

To assign a more descriptive standard name for Ybr074, I propose Protein in FXNA-related Family 1, or Pff1. This name is derived from the PANTHER classification of this putative protease in the FXNA-related family of proteases whose members are listed in Table 5.

The finding that Pff1 is a vacuolar protease was surprising because published data demonstrate that its mammalian counterpart, FXNA, is ER-localized (Garcia-Rudaz et al, 2007). With only 11% sequence identity between Pff1 and FXNA, it may be that their differing sub-cellular localization is attributed to a legitimate cross-species difference, perhaps reflective of a divergence in function as well. In considering the reason for this difference, it is interesting to note that Pff1 has a 16 amino acid C-terminal sequence that is absent from both rat and human FXNA. The C-terminus of transmembrane proteins trafficking through the secretory pathway can be associated with di-basic or di-hydrophobic ER exit signals that mediate interaction with the COPII coat (Nufer et al, 2002; Watanabe & Riezman, 2004). Pff1 contains a C-terminal Ile-Leu, which in the case of Erv41, has been shown to serve as an ER exit signal (Otte & Barlowe, 2002). FXNA has a C-terminal Val-Phe, which is not a proven ER exit signal, but the composition of ER exit signals does display some flexibility and Val and Phe feature prominently within dihydrophobic motifs (Nufer et al, 2002). However, the topological analysis of Pff1 in this study indicates that the C-terminus is lumenal, and therefore cannot interact with the COPII coat in the cytosol to serve as an ER exit signal. Together, the simplest view is that the

C-terminus of Pff1 is not used as an ER-exit module. A more likely explanation is that an epitope tag at the C-terminus of Pff1 may disrupt protein folding and result in ER retention. Indeed, cycloheximide chase analysis comparing N- and C-terminally tagged Ybr074 constructs supports this hypothesis.

The localization data available for FXNA was obtained by immunofluorescence using a FXNA construct bearing a C-terminal FLAG tag (Garcia-Rudaz et al, 2007). This is striking when taken together with immunofluorescence data obtained from Pff1 constructs used in this study. Pff1 constructs bearing an HA tag either at the N-terminus or within the M28 protease domain were localized at the vacuolar membrane (Figure 10). In contrast, Pff1 tagged with HA at the C-terminus was localized to the ER, in congruence with FXNA-FLAG localization. This suggests that placing a tag at the C-terminus may influence the structure of these proteins and cause ER retention (Figure 12). In support of vacuolar localization, untagged Pff1 was identified as a component of the vacuolar membrane in a proteomic screen (Wiederhold et al, 2009). A re-examination of FXNA localization using an epitope tag placed at the N-terminus may be required to resolve this question. I plan to address this issue by examining the stabilities of Pff1-HA and HA-Pff1 by cycloheximide chase analysis. If Pff1 is retained in the ER due to misfolding, it may be targeted for degradation by the ER quality control system, and therefore be less stable than Pff1 that is successfully transported to the vacuole.

The mechanism by which Pff1 may be targeted to the vacuole also merits further investigation. The N-linked glycosylation of Pff1 (Figure 8), and the sub-population of Pff1 somewhat visible in the ER by immunofluorescence (Figure 10), suggest that Pff1 is not targeted to the vacuole by the Cvt pathway. However, transport of Pff1 to the vacuole either via the CPY pathway or the ALP pathway is theoretically possible (Bowers & Stevens, 2005). Since many of

the factors mediating these pathways have been worked out, identifying which transport pathway relays Pff1 to the vacuole may provide clues to some of its interaction partners.

To examine whether Pff1 sorts to the vacuole via the CPY pathway, Pff1 localization can be assayed in class E vacuolar sorting mutants (Raymond et al, 1992). This class of mutants is associated with defects in protein sorting to the MVB, and includes members of the ESCRT complexes. Mutant strains such as *vps27Δ* (ESCRT 0) and *vps23Δ* (ESCRT I) exhibit an accumulation of cargo dependent on the CPY pathway in the MVB, while cargo targeted by the ALP pathway bypasses the MVB and is targeted directly to the vacuole (Bowers & Stevens, 2005; Van Den Hazel et al, 1996).

To investigate the potential dependence of Pff1 on the ALP pathway, strains expressing a mutant allele of the AP3 adaptor complex binding partner, Vps41, can be examined. Cargo sorted by the ALP pathway requires the AP3 adapter complex and Vps41 for vesicle budding from the Golgi and for fusion with the vacuole in a clathrin-independent manner (Bowers & Stevens, 2005). The *vps41-231* allele is characterized by a Gly171Arg mutation in its N-terminal domain, which disrupts binding to the Apl5 subunit of the AP-3 adaptor complex (Darsow et al, 2001). Although *vps41Δ* strains are defective for both CPY and ALP transport, the *vps41-231* mutant allele exhibits a specific defect in ALP trafficking. If Pff1 were found to accumulate in a pre-vacuolar compartment in a *vps41-231* mutant strain or in AP3 mutant strains, this would indicate that Pff1 must be transported to the vacuole via the ALP pathway.

As discussed in Chapter 1, there are seven known proteases in the yeast vacuole. This raises the question of why an eighth protease, such as Pff1, is expressed in this compartment. To answer this question it helps to consider the features of Pff1 that make it unique in comparison to other vacuolar proteases. The most striking feature of Pff1 is that it is the only multi-pass

transmembrane protease identified in the vacuole. As such, Pff1 has the potential to interact with, and possibly influence the activity of other proteins found in the vacuolar membrane. These include vacuolar sorting and fusion proteins, transporters, and the cell wall proteins required for the biogenesis of this structure, such as the GPI-anchored protein, Gas1, and the multi-pass transmembrane protein Fks1, which were discussed in Chapter 4. These interacting proteins may represent substrates of Pff1 or non-substrate partners of Pff1. Identifying vacuolar proteins that physically interact with Pff1 may be informative of its function.

Furthermore, it will be interesting to test whether Pff1 is ubiquitinated. The ubiquitin ligase, Rsp5, is involved in the transport of both endocytic cargo and cargo trafficking to the vacuole via the CPY pathway (Bowers & Stevens, 2005). Intriguingly, Pff1 was found in a large-scale pull down of ubiquitinated proteins (Peng et al, 2003). In addition, this study showed that Endo H-treated Pff1 had a higher molecular mass than was predicted based its amino acid sequence. Therefore, it is possible that Pff1 is ubiquitinated by Rsp5, or the Golgi-associated ubiquitin ligase, Tul1 (Reggiori & Pelham, 2002). It will be interesting to examine the dependence of vacuolar Pff1 and Pff1 retained in the ER on different ubiquitin ligases. It is possible that the E3 ligase interaction between these two forms of Pff1 may shift from the Golgi-associated E3 ligases, mentioned above, to ER-associated E3 ligases such as Hrd1 and Doa10 (Vembar & Brodsky, 2008).

In order to identify proteins that physically interact with Pff1, I will conduct immunoprecipitation experiments using purified vacuoles. Methods for isolating vacuoles from spheroplasted cells by Ficoll gradient centrifugation have been described (Ohsumi & Anraku, 1981; Wiederhold et al, 2009). In order to distinguish Pff1 substrates from non-substrate proteins interacting with Pff1, wild type Pff1 and a catalytically inactive Pff1 mutant will be examined.

Bone fide substrates of Pff1 may be partially or completely degraded in the presence of wild type Pff1, or may accumulate in a strain expressing a catalytically inactive Pff1 mutant.

The structures of select M28 metalloproteases have been solved, including that of the human glutamate carboxypeptidase II (GCP II; PDB ID 3RBU) (Tykvart et al, 2012). Site-directed mutagenesis of the GCP II active site was used to identify mutations that disrupted its protease activity (Speno et al, 1999). These mutations map to zinc-binding residues, which in Pff1 correspond to His156Gly, His256Gly, and Asp168Glu, shown in Figure 33. These amino acid substitutions will be used to generate catalytically inactive Pff1 mutants for immunoprecipitation experiments.

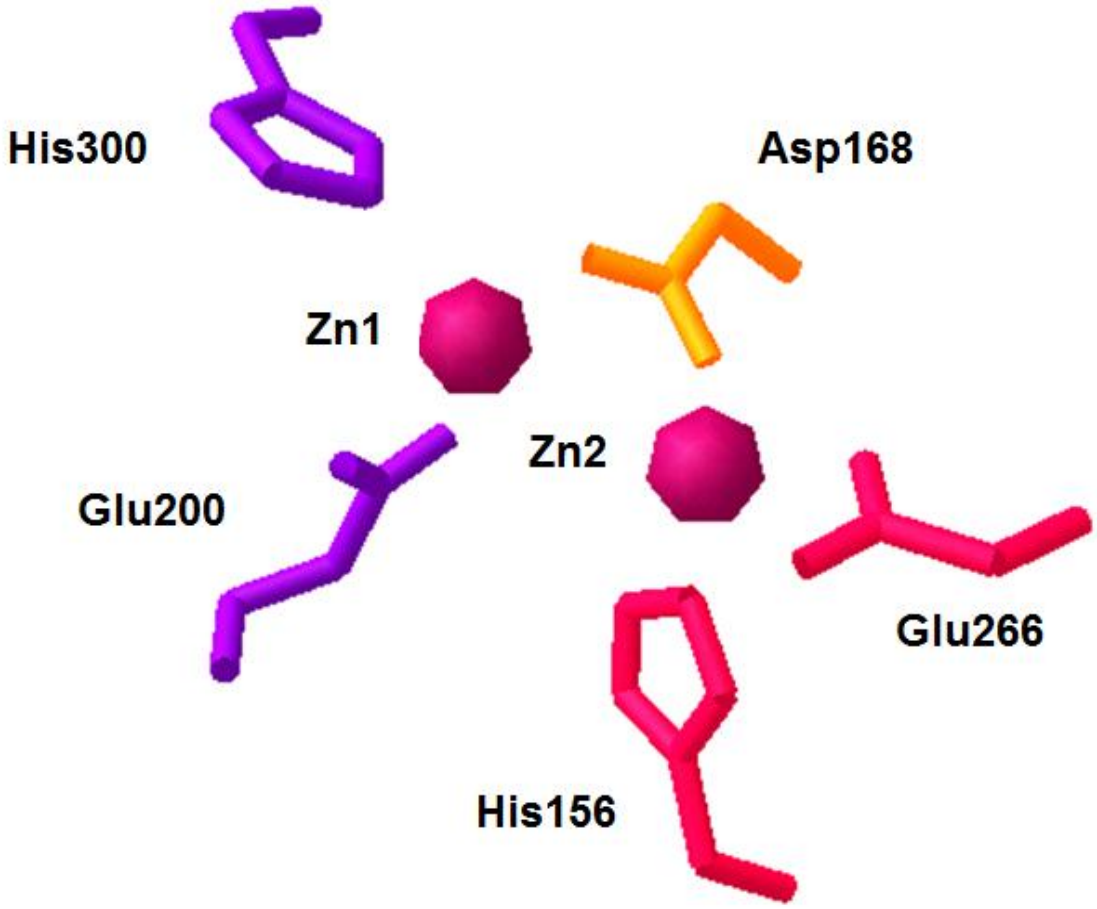

Figure 33: Schematic of Ybr074 (Pff1) active site

The active site contains two Zn^{2+} ions denoted Zn1 and Zn2. Zn1 is coordinated to His300 and Glu200, Zn2 is coordinated to His156 and Glu266, while Asp168 takes part in a bidentate interaction, coordinating both Zn1 and Zn2. Only zinc-binding residues are shown, and the Glu201 residue putatively involved in catalysis is omitted.

Since autophagy is a major catabolic process associated with the vacuole, a role for Pff1 in autophagy must be considered. While many vacuolar proteases are upregulated in response to nitrogen starvation, this was not found to be true in the case of Pff1 (Gasch et al, 2000). Nonetheless, Pff1 may still interact with Atg proteins *en route* to the vacuole to facilitate sorting of autophagosomes to the vacuolar compartment. To test this hypothesis, wild type and *pff1Δ* strains expressing GFP-Atg8 will be constructed and the localization and cleavage of the protein will be assessed as described (Nair et al, 2011). Specifically, GFP-Atg8 can be used as a reporter for proper formation of the autophagosome by fluorescence microscopy. GFP-Atg8 may also be used to examine internalization of the phagocytic body. In wild type cells, the inner membrane of the autophagosome, containing GFP-Atg8, fuses with the vacuole and GFP and degradation of GFP-Atg8 will be visible by Western blot analysis. In the *pff1Δ* strain, GFP-Atg8 may accumulate, indicating a defect in fusion of the autophagosome with the vacuole.

The vacuole is a dynamic buffering compartment that responds to numerous environmental cues by regulating cytosolic concentration of nutrients (He & Klionsky, 2009). The vacuole responds to nutrient stress, osmotic stress, stages of the cell cycle, oxidative stress, and the presence of toxic metals and drugs (Li & Kane, 2009). The proteases responsible for recycling amino acids in this compartment have broad specificities, allowing for non-selective degradation of cargo targeted to the vacuole. Some of these proteases, such as CPY and CpS have partially redundant functions, but are targeted to the vacuole in slightly different ways; as a soluble protease or anchored to the membrane, respectively. Others have catalytic activities that can be modulated by the presence of certain cellular factors; for example, Ape3 activity is affected by Co^{2+} (Yasuhara et al, 1994). These data suggest that the importance of the vacuole's buffering capacity requires an arsenal of proteases, which may interact with different partners

and whose activities may be fine-tuned in response to cellular conditions and environmental stresses. Understanding the cues that influence Pff1 activity will be important to place its function in the context of both cellular physiology and that of other vacuolar proteases. Expression of Pff1, by Northern blot analysis or quantitative RT-PCR, under conditions that trigger the cell wall integrity response, such as via heat stress, calcofluor white treatment, or excess Ca^{2+}, may address this question (Hohmann, 2009; Ram & Klis, 2006; Rodriguez-Pena et al, 2010; Zhao et al, 1998). This experiment might also address the potential role of Pff1 in the maintenance of cell wall integrity, which was raised in this study. However, the effect of Pff1 on the cell wall cannot be affirmed until cell wall related phenotypes of *cdc48-2pff1Δ* yeast have been re-examined, as discussed in Chapter 4.

Overall, this study has shed light on a novel putative protease that adds to the repertoire of the yeast vacuole. Further studies demonstrating Pff1 proteolytic activity and substrate specificity, as well as those breaking down the biological function of Pff1 await further research, and are greatly anticipated.

APPENDIX A

ATTEMPTS TO PURIFY THE PROTEASE DOMAIN OF YBR074 (Pff1)

In order to determine whether Pff1 has proteolytic activity, attempts were made to purify its putative M28 metalloprotease domain in order to conduct proteolytic assays *in vitro*. This section outlines the various cloning, expression, purification, and enzymatic assays used in an effort to elucidate the predicted enzymatic activity of Pff1.

A.1 ASSIGNING PROTEASE DOMAIN BOUNDARIES

An initial attempt at expressing the Pff1 protease domain was made by Douglas Placais using the sequence shown in Table 13. This construct was N-terminally GST-tagged and inserted into a pGEX2T vector with a P_{tac} promoter. However, cloning attempts resulted in rearrangements of the insert, and it was hypothesized that this was the result of toxicity induced by leaky expression of the Pff1 protease domain. To overcome the leaky expression of the Pff1 protease domain, a pET21a(+) vector was tested. In this vector, expression of the Pff1 protease domain, containing a C-terminal 6 x His tag, was under control of a P_{T7} promoter, and expression of T7 polymerase was controlled by a P_{tac} promoter.

Expression of the Pff1 protease domain from the pET21a(+) vector in BL21 (DE3) *E. coli* cells was impeded by low codon usage bias. When Rosetta Gami B (DE3) cells containing the pRARE vector encoding rare tRNAs was used instead, high molecular weight bands were

observed upon expression of the Pff1 protease domain. This suggested that this Pff1 protease domain construct was prone to aggregation. Aggregation of the protein encoding this construct may have been caused by the presence of a cysteine residue near the C-terminus, or by the presence of sequence predicted to constitute the adjacent hydrophobic transmembrane segments on either side of the Pff1 protease domain (Table 13).

In order to increase solubility of the Pff1 protease domain for the purpose of purification, alternative constructs were designed, as part of this dissertation work, using the following rationale. Construct PD_0 was designed to exclude transmembrane segment (TM) 1 based on ConPred II topology prediction, using Glu38 as the first residue. The PD_0 construct also excludes TM 2 and a flanking cysteine residue, leaving Ala341 as the C-terminal residue. Construct PD_1 boundaries are based on those of secondary structure elements within the protease domain. The secondary structure of the *Streptomyces griseus* M28 metalloprotease known as aminopeptidase S (PDB ID: 1CP7) was compared to a secondary structure of the Pff1 protease domain predicted by PSIPRED (http://bioinf.cs.ucl.ac.uk/psipred/) (Figure 34). The PD_1 construct begins at Thr75; three amino acids upstream of a predicted alpha helix, and ends at Ser332; three amino acids downstream of a predicted alpha helix (Figure 34). Construct PD_2 was designed based on the Pff1 M28 domain boundaries assigned by MEROPS (http://merops.sanger.ac.uk/). Finally, construct PD_3 was designed based on the Pff1 M28 domain boundaries assigned by Pfam (http://pfam.sanger.ac.uk/).

Table 13: Pff1 protease domain constructs designed for purification

The name, amino acid boundaries, predicted molecular weight, and amino acid sequence of each construct is shown.

Construct	Boundaries	Molecular Weight	Sequence
$PD_{Placais}$	Tyr33-Cys364	38 kDa	YIFDHERYKLNLPKEDEHPEFNDLLETAWGDLQIITASFHPYTSKENDKVHDYL LKRVLEITGNSSFASVSDDKESERSILFQQQDPFNESSRFSRVTYFESSNILVK LEGKNPEEEGLLLSAHFDSVPTGYGATDDGMGVVSLLANLKYHIKHRPNRTLIF NFNNNEEFGLLGASTYFDHSWSNLTKYVINLEGTGAGGKAVLFRTSDTSTARIY QQSVKENPFGNSIYQQGFYSRYVRSETDYKIYEENGMRGWDVAFYKPRNLYHTI KDSIQYTSKASLWHMLHTSLQLSAYVASNSLDTADQTPACYFDFIGLKFFVISA KTLFYWNC
PD_0	Glu38-Ala341	35 kDa	ERYKLNLPKEDEHPEFNDLLETAWGDLQIITASFHPYTSKENDKVHDYLLKRVL EITGNSSFASVSDDKESERSILFQQQDPFNESSRFSRVTYFESSNILVKLEGKN PEEEGLLLSAHFDSVPTGYGATDDGMGVVSLLANLKYHIKHRPNRTLIFNFNNN EEFGLLGASTYFDHSWSNLTKYVINLEGTGAGGKAVLFRTSDTSTARIYQQSVK ENPFGNSIYQQGFYSRYVRSETDYKIYEENGMRGWDVAFYKPRNLYHTIKDSIQ YTSKASLWHMLHTSLQLSAYVASNSLDTADQTPA
PD_1	Thr75-Ser332	29 kDa	TSKENDKVHDYLLKRVLEITGNSSFASVSDDKESERSILFQQQDPFNESSRFSR VTYFESSNILVKLEGKNPEEEGLLLSAHFDSVPTGYGATDDGMGVVSLLANLKY HIKHRPNRTLIFNFNNNEEFGLLGASTYFDHSWSNLTKYVINLEGTGAGGKAVL FRTSDTSTARIYQQSVKENPFGNSIYQQGFYSRYVRSETDYKIYEENGMRGWDV AFYKPRNLYHTIKDSIQYTSKASLWHMLHTSLQLSAYVASNS
PD_2	Asn96-Ala341	28 kDa	NSSFASVSDDKESERSILFQQQDPFNESSRFSRVTYFESSNILVKLEGKNPEEE GLLLSAHFDSVPTGYGATDDGMGVVSLLANLKYHIKHRPNRTLIFNFNNNEEFG LLGASTYFDHSWSNLTKYVINLEGTGAGGKAVLFRTSDTSTARIYQQSVKENPF GNSIYQQGFYSRYVRSETDYKIYEENGMRGWDVAFYKPRNLYHTIKDSIQYTSK ASLWHMLHTSLQLSAYVASNSLDTADQTPA
PD_3	Glu149-Ser332	21 kDa	EGLLLSAHFDSVPTGYGATDDGMGVVSLLANLKYHIKHRPNRTLIFNFNNNEEF GLLGASTYFDHSWSNLTKYVINLEGTGAGGKAVLFRTSDTSTARIYQQSVKENP FGNSIYQQGFYSRYVRSETDYKIYEENGMRGWDVAFYKPRNLYHTIKDSIQYTS KASLWHMLHTSLQLSAYVASNS

Key

Conf: Confidence (0=low, 9=high)

Pred: Predicted secondary structure (H=helix, E=strand, C=coil)

Pff1: Pff1 amino acid sequence

PSIPRED HFORMAT (PSIPRED V3.0)

```
Conf: 906778553214666226788999998886432101453457999989989887759999
Pred: CHHHHHHHHHHCCCCCHHHHHHHHHHHHHHHHHHCCCCCCCCCCCCCCCCCCCCCHHHHH
Pff1: MKLKSVFRSVLKYRKTNLSLLLLITYSIITLLYIFDHERYKLNLPKEDEHPEFNDLLETA
              10        20        30        40        50        60
Conf: 999999535987899965699999999999986148998634553222201343037887
Pred: HHHHHHHHCCCCCCCCHHHHHHHHHHHHHHHHHHCCCCCCCCCCCCCCCCEEEEEECCCCC
Pff1: WGDLQIITASFHPYTSKENDKVHDYLLKRVLEITGNSSFASVSDDKESERSILFQQQDPF
              70        80        90       100       110       120
Conf: 656652022331100599998378999958999010588899999876821699999999
Pred: CCCCCCEEEEEECCCEEEEEEECCCCCCCCEEEEEECCCCCCCCCCCCCCCCHHHHHHHHHH
Pff1: NESSRFSRVTYFESSNILVKLEGKNPEEEGLLLSAHFDSVPTGYGATDDGMGVVSLLANL
             130       140       150       160       170       180
Conf: 970039999419999729633550115999845355655579987225889921688719
Pred: HHHHCCCCCCEEEEEECCCCCCCCCCHHHHHHCCCCCCCCEEEEEECCCCCCCCEEEEECC
Pff1: KYHIKHRPNRTLIFNFNNNEEFGLLGASTYFDHSWSNLTKYVINLEGTGAGGKAVLFRTS
             190       200       210       220       230       240
Conf: 852899998840158888721112334788889972075764799434752315999798
Pred: CCHHHHHHHHHCCCCCCCCCCCCCCCCCCCCCCCCCHHHHHHCCCCCEEEEEECCCCCCC
Pff1: DTSTARIYQQSVKENPFGNSIYQQGFYSRYVRSETDYKIYEENGMRGWDVAFYKPRNLYH
             250       260       270       280       290       300
Conf: 968982479999999999999999999870999999999928983057269999365036
Pred: CCCCCCCCCCCHHHHHHHHHHHHHHHHHHHCCCCCCCCCCCCCCEEEEECCCEEEEEECCHHH
Pff1: TIKDSIQYTSKASLWHMLHTSLQLSAYVASNSLDTADQTPACYFDFIGLKFFVISAKTLF
             310       320       330       340       350       360
```

```
Conf: 789999999999987531011244543333303210357899999999999652012354
Pred: HHHHHHHHHHHHHHHHHHHEEECCCCCCCCCCCCEEEEHHHHHHHHHHHHHHHHHHCCCCCC
Pff1: YWNCIFLLVSPVVAIGLYLISRDRMTWKSYSWLSWTRFPLSLAAGIIVQKLFSNDIIRSN
             370       380       390       400       410       420
Conf: 431137835799998789999999986201210225743125788999999998643100
Pred: CCCCCCCCHHHHHHHHHHHHHHHHHHHHCCCCCCCCCCCCHHHHHHHHHHHHHHHHHHEE
Pff1: PLTFSRNYFWPISAFFTQVIFTSYVLINCSNFFFPCADMKSLSIIELFIILWTILLFTSK
             430       440       450       460       470       480
Conf: 00137960232026899999999999999999980764332357434478898888875 5
Pred: EECCCCCEEEECHHHHHHHHHHHHHHHHHHHHHHCCCCCCCCCCCCCCCCCCCCCCCCCC
Pff1: LLYSSDYRYTGLYPLSIFFLLSTIAAILRLLALALGMRTRKRLGRECRDHHSNYSSHSQI
             490       500       510       520       530       540
Conf: 776788999899989789898788987899976677898877667888789876556654
Pred: CCCCCCCCCCCCCCCCCCCCCCCCCCCCCCCCCCCCCCCCCCCCCCCCCCCCCCCCCCCC
Pff1: DMERDGQENLEQPQDQLTSSQDDQASIQDDNVSTTSAGPSHNVDEDHGMDSSSQQHDERV
             550       560       570       580       590       600
Conf: 433589888888752233333434784036765420266301011347777401332222
Pred: CCCCCCCCCCCCCCCCCCCCCCCCCCCCEEEEEEEEECCCCCHHHHHHHHHHHHCCCCCCC
Pff1: PLLKGSNSMEEGLSTRENSLKLEYTDYAWIIQFLLIVPIPSFILFNSVDVIMDALNHTVQ
             610       620       630       640       650       660
Conf: 3543112466777676544214765521210103678999999987542035799999999
Pred: CCCCCHHHHHHHHHHHHHHHCCCCCCEEEECHHHHHHHHHHHHHHHHHHCCCCCCCCCCC
Pff1: EGSKATFDVLRFGMVGSILIALPILPFFYKVNYITISLTALLFLISASKTLLVHPFTNSN
             670       680       690       700       710       720
Conf: 92189999964599996469997568774788852199987899714311089990003 8
Pred: CCEEEEEEEEECCCCCCCEEEEECCCCCCHHHHHHCCCCCCCCCCEEEEEECCCCCCCCEE
Pff1: PLKVRFSQNIDLSQGNAASVHVLGREGNFLKPMLQDLPSIKYSSTHINCTSVTNGMELCM
             730       740       750       760       770       780
Conf: 503899744799999855553999997068887679999706899999357511899966
Pred: EECCCCCCCCCCCCCCCCCCEEEEEEEECCCCCCCCCCCCEEEEEEEECCCCCEEEEEC
Pff1: YDGMQPNLLSTNGNTNISSMVKVHVLHNNRNSTERSPYEPIVAELLLEVKENRACTLTFE
             790       800       810       820       830       840
```

```
Conf: 888898980699995148999876664542237899553796132389973599699746
Pred: CCCCCCCCEEEEEEEECCCCCCCCCCCCCCCCCCCCCCCEEEEECCCCCCCCCEEEEEEECC
Pff1: SRHQAKSPVREITVYQKKNSAPQKANITKTIKSASGINELQLHKLDFDQETYHIGVQWFP
             850       860       870       880       890       900
Conf: 765899965555798887108999992038986545885468776135875508892899
Pred: CCCCCCCCCCCCCCCCCCCCEEEEEEEEECCCCCCCCCCCCCCCCCCCHHHHHHCCCCCEEE
Pff1: KLLTDGNVEDDKLGTKDELSVSISCYWGEYDSESVVNGTAVRKIPAFDELINYAPLSFSF
             910       920       930       940       950       960
Conf: 3068840899988989
Pred: EECCCCEEEEEEEEC
Pff1: TNEQKGLVIVKDAIIL
             970
```

Figure 34: Pff1 secondary structure predication using PSIPRED version 3.0

The transmembrane segments of Pff1 predicted using ConPredII are highlighted in grey. The M28 domain as predicted by the MEROPS database is highlighted in yellow, with conserved metal-binding residues in bold and underlined.

A.2 CLONING AND EXPRESSION OF THE PFF1 PROTEASE DOMAIN

The protease domain constructs described above were cloned into the vectors shown in Table 14. Numerous attempts to clone Pff1 protease domain into these vectors failed, with the exception of the pBAD/gIII A vector. The tightly regulated pBAD promoter is dependent on the presence of L-arabinose for induction, and can be repressed by the presence of glucose. Constructs PD_0, PD_1, PD_2 and PD_3 were successfully cloned into the pBAD vector and induced in TOP10 *E. coli* cells using 0.2% L-Arabinose at 37°C. TOP10 cells were used because they do not metabolize L-arabinose. Although protease domain expression increased over time, the optical density of the

bacterial culture expressing the protease domain began to decrease after 4 h of induction (Figure 35A). This observation supports the hypothesis that Pff1 protease domain expression is toxic in *E. coli*.

Table 14: Vectors used in attempts to clone Pff1 protease domain for purification

Vector	Promoter	Tag	Tag location	Cleavage site	Secretion Signal	Localization
pMAL-p4X	P_{tac}	6xHIS-MBP	N-terminal	Factor Xa	*malE* signal sequence	periplasmic space
pMAL-c4X	P_{tac}	MBP	N-terminal	Factor Xa	None	cytosol
pLC3	T_7	6xHIS-MBP	N-terminal	TEV	None	cytosol
pBAD/gIII A	P_{BAD}	myc-6xHIS	C-terminal	N/A	Gene III secretion signal	periplasmic space

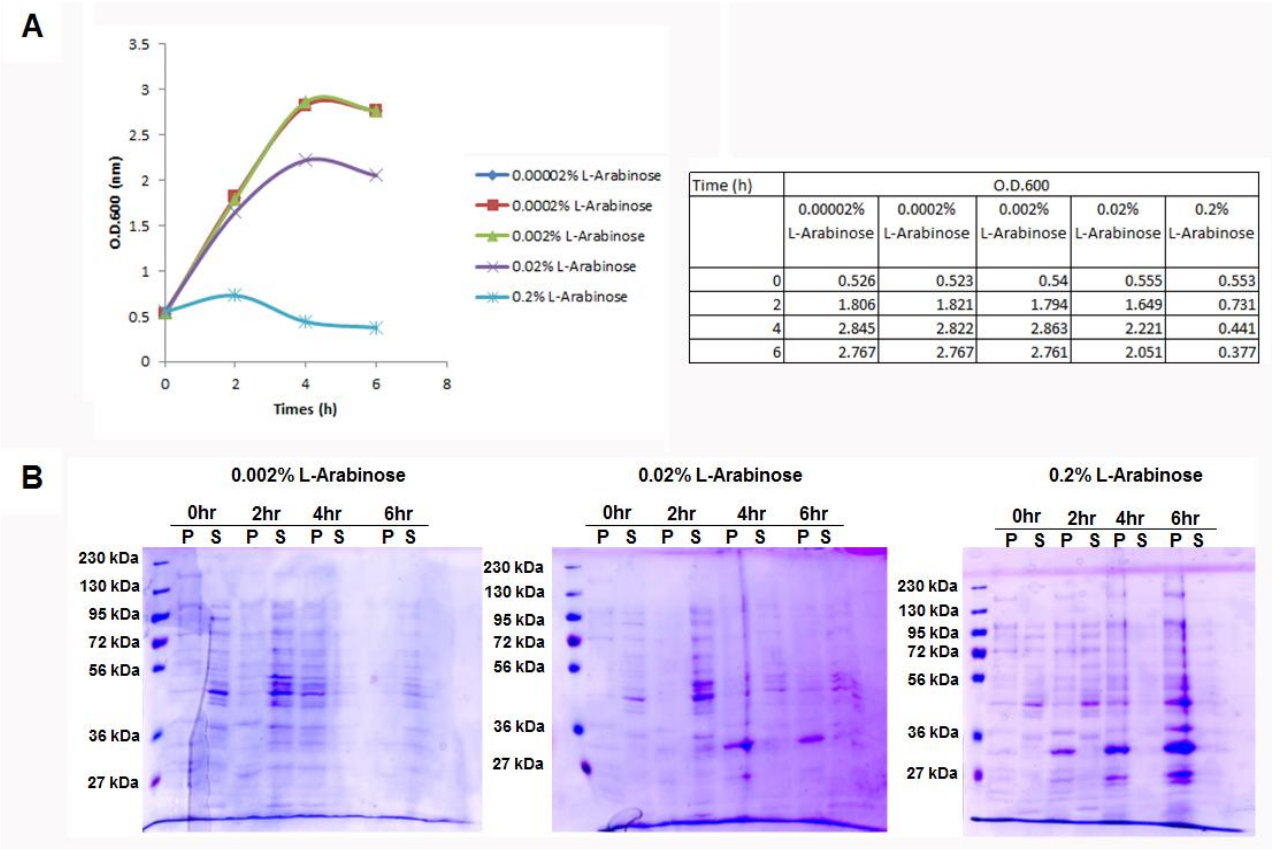

Time (h)	O.D.600				
	0.00002% L-Arabinose	0.0002% L-Arabinose	0.002% L-Arabinose	0.02% L-Arabinose	0.2% L-Arabinose
0	0.526	0.523	0.54	0.555	0.553
2	1.806	1.821	1.794	1.649	0.731
4	2.845	2.822	2.863	2.221	0.441
6	2.767	2.767	2.761	2.051	0.377

Figure 35: Expression of PD_2 from the pBAD vector

A) Optical density of TOP 10 *E.coli* expressing PD_2 at 37°C over the course of 6 h, induced by the indicated amounts of L-Arabinose. $O.D._{600}$ values are tabulated on the right (n=1) B) Cells expressing PD_2 were collected at the indicted time points, lysed, and separated into

supernatant and pellet fractions. Protein samples were normalized to the culture $O.D._{600}$ and equal quantities of protein were resolved by 10% SDS-PAGE and visualized using Coomassie brilliant blue stain. PD_2 had an apparent molecular weight of ~30 kDa and fractionated with the insoluble pellet fraction.

A.3 PILOT PURIFICATION OF THE PFF1 PROTEASE DOMAIN

A pilot purification of PD_2 was conducted using native purification buffer, or denaturing purification buffers containing 6 M urea, 1% Triton X-100, or 6 M guanidine hydrochloride (GnCl).

Native purification buffer:	50 mM NaH_2PO_4, pH 7.8
	0.5 M NaCl
6M GnCl lysis buffer:	6 M guanidine hydrochloride
	20 mM sodium phosphate pH 7.8
	500 mM NaCl
6M urea lysis buffer:	6M urea
	20 mM sodium phosphate pH 7.8
	500 mM NaCl
1% Triton X-100 lysis buffer:	1% Triton X-100
	20 mM sodium phosphate pH 7.8
	500 mM NaCl

A 250mL culture was induced using 0.2% L-Arabinose for 4 h at 37°C. Cells were harvested by centrifugation at 5000 g for 10 min at 4°C in a GSA rotor. The pellet was re-suspended 32 mL

native purification buffer and split into four 8 mL samples. Each 8 mL sample was treated using 8 mg of chicken egg lysozyme for 30 min on ice and in the presence of protease inhibitors (PMSF, Leupeptin, and Pepstatin A). Cells were then lysed by sonication on ice in four 30 sec pulses with 1 min intervals on ice between pulses. Lysates were cleared by centrifugation at 3000 *g* for 15 min at 4°C in an SS-34 rotor. Cleared lysates were re-suspended in 8 mL of native binding buffer, 6M GnCl lysis buffer, 6M urea buffer, or 1% Triton X-100 buffer. Cells were incubated on ice for 20 min with occasional mixing to ensure thorough lysis. Lysates were centrifuged at 3000 *g* for 15 min at 4°C. Supernatants were added to 2 mL of equilibrated Ni^{2+}-NTA resin and allowed to bind in batch on a nutator for 60 min at 4°C. The resin was allowed to settle, the flow through was collected, and the resin was washed twice with 8 mL wash buffer (10 mM imidazole, 20 mM sodium phosphate pH 7.8, 500 mM NaCl). SDS-PAGE sample buffer was added to 10 μL of resin from each in batch purification and protein bound to the resin was resolved on 10% SDS-polyacrylamide gel and visualized by Coomassie brilliant blue staining (Figure 36). Purification using 6 M guanidine hydrochloride lysis buffer appeared to produce the best combination of yield and purity.

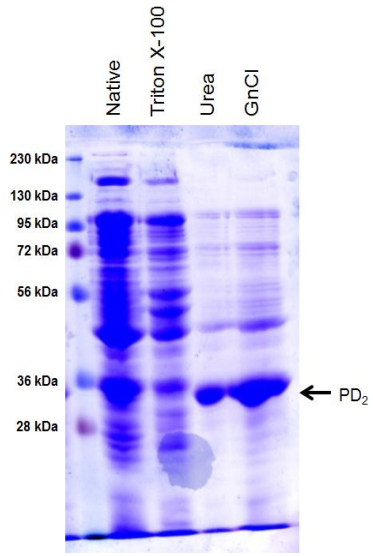

Figure 36: Pilot purification of PD2

PD2 (~30 kDa) is shown by coomassie blue staining of a 10% SDS-PAGE gel. PD_2-myc-6xHIS purified in batch using native binding buffer, 1% Triton X-100 lysis buffer, 6 M urea lysis buffer, or 6 M guanidine hydrochloride (GnCl) lysis buffer.

A.4 PURIFICATION PROCEDURE FOR PFF1 PROTEASE DOMAIN

Cells were grown in 1 L Luria broth (LB) supplemented with 200 µg/mL ampicillin at 37°C to an $O.D._{600}$= 0.7-0.9. Pff1 protease domain expression was induced with 0.2% L-Arabinose for 4 h at 37°C. Cells were spun down in two 500 mL batches at 5000 *g* for 6 min at 4°C in an F7S rotor. The cell pellet was re-suspended in 10 mL 6 M GnCl lysis buffer supplemented with protease inhibitors (PMSF, Leupeptin, Pepstatin A). Cells were then lysed by sonication in three 30 sec pulses with 1 min intervals on ice between pulses to prevent heat-induced protein denaturation. Lysates were cleared by centrifugation at 12 000 *g* for 15 min at 4°C using an SS-34 rotor. The cleared lysate was added to 5 mL of equilibrated Ni^{2+}-NTA resin and the His-

tagged Pff1 protease domain was allowed to bind the resin in batch on a rocker for 60 min at 4°C. The resin was allowed to settle and the flow-through was removed. The resin was washed four times using 15 mL of 6 M GnCl lysis buffer by incubation for 5 min at 4°C. Protein was then eluted in 8-10 steps from the resin using 1 mL washes with elution buffer. This protocol typically yielded purified Pff1 protease domain at a concentration of approximately 0.5 mg/mL.

Since SDS precipitates in the presence of guanidine hydrochloride, 50 µL of each protein purification sample was TCA precipitated and acetone washed prior to re-suspension in SDS-PAGE sample buffer. Protein purification samples were resolved by 10% SDS-PAGE gels and protein was visualized by Coomassie brilliant blue staining.

6M GnCl lysis buffer:	6 M guanidine hydrochloride
	10 mM imidazole
	20 mM sodium phosphate pH 7.8
	500 mM NaCl
Elution buffer:	6 M guanidine hydrochloride
	500 mM imidazole
	50 mM NaH_2PO_4, pH 7.8
	0.5 M NaCl

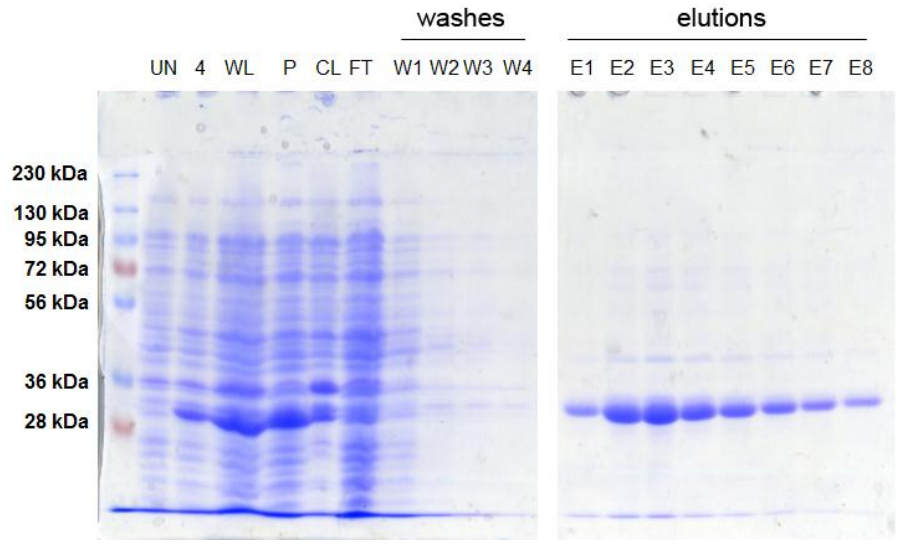

Figure 37: PD_2 in batch purification gel

10% SDS-polyacrylamide gel in which protein is visualized by Coomassie brilliant blue staining. Samples shown are protein from uninduced cells (UN), cells induced for 4 h (4), whole lysate (WL), pellet (P), cleared lysate (CL), flow through (FT), washes (W1-4), and elutions (E1-8). PD_2, with an apparent molecular mass of ~30 kDa, is enriched in elution fractions.

A.5 REFOLDING THE PFF1 PROTEASE DOMAIN

In order to use the purified Pff1 protease domain in an *in vitro* enzymatic assay, the protease domain must be re-folded back into its native structure. To do this, the guanidine hydrochloride had to be removed from the eluted protein sample by dialysis. Solubility of PD_2 could be maintained in as low as 2M guanidine hydrochloride, but any further reduction in guanidine hydrochloride concentration resulted in PD_2 crashing out of solution (Figure 37).

This result was observed after overnight dialysis at 4°C of 500 µL of purified PD_2 into 4 M GnCl, 150 mM NaCl, 250 mM sorbitol, 10% glycerol, 400 mM arginine pH 7.8. In a second

step, the protein was dialyzed for 5.5 h at 4°C into a solution containing 2 M GnCl, 150 mM NaCl, 250 mM sorbitol, 10% glycerol, 400 mM arginine pH 7.8 (Figure 37). Finally, the protein was dialyzed overnight at 4°C into 1 M GnCl, 150 mM NaCl, 250 mM sorbitol, 10% glycerol, 400 mM arginine pH 7.8 in the presence or absence of 1 mM $ZnCl_2$. Since zinc is a cofactor for M28 family metalloproteases, I hypothesized that the presence of zinc in the dialysis buffer might facilitate refolding. However, zinc did not have an effect on PD_2 solubility under these conditions.

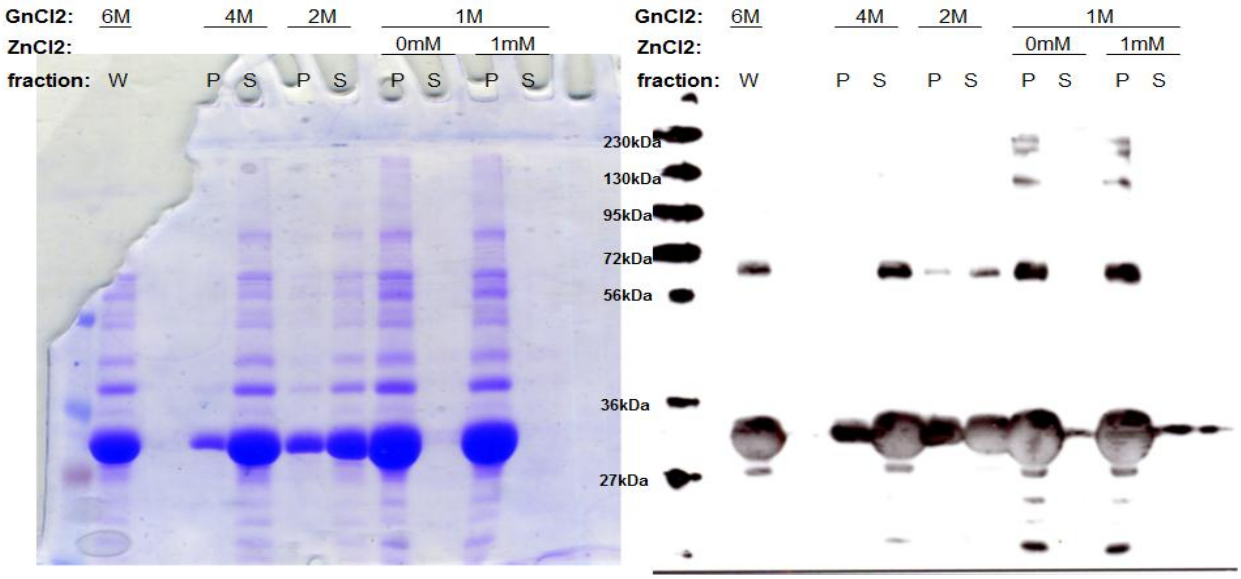

Figure 38: Refolding of PD_2 by dialysis

The left panel shows a Coomassie brilliant blue stained 10% SDS-polyacrylamide gel of PD_2 samples. At 6 M GnCl the whole (W) protein sample was loaded, while at 4 M, 2 M, and 1 M GnCl each sample was fractionated by centrifugation into an insoluble pellet (P) and soluble (S) fraction. Zinc chloride was omitted from all dialysis buffers except the 1 M GnCl buffer, as indicated. The right panel shows the same samples analyzed by western blot analysis using an anti-5XHis antibody to visualize PD_2 protein.

In addition to dialysis, fast dilution of PD_2 into various refolding buffers was attempted based on previous successes of this method (Vincentelli et al, 2004). Purified PD_2 was diluted 20-fold into various refolding buffers, listed in Table 15, in a 96-well plate. Isopropanol was used as a negative control and elution buffer was used as a positive control for PD_2 solubility. Differences among the refolding buffers in maintaining PD_2 solubility could not be reliably ascertained by measuring absorbance because precipitated protein settled to the bottom of the wells and resulted in spurious readings. To overcome this problem, samples were collected from the 96-well plates and separated by centrifugation into insoluble and soluble fractions. Protein in these fractions was resolved by 10% SDS-PAGE and visualized by silver staining. Although there may have been a tendency towards more protein partitioning to the soluble fraction in buffers containing arginine at pH 8 or 9, these results were also inconsistent.

Table 15: Refolding buffers tested on PD_2 in a 96-well plate format

Row	Column	Buffer
A	1	isopropanol
B	1	elution buffer
C	1	50 mM sodium acetate pH 4
D	1	50 mM sodium acetate pH 4, 100 mM NaCl
E	1	50 mM sodium acetate pH 4, 200 mM NaCl
F	1	50 mM sodium acetate pH 4, 20% glycerol, 50 µM $CaCl_2$, 50 µM $MgCl_2$, 50 µM $ZnCl_2$, 50 µM $NiCl_2$, 50 µM $CuSO_4$
G	1	50 mM sodium acetate pH 4, 0.05% PEG, 500 mM glucose
H	1	50 mM sodium acetate pH 4, 1 mM EDTA
A	3	50 mM sodium acetate pH 4, 800 mM arginine
B	3	50 mM MES pH 5
C	3	50 mM MES pH 5, 100 mM NaCl
D	3	50 mM MES pH 5, 200 mM NaCl
E	3	50 mM MES pH 5, 20% glycerol, 50 µM CaCl2, 50 µM MgCl2, 50 µM ZnCl2, 50 µM NiCl2, 50 µM CuSO4
F	3	50 mM MES pH 5, 0.05% PEG, 500 mM glucose
G	3	50 mM MES pH 5, 1 mM EDTA
H	3	50 mM MES pH 5, 800 mM arginine
A	5	50 mM MES pH 6
B	5	50 mM MES pH 6, 100 mM NaCl
C	5	50 mM MES pH 6, 200 mM NaCl
D	5	50 mM MES pH 6, 20% glycerol, 50 µM CaCl2, 50 µM MgCl2, 50 µM ZnCl2, 50 µM NiCl2, 50 µM CuSO4
E	5	50 mM MES pH 6, 0.05% PEG, 500 mM glucose
F	5	50 mM MES pH 6, 1 mM EDTA
G	5	50 mM MES pH 6, 800 mM arginine
H	5	50 mM Tris pH 7
A	7	50 mM Tris pH 7, 100 mM NaCl
B	7	50 mM Tris pH 7, 200 mM NaCl
C	7	50 mM Tris pH 7, 20% glycerol, 50 µM CaCl2, 50 µM MgCl2, 50 µM ZnCl2, 50 µM NiCl2, 50 µM CuSO4
D	7	50 mM Tris pH 7, 0.05% PEG, 500 mM glucose
E	7	50 mM Tris pH 7, 1 mM EDTA
F	7	50 mM Tris pH 7, 800 mM arginine
G	7	50 mM Tris pH 8
H	7	50 mM Tris pH 8, 100 mM NaCl
A	9	50 mM Tris pH 8, 200 mM NaCl
B	9	50 mM Tris pH 8, 20% glycerol, 50 µM CaCl2, 50 µM MgCl2, 50 µM ZnCl2, 50 µM NiCl2, 50 µM CuSO4
C	9	50 mM Tris pH 8, 0.05% PEG, 500 mM glucose
D	9	50 mM Tris pH 8, 1 mM EDTA
E	9	50 mM Tris pH 8, 800 mM arginine
F	9	50 mM CHES pH 9
G	9	50 mM CHES pH 9, 100 mM NaCl
H	9	50 mM CHES pH 9, 200 mM NaCl
A	11	50 mM CHES pH 9, 20% glycerol, 50 µM CaCl2, 50 µM MgCl2, 50 µM ZnCl2, 50 µM NiCl2, 50 µM CuSO4
B	11	50 mM CHES pH 9, 0.05% PEG, 500 mM glucose
C	11	50 mM CHES pH 9, 1 mM EDTA
D	11	50 mM CHES pH 9, 800 mM arginine
E	11	50 mM MES pH 5, 800 mM arginine, 50 µM CaCl2, 50 µM MgCl2, 50 µM ZnCl2, 50 µM NiCl2, 50 µM CuSO4
F	11	50 mM MES pH 6, 800 mM arginine, 50 µM CaCl2, 50 µM MgCl2, 50 µM ZnCl2, 50 µM NiCl2, 50 µM CuSO4
G	11	50 mM Tris pH 7, 800 mM arginine, 50 µM CaCl2, 50 µM MgCl2, 50 µM ZnCl2, 50 µM NiCl2, 50 µM CuSO4
H	11	50 mM Tris pH 8, 800 mM arginine, 50 µM CaCl2, 50 µM MgCl2, 50 µM ZnCl2, 50 µM NiCl2, 50 µM CuSO4

Arginine has been used successfully to refold nucleotide binding domain (NBD) 1 of the cystic fibrosis transmembrane conductance regulator (CFTR) from a purification buffer containing 6 M guanidine hydrochloride (Qu & Thomas, 1996). It has been proposed that the guanidinium group of arginine helps solubilize polar residues, while its aliphatic 3-carbon chain may protect hydrophobic regions of the protein from aggregation. In order to assess whether arginine may be an effective refolding reagent for PD_2, a similar re-folding buffer was tested. Refolding buffer containing 100 mM Tris-HCl pH 8.0, 400 mM L-arginine-HCl, 2 mM EDTA, 1 mM DTT, and 1 mM $ZnCl_2$500 µL was used to dilute 500 µL of purified PD_2 in 6 M GnCl-containing elution buffer 50-fold. The diluted protein was incubated on a nutator overnight at 4°C. Soluble PD_2 was isolated by centrifugation at 16 000 *g* for 20 min at 4°C in an SS-34 rotor. The supernatant fraction was TCA precipitated and the protein resolved on a 10% SDS-polyacrylamide gel and visualized by Coomassie brilliant blue staining and silver staining. Using the same treatment in which L-arginine in the refolding buffer was replaced with L-histidine also produced some soluble PD_2 but at a lower level. This suggests that L-arginine promotes PD_2 solubility in the course of protein refolding.

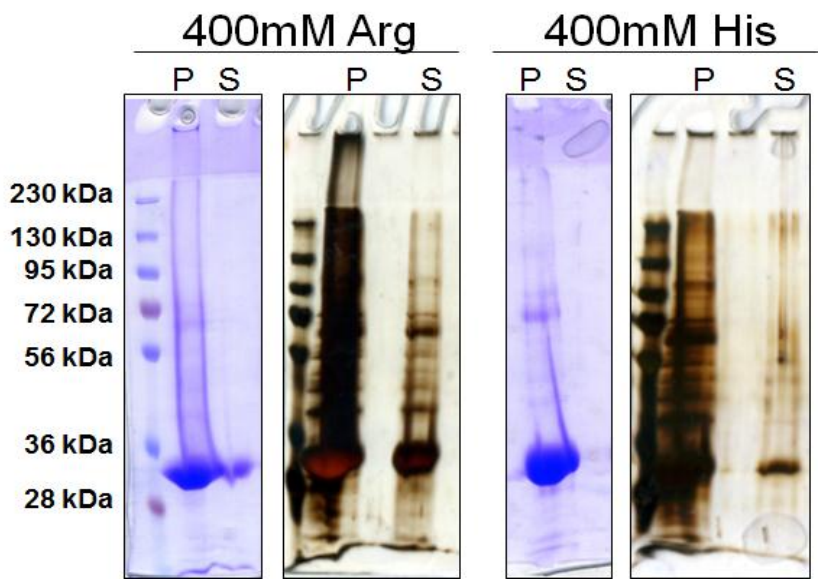

Figure 39: Fast dilution of PD_2 in refolding buffer containing L-arginine or L-histidine

Purified PD_2 was diluted 50 fold from a 6 M GnCl elution buffer to a refolding buffer containing L-arginine or L-histidine. Protein partitioning to the pellet and supernatant fractions is shown resolved by 10% SDS-PAGE and visualized by Coomiassie brilliant blue staining and silver staining.

A.6 ASSAYS FOR PROTEOLYTIC ACTIVITY

In order to test the proteolytic activity of the Pff1 protease domain two different colorimetric assay were employed: an azocasein cleavage assay and an L-leucine p-nitroanilide (LeuNA) cleavage assay. The azocasein assay is targeted towards endopeptidases, while the LeuNA assay is targeted towards exopeptidases.

The azocasein cleavage assay was performed as follows. Azocasein powder (Sigma) was dissolved in a 0.5% (w/v) sodium carbonate solution to produce a 2.5% (w/v) azocasein solution.

500 μL of this azocasein solution was mixed with 300 μL of 0.5% (w/v) sodium carbonate and allowed to equilibrate at 37°C. The equilibrated mixture was supplemented with 200 μL of purified Pff1 protease domain and incubated with shaking in a 37 °C water bath for 30 min. The reaction was stopped using 4 mL of 5% TCA, forming a yellow precipitate. This precipitate was separated from the solution by centrifugation at 12 000 *g* for 10 min at 4°C in an SS-34 rotor. 1 mL of the clear supernatant was transferred to a fresh borosilicate culture tube and mixed with 3 mL of 0.5 M NaOH, producing a yellowish color. Absorbance was measured at 440 nm. Trypsin was used as a positive control for this assay.

It was found that imidazole in the elution buffer interfered with the azocasein assay by resulting in absorbance at 440 nm even in the absence of any protein. Therefore, for future reference it is important to note that Pff1 protease activity cannot be tested without dialyzing out the imidazole first.

Although the possibility that Pff1 is an endopeptidase cannot be excluded, it is important to note that the M28 family of metalloproteases is comprised of exopeptidases. Among these are the *S. griseus* aminopeptidase, SGAP, and the *Vibrio proteolyticus* (also known as *Aeromonas proteolytica*) aminiopeptidase, AAP. Both of these aminopeptidase exhibit a specificity for leucine at their substrate binding site and have shown proteolytic activity in the presence of the substrate LeuNA (Arima et al, 2006).

The LeuNA cleavage assay was modified from the Sigma protocol and performed as a 96-well plate assay in the following manner. In each well, 933 μL of 50 mM sodium phosphate buffer, pH 7.2 was mixed with 33 μL of 24 mM LeuNA solution prepared in methanol. The mixed solution was equilibrated at 37°C and the absorbance at 405 nm was monitored until it remained constant. Then 33 μL of enzyme was added, the solution was mixed and the A_{405} was

read every minute for 6 min. Leucine aminopeptidase, microsomal, porcine kidney (Sigma) was used as a positive control, and buffer was used as a negative control. Although a steady increase in A_{405} was observed for the positive control, leucine aminopeptidase, none was observed for purified PD_2 or PD_0 (data not shown). Furthermore, it was observed that L-arginine inhibited the positive control reaction completely. This suggests that the activity of Pff1 protease domain refolded in the presence of L-arginine cannot be determined using this assay.

BIBLIOGRAPHY

Adachi W, Suzuki NN, Fujioka Y, Suzuki K, Ohsumi Y, Inagaki F (2007) Crystallization of Saccharomyces cerevisiae aminopeptidase 1, the major cargo protein of the Cvt pathway. *Acta crystallographica Section F, Structural biology and crystallization communications* **63:** 200-203

Adamis PD, Mannarino SC, Riger CJ, Duarte G, Cruz A, Pereira MD, Eleutherio EC (2009) Lap4, a vacuolar aminopeptidase I, is involved in cadmium-glutathione metabolism. *Biometals : an international journal on the role of metal ions in biology, biochemistry, and medicine* **22:** 243-249

Adams A, Kaiser C, Cold Spring Harbor Laboratory. (1998) *Methods in yeast genetics : a Cold Spring Harbor Laboratory course manual*, 1997 edn. Plainview, N.Y.: Cold Spring Harbor Laboratory Press.

Ahner A, Nakatsukasa K, Zhang H, Frizzell RA, Brodsky JL (2007) Small heat-shock proteins select deltaF508-CFTR for endoplasmic reticulum-associated degradation. *Molecular biology of the cell* **18:** 806-814

Ahner A, University of Pittsburgh. School of Arts and Sciences. (2005) THE ROLE OF CYTOPLASMIC CHAPERONES IN THE BIOGENESIS, MATURATION, AND DEGRADATION OF CYTOPLASMIC AND INTEGRAL MEMBRANE PROTEINS. University of Pittsburgh, Pittsburgh, PA.

Alder NN, Johnson AE (2004) Cotranslational membrane protein biogenesis at the endoplasmic reticulum. *The Journal of biological chemistry* **279:** 22787-22790

Alper BJ, Rowse JW, Schmidt WK (2009) Yeast Ste23p shares functional similarities with mammalian insulin-degrading enzymes. *Yeast* **26:** 595-610

Altschul SF, Madden TL, Schaffer AA, Zhang J, Zhang Z, Miller W, Lipman DJ (1997) Gapped BLAST and PSI-BLAST: a new generation of protein database search programs. *Nucleic acids research* **25:** 3389-3402

Altschul SF, Wootton JC, Gertz EM, Agarwala R, Morgulis A, Schaffer AA, Yu YK (2005) Protein database searches using compositionally adjusted substitution matrices. *The FEBS journal* **272:** 5101-5109

Arai M, Mitsuke H, Ikeda M, Xia JX, Kikuchi T, Satake M, Shimizu T (2004) ConPred II: a consensus prediction method for obtaining transmembrane topology models with high reliability. *Nucleic acids research* **32:** W390-393

Arima J, Uesugi Y, Iwabuchi M, Hatanaka T (2006) Study on peptide hydrolysis by aminopeptidases from Streptomyces griseus, Streptomyces septatus and Aeromonas proteolytica. *Applied microbiology and biotechnology* **70:** 541-547

Baba M, Osumi M, Scott SV, Klionsky DJ, Ohsumi Y (1997) Two distinct pathways for targeting proteins from the cytoplasm to the vacuole/lysosome. *The Journal of cell biology* **139:** 1687-1695

Barrowman J, Michaelis S (2009) ZMPSTE24, an integral membrane zinc metalloprotease with a connection to progeroid disorders. *Biological chemistry* **390:** 761-773

Beau I, Esclatine A, Codogno P (2008) Lost to translation: when autophagy targets mature ribosomes. *Trends in cell biology* **18:** 311-314

Bermejo C, Garcia R, Straede A, Rodriguez-Pena JM, Nombela C, Heinisch JJ, Arroyo J (2010) Characterization of sensor-specific stress response by transcriptional profiling of wsc1 and mid2 deletion strains and chimeric sensors in Saccharomyces cerevisiae. *Omics : a journal of integrative biology* **14:** 679-688

Bernales S, Schuck S, Walter P (2007) ER-phagy: selective autophagy of the endoplasmic reticulum. *Autophagy* **3:** 285-287

Bhamidipati A, Denic V, Quan EM, Weissman JS (2005) Exploration of the topological requirements of ERAD identifies Yos9p as a lectin sensor of misfolded glycoproteins in the ER lumen. *Molecular cell* **19:** 741-751

Bleackley MR, Young BP, Loewen CJ, MacGillivray RT (2011) High density array screening to identify the genetic requirements for transition metal tolerance in Saccharomyces cerevisiae. *Metallomics : integrated biometal science* **3:** 195-205

Blom N, Sicheritz-Ponten T, Gupta R, Gammeltoft S, Brunak S (2004) Prediction of post-translational glycosylation and phosphorylation of proteins from the amino acid sequence. *Proteomics* **4:** 1633-1649

Boeke JD, Trueheart J, Natsoulis G, Fink GR (1987) 5-Fluoroorotic acid as a selective agent in yeast molecular genetics. *Methods in enzymology* **154:** 164-175

Boettner DR, Chi RJ, Lemmon SK (2012) Lessons from yeast for clathrin-mediated endocytosis. *Nature cell biology* **14:** 2-10

Bonifacino JS (2004) The GGA proteins: adaptors on the move. *Nature reviews Molecular cell biology* **5:** 23-32

Boone C, Sommer SS, Hensel A, Bussey H (1990) Yeast KRE genes provide evidence for a pathway of cell wall beta-glucan assembly. *The Journal of cell biology* **110:** 1833-1843

Bowers K, Stevens TH (2005) Protein transport from the late Golgi to the vacuole in the yeast Saccharomyces cerevisiae. *Biochimica et biophysica acta* **1744:** 438-454

Bowman BJ, Bowman EJ (1986) H+-ATPases from mitochondria, plasma membranes, and vacuoles of fungal cells. *The Journal of membrane biology* **94:** 83-97

Boyartchuk VL, Rine J (1998) Roles of prenyl protein proteases in maturation of Saccharomyces cerevisiae a-factor. *Genetics* **150:** 95-101

Braakman I, Bulleid NJ (2011) Protein folding and modification in the mammalian endoplasmic reticulum. *Annual review of biochemistry* **80:** 71-99

Brachat S, Dietrich FS, Voegeli S, Zhang Z, Stuart L, Lerch A, Gates K, Gaffney T, Philippsen P (2003) Reinvestigation of the Saccharomyces cerevisiae genome annotation by comparison to the genome of a related fungus: Ashbya gossypii. *Genome biology* **4:** R45

Brachmann CB, Davies A, Cost GJ, Caputo E, Li J, Hieter P, Boeke JD (1998) Designer deletion strains derived from Saccharomyces cerevisiae S288C: a useful set of strains and plasmids for PCR-mediated gene disruption and other applications. *Yeast* **14:** 115-132

Braun NA, Morgan B, Dick TP, Schwappach B (2010) The yeast CLC protein counteracts vesicular acidification during iron starvation. *Journal of cell science* **123:** 2342-2350

Bredemeyer AJ, Lewis RM, Malone JP, Davis AE, Gross J, Townsend RR, Ley TJ (2004) A proteomic approach for the discovery of protease substrates. *Proceedings of the National Academy of Sciences of the United States of America* **101:** 11785-11790

Brittle EE, Waters MG (2000) Cell biology. ER-to-Golgi traffic--this bud's for you. *Science* **289:** 403-404

Broach JR, Pringle JR, Jones EW (1991) *The Molecular and cellular biology of the yeast Saccharomyces*, Cold Spring Harbor, N.Y.: Cole Spring Harbor Laboratory Press.

Brocker C, Kuhlee A, Gatsogiannis C, Balderhaar HJ, Honscher C, Engelbrecht-Vandre S, Ungermann C, Raunser S (2012) Molecular architecture of the multisubunit homotypic fusion and vacuole protein sorting (HOPS) tethering complex. *Proceedings of the National Academy of Sciences of the United States of America* **109:** 1991-1996

Brodsky JL, Hamamoto S, Feldheim D, Schekman R (1993) Reconstitution of protein translocation from solubilized yeast membranes reveals topologically distinct roles for BiP and cytosolic Hsc70. *The Journal of cell biology* **120:** 95-102

Brodsky JL, Lawrence JG, Caplan AJ (1998) Mutations in the cytosolic DnaJ homologue, YDJ1, delay and compromise the efficient translation of heterologous proteins in yeast. *Biochemistry* **37:** 18045-18055

Buchan DW, Ward SM, Lobley AE, Nugent TC, Bryson K, Jones DT (2010) Protein annotation and modelling servers at University College London. *Nucleic acids research* **38:** W563-568

Bussey H (1991) K1 killer toxin, a pore-forming protein from yeast. *Molecular microbiology* **5:** 2339-2343

Carotti C, Ragni E, Palomares O, Fontaine T, Tedeschi G, Rodriguez R, Latge JP, Vai M, Popolo L (2004) Characterization of recombinant forms of the yeast Gas1 protein and identification of

residues essential for glucanosyltransferase activity and folding. *European journal of biochemistry / FEBS* **271:** 3635-3645

Carvalho P, Stanley AM, Rapoport TA (2010) Retrotranslocation of a misfolded luminal ER protein by the ubiquitin-ligase Hrd1p. *Cell* **143:** 579-591

Castillon GA, Aguilera-Romero A, Manzano-Lopez J, Epstein S, Kajiwara K, Funato K, Watanabe R, Riezman H, Muniz M (2011) The yeast p24 complex regulates GPI-anchored protein transport and quality control by monitoring anchor remodeling. *Molecular biology of the cell* **22:** 2924-2936

Cheng J, Randall AZ, Sweredoski MJ, Baldi P (2005) SCRATCH: a protein structure and structural feature prediction server. *Nucleic acids research* **33:** W72-76

Clark NL, Alani E, Aquadro CF (2012) Evolutionary rate covariation reveals shared functionality and coexpression of genes. *Genome research* **22:** 714-720

Claros MG, von Heijne G (1994) TopPred II: an improved software for membrane protein structure predictions. *Computer applications in the biosciences : CABIOS* **10:** 685-686

Cohen Y, Schuldiner M (2011) Advanced methods for high-throughput microscopy screening of genetically modified yeast libraries. *Methods Mol Biol* **781:** 127-159

Collins GA, Gomez TA, Deshaies RJ, Tansey WP (2010) Combined chemical and genetic approach to inhibit proteolysis by the proteasome. *Yeast* **27:** 965-974

Cowles CR, Odorizzi G, Payne GS, Emr SD (1997) The AP-3 adaptor complex is essential for cargo-selective transport to the yeast vacuole. *Cell* **91:** 109-118

Dargemont C, Ossareh-Nazari B (2012) Cdc48/p97, a key actor in the interplay between autophagy and ubiquitin/proteasome catabolic pathways. *Biochimica et biophysica acta* **1823:** 138-144

Darsow T, Katzmann DJ, Cowles CR, Emr SD (2001) Vps41p function in the alkaline phosphatase pathway requires homo-oligomerization and interaction with AP-3 through two distinct domains. *Molecular biology of the cell* **12:** 37-51

de Nobel H, Ruiz C, Martin H, Morris W, Brul S, Molina M, Klis FM (2000) Cell wall perturbation in yeast results in dual phosphorylation of the Slt2/Mpk1 MAP kinase and in an Slt2-mediated increase in FKS2-lacZ expression, glucanase resistance and thermotolerance. *Microbiology* **146 (Pt 9):** 2121-2132

de Nobel JG, Klis FM, Priem J, Munnik T, van den Ende H (1990) The glucanase-soluble mannoproteins limit cell wall porosity in Saccharomyces cerevisiae. *Yeast* **6:** 491-499

DeLaBarre B, Brunger AT (2003) Complete structure of p97/valosin-containing protein reveals communication between nucleotide domains. *Nature structural biology* **10:** 856-863

Denning GM, Anderson MP, Amara JF, Marshall J, Smith AE, Welsh MJ (1992) Processing of mutant cystic fibrosis transmembrane conductance regulator is temperature-sensitive. *Nature* **358:** 761-764

Dietrich FS, Voegeli S, Brachat S, Lerch A, Gates K, Steiner S, Mohr C, Pohlmann R, Luedi P, Choi S, Wing RA, Flavier A, Gaffney TD, Philippsen P (2004) The Ashbya gossypii genome as a tool for mapping the ancient Saccharomyces cerevisiae genome. *Science* **304:** 304-307

Dong H, Czaja MJ (2011) Regulation of lipid droplets by autophagy. *Trends in endocrinology and metabolism: TEM* **22:** 234-240

Dubois M, Gilles KA, Hamilton JK, Rebers PA, Smith F (1956) Colorimetric Method for Determination of Sugars and Related Substances. *Anal Chem* **28:** 350-356

Duden R (2003) ER-to-Golgi transport: COP I and COP II function (Review). *Molecular membrane biology* **20:** 197-207

Dunn BM (2002) Structure and mechanism of the pepsin-like family of aspartic peptidases. *Chemical reviews* **102:** 4431-4458

Dunn WA, Jr., Cregg JM, Kiel JA, van der Klei IJ, Oku M, Sakai Y, Sibirny AA, Stasyk OV, Veenhuis M (2005) Pexophagy: the selective autophagy of peroxisomes. *Autophagy* **1:** 75-83

Egea PF, Stroud RM (2010) Lateral opening of a translocon upon entry of protein suggests the mechanism of insertion into membranes. *Proceedings of the National Academy of Sciences of the United States of America* **107:** 17182-17187

Epple UD, Suriapranata I, Eskelinen EL, Thumm M (2001) Aut5/Cvt17p, a putative lipase essential for disintegration of autophagic bodies inside the vacuole. *Journal of bacteriology* **183:** 5942-5955

Farley PC, Shepherd MG, Sullivan PA (1986) The purification and properties of yeast proteinase B from Candida albicans. *The Biochemical journal* **236:** 177-184

Finley D (2009) Recognition and processing of ubiquitin-protein conjugates by the proteasome. *Annual review of biochemistry* **78:** 477-513

Fratti RA, Jun Y, Merz AJ, Margolis N, Wickner W (2004) Interdependent assembly of specific regulatory lipids and membrane fusion proteins into the vertex ring domain of docked vacuoles. *The Journal of cell biology* **167:** 1087-1098

Friedberg I (2006) Automated protein function prediction--the genomic challenge. *Briefings in bioinformatics* **7:** 225-242

Froquet R, Cherix N, Birke R, Benghezal M, Cameroni E, Letourneur F, Mosch HU, De Virgilio C, Cosson P (2008) Control of cellular physiology by TM9 proteins in yeast and Dictyostelium. *The Journal of biological chemistry* **283:** 6764-6772

Fujiki Y, Hubbard AL, Fowler S, Lazarow PB (1982) Isolation of intracellular membranes by means of sodium carbonate treatment: application to endoplasmic reticulum. *The Journal of cell biology* **93:** 97-102

Fujita M, Yoko OT, Jigami Y (2006) Inositol deacylation by Bst1p is required for the quality control of glycosylphosphatidylinositol-anchored proteins. *Molecular biology of the cell* **17:** 834-850

Fundoiano-Hershcovitz Y, Rabinovitch L, Langut Y, Reiland V, Shoham G, Shoham Y (2004) Identification of the catalytic residues in the double-zinc aminopeptidase from Streptomyces griseus. *FEBS letters* **571:** 192-196

Gakh O, Cavadini P, Isaya G (2002) Mitochondrial processing peptidases. *Biochimica et biophysica acta* **1592:** 63-77

Ganguli D, Kumar C, Bachhawat AK (2007) The alternative pathway of glutathione degradation is mediated by a novel protein complex involving three new genes in Saccharomyces cerevisiae. *Genetics* **175:** 1137-1151

Garcia-Rudaz C, Luna F, Tapia V, Kerr B, Colgin L, Galimi F, Dissen GA, Rawlings ND, Ojeda SR (2007) Fxna, a novel gene differentially expressed in the rat ovary at the time of folliculogenesis, is required for normal ovarian histogenesis. *Development* **134:** 945-957

Garcia R, Rodriguez-Pena JM, Bermejo C, Nombela C, Arroyo J (2009) The high osmotic response and cell wall integrity pathways cooperate to regulate transcriptional responses to zymolyase-induced cell wall stress in Saccharomyces cerevisiae. *The Journal of biological chemistry* **284:** 10901-10911

Garre E, Matallana E (2009) The three trehalases Nth1p, Nth2p and Ath1p participate in the mobilization of intracellular trehalose required for recovery from saline stress in Saccharomyces cerevisiae. *Microbiology* **155:** 3092-3099

Garza RM, Sato BK, Hampton RY (2009) In vitro analysis of Hrd1p-mediated retrotranslocation of its multispanning membrane substrate 3-hydroxy-3-methylglutaryl (HMG)-CoA reductase. *The Journal of biological chemistry* **284:** 14710-14722

Gasch AP, Spellman PT, Kao CM, Carmel-Harel O, Eisen MB, Storz G, Botstein D, Brown PO (2000) Genomic expression programs in the response of yeast cells to environmental changes. *Molecular biology of the cell* **11:** 4241-4257

Ghaemmaghami S, Huh WK, Bower K, Howson RW, Belle A, Dephoure N, O'Shea EK, Weissman JS (2003) Global analysis of protein expression in yeast. *Nature* **425:** 737-741

Gimeno CJ, Ljungdahl PO, Styles CA, Fink GR (1992) Unipolar cell divisions in the yeast S. cerevisiae lead to filamentous growth: regulation by starvation and RAS. *Cell* **68:** 1077-1090

Girao H, Geli MI, Idrissi FZ (2008) Actin in the endocytic pathway: from yeast to mammals. *FEBS letters* **582:** 2112-2119

Glickman MH, Rubin DM, Fu H, Larsen CN, Coux O, Wefes I, Pfeifer G, Cjeka Z, Vierstra R, Baumeister W, Fried V, Finley D (1999) Functional analysis of the proteasome regulatory particle. *Molecular biology reports* **26:** 21-28

Goder V, Melero A (2011) Protein O-mannosyltransferases participate in ER protein quality control. *Journal of cell science* **124:** 144-153

Goffeau A, Barrell BG, Bussey H, Davis RW, Dujon B, Feldmann H, Galibert F, Hoheisel JD, Jacq C, Johnston M, Louis EJ, Mewes HW, Murakami Y, Philippsen P, Tettelin H, Oliver SG (1996) Life with 6000 genes. *Science* **274:** 546, 563-547

Golovina EA, Golovin AV, Hoekstra FA, Faller R (2009) Water replacement hypothesis in atomic detail--factors determining the structure of dehydrated bilayer stacks. *Biophysical journal* **97:** 490-499

Goto M (2007) Protein O-glycosylation in fungi: diverse structures and multiple functions. *Bioscience, biotechnology, and biochemistry* **71:** 1415-1427

Grenson M (1966) Multiplicity of the amino acid permeases in Saccharomyces cerevisiae. II. Evidence for a specific lysine-transporting system. *Biochimica et biophysica acta* **127:** 339-346

Guerriero CJ, Brodsky JL (2012) The delicate balance between secreted protein folding and endoplasmic reticulum-associated degradation in human physiology. *Physiological reviews* **92:** 537-576

Guldal CG, Broach J (2006) Assay for adhesion and agar invasion in S. cerevisiae. *Journal of visualized experiments : JoVE***:** 64

He C, Klionsky DJ (2009) Regulation mechanisms and signaling pathways of autophagy. *Annual review of genetics* **43:** 67-93

Hebert DN, Molinari M (2007) In and out of the ER: protein folding, quality control, degradation, and related human diseases. *Physiological reviews* **87:** 1377-1408

Hedstrom L (2002) Serine protease mechanism and specificity. *Chemical reviews* **102:** 4501-4524

Helenius A, Aebi M (2004) Roles of N-linked glycans in the endoplasmic reticulum. *Annual review of biochemistry* **73:** 1019-1049

Herzig Y, Sharpe HJ, Elbaz Y, Munro S, Schuldiner M (2012) A systematic approach to pair secretory cargo receptors with their cargo suggests a mechanism for cargo selection by Erv14. *PLoS biology* **10:** e1001329

Hirayama H, Fujita M, Yoko-o T, Jigami Y (2008) O-mannosylation is required for degradation of the endoplasmic reticulum-associated degradation substrate Gas1*p via the ubiquitin/proteasome pathway in Saccharomyces cerevisiae. *Journal of biochemistry* **143:** 555-567

Hohmann S (2009) Control of high osmolarity signalling in the yeast Saccharomyces cerevisiae. *FEBS letters* **583:** 4025-4029

Hopper AK, Magee PT, Welch SK, Friedman M, Hall BD (1974) Macromolecule synthesis and breakdown in relation to sporulation and meiosis in yeast. *Journal of bacteriology* **119:** 619-628

Horton P, Park KJ, Obayashi T, Fujita N, Harada H, Adams-Collier CJ, Nakai K (2007) WoLF PSORT: protein localization predictor. *Nucleic acids research* **35:** W585-587

Hsieh MT, Chen RH (2011) Cdc48 and cofactors Npl4-Ufd1 are important for G1 progression during heat stress by maintaining cell wall integrity in Saccharomyces cerevisiae. *PloS one* **6:** e18988

Huang X, Miller W (1991) A time-efficient, linear-space local similarity algorithm. *Advances in Applied Mathematics* **12:** 337-357

Hubbers CU, Clemen CS, Kesper K, Boddrich A, Hofmann A, Kamarainen O, Tolksdorf K, Stumpf M, Reichelt J, Roth U, Krause S, Watts G, Kimonis V, Wattjes MP, Reimann J, Thal DR, Biermann K, Evert BO, Lochmuller H, Wanker EE, Schoser BG, Noegel AA, Schroder R (2007) Pathological consequences of VCP mutations on human striated muscle. *Brain : a journal of neurology* **130:** 381-393

Hughes H, Stephens DJ (2008) Assembly, organization, and function of the COPII coat. *Histochemistry and cell biology* **129:** 129-151

Huh WK, Falvo JV, Gerke LC, Carroll AS, Howson RW, Weissman JS, O'Shea EK (2003) Global analysis of protein localization in budding yeast. *Nature* **425:** 686-691

Hutchins MU, Klionsky DJ (2001) Vacuolar localization of oligomeric alpha-mannosidase requires the cytoplasm to vacuole targeting and autophagy pathway components in Saccharomyces cerevisiae. *The Journal of biological chemistry* **276:** 20491-20498

Hutt DM, Roth DM, Chalfant MA, Youker RT, Matteson J, Brodsky JL, Balch WE (2012) FK506 Binding Protein 8 Peptidylprolyl Isomerase Activity Manages a Late Stage of Cystic Fibrosis Transmembrane Conductance Regulator (CFTR) Folding and Stability. *The Journal of biological chemistry* **287:** 21914-21925

Ikeda M, Arai M, Lao DM, Shimizu T (2002) Transmembrane topology prediction methods: a re-assessment and improvement by a consensus method using a dataset of experimentally-characterized transmembrane topologies. *In silico biology* **2:** 19-33

Janda CY, Li J, Oubridge C, Hernandez H, Robinson CV, Nagai K (2010) Recognition of a signal peptide by the signal recognition particle. *Nature* **465:** 507-510

Jarosch E, Taxis C, Volkwein C, Bordallo J, Finley D, Wolf DH, Sommer T (2002) Protein dislocation from the ER requires polyubiquitination and the AAA-ATPase Cdc48. *Nature cell biology* **4:** 134-139

Jendretzki A, Wittland J, Wilk S, Straede A, Heinisch JJ (2011) How do I begin? Sensing extracellular stress to maintain yeast cell wall integrity. *European journal of cell biology* **90:** 740-744

Jensen TJ, Loo MA, Pind S, Williams DB, Goldberg AL, Riordan JR (1995) Multiple proteolytic systems, including the proteasome, contribute to CFTR processing. *Cell* **83:** 129-135

Jin R, Dobry CJ, McCown PJ, Kumar A (2008) Large-scale analysis of yeast filamentous growth by systematic gene disruption and overexpression. *Molecular biology of the cell* **19:** 284-296

Jones GM, Stalker J, Humphray S, West A, Cox T, Rogers J, Dunham I, Prelich G (2008) A systematic library for comprehensive overexpression screens in Saccharomyces cerevisiae. *Nature methods* **5:** 239-241

Jorgensen MU, Emr SD, Winther JR (1999) Ligand recognition and domain structure of Vps10p, a vacuolar protein sorting receptor in Saccharomyces cerevisiae. *European journal of biochemistry / FEBS* **260:** 461-469

Jules M, Guillou V, Francois J, Parrou JL (2004) Two distinct pathways for trehalose assimilation in the yeast Saccharomyces cerevisiae. *Applied and environmental microbiology* **70:** 2771-2778

Julius D, Blair L, Brake A, Sprague G, Thorner J (1983) Yeast alpha factor is processed from a larger precursor polypeptide: the essential role of a membrane-bound dipeptidyl aminopeptidase. *Cell* **32:** 839-852

Jung G, Ueno H, Hayashi R (1999) Carboxypeptidase Y: structural basis for protein sorting and catalytic triad. *Journal of biochemistry* **126:** 1-6

Kabeya Y, Noda NN, Fujioka Y, Suzuki K, Inagaki F, Ohsumi Y (2009) Characterization of the Atg17-Atg29-Atg31 complex specifically required for starvation-induced autophagy in Saccharomyces cerevisiae. *Biochemical and biophysical research communications* **389:** 612-615

Kakinuma Y, Ohsumi Y, Anraku Y (1981) Properties of H+-translocating adenosine triphosphatase in vacuolar membranes of SAccharomyces cerevisiae. *The Journal of biological chemistry* **256:** 10859-10863

Karreman RJ, Lindsey GG (2007) Modulation of Congo-red-induced aberrations in the yeast Saccharomyces cerevisiae by the general stress response protein Hsp12p. *Canadian journal of microbiology* **53:** 1203-1210

Karunanithi S, Vadaie N, Chavel CA, Birkaya B, Joshi J, Grell L, Cullen PJ (2010) Shedding of the mucin-like flocculin Flo11p reveals a new aspect of fungal adhesion regulation. *Current biology : CB* **20:** 1389-1395

Kelley LA, Sternberg MJ (2009) Protein structure prediction on the Web: a case study using the Phyre server. *Nature protocols* **4:** 363-371

Khalfan WA, Klionsky DJ (2002) Molecular machinery required for autophagy and the cytoplasm to vacuole targeting (Cvt) pathway in S. cerevisiae. *Current opinion in cell biology* **14:** 468-475

Kim J, Scott SV, Oda MN, Klionsky DJ (1997) Transport of a large oligomeric protein by the cytoplasm to vacuole protein targeting pathway. *The Journal of cell biology* **137:** 609-618

Kim PS, Arvan P (1998) Endocrinopathies in the family of endoplasmic reticulum (ER) storage diseases: disorders of protein trafficking and the role of ER molecular chaperones. *Endocrine reviews* **19:** 173-202

Kissova I, Salin B, Schaeffer J, Bhatia S, Manon S, Camougrand N (2007) Selective and non-selective autophagic degradation of mitochondria in yeast. *Autophagy* **3:** 329-336

Kitamura K, Yamamoto Y (1972) Purification and properties of an enzyme, zymolyase, which lyses viable yeast cells. *Archives of biochemistry and biophysics* **153:** 403-406

Klausner RD, Lippincott-Schwartz J, Bonifacino JS (1990) The T cell antigen receptor: insights into organelle biology. *Annual review of cell biology* **6:** 403-431

Klein T, Bischoff R (2011) Physiology and pathophysiology of matrix metalloproteases. *Amino acids* **41:** 271-290

Klionsky DJ, Herman PK, Emr SD (1990) The fungal vacuole: composition, function, and biogenesis. *Microbiological reviews* **54:** 266-292

Klis FM, Boorsma A, De Groot PW (2006) Cell wall construction in Saccharomyces cerevisiae. *Yeast* **23:** 185-202

Klis FM, Mol P, Hellingwerf K, Brul S (2002) Dynamics of cell wall structure in Saccharomyces cerevisiae. *FEMS microbiology reviews* **26:** 239-256

Knop M, Finger A, Braun T, Hellmuth K, Wolf DH (1996) Der1, a novel protein specifically required for endoplasmic reticulum degradation in yeast. *The EMBO journal* **15:** 753-763

Kofla G, Ruhnke M (2011) Pharmacology and metabolism of anidulafungin, caspofungin and micafungin in the treatment of invasive candidosis: review of the literature. *European journal of medical research* **16:** 159-166

Koh JL, Ding H, Costanzo M, Baryshnikova A, Toufighi K, Bader GD, Myers CL, Andrews BJ, Boone C (2010) DRYGIN: a database of quantitative genetic interaction networks in yeast. *Nucleic acids research* **38:** D502-507

Kominami E, Hoffschulte H, Leuschel L, Maier K, Holzer H (1981) The substrate specificity of proteinase B from baker's yeast. *Biochimica et biophysica acta* **661:** 136-141

Kondo H, Shibano Y, Amachi T, Cronin N, Oda K, Dunn BM (1998) Substrate specificities and kinetic properties of proteinase A from the yeast Saccharomyces cerevisiae and the development of a novel substrate. *Journal of biochemistry* **124:** 141-147

Koppen M, Langer T (2007) Protein degradation within mitochondria: versatile activities of AAA proteases and other peptidases. *Critical reviews in biochemistry and molecular biology* **42:** 221-242

Kraft C, Reggiori F, Peter M (2009) Selective types of autophagy in yeast. *Biochimica et biophysica acta* **1793:** 1404-1412

Krick R, Bremer S, Welter E, Schlotterhose P, Muehe Y, Eskelinen EL, Thumm M (2010) Cdc48/p97 and Shp1/p47 regulate autophagosome biogenesis in concert with ubiquitin-like Atg8. *The Journal of cell biology* **190:** 965-973

Krick R, Muehe Y, Prick T, Bremer S, Schlotterhose P, Eskelinen EL, Millen J, Goldfarb DS, Thumm M (2008) Piecemeal microautophagy of the nucleus requires the core macroautophagy genes. *Molecular biology of the cell* **19:** 4492-4505

Kruckeberg AL, Ye L, Berden JA, van Dam K (1999) Functional expression, quantification and cellular localization of the Hxt2 hexose transporter of Saccharomyces cerevisiae tagged with the green fluorescent protein. *The Biochemical journal* **339 (Pt 2):** 299-307

Lachmann J, Ungermann C, Engelbrecht-Vandre S (2011) Rab GTPases and tethering in the yeast endocytic pathway. *Small GTPases* **2:** 182-186

Lauwers E, Erpapazoglou Z, Haguenauer-Tsapis R, Andre B (2010) The ubiquitin code of yeast permease trafficking. *Trends in cell biology* **20:** 196-204

Lauwers E, Jacob C, Andre B (2009) K63-linked ubiquitin chains as a specific signal for protein sorting into the multivesicular body pathway. *The Journal of cell biology* **185:** 493-502

Lederkremer GZ (2009) Glycoprotein folding, quality control and ER-associated degradation. *Current opinion in structural biology* **19:** 515-523

Lee C, Schwartz MP, Prakash S, Iwakura M, Matouschek A (2001) ATP-dependent proteases degrade their substrates by processively unraveling them from the degradation signal. *Molecular cell* **7:** 627-637

Lee DH, Goldberg AL (1998) Proteasome inhibitors: valuable new tools for cell biologists. *Trends in cell biology* **8:** 397-403

Lee MJ, Lee BH, Hanna J, King RW, Finley D (2011) Trimming of ubiquitin chains by proteasome-associated deubiquitinating enzymes. *Molecular & cellular proteomics : MCP* **10:** R110 003871

Leon S, Haguenauer-Tsapis R (2009) Ubiquitin ligase adaptors: regulators of ubiquitylation and endocytosis of plasma membrane proteins. *Experimental cell research* **315:** 1574-1583

Lesage G, Bussey H (2006) Cell wall assembly in Saccharomyces cerevisiae. *Microbiology and molecular biology reviews : MMBR* **70:** 317-343

Lesage G, Shapiro J, Specht CA, Sdicu AM, Menard P, Hussein S, Tong AH, Boone C, Bussey H (2005) An interactional network of genes involved in chitin synthesis in Saccharomyces cerevisiae. *BMC genetics* **6:** 8

Li H, Page N, Bussey H (2002) Actin patch assembly proteins Las17p and Sla1p restrict cell wall growth to daughter cells and interact with cis-Golgi protein Kre6p. *Yeast* **19:** 1097-1112

Li SC, Kane PM (2009) The yeast lysosome-like vacuole: endpoint and crossroads. *Biochimica et biophysica acta* **1793:** 650-663

Li WW, Li J, Bao JK (2012) Microautophagy: lesser-known self-eating. *Cellular and molecular life sciences : CMLS* **69:** 1125-1136

Lippincott-Schwartz J, Bonifacino JS, Yuan LC, Klausner RD (1988) Degradation from the endoplasmic reticulum: disposing of newly synthesized proteins. *Cell* **54:** 209-220

Liu J, Kaksonen M, Drubin DG, Oster G (2006) Endocytic vesicle scission by lipid phase boundary forces. *Proceedings of the National Academy of Sciences of the United States of America* **103:** 10277-10282

Longtine MS, McKenzie A, 3rd, Demarini DJ, Shah NG, Wach A, Brachat A, Philippsen P, Pringle JR (1998) Additional modules for versatile and economical PCR-based gene deletion and modification in Saccharomyces cerevisiae. *Yeast* **14:** 953-961

Lorenz MC, Cutler NS, Heitman J (2000) Characterization of alcohol-induced filamentous growth in Saccharomyces cerevisiae. *Molecular biology of the cell* **11:** 183-199

Lu H, Salimian S, Gamelin E, Wang G, Fedorowski J, LaCourse W, Greenberg JT (2009) Genetic analysis of acd6-1 reveals complex defense networks and leads to identification of novel defense genes in Arabidopsis. *The Plant journal : for cell and molecular biology* **58:** 401-412

Manandhar SP, Hildebrandt ER, Jacobsen WH, Santangelo GM, Schmidt WK (2010) Chemical inhibition of CaaX protease activity disrupts yeast Ras localization. *Yeast* **27:** 327-343

Mansfeld J (2007) Metalloproteases. In *Industrial enzymes: structure, function, and applications*, Polaina JaM, A.P. (ed), 14. Dordrecht, The Netherlands: Springer

Marchler-Bauer A, Lu S, Anderson JB, Chitsaz F, Derbyshire MK, DeWeese-Scott C, Fong JH, Geer LY, Geer RC, Gonzales NR, Gwadz M, Hurwitz DI, Jackson JD, Ke Z, Lanczycki CJ, Lu F, Marchler GH, Mullokandov M, Omelchenko MV, Robertson CL, Song JS, Thanki N, Yamashita RA, Zhang D, Zhang N, Zheng C, Bryant SH (2011) CDD: a Conserved Domain Database for the functional annotation of proteins. *Nucleic acids research* **39:** D225-229

Marcusson EG, Horazdovsky BF, Cereghino JL, Gharakhanian E, Emr SD (1994) The sorting receptor for yeast vacuolar carboxypeptidase Y is encoded by the VPS10 gene. *Cell* **77:** 579-586

Mari M, Tooze SA, Reggiori F (2011) The puzzling origin of the autophagosomal membrane. *F1000 biology reports* **3:** 25

Marie M, Sannerud R, Avsnes Dale H, Saraste J (2008) Take the 'A' train: on fast tracks to the cell surface. *Cellular and molecular life sciences : CMLS* **65:** 2859-2874

Marty F (1999) Plant vacuoles. *The Plant cell* **11:** 587-600

Mason DA, Shulga N, Undavai S, Ferrando-May E, Rexach MF, Goldfarb DS (2005) Increased nuclear envelope permeability and Pep4p-dependent degradation of nucleoporins during hydrogen peroxide-induced cell death. *FEMS yeast research* **5:** 1237-1251

May C, Brosseron F, Chartowski P, Meyer HE, Marcus K (2012) Differential Proteome Analysis Using 2D-DIGE. *Methods Mol Biol* **893:** 75-82

McCracken AA, Brodsky JL (1996) Assembly of ER-associated protein degradation in vitro: dependence on cytosol, calnexin, and ATP. *The Journal of cell biology* **132:** 291-298

Mechler B, Muller M, Muller H, Meussdoerffer F, Wolf DH (1982) In vivo biosynthesis of the vacuolar proteinases A and B in the yeast Saccharomyces cerevisiae. *The Journal of biological chemistry* **257:** 11203-11206

Meissner D, Odman-Naresh J, Vogelpohl I, Merzendorfer H (2010) A novel role of the yeast CaaX protease Ste24 in chitin synthesis. *Molecular biology of the cell* **21:** 2425-2433

Mellman I, Warren G (2000) The road taken: past and future foundations of membrane traffic. *Cell* **100:** 99-112

Meyer H, Bug M, Bremer S (2012) Emerging functions of the VCP/p97 AAA-ATPase in the ubiquitin system. *Nature cell biology* **14:** 117-123

Mi H, Dong Q, Muruganujan A, Gaudet P, Lewis S, Thomas PD (2010) PANTHER version 7: improved phylogenetic trees, orthologs and collaboration with the Gene Ontology Consortium. *Nucleic acids research* **38:** D204-210

Mizushima N (2007) Autophagy: process and function. *Genes & development* **21:** 2861-2873

Moehle CM, Dixon CK, Jones EW (1989) Processing pathway for protease B of Saccharomyces cerevisiae. *The Journal of cell biology* **108:** 309-325

Morales Quinones M, Winston JT, Stromhaug PE (2012) Propeptide of aminopeptidase 1 protein mediates aggregation and vesicle formation in cytoplasm-to-vacuole targeting pathway. *The Journal of biological chemistry* **287:** 10121-10133

Moreira KE, Walther TC, Aguilar PS, Walter P (2009) Pil1 controls eisosome biogenesis. *Molecular biology of the cell* **20:** 809-818

Munn AL, Heese-Peck A, Stevenson BJ, Pichler H, Riezman H (1999) Specific sterols required for the internalization step of endocytosis in yeast. *Molecular biology of the cell* **10:** 3943-3957

Myers EW, Miller W (1988) Optimal alignments in linear space. *Computer applications in the biosciences : CABIOS* **4:** 11-17

Naik RR, Jones EW (1998) The PBN1 gene of Saccharomyces cerevisiae: an essential gene that is required for the post-translational processing of the protease B precursor. *Genetics* **149:** 1277-1292

Nair U, Thumm M, Klionsky DJ, Krick R (2011) GFP-Atg8 protease protection as a tool to monitor autophagosome biogenesis. *Autophagy* **7:** 1546-1550

Nakai K, Horton P (1999) PSORT: a program for detecting sorting signals in proteins and predicting their subcellular localization. *Trends in biochemical sciences* **24:** 34-36

Nakatsukasa K, Brodsky JL (2010) in vitro reconstitution of the selection, ubiquitination, and membrane extraction of a polytopic ERAD substrate. *Methods Mol Biol* **619:** 365-376

Nakatsukasa K, Huyer G, Michaelis S, Brodsky JL (2008) Dissecting the ER-associated degradation of a misfolded polytopic membrane protein. *Cell* **132:** 101-112

Nebes VL, Jones EW (1991) Activation of the proteinase B precursor of the yeast Saccharomyces cerevisiae by autocatalysis and by an internal sequence. *The Journal of biological chemistry* **266:** 22851-22857

Ng DT, Spear ED, Walter P (2000) The unfolded protein response regulates multiple aspects of secretory and membrane protein biogenesis and endoplasmic reticulum quality control. *The Journal of cell biology* **150:** 77-88

Nice DC, Sato TK, Stromhaug PE, Emr SD, Klionsky DJ (2002) Cooperative binding of the cytoplasm to vacuole targeting pathway proteins, Cvt13 and Cvt20, to phosphatidylinositol 3-phosphate at the pre-autophagosomal structure is required for selective autophagy. *The Journal of biological chemistry* **277:** 30198-30207

Nishikawa SI, Fewell SW, Kato Y, Brodsky JL, Endo T (2001) Molecular chaperones in the yeast endoplasmic reticulum maintain the solubility of proteins for retrotranslocation and degradation. *The Journal of cell biology* **153:** 1061-1070

Nishizawa M, Yasuhara T, Nakai T, Fujiki Y, Ohashi A (1994) Molecular cloning of the aminopeptidase Y gene of Saccharomyces cerevisiae. Sequence analysis and gene disruption of a new aminopeptidase. *The Journal of biological chemistry* **269:** 13651-13655

Nolan S, Cowan AE, Koppel DE, Jin H, Grote E (2006) FUS1 regulates the opening and expansion of fusion pores between mating yeast. *Molecular biology of the cell* **17:** 2439-2450

Nufer O, Guldbrandsen S, Degen M, Kappeler F, Paccaud JP, Tani K, Hauri HP (2002) Role of cytoplasmic C-terminal amino acids of membrane proteins in ER export. *Journal of cell science* **115:** 619-628

Nwaka S, Holzer H (1998) Molecular biology of trehalose and the trehalases in the yeast Saccharomyces cerevisiae. *Progress in nucleic acid research and molecular biology* **58:** 197-237

Nwaka S, Mechler B, Holzer H (1996) Deletion of the ATH1 gene in Saccharomyces cerevisiae prevents growth on trehalose. *FEBS letters* **386:** 235-238

Ohsumi Y, Anraku Y (1981) Active transport of basic amino acids driven by a proton motive force in vacuolar membrane vesicles of Saccharomyces cerevisiae. *The Journal of biological chemistry* **256:** 2079-2082

Orij R, Postmus J, Ter Beek A, Brul S, Smits GJ (2009) In vivo measurement of cytosolic and mitochondrial pH using a pH-sensitive GFP derivative in Saccharomyces cerevisiae reveals a relation between intracellular pH and growth. *Microbiology* **155:** 268-278

Otte S, Barlowe C (2002) The Erv41p-Erv46p complex: multiple export signals are required in trans for COPII-dependent transport from the ER. *The EMBO journal* **21:** 6095-6104

Page N, Gerard-Vincent M, Menard P, Beaulieu M, Azuma M, Dijkgraaf GJ, Li H, Marcoux J, Nguyen T, Dowse T, Sdicu AM, Bussey H (2003) A Saccharomyces cerevisiae genome-wide mutant screen for altered sensitivity to K1 killer toxin. *Genetics* **163:** 875-894

Parlati F, Dominguez M, Bergeron JJ, Thomas DY (1995) Saccharomyces cerevisiae CNE1 encodes an endoplasmic reticulum (ER) membrane protein with sequence similarity to calnexin and calreticulin and functions as a constituent of the ER quality control apparatus. *The Journal of biological chemistry* **270:** 244-253

Parr CL, Keates RA, Bryksa BC, Ogawa M, Yada RY (2007) The structure and function of Saccharomyces cerevisiae proteinase A. *Yeast* **24:** 467-480

Parsons AB, Brost RL, Ding H, Li Z, Zhang C, Sheikh B, Brown GW, Kane PM, Hughes TR, Boone C (2004) Integration of chemical-genetic and genetic interaction data links bioactive compounds to cellular target pathways. *Nature biotechnology* **22:** 62-69

Paz Y, Elazar Z, Fass D (2000) Structure of GATE-16, membrane transport modulator and mammalian ortholog of autophagocytosis factor Aut7p. *The Journal of biological chemistry* **275:** 25445-25450

Pena-Castillo L, Hughes TR (2007) Why are there still over 1000 uncharacterized yeast genes? *Genetics* **176:** 7-14

Peng J, Schwartz D, Elias JE, Thoreen CC, Cheng D, Marsischky G, Roelofs J, Finley D, Gygi SP (2003) A proteomics approach to understanding protein ubiquitination. *Nature biotechnology* **21:** 921-926

Pereira C, Chaves S, Alves S, Salin B, Camougrand N, Manon S, Sousa MJ, Corte-Real M (2010) Mitochondrial degradation in acetic acid-induced yeast apoptosis: the role of Pep4 and the ADP/ATP carrier. *Molecular microbiology* **76:** 1398-1410

Pittman JK (2011) Vacuolar Ca(2+) uptake. *Cell calcium* **50:** 139-146

Pollastri G, Przybylski D, Rost B, Baldi P (2002) Improving the prediction of protein secondary structure in three and eight classes using recurrent neural networks and profiles. *Proteins* **47:** 228-235

Preston RA, Murphy RF, Jones EW (1989) Assay of vacuolar pH in yeast and identification of acidification-defective mutants. *Proceedings of the National Academy of Sciences of the United States of America* **86:** 7027-7031

Prosser DC, Drivas TG, Maldonado-Baez L, Wendland B (2011) Existence of a novel clathrin-independent endocytic pathway in yeast that depends on Rho1 and formin. *The Journal of cell biology* **195:** 657-671

Punta M, Coggill PC, Eberhardt RY, Mistry J, Tate J, Boursnell C, Pang N, Forslund K, Ceric G, Clements J, Heger A, Holm L, Sonnhammer EL, Eddy SR, Bateman A, Finn RD (2012) The Pfam protein families database. *Nucleic acids research* **40:** D290-301

Pyo JO, Nah J, Jung YK (2012) Molecules and their functions in autophagy. *Experimental & molecular medicine* **44:** 73-80

Qiu QS (2012) V-ATPase, ScNhx1p and yeast vacuole fusion. *Journal of genetics and genomics = Yi chuan xue bao* **39:** 167-171

Qu BH, Thomas PJ (1996) Alteration of the cystic fibrosis transmembrane conductance regulator folding pathway. *The Journal of biological chemistry* **271:** 7261-7264

Rabinovich E, Kerem A, Frohlich KU, Diamant N, Bar-Nun S (2002) AAA-ATPase p97/Cdc48p, a cytosolic chaperone required for endoplasmic reticulum-associated protein degradation. *Molecular and cellular biology* **22:** 626-634

Ram AF, Klis FM (2006) Identification of fungal cell wall mutants using susceptibility assays based on Calcofluor white and Congo red. *Nature protocols* **1:** 2253-2256

Rawlings ND, Barrett AJ (1993) Evolutionary families of peptidases. *The Biochemical journal* **290 (Pt 1):** 205-218

Rawlings ND, Barrett AJ (1995) Evolutionary families of metallopeptidases. *Methods in enzymology* **248:** 183-228

Rawlings ND, Barrett AJ, Bateman A (2012) MEROPS: the database of proteolytic enzymes, their substrates and inhibitors. *Nucleic acids research* **40:** D343-350

Raymond CK, Howald-Stevenson I, Vater CA, Stevens TH (1992) Morphological classification of the yeast vacuolar protein sorting mutants: evidence for a prevacuolar compartment in class E vps mutants. *Molecular biology of the cell* **3:** 1389-1402

Reggiori F, Klionsky DJ (2002) Autophagy in the eukaryotic cell. *Eukaryotic cell* **1:** 11-21

Reggiori F, Pelham HR (2002) A transmembrane ubiquitin ligase required to sort membrane proteins into multivesicular bodies. *Nature cell biology* **4:** 117-123

Rimon N, Schuldiner M (2011) Getting the whole picture: combining throughput with content in microscopy. *Journal of cell science* **124:** 3743-3751

Roberts CJ, Pohlig G, Rothman JH, Stevens TH (1989) Structure, biosynthesis, and localization of dipeptidyl aminopeptidase B, an integral membrane glycoprotein of the yeast vacuole. *The Journal of cell biology* **108:** 1363-1373

Rodriguez-Pena JM, Garcia R, Nombela C, Arroyo J (2010) The high-osmolarity glycerol (HOG) and cell wall integrity (CWI) signalling pathways interplay: a yeast dialogue between MAPK routes. *Yeast* **27:** 495-502

Romisch K (2005) Endoplasmic reticulum-associated degradation. *Annual review of cell and developmental biology* **21:** 435-456

Rusnak F, Mertz P (2000) Calcineurin: form and function. *Physiological reviews* **80:** 1483-1521

Santamaria R, Rizzetto L, Bromley M, Zelante T, Lee W, Cavalieri D, Romani L, Miller B, Gut I, Santos M, Pierre P, Bowyer P, Kapushesky M (2011) Systems biology of infectious diseases: a focus on fungal infections. *Immunobiology* **216:** 1212-1227

Santos A, Marquina D, Leal JA, Peinado JM (2000) (1-->6)-beta-D-glucan as cell wall receptor for Pichia membranifaciens killer toxin. *Applied and environmental microbiology* **66:** 1809-1813

Sato K, Nakano A (2007) Mechanisms of COPII vesicle formation and protein sorting. *FEBS letters* **581:** 2076-2082

Sbardella D, Fasciglione GF, Gioia M, Ciaccio C, Tundo GR, Marini S, Coletta M (2012) Human matrix metalloproteinases: an ubiquitarian class of enzymes involved in several pathological processes. *Molecular aspects of medicine* **33:** 119-208

Schauer A, Knauer H, Ruckenstuhl C, Fussi H, Durchschlag M, Potocnik U, Frohlich KU (2009) Vacuolar functions determine the mode of cell death. *Biochimica et biophysica acta* **1793:** 540-545

Schneider CA, Rasband WS, Eliceiri KW (2012) NIH Image to ImageJ: 25 years of image analysis. *Nature methods* **9:** 671-675

Schu P (2008) Aminopeptidase I enzymatic activity. *Methods in enzymology* **451:** 67-78

Schwarz F, Aebi M (2011) Mechanisms and principles of N-linked protein glycosylation. *Current opinion in structural biology* **21:** 576-582

Scott SV, Baba M, Ohsumi Y, Klionsky DJ (1997) Aminopeptidase I is targeted to the vacuole by a nonclassical vesicular mechanism. *The Journal of cell biology* **138:** 37-44

Shei GJ, Broach JR (1995) Yeast silencers can act as orientation-dependent gene inactivation centers that respond to environmental signals. *Molecular and cellular biology* **15:** 3496-3506

Shimoi H, Kitagaki H, Ohmori H, Iimura Y, Ito K (1998) Sed1p is a major cell wall protein of Saccharomyces cerevisiae in the stationary phase and is involved in lytic enzyme resistance. *Journal of bacteriology* **180:** 3381-3387

Shirahama K, Yazaki Y, Sakano K, Wada Y, Ohsumi Y (1996) Vacuolar function in the phosphate homeostasis of the yeast Saccharomyces cerevisiae. *Plant & cell physiology* **37:** 1090-1093

Singer MA, Lindquist S (1998) Thermotolerance in Saccharomyces cerevisiae: the Yin and Yang of trehalose. *Trends in biotechnology* **16:** 460-468

Smith MH, Ploegh HL, Weissman JS (2011) Road to ruin: targeting proteins for degradation in the endoplasmic reticulum. *Science* **334:** 1086-1090

Snider C, Jayasinghe S, Hristova K, White SH (2009) MPEx: a tool for exploring membrane proteins. *Protein science : a publication of the Protein Society* **18:** 2624-2628

Sousa MJ, Azevedo F, Pedras A, Marques C, Coutinho OP, Preto A, Geros H, Chaves SR, Corte-Real M (2011) Vacuole-mitochondrial cross-talk during apoptosis in yeast: a model for understanding lysosome-mitochondria-mediated apoptosis in mammals. *Biochemical Society transactions* **39:** 1533-1537

Spear ED, Ng DT (2003) Stress tolerance of misfolded carboxypeptidase Y requires maintenance of protein trafficking and degradative pathways. *Molecular biology of the cell* **14:** 2756-2767

Speno HS, Luthi-Carter R, Macias WL, Valentine SL, Joshi AR, Coyle JT (1999) Site-directed mutagenesis of predicted active site residues in glutamate carboxypeptidase II. *Molecular pharmacology* **55:** 179-185

Spormann DO, Heim J, Wolf DH (1991) Carboxypeptidase yscS: gene structure and function of the vacuolar enzyme. *European journal of biochemistry / FEBS* **197:** 399-405

Stirling CJ, Rothblatt J, Hosobuchi M, Deshaies R, Schekman R (1992) Protein translocation mutants defective in the insertion of integral membrane proteins into the endoplasmic reticulum. *Molecular biology of the cell* **3:** 129-142

Subramanian S, Woolford CA, Drill E, Lu M, Jones EW (2006) Pbn1p: an essential endoplasmic reticulum membrane protein required for protein processing in the endoplasmic reticulum of budding yeast. *Proceedings of the National Academy of Sciences of the United States of America* **103:** 939-944

Sullivan ML, Youker RT, Watkins SC, Brodsky JL (2003) Localization of the BiP molecular chaperone with respect to endoplasmic reticulum foci containing the cystic fibrosis transmembrane conductance regulator in yeast. *The journal of histochemistry and cytochemistry : official journal of the Histochemistry Society* **51:** 545-548

Sun Y, Kaksonen M, Madden DT, Schekman R, Drubin DG (2005) Interaction of Sla2p's ANTH domain with PtdIns(4,5)P2 is important for actin-dependent endocytic internalization. *Molecular biology of the cell* **16:** 717-730

Suzuki K, Kirisako T, Kamada Y, Mizushima N, Noda T, Ohsumi Y (2001) The pre-autophagosomal structure organized by concerted functions of APG genes is essential for autophagosome formation. *The EMBO journal* **20:** 5971-5981

Suzuki NN, Yoshimoto K, Fujioka Y, Ohsumi Y, Inagaki F (2005) The crystal structure of plant ATG12 and its biological implication in autophagy. *Autophagy* **1:** 119-126

Takeshige K, Baba M, Tsuboi S, Noda T, Ohsumi Y (1992) Autophagy in yeast demonstrated with proteinase-deficient mutants and conditions for its induction. *The Journal of cell biology* **119:** 301-311

Tang B, Nirasawa S, Kitaoka M, Hayashi K (2002) The role of the N-terminal propeptide of the pro-aminopeptidase processing protease: refolding, processing, and enzyme inhibition. *Biochemical and biophysical research communications* **296:** 78-84

Tang J, Wong RN (1987) Evolution in the structure and function of aspartic proteases. *Journal of cellular biochemistry* **33:** 53-63

Teichert U, Mechler B, Muller H, Wolf DH (1989) Lysosomal (vacuolar) proteinases of yeast are essential catalysts for protein degradation, differentiation, and cell survival. *The Journal of biological chemistry* **264:** 16037-16045

Thomas PD, Kejariwal A, Campbell MJ, Mi H, Diemer K, Guo N, Ladunga I, Ulitsky-Lazareva B, Muruganujan A, Rabkin S, Vandergriff JA, Doremieux O (2003) PANTHER: a browsable database of gene products organized by biological function, using curated protein family and subfamily classification. *Nucleic acids research* **31:** 334-341

Thumm M (2000) Structure and function of the yeast vacuole and its role in autophagy. *Microscopy research and technique* **51:** 563-572

Tirosh B, Furman MH, Tortorella D, Ploegh HL (2003) Protein unfolding is not a prerequisite for endoplasmic reticulum-to-cytosol dislocation. *The Journal of biological chemistry* **278:** 6664-6672

Tong AH, Boone C (2006) Synthetic genetic array analysis in Saccharomyces cerevisiae. *Methods Mol Biol* **313:** 171-192

Tong AH, Evangelista M, Parsons AB, Xu H, Bader GD, Page N, Robinson M, Raghibizadeh S, Hogue CW, Bussey H, Andrews B, Tyers M, Boone C (2001) Systematic genetic analysis with ordered arrays of yeast deletion mutants. *Science* **294:** 2364-2368

Travers KJ, Patil CK, Wodicka L, Lockhart DJ, Weissman JS, Walter P (2000) Functional and genomic analyses reveal an essential coordination between the unfolded protein response and ER-associated degradation. *Cell* **101:** 249-258

Trumbly RJ, Bradley G (1983) Isolation and characterization of aminopeptidase mutants of Saccharomyces cerevisiae. *Journal of bacteriology* **156:** 36-48

Tykvart J, Sacha P, Barinka C, Knedlik T, Starkova J, Lubkowski J, Konvalinka J (2012) Efficient and versatile one-step affinity purification of in vivo biotinylated proteins: expression, characterization and structure analysis of recombinant human glutamate carboxypeptidase II. *Protein expression and purification* **82:** 106-115

Unlu M, Morgan ME, Minden JS (1997) Difference gel electrophoresis: a single gel method for detecting changes in protein extracts. *Electrophoresis* **18:** 2071-2077

Uttenweiler A, Mayer A (2008) Microautophagy in the yeast Saccharomyces cerevisiae. *Methods Mol Biol* **445:** 245-259

Valdivia RH, Baggott D, Chuang JS, Schekman RW (2002) The yeast clathrin adaptor protein complex 1 is required for the efficient retention of a subset of late Golgi membrane proteins. *Developmental cell* **2:** 283-294

van den Hazel HB, Kielland-Brandt MC, Winther JR (1992) Autoactivation of proteinase A initiates activation of yeast vacuolar zymogens. *European journal of biochemistry / FEBS* **207:** 277-283

Van Den Hazel HB, Kielland-Brandt MC, Winther JR (1996) Review: biosynthesis and function of yeast vacuolar proteases. *Yeast* **12:** 1-16

van Dijken JP, Bauer J, Brambilla L, Duboc P, Francois JM, Gancedo C, Giuseppin ML, Heijnen JJ, Hoare M, Lange HC, Madden EA, Niederberger P, Nielsen J, Parrou JL, Petit T, Porro D, Reuss M, van Riel N, Rizzi M, Steensma HY, Verrips CT, Vindelov J, Pronk JT (2000) An interlaboratory comparison of physiological and genetic properties of four Saccharomyces cerevisiae strains. *Enzyme and microbial technology* **26:** 706-714

Vembar SS, Brodsky JL (2008) One step at a time: endoplasmic reticulum-associated degradation. *Nature reviews Molecular cell biology* **9:** 944-957

Vembar SS, Jonikas MC, Hendershot LM, Weissman JS, Brodsky JL (2010) J domain co-chaperone specificity defines the role of BiP during protein translocation. *The Journal of biological chemistry* **285:** 22484-22494

Veses V, Richards A, Gow NA (2008) Vacuoles and fungal biology. *Current opinion in microbiology* **11:** 503-510

Vincentelli R, Canaan S, Campanacci V, Valencia C, Maurin D, Frassinetti F, Scappucini-Calvo L, Bourne Y, Cambillau C, Bignon C (2004) High-throughput automated refolding screening of inclusion bodies. *Protein science : a publication of the Protein Society* **13:** 2782-2792

von Heijne G (1992) Membrane protein structure prediction. Hydrophobicity analysis and the positive-inside rule. *Journal of molecular biology* **225:** 487-494

Wang W, Malcolm BA (1999) Two-stage PCR protocol allowing introduction of multiple mutations, deletions and insertions using QuikChange Site-Directed Mutagenesis. *BioTechniques* **26:** 680-682

Ward CL, Kopito RR (1994) Intracellular turnover of cystic fibrosis transmembrane conductance regulator. Inefficient processing and rapid degradation of wild-type and mutant proteins. *The Journal of biological chemistry* **269:** 25710-25718

Ward CL, Omura S, Kopito RR (1995) Degradation of CFTR by the ubiquitin-proteasome pathway. *Cell* **83:** 121-127

Watanabe D, Abe M, Ohya Y (2001) Yeast Lrg1p acts as a specialized RhoGAP regulating 1,3-beta-glucan synthesis. *Yeast* **18:** 943-951

Watanabe R, Riezman H (2004) Differential ER exit in yeast and mammalian cells. *Current opinion in cell biology* **16:** 350-355

Watts GD, Wymer J, Kovach MJ, Mehta SG, Mumm S, Darvish D, Pestronk A, Whyte MP, Kimonis VE (2004) Inclusion body myopathy associated with Paget disease of bone and frontotemporal dementia is caused by mutant valosin-containing protein. *Nature genetics* **36:** 377-381

Weidberg H, Shvets E, Elazar Z (2011) Biogenesis and cargo selectivity of autophagosomes. *Annual review of biochemistry* **80:** 125-156

Weinberg J, Drubin DG (2012) Clathrin-mediated endocytosis in budding yeast. *Trends in cell biology* **22:** 1-13

Werner ED, Brodsky JL, McCracken AA (1996) Proteasome-dependent endoplasmic reticulum-associated protein degradation: an unconventional route to a familiar fate. *Proceedings of the National Academy of Sciences of the United States of America* **93:** 13797-13801

Westphal V, Marcusson EG, Winther JR, Emr SD, van den Hazel HB (1996) Multiple pathways for vacuolar sorting of yeast proteinase A. *The Journal of biological chemistry* **271:** 11865-11870

Wiederhold E, Gandhi T, Permentier HP, Breitling R, Poolman B, Slotboom DJ (2009) The yeast vacuolar membrane proteome. *Molecular & cellular proteomics : MCP* **8:** 380-392

Wiemken A, Matile P, Moor H (1970) Vacuolar dynamics in synchronously budding yeast. *Archiv fur Mikrobiologie* **70:** 89-103

Winzeler EA, Castillo-Davis CI, Oshiro G, Liang D, Richards DR, Zhou Y, Hartl DL (2003) Genetic diversity in yeast assessed with whole-genome oligonucleotide arrays. *Genetics* **163:** 79-89

Wolf DH, Ehmann C (1981) Carboxypeptidase S- and carboxypeptidase Y-deficient mutants of Saccharomyces cerevisiae. *Journal of bacteriology* **147:** 418-426

Wolf DH, Stolz A (2012) The Cdc48 machine in endoplasmic reticulum associated protein degradation. *Biochimica et biophysica acta* **1823:** 117-124

Wright CM, Fewell SW, Sullivan ML, Pipas JM, Watkins SC, Brodsky JL (2007) The Hsp40 molecular chaperone Ydj1p, along with the protein kinase C pathway, affects cell-wall integrity in the yeast Saccharomyces cerevisiae. *Genetics* **175:** 1649-1664

Xie Y, Varshavsky A (2001) RPN4 is a ligand, substrate, and transcriptional regulator of the 26S proteasome: a negative feedback circuit. *Proceedings of the National Academy of Sciences of the United States of America* **98:** 3056-3061

Xie Z, Klionsky DJ (2007) Autophagosome formation: core machinery and adaptations. *Nature cell biology* **9:** 1102-1109

Yamanaka K, Sasagawa Y, Ogura T (2012) Recent advances in p97/VCP/Cdc48 cellular functions. *Biochimica et biophysica acta* **1823:** 130-137

Yan A, Lennarz WJ (2005) Unraveling the mechanism of protein N-glycosylation. *The Journal of biological chemistry* **280:** 3121-3124

Yang Z, Klionsky DJ (2009) An overview of the molecular mechanism of autophagy. *Current topics in microbiology and immunology* **335:** 1-32

Yasuhara T, Nakai T, Ohashi A (1994) Aminopeptidase Y, a new aminopeptidase from Saccharomyces cerevisiae. Purification, properties, localization, and processing by protease B. *The Journal of biological chemistry* **269:** 13644-13650

Yorimitsu T, Klionsky DJ (2007) Endoplasmic reticulum stress: a new pathway to induce autophagy. *Autophagy* **3:** 160-162

Youker RT, Walsh P, Beilharz T, Lithgow T, Brodsky JL (2004) Distinct roles for the Hsp40 and Hsp90 molecular chaperones during cystic fibrosis transmembrane conductance regulator degradation in yeast. *Molecular biology of the cell* **15:** 4787-4797

Yuga M, Gomi K, Klionsky DJ, Shintani T (2011) Aspartyl aminopeptidase is imported from the cytoplasm to the vacuole by selective autophagy in Saccharomyces cerevisiae. *The Journal of biological chemistry* **286:** 13704-13713

Zhang Y, Nijbroek G, Sullivan ML, McCracken AA, Watkins SC, Michaelis S, Brodsky JL (2001) Hsp70 molecular chaperone facilitates endoplasmic reticulum-associated protein degradation of cystic fibrosis transmembrane conductance regulator in yeast. *Molecular biology of the cell* **12:** 1303-1314

Zhao C, Jung US, Garrett-Engele P, Roe T, Cyert MS, Levin DE (1998) Temperature-induced expression of yeast FKS2 is under the dual control of protein kinase C and calcineurin. *Molecular and cellular biology* **18:** 1013-1022

Zhou G, Li H, DeCamp D, Chen S, Shu H, Gong Y, Flaig M, Gillespie JW, Hu N, Taylor PR, Emmert-Buck MR, Liotta LA, Petricoin EF, 3rd, Zhao Y (2002) 2D differential in-gel electrophoresis for the identification of esophageal scans cell cancer-specific protein markers. *Molecular & cellular proteomics : MCP* **1:** 117-124

Ziman M, Chuang JS, Schekman RW (1996) Chs1p and Chs3p, two proteins involved in chitin synthesis, populate a compartment of the Saccharomyces cerevisiae endocytic pathway. *Molecular biology of the cell* **7:** 1909-1919

Zinser E, Paltauf F, Daum G (1993) Sterol composition of yeast organelle membranes and subcellular distribution of enzymes involved in sterol metabolism. *Journal of bacteriology* **175:** 2853-2858

Zinser E, Sperka-Gottlieb CD, Fasch EV, Kohlwein SD, Paltauf F, Daum G (1991) Phospholipid synthesis and lipid composition of subcellular membranes in the unicellular eukaryote Saccharomyces cerevisiae. *Journal of bacteriology* **173:** 2026-2034